S-Matrix Analysis of Vibrational and Alignment Effects in Intense-Field Multiphoton Ionization of Molecules

Arvid Requate

Mar. 2007

Dissertation

zur Erlangung des Doktorgrades der Naturwissenschaften
an der Fakultät für Physik der Universität Bielefeld

Referenten: Prof. F. H. M. Faisal Ph.D.,
Fakultät für Physik, Universität Bielefeld
Dr. A. Becker,
Max-Planck-Institut für Physik komplexer Systeme, Dresden

Vorwort

Die vorliegende Dissertation wurde in der Arbeitsgruppe *Theoretische Atom-, Molekül- und Laserphysik* unter der Leitung von Prof. F.H.M. Faisal Ph.D. an der Fakultät für Physik der Universität Bielefeld begonnen und in der Arbeitsgruppe *Nichtlineare Prozesse in starken Feldern* unter der Leitung von A. Becker an dem Max-Planck-Institut für Physik komplexer Systeme (MPIPKS) fertig gestellt. Die quantenchemischen Berechnungen mit dem GAMESS Paket wurden auf den Rechnern der Fakultät für Physik der Universität Bielefeld vorgenommen, während die numerischen S-Matrix Rechnungen zum größten Teil auf den Linux Rechnern des MPIPKS durchgeführt wurden.

Teile der in Kapitel 4 dargestellten Ergebnisse wurden in der Publikation

S-matrix theory of inelastic vibronic ionization of molecules in intense laser fields
A. Requate, A. Becker und F. H. M. Faisal, Phys. Rev. A **73** (2006) 033406

dargestellt. Die Arbeit wurde in englischer Sprache verfasst, um die relative Sprachbarriere gering zu gestalten, da Englisch derzeit die Hauptsprache des Fachgebiets darstellt.

Außer der in der Bibliographie angegebenen Literatur wurden folgende Programmpakete zur Erstellung und Auswertung der numerischen Simulationen sowie der Dissertationsschrift verwendet: GNU Compiler Collection (GCC), GNU Scientific Library (GSL), CERN Class Library for High Energy Physics (CLHEP), GAMESS, GaussSum, Python, Xmgrace sowie Pybliographic, Kile, Xfig und pdfeTeX einschließlich verschiedener Pakete, allen voran LaTeX, KOMA-Script, `amsmath`, `graphicx`, `hyperref` und `natbib`. Der verwendete Fortran Programmcode zur Berechnung der generalisierten Bessel-Funktionen ist eine Entwicklung früherer Mitglieder der Arbeitsgruppe "Theoretische Atom-, Molekül- und Laserphysik" an der Fakultät für Physik der Universität Bielefeld.

Contents

1. Introduction and Outline

In one of his three groundbreaking papers of 1905 Albert Einstein introduced the concept that light has a corpuscular character in the process of the *Photoeffect* [1]. In this process an electron bound to an atom is ionized into the continuum by absorption of a single photon from a light source. Experimentally it was found that it was the frequency and not the intensity of the light, which is the crucial parameter that decided whether the process would be possible or not. Einstein's theory was complementary to the established way to describe light as an electromagnetic wave according to Maxwell's laws. The success of both models in different areas of physics was the foundation of the wave-particle dualism of light as a figure of thought. In the course of her Ph.D. thesis [2, 3], which was finally published 1931, Maria Goeppert-Mayer theoretically predicted the possibility of the simultaneous absorption of two photons. The cross sections for this process are considerably smaller than the ones for single photon absorption. It was not until 1950, that the first experimental evidence for processes of this kind could be found by means of radio-frequency spectroscopy [4]. About ten years later, further experimental confirmation was obtained [5] in experiments with a maser source which was realized only a couple of years earlier [6]. With the advent of sources of laser light [7, 8] of ever increasing intensity, it became possible to study the absorption of multiple photons in elementary electronic transition process in atoms and molecules [9, 10].

The electric field strength that binds the electron in its ground state to the proton inside the Hydrogen atom is

$$|\vec{E}| = \frac{e}{4\pi\epsilon_0 a_0^2} = 5.14 \times 10^9 \frac{\mathrm{V}}{\mathrm{cm}} \,, \tag{1.1}$$

where e is the charge of an electron, a_0 is the Bohr radius and ϵ_0 is the dielectric constant for vacuum. The only practicable way to achieve field strengths of this order of magnitude in a laboratory is in form of the temporally varying electric field of an electromagnetic wave. The corresponding magnetic field component is found to be less important for the dynamics for intensities that are lower than the relativistic threshold intensity of about $10^{19}\,\mathrm{W/cm^2}$. At that intensity the average kinetic energy of an electron in the field starts to exceed to the electronic rest energy:

$$eE_0\lambda > 2\pi m_e c^2 \,, \tag{1.2}$$

with the wavelength $\lambda = c/2\pi\omega$; m_e denotes the mass of the electron and c the speed of light. The measure for the average kinetic energy of an elementary charge

in an electromagnetic wave with E-field $E(t) = E_0 \sin(\omega t + \phi_0)$ is the ponderomotive energy

$$U_p = \frac{e^2 E_0^2}{4 m_e \omega^2} \,. \tag{1.3}$$

At the field intensity of $I_{\text{a.u.}} = 3.51 \times 10^{16}\,\text{W/cm}^2$ the strength of the electric field of the laser is of the same size as the electric field in the field free hydrogen atom.

$$I_0 = \frac{1}{2} c \epsilon_0 E_0^2 \text{ [in S.I.], and } I_0 = E_0^2 \text{ [in a.u.]} \,. \tag{1.4}$$

Boosted by the development of Chirped Pulse Amplification [11–13] laser technology evolved at a fast pace up to the point that today intensities above $10^{21}\,\text{W/cm}^2$ can be focused on atomic and molecular systems [14, 15]. But already at intensities much below $I_{\text{a.u.}}$, ionization processes occur, as the bound system is distorted nonlinearly by the field and mechanisms as tunneling and intense-field multiphoton ionization are quantum mechanically possible.

The usage of pulsed laser beams also introduces another interesting advantage of the laser over static fields for the study of transition processes in atoms and molecules, that is ultrashort interaction times. Nowadays already few cycle pulses are experimentally controllable [16, 17]. Since one cycle of the laser field of 800 nm wavelength takes 2.67 fs, the interaction time with the Coulombic system is on the scale of femtoseconds ($1\,\text{fs} = 10^{-15}\,\text{s}$). Taking into account that the peak intensity of the pulse is only achieved at the central oscillation of the pulse, effective interaction times on the attosecond time scale ($1\,\text{as} = 10^{-18}\,\text{s}$) can be realized with lasers of higher frequency, e.g. in the XUV domain (a period of 14 nm radiation extends over $T_0 \approx 46\,\text{as}$) [18]. Series (or *trains*) of XUV attosecond pulses have also been produced by emission of high-harmonic frequency radiation in electron recollision processes [19]. Today it is a matter of active research to generate isolated XUV attosecond pulses, for which theoretical concepts exist (see [16] for references).

Given these ultra short interaction times, that nearly reach the domain of characteristic times of electronic motion (1 a.u. of time $\approx 24.2\,\text{as}$, see definition of atomic units in section A), and given the tunability of the laser frequency by means such as optical parametric amplification and high harmonic generation, today it is realistic to think about mechanisms of controlled manipulation of atoms and molecules. One of the most interesting applications is the probing and control of chemical reactions on femtosecond time scales [20, 21] by *pump-probe techniques* [22].

For the theoretical description such processes provide at least two major challenges. The first and most obvious is the fact that these processes involve many interacting physical entities or bodies. The second is that the dynamics of the process is determined by two interactions, the Coulomb interaction of the electrons with the bound system, and their interaction with the laser field, and that these two interactions are of comparable strength. Both challenges demand for a systematic approach to

successively account for one specific two-body interaction at each step of the theoretical description. The Intense-Field Many-Body S-Matrix Theory (IMST) has been developed to meet this demand [23–26]. Widely recognized for the successful identification of *Nonsequential Double Ionization* as an essential mechanism in the double ionization of atoms [27–32] it and its precursor, the KFR theory, has become a standard approach for the identification of interaction mechanisms in bound-continuum transitions. These approaches go beyond the traditional perturbation theory, as they do not rely on one interaction being only of perturbative influence as compared to the other interaction. As such it can explain processes that are occurring in a domain where for this reason perturbation theory breaks down.

While there has been considerable progress in the last years in the general understanding of mechanisms of intense-field processes in atoms, molecules and clusters, the number of questions left unconsidered increases with number of internal degrees of freedom of these systems. In the case of clusters quasiclassical treatments of many-body behavior have been shown to result in working models that can explain the special features of these systems in intense laser fields [33], such as the observed increased energy transfer from the field and the resulting high charge states of the atomic ions, to name only two. For single molecules on the other hand a fully quantum mechanical treatment is necessary due to the quantization of the energy of their electronic, vibrational and rotational states. For small molecules this kind of analysis is feasible due to the restricted number of internal degrees of freedom. The very first insight into the sequence of physical processes in molecular systems is gained by considering the implications of the large difference in the masses of the electrons and the nuclei. This results in the Born-Oppenheimer separation of the Hamilton operator for molecular systems and in the conclusion that the electrons are the primary interaction partners to the field. Internuclear dynamics is taking place subsequently on a considerably longer time scale. It is the topic of this thesis to analyze the interplay of ionization processes in intense laser fields with molecular degrees of freedom. On the one hand it presents a quantum mechanical analysis of the effect of multi-photon ionization on the state of internuclear vibration of molecules and on the other hand it considers the role of molecular alignment, i.e. the angle of the internuclear axis to the polarization of the laser field, in *Nonsequential Double Ionization*. The latter is assessed by a separation of the full process into *Above Threshold Ionization* (ATI) and subsequent electron impact ionization in the laser field $(e + N\omega, 2e)$. Since the alignment dependence of ATI rates is well understood in terms of the symmetry of the molecular orbital of the ionized electron [34–37], this thesis undertakes the corresponding analysis for the final $(e + N\omega, 2e)$ step to obtain a deeper understanding of the interplay of these two processes in diatomic molecules.

The following chapter 2 gives an overview of the mechanisms of strong field ionization, highlighting the most important results of experimental and theoretical research. Starting from the basic mechanisms of single ionization, i.e. photoeffect, tunneling and intense-field multiphoton ionization an introduction is given to the

different subsequent effects, such as elastic and inelastic recollision in general and double and multiple ionization in particular. The effects of the specific electronic and vibrational structure of molecules on processes in intense laser fields are discussed.

Chapter 3 introduces to different theoretical methods of atomic and molecular and laser physics, such as the numerical evolution of wavefunctions according to the time dependent Schrödinger equation (TDSE) on the one hand and Floquet methods on the other hand. The TDSE section contains a short overview over the *Virtual NPSF Lab* (section 3.1.1), a project currently in process at the group *Nonlinear Processes in Strong Fields* (NPSF) at the Max Planck Institute for the Physics of Complex Systems (MPIPKS), where part of the research for this thesis was supervised. Some of the key points of the theoretical and technical approach in this project are highlighted with an emphasis on the quantum mechanical description of electron pair states in intense laser fields, which represent an essential part of the final states of double ionization processes. Special consideration is given in this chapter to an account of the Intense-Field Many-Body S-Matrix Theory (IMST) which constitutes the theoretical framework of this thesis.

In chapter 4 the process of *Inelastic Vibronic Ionization* of molecules in intense laser fields is analyzed, applying the framework of S-matrix theory. To this end, the Born-Oppenheimer separation of electronic and nuclear dynamics is introduced and the difference between the Franck-Condon principle for electronic transitions in molecules and the Franck-Condon approximation is discussed. An overview is given over so called non-Franck-Condon effects in molecular electronic transitions, laying emphasis on a particularly clean and at first glance irritating experimental result for the ionization of H_2 in intense laser fields. In section 4.3 the S-matrix theory for *Inelastic Vibronic Ionization* is derived and the quantum mechanical boundary conditions, i.e. the initial and final states, are defined. Section 4.4 discusses the results of the numerical calculations for small diatomic molecules in comparison with the experimental data. Different levels of approximation are compared – the fully coherent Born-Oppenheimer, the 'frozen' MO and the Franck-Condon overlap approximation – and the applicability of the Franck-Condon approximation to the strongly nonlinear process of multiphoton ionization of molecules in an intense laser field is verified. Effects of the variation of isotopes and of laser polarization are shown. The interpretation of the photoelectron or scattering phase terms that appear in the first order S-matrix rate expression leads to a discussion of the emergence of momentum conservation in the context of IMST (section 4.4.4). Subsequently the theory is applied to more complex diatomic molecules, homo- as well as heteronuclear ones. The extension to polyatomic molecules is exemplified by the application to a linear triatomic molecule.

The final chapter 5 of this thesis is devoted to the analysis of the alignment dependence of *Nonsequential Double Ionization* (NSDI) of diatomic molecules. This is done from two perspectives. First, the electron impact ionization of diatomic molecules

in the presence of a laser field $(e + N\omega, 2e)$ is treated, which according to present physical understanding constitutes the mechanism of secondary ionization in NSDI. On the other hand, to connect to current experimental research and to relate the $(e+N\omega, 2e)$ analysis back to the context of *Nonsequential Double Ionization*, a model formula for NSDI is used, which combines the two separate first order S-matrix expressions for the initial step (intense-field multiphoton ionization) and the final step (laser assisted electron impact ionization) to obtain an approximation for the rates of *Nonsequential Double Ionization* of diatomic molecules. To this end the first order IMST expression for the $(e + N\omega, 2e)$ process is derived in section 5.1.2 considering spin-correlation between projectile and target electron, allowing for exchange scattering. An argument is brought forward, that ionization of the secondary electron after collision of the primary/projectile electron with the nuclei is beyond the scope of a first order S-matrix approach, resulting in vanishing first order transition amplitudes for this mechanism. Following up the discussion of the momentum of electron pair states in section 3.1.1 on the one hand and on the emergence of momentum conservation in IMST (section 4.4.4) on the other hand, the consideration of the recoil momentum of the molecular ion in the framework of IMST and its specific role in the first order S-matrix expression for laser assisted electron impact ionization are discussed in section 5.1.3. The dependence of ionization rates on the angle of alignment between the internuclear axis and the direction of laser polarization is analyzed in terms of the symmetry of the molecular orbital of the secondary electron. The effect of the spin on this process is analyzed in section 5.1.5. To focus on two salient degrees of freedom that distinguish a diatomic molecule from an atom, two kinds of calculated spectra are presented in the final part of chapter 5: Following up to the analysis in the first part of chapter 5, the variation of the NSDI rates with the alignment angle between the internuclear axis of the molecule and the direction of laser polarization is shown. Additionally, based on the verified applicability of the Franck-Condon approximation in strongly nonlinear processes in intense laser fields (shown in chapter 4), the distribution of the vibrational states of the molecular dication after NSDI is predicted within the limits of the approximations applied.

Chapter 6 summarizes the conclusions and gives an outlook from the perspective gained in the course of this thesis.

In this thesis atomic units will be used, where $e = m_e = \hbar = 1$. Details of this system of units are noted in section A. In some formulae the respective quantities are written down explicitly for convenience, to give familiar combinations of quantities that are less irritating for a quick check of units.

2. Mechanisms of Strong Field Ionization

This chapter gives an overview of the mechanisms of single and multiple ionization of atoms and molecules in intense laser fields.

2.1. Single Ionization

One of the most surprising experimental findings in the research on the interaction of intense laser fields with atoms and molecules has been the detection of a discrete structure in the kinetic energy spectra of ionized electrons [38–40]. The spectra showed equally spaced peaks in the detection yields, separated by the energy of one photon. The phenomenon was dubbed *Above Threshold Ionization* (ATI) [41], as the electrons can absorb more than the threshold energy necessary to make the transition from a specific bound state of the Coulomb potential to an energetically low lying continuum state. The discovery was surprising, since a free electron cannot absorb single photons, because the momentum is not conserved in that process. It emphasized that the ionizing electron is still in the vicinity of the parent ion directly after its first transition to a low lying continuum state. The effect was first explained as a two step process [38]. In this picture, the electron enters the continuum at threshold energy and then absorbs additional photons by *Inverse Bremsstrahlung* in the field of the parent ion. The differential cross section for the combination of the two steps has been found to be [42–44]

$$\frac{d\sigma_{fi}^{(M)}}{d\Omega} = \frac{k_f}{k_i} J_M^2 \left[\boldsymbol{\alpha}_0 \cdot (\boldsymbol{k}_f - \boldsymbol{k}_i)\right] \frac{d\sigma_{fi}^{(N_0)}}{d\Omega} \tag{2.1}$$

where M is the number of excess photons absorbed on top of the N_0 threshold and the momentum of the charged particle changes from $\boldsymbol{k}_i$ to $\boldsymbol{k}_f$.

$$\boldsymbol{\alpha}_0 = \frac{q\boldsymbol{A}_0}{m_e c\omega} \tag{2.2}$$

is the quiver radius of the electron (of charge $q = -1\,\text{a.u.}$) in the laser field with an amplitude vector $\boldsymbol{A}_0$ of the vector potential. The symbol J_M denotes a Bessel function of first kind of Mth order. While this derivation is consistent with the multiphoton nature of the process, one still needs the basic differential cross section $\frac{d\sigma_{fi}^{(N_0)}}{d\Omega}$ for multiphoton threshold ionization to predict the cross section for the N_0+M photon process.

When on the other hand the theoretical description for the intense-field, nonperturbative *Multiphoton Ionization* (MPI) had been found independently by Keldysh, Faisal and Reiss (KFR) [45–47], it became clear that the ATI process can be understood as a direct (single-step) mechanism of ionization by simultaneous absorption of $N = N_0 + M$ photons in the vicinity of the binding potential. It thus proved to be a more effective explanation than the initially proposed two-step model for ATI.

After a short note on the quantum mechanical description of the bound electrons in ionization processes we will give an account of the two general physical mechanisms that have been identified in intense-field ionization. The first is *Tunneling Ionization* which limits into *Over the Barrier Ionization* for higher field strengths. It enjoys a high popularity due to the general simplicity of its application but is limited to a certain domain of field parameters (intensity and wavelength), related to the given ionization potential. Specifically it cannot explain the quantized photonic structure of the ATI effect. The second mechanism discussed is the intense-field *Multiphoton Ionization* (MPI) which includes the "tunnel-mechanism" as a special case [26]. This section about single ionization closes with an account of the electronic recollision process, which may occur subsequently to single ionization in the laser field.

2.1.1. Quantum Mechanical Description of the Bound System

Neglecting the possibility of spin-flips, each occupied electronic state in the initially prepared bound Coulombic system is related to exactly one possible final state of the system after an effective N-photon ionization, depending on which electron was transferred into a continuum state of the ion. Correspondingly, directly after ionization, i.e. without further relaxation processes, the ion is left either in the ground state or, if an inner-shell electron was ionized, in a specific excited state. Energy conservation demands that $N\hbar\omega - E_T(i,f) - U_p = E_{\text{kin}}(i,f,N)$, where $E_T(i,f)$ denotes the energy difference between the final state of the ion and initial state of the bound Coulombic system. $E_{\text{kin}}(i,f,N)$ is the time averaged kinetic energy of the ionized electron in the field.

If the initial and final states of the Coulombic system are described as products of the wavefunctions of the single electrons, the final ground or unrelaxed excited state of the ion corresponds directly to the initial spatial state of the electron that was ionized. This assumption is usually made and is equivalent to the physical assumption that there is no "hidden" implicit correlation between the electrons of the initial bound system beyond the explicit correlation by the Coulomb potential that defines the Hamiltonian for the bound system[1]. In quantum chemistry the spatial wavefunctions of the electrons are frequently referred to as spatial orbitals.

Without the consideration of the effect of magnetic fields or relativistic effects in the initial system two electrons occupying the same spatial orbital but differing

[1] If the Hamiltonian is replaced by an approximative one like in Hartree-Fock calculations, this explicit correlation is lost to an extend that depends on the type of approximation.

in their spin have the same energy, i.e. they are degenerate. Consequently, in an effective N-photon transition, for each transition energy $E_T(i,f)$ there are up to two electronic initial states, differing only in spin, that define possible channels to the detection of an electron with kinetic energy $E_{\mathrm{kin}}(i,f,N)$. Thus there is a one to one correspondence between the kinetic energy of the finally ionized electron and the spatial orbital it initially originates from. For a given frequency of the laser field, the ionization from the highest occupied orbitals achieves the highest values of kinetic energy.

In the scope of this work, a process of single ionization *of an atom* is called *elastic* for the other constituents of the residual ion, if they can be treated as passive, in the sense that they do not gain or loose energy. In contrast a process that deposits more energy in the ion than necessary to create it from its parent by removal of a specific electron is called *inelastic*. In *elastic* single ionization of atoms the finally bound electrons are occupying orbitals of the same quantum numbers as in the initial atom, while in *inelastic* processes at least one of the electrons undergoes a transition to a different, previously unoccupied spatial orbital. In this terminology *elastic* atomic single ionization corresponds to a single active electron process, where all other electrons are spectators.

In the theoretical models used in this thesis, in each step of the processes discussed, there will be one of the bound electrons which is active in the sense that it undergoes a transition as a result of energy exchange with the laser field or due to interaction with an unbound scattering electron. In this sense the other electrons are inactive. Due to electronic correlation it is possible though that their states adapt slightly once an electron leaves the bound system. In the context of single active electron theories the correlation with the remaining electrons can be expressed in terms of the one-electron state

$$\begin{aligned} |\,\phi_i(\boldsymbol{r}_1)\,\rangle &= \langle\,\Phi_f(\mathbf{r}_2,\ldots,\mathbf{r}_N)\,|\,\Phi_i(\mathbf{r}_1,\mathbf{r}_2,\ldots,\mathbf{r}_N)\,\rangle \\ &= |\,\phi_i'(\boldsymbol{r}_1)\,\rangle\langle\,\Phi_f(\mathbf{r}_2,\ldots,\mathbf{r}_N)\,|\,\Phi_i'(\mathbf{r}_2,\ldots,\mathbf{r}_N)\,\rangle\;, \end{aligned} \tag{2.3}$$

where

$$|\,\Phi_i(\mathbf{r}_1,\mathbf{r}_2,\ldots,\mathbf{r}_N)\,\rangle = |\,\phi_i'(\boldsymbol{r}_1)\,\rangle\;|\,\Phi_i'(\mathbf{r}_2,\ldots,\mathbf{r}_N)\,\rangle \tag{2.4}$$

is the initial state of the bound N-electron system and $|\Phi_f(\mathbf{r}_2,\ldots,\mathbf{r}_N)\,\rangle$ is the final state of the ionized bound $N-1$ electron system. This one-electron state is known as *Dyson orbital*, *Feynman-Dyson amplitude* or *generalized overlap amplitude* [48–50]. It comprises the electronic correlation between the initial and final state of the bound multielectron system and thus allows to represent the multielectron system by an effective one electron state. If the single active electron ansatz is valid for the given physical process, the overlap matrix element just contributes a constant factor. In cases where electronic correlation is found to be of minor effect in quantum chemical calculations, i.e. when the overlap matrix element of the passive electrons is close to one, the active electron can be described just by the spatial orbital $|\phi_i(\boldsymbol{r}_1)\,\rangle$

it occupied at the moment of transition. This is usually a good approximation for outer valence electrons [51]. Relaxation processes, e.g. fluorescence, are considered as subsequent quantum mechanical transitions.

Selecting an interval of values for the measurement of the kinetic energy of the ionized electrons determines which channels of ionization are possible for *elastic* single ionization, i.e. which initially occupied spatial orbitals have to be considered as active in a N-photon absorption to achieve a certain value for the kinetic energy of the ionized electron. Since the kinetic energy is positively definite, the ionization channels to final states with $E_T(i,f) > N\hbar\omega - U_p$ are closed for an effective N-photon absorption. Consequently all spatial orbitals that are energetically more than $N\hbar\omega - U_p$ below the single ionization continuum are inactive for N-photon absorption processes. The minimal number of photons needed to achieve single ionization is determined as

$$N_0 = \left\lceil \frac{I_p + U_p}{\hbar\omega} \right\rceil \ , \tag{2.5}$$

where I_p is the first ionization potential.

2.1.2. Tunneling Ionization

Tunneling Ionization makes use of a quasistatic consideration of the effect of the electrical component of the laser field. Keldysh [45] established a criterion for atomic systems that is widely understood as distinguishing the domain of validity for this mechanism. Conceptually it is a criterion, that determines the temporal conditions on the laser field that allow *Tunneling Ionization* to occur. Thus, actually it only establishes the limits of applicability of the tunneling model. It can be derived from quasiclassical considerations [52].

According to the *virial theorem* the mean kinetic energy of the bound electron in a Coulomb field is half of its mean potential energy, $2\langle T_e\rangle = I_p$. In the quasistatic picture of the effect of the laser field on the bound system, the Coulombic $1/r$ potential is bent down by the electric field component of the laser (see Fig. 2.1). A potential barrier of finite width of the order of $I_p/(eE_0)$ $\left(\text{more precisely } 2\sqrt{I_p^2/(eE_0)^2 - 1/E_0}\right)$ is formed, where I_p is the ionization potential of the atom, E_0 is the electric field strength and e is the absolute value of the electron charge ($q = -e = -1$ in atomic units, see section A). The time to tunnel through the potential barrier can be estimated by the time to traverse it:

$$\tau_t = \frac{\sqrt{2m_e I_p}}{eE_0} \ . \tag{2.6}$$

For tunneling this time has to be much smaller than the half-period of the laser field and thus

$$\frac{\pi}{\omega} \gg \tau_t \Rightarrow \gamma \equiv \sqrt{\frac{I_p}{2U_p}} \ll 1 \ . \tag{2.7}$$

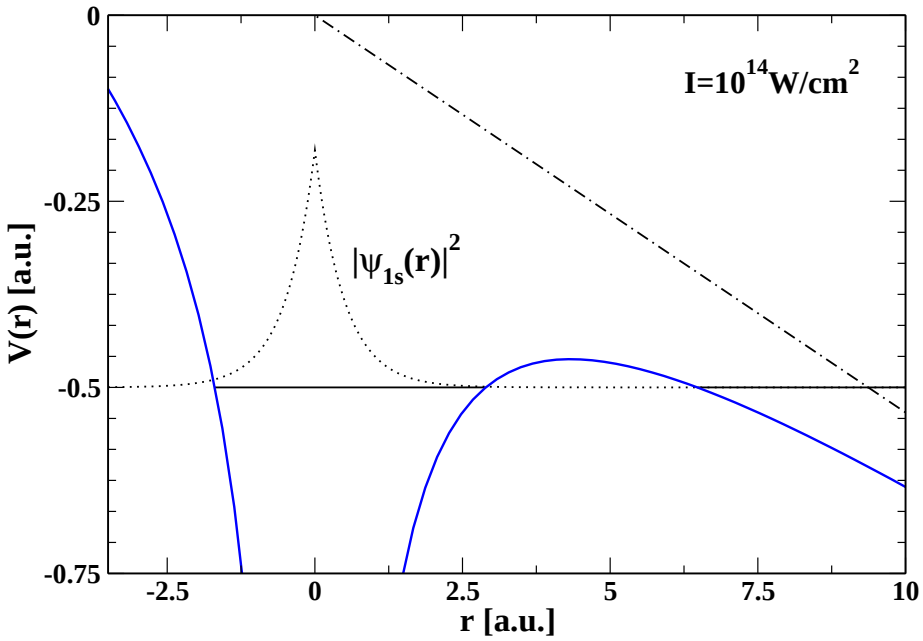

Figure 2.1.: Energy diagram of *Tunneling Ionization* of an hydrogen atom in a laser field of intensity $I = 10^{14}\,\mathrm{W/cm^2}$. For a 1064 nm Nd:YAG laser the Keldysh parameter is $\gamma \approx 0.85$, for a 10.64 μm CO_2 laser $\gamma \approx 0.085$.

This condition on the Keldysh parameter γ defines a relation between the intensity and the frequency of the laser field, that depends parametrically on the ionization potential. Thus, the condition for tunneling ionization can also be read again in terms of the virial theorem as $\langle T_e \rangle \ll U_p$. As will be shown, in the theory of intense-field Multiphoton Ionization the ponderomotive energy also increases the transition energy that is necessary for the electron to go over into a continuum state. For this reason it is also frequently referred to as the *ponderomotive potential*. It can be interpreted as the effective potential of the field dressed continuum states above field free continuum. Thus the tunneling condition can be read as stating that, for tunneling to the field dressed continuum to occur, this additional potential must be large on the scale of the average kinetic energy of the bound electron.

In the tunneling domain, a quasiclassical approximation for the single ionization rate of atoms in static electric fields that are much weaker than the intra-atomic field strength has been given by Landau and Lifshits [53]. Ionization in a monochromatic oscillating field has first been treated by Keldysh [45], considering the field-dressed continuum states but neglecting the Coulomb interaction of the ionized electron with the parent ion. Perelomov, Popov and Terent'ev [54–56] considered this correlation in the final state more accurately, averaging the static field expression over a cycle of a laser pulse of arbitrary polarization. Their formula holds under the adiabaticity condition of Keldysh. Subsequently it was extended by Ammosov, Delone and

Krainov ([57], see also [58]) to atoms and atomic ions of higher nuclear charge that can be in arbitrary electronic states. It is commonly referred to as *ADK-theory*:

$$\Gamma = C^2_{n^*l^*} f_{l,m} \left(\frac{2F_0}{E_0}\right)^{2n^*-|m|-1} A(E_0,\omega,\epsilon)\, I_p \exp\left(-\frac{2}{3}\frac{F_0}{E_0}\right) , \tag{2.8}$$

where E_0 is the field strength of the electrical field, $F_0 = (\sqrt{2I_p})^3$ is the atomic field strength and $n^* = Z/\sqrt{2I_p}$ is the effective principal quantum number of a Coulombic system of charge state Z. The coefficients $C_{n^*l^*}$ are usually determined from a fit of a wavefunction from numerical quantum chemical calculations to the asymptotic behavior of a bound Coulomb state. The angular momentum is taken into account by the factor

$$f_{l,m} = \frac{(2l+1)(l+|m|)!}{2^{|m|}(|m|)!(l-|m|)!} , \tag{2.9}$$

where l and m are the angular momentum and magnetic quantum numbers of the ionizing electron respectively. The third factor in Eq. (2.8), which was improved by Perelomov, Popov and Terent'ev as compared to the original derivation of Keldysh, approximatively takes into account the Coulomb interaction of the atomic ion with the ionized electron. The factor $A(E_0,\omega,\epsilon)$ enters from the averaging over one period of the oscillating field:

$$A(E_0,\omega,\epsilon) = \left[\frac{\epsilon(1+\epsilon)}{2}\right]^{-\frac{1}{2}} a\left(\frac{1-\epsilon}{3\epsilon}\frac{F_0}{E_0}\right) , \tag{2.10}$$

$$a(x) = e^{-x} I_0(x) , \tag{2.11}$$

where $0 \leq \epsilon \leq 1$ is the ellipticity of the laser and $I_0(x)$ is the Bessel function of imaginary argument. Thus, for circular polarization the cycle averaged rate is identical to the rate in a static field. For linear polarization this factor reduces to $\sqrt{\frac{3}{\pi}E_0/F_0}$.

The process can be understood as the transmission of the tail of the bound wavefunction through the potential barrier, where it is attenuated exponentially as it lacks the classically required energy to pass it. The electron is promoted to the continuum with zero momentum at a distance of about $2I_p/E_0$ (in a.u.) from the parent ion. Based on this picture, the "simple man's theory" [59, 60] explains the width of the ATI spectrum of the directly ionized electrons. This is obtained by calculating the maximal amount of cycle averaged kinetic energy that an electron can gain from the oscillating electric field $E(t) = E_0 \sin(\omega t + \phi_0)$:

$$\langle E_{\text{kin}} \rangle = U_p + (\sqrt{2U_p}\cos(\omega t_0 + \phi_0) + \sqrt{m_e} 2v_0)^2 . \tag{2.12}$$

Assuming that the electron enters continuum with zero velocity v_0, it may gain up to $2\,U_p$ from the field as drift energy additionally to the basic quiver energy U_p.

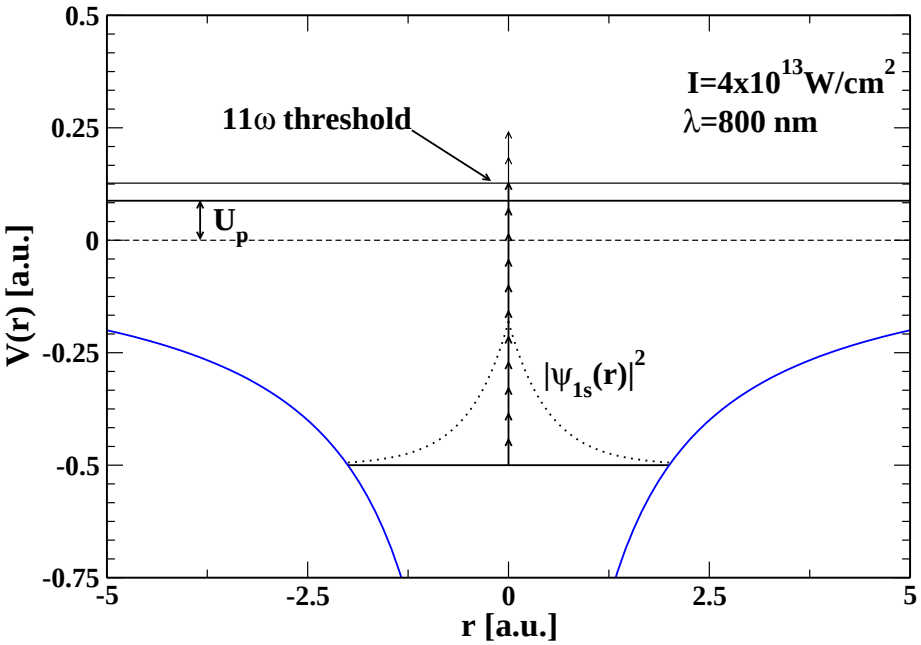

Figure 2.2.: Energy diagram of intense-field *Multiphoton Ionization* of an hydrogen atom in a 800 nm field of a Ti:Sapphire laser of intensity $I = 4 \times 10^{13}\,\mathrm{W/cm^2}$. The Keldysh parameter for this setting is $\gamma \approx 1.8$.

Please note, that the ADK rate for single ionization is independent of the wavelength of the laser field. This is a signature of the quasistatic nature of its derivation. While neglected, the quantized nature of energy transfer from the field is valid also in the tunneling domain and thus signatures of a quantized multiphoton absorption should also be detectable. Recently evidence for such signatures was found experimentally [61, 62] that could partly be explained from the theory of intense-field Multiphoton Ionization [63, 64].

If finally the peak electrical field strength of the laser field gets large enough to suppress the Coulomb barrier for the upper bound states to or below their binding energy (*barrier suppression ionization* [65]), the dynamics of the system will be dominated by the interaction with the electrical field. The ADK formula has been modified to take into account these repeated barrier suppressions during the laser cycle ([66], for a recent review see [67]). In a linearly polarized laser field it is possible though, that the interaction with the parent ion becomes important again when the electron passes by close enough in a subsequent reversal of the field direction (see section 2.1.4).

2.1.3. Intense-Field Multiphoton Ionization

Historically the theory of *Multiphoton Ionization* (MPI) originates from perturbative theoretical considerations [2, 3]. In this approach, the intensity is limited to be small enough as to not significantly disturb the structure of the initially bound system. Today this is frequently referred to as *perturbative MPI* in contrast to the non-perturbative MPI-theories of the type of the Keldysh-Faisal-Reiss (KFR) [45–47] and the Intense-Field Many-Body S-Matrix Theory (IMST) [23, 24] described below. The theory of *Multiphoton Ionization* takes into account the quantized transfer of energy from the field to the electron. From the lowest order perturbation theory (LOPT) of nonresonant multiphoton ionization the ionization rate is found to follow a power law dependence on the laser intensity ([68], Section 2.6):

$$\Gamma_{fi}^{(N)} = \sigma_{fi}^{(N)} I^N \ , \tag{2.13}$$

where $\sigma_{fi}^{(N)}$ is the generalized cross section for N-photon ionization depending on the transition matrix element between initial and final stationary quantum states and on the photon frequency. The intensity I is measured in atomic units (see section A), i.e. is smaller than unity in the domain considered. In the interpretations of the ATI experiments [69, 70] this dependence was found to hold also for above the threshold photon number N_0

$$\Gamma_{fi}^{(N_0+M)} = \sigma_{fi}^{(N_0+M)} I^{(N_0+M)} \ . \tag{2.14}$$

Gontier and Trahin [69] argued that the limited interaction time of the atoms passing through the focus of the laser does not allow the interpretation of the ATI peaks as a result of a two-step process, where in the first step the electrons are ionized to continuum at threshold and subsequently gain energy by the initially proposed mechanism of *Inverse Bremsstrahlung* Eq. (2.1). They concluded that the ATI process must be seen as an elementary act of simultaneous absorption of $N = N_0 + M$ photons.

In the experimental ATI spectra it was found that with increasing intensity the lowest order ATI peaks were disappearing [39]. Theoretically this observation was attributed to a closing of the transition channel to the low energy continuum states corresponding to the threshold or lowest order ATI peak. It could be explained by the AC Stark shift of the continuum states by the ponderomotive energy U_p [71]. Thus also the higher-energetic electrons enter continuum with a kinetic energy that is reduced by the amount of U_p, but they gain this energy again upon leaving the focus of the laser field on the way to the field free area of detection [72].

While the perturbative foundation of the theory of *Multiphoton Ionization* is limited to low intensities, the general non-perturbative quantum mechanical treatment of the process is established in the KFR theory [45–47]. In this, the interaction between the laser and the bound system is treated as a scattering process, where the coupling between the electron and the laser has the role of the interaction potential. Consequently its rigorous theoretical foundations lie in the S-matrix theory of potential scattering [73]. The KFR-model has successfully been extended to scattering

processes of second and higher order resulting in the framework of the Intense-Field Many-Body S-Matrix Theory (IMST) [23, 24]. The theoretical foundations will be reviewed and extended in detail in section 3.3.

In contrast to ionization processes involving only a single photon, in intense-field *Multiphoton Ionization* for each initially occupied spatial orbital of the atom there is a discrete band of possible values for the kinetic energy of the finally ionized electron, corresponding to an increasing number of absorbed photons or a rising photon order. This also means that ionization is possible from *every* initially occupied spatial orbital. The ionization from the highest occupied orbitals is achievable with the lowest photon order. Since the ionization rate drops with increasing photon order, ionization of electrons from the highest occupied orbitals contributes most to the ionization signal, if no intermediate resonances are involved.

2.1.4. Recollision

Once an electron is ionized from the bound Coulombic system it may return to the parent ion again as a result of the reversal of the field direction. In this case, the process of *recollision* [74] can occur. The electron can scatter

- *elastically* (i.e. without change in the internal state of the parent ion)
- *inelastically* (excitation or ionization of the parent ion, discussed in section 2.2)

or it can recombine (generating high harmonics of the base photon frequency). In a semiclassical picture the electron scatters *elastically* with the parent ion and simultaneously absorbs additional photons from the laser field in a process of *Inverse Bremsstrahlung* (see Eq. (2.1)). This mechanism was successfully applied to provide an explanation for the extension of the ATI spectrum beyond the semi-classically achievable limit of $2\,U_p$ (Eq. (2.12)). By this *three step mechanism* the experimentally determined extension [75] of the kinetic energy spectrum in a plateau up to $10\,U_p$ can be obtained. Alternatively to the "classical rescattering" model [76], this process can also be described fully quantum mechanically in the framework of the Intense-Field Many-Body S-Matrix Theory (IMST) [25, 26] as a second order process, Coulomb-correlating the field dressed electron, that is multiphoton-ionized in the first interaction, with the residual ion in the second interaction.

2.2. Double and Multiple Ionization

Processes of multiple ionization were first explained as a successive removal of the outermost electrons during the rising edge of the laser pulse. Within this concept of sequential ionization the occurrence of charge states of atoms and their saturation intensities could be predicted [77]. With the collection of more experimental data over a larger dynamical range of the ion yields, deviations of several orders of magnitude

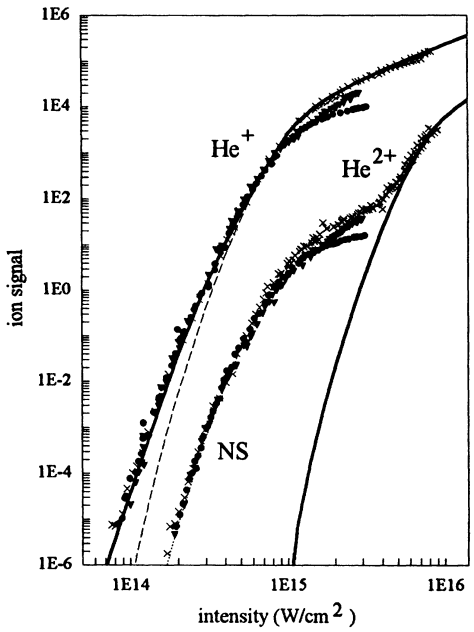

Figure 2.3.: Double logarithmic plot of the ion yields of single (He^+) and double (He^{2+}) ionization (from [79]). In the nonsequential domain (NS) the experimental results deviate by up to six orders of magnitude from the theoretical predictions for sequential double ionization. At intensities above the saturation intensity the ionization signal scales as $I_0^{3/2}$ due to the scaling law of the Gaussian focal volume [81, 82].

were found, compared to the predicted rates for sequential double ionization [78, 79]. The canonical object of research for this process is the Helium atom, but experiments were also performed on other noble gases [79, 80], which also allow the analysis of even higher degrees of ionization. In these experiments for multiple ionization a strong increase of the ionization yield was found below certain intensities. Because of its characteristic visual appearance in double logarithmic plots this change in slope is widely referred to as the "knee" structure (see Fig. 2.3) of *Nonsequential Double Ionization* (NSDI).

The increased ionization yields can be explained by a nonsequential process, where the emission of the second electron is facilitated by the Coulomb correlation with the first one. This correlation can become significant at different stages of the ionization process of the first electron and accordingly different mechanisms of nonsequential multiple ionization have been proposed (for reviews see [83, 84]).

The first correlated mechanism of double ionization is the so called *On the way out* or *Two-Step-One* (TS1) process which is known from single-photon double ionization [85, 86]. In this process, the coupling of the laser field to the electrons drives a first active electron in such a way that in leaving the binding potential of the parent

ion it scatters with another electron and transfers enough energy to this electron to leave the binding potential as well. This process is likely to involve two electrons of the same spatial orbital to minimize the average distance between the scattering partners. As a characteristic feature of this process, for increasing kinetic energy of the first electron, the two ionized electrons are likely to leave the parent ion in the same direction. In the case of linear polarization this direction is along the polarization axis of the laser. Both electrons will also leave the ion in the same laser half-cycle.

Another highly correlated mechanism has been proposed [87, 88] by the name of *Collective Tunneling*. According to this mechanism, two electrons tunnel through the potential barrier in the same half-cycle of the laser pulse. Though similar to the result of *On the way out* mechanism with respect to the timing of the electron release and the correlation of electron momenta, its understanding of electron-electron correlation is very different. For this model to work, the two electrons must form a collective tunneling mode, where they jointly move away from the nucleus, mutually screening its attractive potential. Thus this model suffers two weaknesses, first missing an explanation for the origin of this highly correlated motion, and second the instability of this state. If some evidence for this mechanism can be found, it would work despite the repulsive nature of the Coulomb correlation of the two electrons and not because of it.

Similarly the mechanism of electron *Shake-Off* [78] is not explicitly taking into account the dynamical Coulomb correlation between the two ionizing electrons, but merely the collective correlation of the first electron with all other charged particles of the system in its initial state. The basic idea of this mechanism is the fact that the eigenfunctions of the bound Coulombic system change when one of the electrons is ionized. During the act of single ionization of the first electron, the remaining bound electrons, occupying the eigenfunctions of the neutral Coulombic system, are projected with a certain probability onto unbound continuum eigenfunctions of the singly ionized system. As a result another electron might suddenly be transferred into a continuum state. For this process to occur it is essential that the first electron leaves the system so quickly that an adiabatic transition of the remaining electrons is not possible. It is deemed that the highest occupied spatial orbitals have the largest overlap with the new continuum states. In this process the kinetic energy of the two ionized electrons is distributed very asymmetrically. The active electron is fast, while the passively ionized electron has a low kinetic energy. While this mechanism is dominant for the single photon double ionization by synchrotron radiation for large photon energies [86], it has been shown that this mechanism is of minor efficiency in the strong field regime of laser ionization [32]. Recently it has been shown [26, 89] that the same holds for the analog process of *Shakeup*, where the second electron is transferred to an excited state during single ionization.

If the first electron leaves the ion in an act of single ionization, in strong fields it can also induce the process of *Ionization by Inelastic Recollision* [74, 90], in which it

transfers enough energy to another bound electron for it to leave the singly charged ion as well. The first idea of this process was dubbed *Antenna mechanism*, where the electron that is ionized first absorbs enough energy from the laser field to distribute it among other electrons to leave the Coulombic binding potential too [91, 92], but it failed to allow quantitative predictions for the time delay and the return energy. In its final step this process is similar to a regular $(e, 2e)$ scattering process (see section 5). In contrast to the *On the way out* mechanism, there is a time delay of the order of 2/3 of the laser cycle between the production of the singly charged ion and the doubly charged state. This delay is on the time scale of molecular vibrations and thus may result in measurable effects in molecular double ionization to distinguish the *On the way out* mechanism from the process of *inelastic Recollision*. The unique feature that distinguishes the *Recollision* mechanism from all other mechanisms of double ionization, is the strong dependence on the linear polarization of the laser field. This is necessary for the projectile electron to return to the parent ion again with high enough probability. While the wavepacket of the ionized electron spreads with time, its overlap with the parent ion at the times of return decreases rapidly with increasing ellipticity of the polarization. This dependence of the yield for double ionization on the polarization of the laser field is confirmed experimentally [93, 94].

The framework of the Intense-Field Many-Body S-Matrix Theory (IMST) [25, 26], described in section 3.3, provides a complete quantum mechanical treatment of the double ionization and comprises these four (as well as other) mechanisms in the first two orders of the S-matrix expansion. This is in contrast to the "classical rescattering" [74, 76], that models the field propagation of the electron classically and specifically does not take into account the *On the way out* mechanism. It is shown within this theory that the Feynman diagram in Fig. 2.4, represents the leading contributions. It represents in which order the coupling to the laser field and the interelectron correlation is considered. At the initial time t_i both electrons (represented by the two solid upward lines) in the He atom are correlated by their Coulomb interaction, visualized by the dashed line. Then, at some later time t_1, one of the two electrons is activated by the direct interaction with the laser field, absorbing enough photons to overcome the ionization barrier, which is increased beyond the field free ionization potential by the ponderomotive energy that is required by the electron to enter the laser dressed continuum. Following the time axis of the diagram the two fermionic parts of the physical system are then evolving separately, the ionized electron driven by the field as a wavepacket ($\{\boldsymbol{k}\}$) of Gordon-Volkov states and the bound electron continuing to be dominated by the binding potential of the cation. At time t_2 the Coulomb interaction between the two electrons becomes significant again, represented by the connecting line labeled as V_C. At the final time t_f we are interested in the case where both electrons are unbound, moving with the drift momenta $\mathbf{k}_a$ and $\mathbf{k}_b$. The energy consumption of the process is balanced by the reduction of photons in the laser field.

Finally to complete the possible channels of *inelastic Recollision*, the mechanism

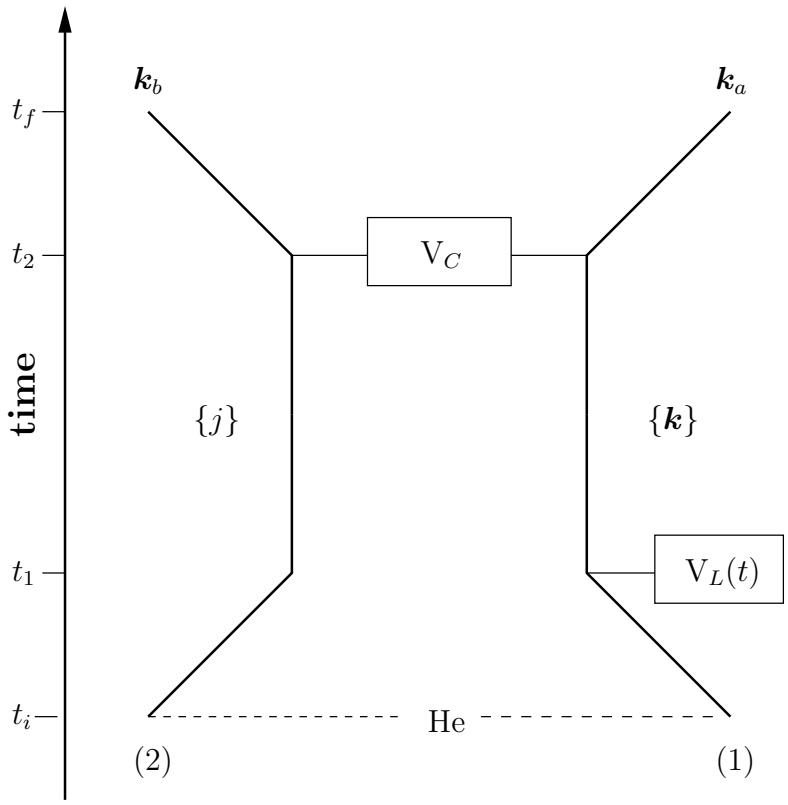

Figure 2.4.: Feynman diagram of the second order process that gives the dominant contribution to *Nonsequential Double Ionization* (NSDI) in infrared laser fields.

of *Recollision Excitation with Subsequent field Ionization* (RESI) [95] has been found to be important in the double ionization of He and Ar [96–98]. This process can be thought of to proceed in four steps, the first two, single ionization and field driven propagation of the electron, being common to all ATI processes. In contrast to *Ionization by Inelastic Recollision* in the third step a bound electron is not transferred directly to a continuum state but to an excited bound state, from which it is field-ionized with increased probability in the final step. Frequently this second, uncorrelated, sequential ionization process is modeled as a tunneling process, but this is not mandatory. In the framework of the Intense-Field Many-Body S-Matrix Theory (IMST), the process would be described as a third order process.

2.3. Molecular Ionization

Compared to atoms, molecules offer additional degrees of freedom. Without loss of generality the discussion below focuses on diatomic molecules first. For these one has as additional parameters first the internuclear distance and second the angle of

alignment of the molecular axis with respect to the direction of polarization of the laser. For heteronuclear molecules the term *orientation* is used instead, since in this case the molecules are not symmetric with respect to inversion about the center of mass (they represent the point group $C_{\infty,\nu}$ and not $D_{\infty,h}$ as in the case of homonuclear diatomics). Thus, one can attribute a directedness to a heteronuclear molecule. Since the polarization of the laser breaks the isotropy of space, the physical situation is distinguishably different if the direction of the heteronuclear molecule is reversed in the presence of the laser field. Furthermore there are two additional *dynamic* degrees of freedom: The first is the vibrational state of the molecule and the second is its rotational state.

When dealing with electronic transitions in molecules, the internuclear distances and orientations are usually treated as fixed during the process, since, according to the Born-Oppenheimer approximation [99], the electronic transition is much faster, evolving on an attosecond time scale ($1\,\mathrm{as} = 10^{-18}\,\mathrm{s}$) [18], than the motion of the nuclei. The vibrational motion occurs on a scale of femtoseconds ($10^{-15}\,\mathrm{s}$) and periods of rotation are typically on a scale of picoseconds ($10^{-12}\,\mathrm{s}$). Accordingly in ionization processes the molecule and its ion are usually taken to have a rigid structure of nuclei at fixed equilibrium distances.

From this rigid molecular model one can already anticipate new effects in processes of single ionization when comparing diatomic molecules to atoms. In the S-matrix analysis it has been shown that the symmetry property *gerade* or *ungerade* of the wavefunction of the ionizing electron causes constructive or destructive interference effects in the outgoing wavefunction of the ionized electron [34, 36, 100]. This analysis was able to explain the experimental observation, that, for the case of molecular oxygen, the ionization yields are suppressed [101, 102, 35] as compared to the ionization signal from Xe atoms, having an ionization potential of comparable magnitude [34]. The ionization rate also shows an alignment dependence with respect to angle of the internuclear axis to the polarization of the laser field [103, 37]. The alignment has been shown to be controllable [104, 105] by interaction of the induced dipole moment with an intense laser pulse of nanosecond duration [106, 107].

The variation of the internuclear distance itself brings up several interesting effects, such as vibrational suppression of ionization [108], *bond softening* [109–112] and the related effect of *bond hardening* [113, 114] as well as *enhanced ionization* [115, 116, 112] of molecules and their ions for stretched internuclear separations in the process of ionization. Vibrational motion can partially explain the suppressed ionization rates for D_2 that are detected experimentally [117] despite its *gerade* ground state symmetry. The latter two effects are well understood in terms of adiabatic field dressed states ([109], see section 3) and both have slightly different mechanisms for molecules with an even number of electrons (e.g. neutral H_2) on one hand and molecules with an odd number of electrons (e.g. the H_2^+ cation) on the other hand. For odd-electronic molecular configurations the first excited electronic state is coupled to the ground state by the oscillating electrical field component of the laser field.

For even-electronic configurations this coupling was shown to be spin-forbidden, but Saenz [112] showed for the case of H_2 that a higher lying state of ionic character is coupled to the ground state of the neutral molecule. This coupling is interpreted in terms of the creation of adiabatic field dressed states, that avoid to cross each other if they have the same symmetry. Treated on the basis of the field free potential curves of the molecule, the adiabatic field dressed potential curves are diabatic mixtures of the field free potential curves shifted by multiples of the photon energy. Compared to the field free case, the potential wells of the adiabatic field dressed states are less deep and thus support less vibrational states for the nuclear motion. The dissociation barrier of the states is lowered with respect to the field free molecule and thus the bond is softened. In dissociation experiments with intense lasers, fragments of molecular dissociation are found at very low energies, on the order of the quanta of vibrational motion [110]. The first evidence of the theoretically predicted effect of *bond softening* was found with molecules in a static electric field [118].

This coupling of states by the photon field also effects the ionization dynamics of molecules. The effect of *enhanced ionization* is complementary to the effect of *bond softening*, but it is based on the same theoretical analysis. Instead of following the adiabatic potential curves in the field, in the regions of avoided crossing the electrons can make diabatic transitions from the adiabatic ground state to the excited state. These diabatic transitions are favored the quicker the potentials change that act on the electrons, i.e. as either the speed of nuclear motion increases or the rise time of the electric field component of the laser decreases ([112] and references therein). Once the electronic wavefunction gained a considerable admixture of the excited state, its ionization potential is reduced and thus ionization rates can rise at the internuclear distances that correspond to regions of avoided crossings. Based on the ideas of Codling and Frasinski [119], that explained the production of asymmetric charge states in multiphoton multiple ionization processes of di- and triatomic molecules, the mechanism of *charge resonant enhanced ionization* (CREI) was first predicted by Zuo and Bandrauk [116] for the H_2^+ cation. The existence of critical internuclear distances, where ionization is enhanced, were recently confirmed in a pump-probe experiment with H_2 and D_2 [120]. First evidence for *enhanced ionization* of neutral H_2 was found in time dependent numerical calculations [121], and could be explained along the same lines as *bond softening* discussed above by Saenz [122]. A similar mechanism may be suspected to contribute to the puzzling non-suppression [34, 123, 124] of the single ionization signal of molecular fluorine (F_2, [125]) because this species is known to exhibit strong correlation between the electrons.

Quite early it was argued [109] that in an intense laser field these diabatic effects, that occur at certain ranges of the internuclear distance R, invalidate the ansatz of Condon, which is based on the overlap of stationary quantum states. Additionally in the quasistatic theoretical model of tunneling ionization, the quantum mechanical concept of stationary states with quantized, fixed energies is not applicable.

Quantum mechanically the atomic constituents of the molecule constantly move

around their equilibrium positions. Without loss of generality, the following discussion starts with diatomic molecules. The motion of each atomic nucleus is confined by the potential well $V(R)$ that is build up by the superposition of the mean attractive Coulomb field of the electrons and the Coulomb field of the other nuclei which is repelling them from each other. The possible states of vibration in this binding potential are quantized. If an electron is removed from the molecular system, the internuclear potential changes. The internuclear equilibrium distance relaxes to a value that usually differs from the equilibrium distance of the parent molecule. If this electron occupied an orbital of bonding symmetry, the position of the minimum of the potential well is shifted to a higher internuclear distance in the ion. If on the other hand the ionization frees a formerly occupied orbital of antibonding symmetry, the minimum shifts to a lower internuclear distance as the bond weakening charge distribution is removed. Thus the ionization of an electron from a molecule initiates a change of the internuclear motion. If the molecule initially was in one specific vibrational eigenstate, the molecular ion is put into a coherent superposition of vibrational eigenstates of the new bonding potential. While the expectation value for the internuclear distance $\langle R \rangle(t) = \langle\, \Psi(R,t)|R|\Psi(R,t) \,\rangle$ is a stationary quantity for a pure eigenstate, it changes periodically with time in the molecular ion. This coherent superposition of vibrational eigenstates forms a *wavepacket* that moves periodically along the R-axis as time evolves.

In double ionization of bi-electronic molecules like H_2 and isotopic variants, this moving wavepacket can be mapped by the kinetic energy of the ionic fragments if they dissociate after the ionization of the second electron [126–128]. This kind of dissociation is traditionally referred to as *Coulomb explosion* [129]. Since the internuclear potential $V(R)$ of the doubly ionized H_2 is strictly repulsive, there is a one to one correspondence of internuclear distance to the potential energy that is converted into kinetic energy. This correspondence is known as *reflection principle* [130–134]. The ionization of the first electron can be regarded as the start of a molecular clock [135], that can be read by measuring the kinetic energy of the molecular fragments as a function of the time delay between single and double ionization. If on the other hand this delay is unknown as in the usual case, information about it can be gained from the kinetic energy spectrum of the molecular fragments. Experimental techniques involving dissociation of the molecules and measurement of the *kinetic energy release* (KER) are also frequently applied to other diatomic molecules to reveal the binding energy of the highest excited electron following processes of excitation or ionization (see section 4.2).

In double ionization the alignment of the molecule plays a role as well for the ionization of the second electron. While the mechanism for this is nearly trivial for sequential ionization, for a nonsequential process it can be thought of as a scattering process of the first electron on a molecular ion that is aligned to its direction of propagation in a certain way. Analogous to the atomic case, the application of the Intense-Field Many-Body S-Matrix Theory (IMST) [25, 26], intrinsically con-

siders both processes, *On the way out* and *inelastic Recollision* coherently, and the orientation of the internuclear axis enters as an adiabatic parameter to the molecular wavefunction.

3. Overview of Theoretical Methods

In atomic and molecular physics it has become possible to calculate and measure certain quantities with very high precision. On the theoretical side much of this success was possible due to the clearly defined and known interaction laws and the limited extent of the physical system under consideration. The Coulomb interaction is governing the dynamics of the electrons, while e.g. the influence of gravitation of the molecular constituents is negligible. In contrast, research in nuclear structure or solid state physics, e.g., must cope with the lack of knowledge of the precise form of the many-body interaction of the nuclear or condensed matter constituents. Yet, the solution of the time dependent Schrödinger equation (TDSE) to a given Hamiltonian still is a nontrivial task. Specifically the Schrödinger equation for the single atom or molecule is still lacking general solutions for Coulombic systems with more than one electron. Moreover, for dynamic problems such as collisions or interactions of atoms and molecules with strong time-varying electromagnetic fields, even for systems with only one or a few electrons, such a high precision description of observables is not often achievable in calculations. A wide range of theoretical approaches have been and continue to be developed to obtain approximative solutions to given specific conditions of the problem. All techniques have their virtue for specific domains and often several are used independently to gather more insight into the problem at hand.

3.1. Time-dependent Methods

The techniques divide into two basic categories, which I call discrete (usually 'local') and continuous ones, distinguishing them by the nature of the time evolution applied [136]. Discrete techniques of approximation to the time dependent Schrödinger equation are evolving a given initial solution at one time to the next time step according to the differential equation. These techniques are frequently referred to as *TDSE methods* or *direct solution of the TDSE* [137, 138]. The initial solution is either taken from an analytical calculation or for consistency is converged on the same discrete grid according to a variational principle or by imaginary time propagation. Since the numerical TDSE evolution is computationally very demanding, not only the granularity of the grid but also its extent has to be limited. Several techniques for the compensation of artifacts originating from these truncations have been developed, such as boundary mask functions [139], complex absorbing potentials [140] and exterior complex scaling [141]. Additionally to these confinements, researchers frequently try to reduce the number of dimensions of the problem to the coordinates that undergo the essential dynamics of the process. For this reason and also to check

basic assumptions it is not uncommon to analyze one dimensional (1D) models, that only consider the motion of the Coulombic system along the direction of the electric field component of the laser (e.g. [142, 143]). On the other hand, due to the advance in processor speeds and computer memory, by now it has become possible to tackle the full dimensional TDSE equation numerically for the case of He [144, 145]. In the next section we will briefly discuss the current advancement of a different approach which reduces the full dimensional calculations to the degrees of freedom that are essential for the physical system at hand [146, 147].

All approximative techniques to the solution of the time dependent Schrödinger equation can be thought of as evolving the initial solution into an orthonormal set of known basis functions. The 'local' techniques choose the position or the dual momentum eigenfunctions to evolve the initial solution and necessarily must restrict their description also to a discrete set of the complete, continuous set of possible basis functions. Thus these techniques are finite-difference, finite-element methods that, apart from time, also discretize space into a grid of a certain granularity that is chosen small enough to cover the physical scale of the quantities involved, e.g. to hold the shortest de Broglie wavelength that occurs for the ionized electron. The approximative solution obtained by these methods is a discrete one. While analytically the description of the physical system is equivalently expressible in different bases, the limitations of numerical calculations impose losses of information, that may prohibit this mapping and make it important to choose physically relevant states as the basis of the numerical description. E.g. states that are not well localized in position or momentum space are not efficiently and accurately representable in these particular bases. There are also approaches to perform TDSE calculations in other basis spaces, e.g. on B-splines [148] or spherical harmonics [148].

3.1.1. Virtual NPSF Lab

While one dimensional TDSE calculations have been quite successful for situations of single-ionization, multi-electron dynamics does not seem to be accurately describable without giving the electrons the extra degree of freedom to repel each other while being driven by the field. To this end models that go beyond one dimensional approaches have recently been developed [146], and are now applied in the creation of an efficient software for the numerical simulation of virtual laser experiments. The technical concept of this approach is to create a library of software routines [149] that allow to calculate and propagate a discretized wavefunction according to a selectable Hamiltonian on a spatio-temporal grid, currently by using a Crank-Nicholson finite-difference iterative method [150]. Applying object oriented software engineering concepts [151], the code is designed in such a way that all physical characteristics of the system are flexibly adaptable. This allows virtual laser experiments with different physical systems such as the Helium atom [146] and small molecular systems like H_2 with a fixed internuclear radius [147] and H_2^+ with moving nuclei. The idea

was born out of the observation that several systems of current interest in atomic and molecular laser physics are governed by Hamiltonians of similar general structure. All systems covered so far are three- and four-body systems which can be reduced to an effective two-body problem due to the large mass of the nuclear centers. The dimensionality of the problem is further reduced by the observation that the laser only couples to the center of mass coordinate of two charged particles of identical charge-to-mass ratio. To use different pulse shapes, the carrier frequency of the laser can be modulated by different analytical or experimentally recorded pulse shapes. The temporal discretization of the propagation is obtained by a discretization of the field generated by the laser pulse with a variable time step suitable for the desired spectral resolution. To allow efficient simulation of pump-probe experiments, where the two pulses usually have very different spectral and temporal characteristics, two pulses can be superposed by analytic calculation of the combined laser pulse and ensuing discretization of the generated field at the highest resolution necessary at a given time. This concept of a separation of the laser object from the discretized field object decouples the Hamiltonian from the specifics of field generation. The Hamiltonian is only coupling to either the electric field $\mathbf{E}(t)$ or its vector potential $\mathbf{A}(t)$ at each instant of the simulation time depending on the choice of gauge. For a diatomic molecule with two electrons like H_2 or HD in the laser field the Hamiltonian can be written in the different gauges as:

$$\begin{aligned} H^{(LG)} =& \frac{1}{4}\mathbf{k}_{\mathrm{CM}}^2 + \mathbf{k}_{\mathrm{rel}}^2 + 2\mathbf{r}_{\mathrm{CM}}\mathbf{E}(t) + V_{\mathrm{coul}} \\ &+ \frac{1}{2M}\mathbf{P}_{\mathrm{CM}}^2 + \frac{1}{2\mu}\mathbf{P}_{\mathrm{rel}}^2 - (Z_A + Z_B)\mathbf{R}_{\mathrm{CM}}\mathbf{E}(t) - Z_{\mathrm{rel}}\mathbf{R}_{\mathrm{rel}}\mathbf{E}(t) \end{aligned} \tag{3.1}$$

$$\begin{aligned} H^{(VG)} =& \frac{1}{4}\left(\mathbf{k}_{\mathrm{CM}} + 2\frac{\mathbf{A}(t)}{c}\right)^2 + \mathbf{k}_{\mathrm{rel}}^2 + V_{\mathrm{coul}} \\ &+ \frac{1}{2M}\left(\mathbf{P}_{\mathrm{CM}} - (Z_A + Z_B)\frac{\mathbf{A}(t)}{c}\right)^2 + \frac{1}{2\mu}\left(\mathbf{P}_{\mathrm{rel}} - Z_{\mathrm{rel}}\frac{\mathbf{A}(t)}{c}\right)^2 , \end{aligned} \tag{3.2}$$

where M and μ denote the total and reduced masses of the molecule and

$$V_{\mathrm{coul}} = \frac{1}{r_{\mathrm{rel}}} + \frac{Z_A Z_B}{R_{\mathrm{rel}}} - \sum_{i=1}^{2}\sum_{j=A,B}\frac{Z_j}{|\mathbf{r}_i - \mathbf{R}_k|} . \tag{3.3}$$

The center of mass and relative momenta of the nuclei A and B are denoted as $\mathbf{P}_{\mathrm{CM}}$ and $\mathbf{P}_{\mathrm{rel}}$ respectively. The corresponding quantities for the electrons are referred to by the letter k. Note that $\mathbf{P}_{\mathrm{CM}}$ references the nuclear center of mass while $\mathbf{k}_{\mathrm{CM}}$ references the center of mass of the electrons. One recognizes that the field couples to the internuclear coordinate R_{rel} of the nuclei directly only through what may be referred to as the *relative charge*

$$Z_{\mathrm{rel}} \equiv \mu\left(\frac{Z_A}{m_A} - \frac{Z_B}{m_B}\right) \tag{3.4}$$

of the two nuclear centers with charge-to-mass ratios of Z_A/m_A and Z_B/m_B respectively. The name is appropriate due to the structural similarity to the expression for the relative momenta.

The splitting of the Hamiltonian into center of mass and relative momenta Eq. (3.2) directly leads to a new interpretation of the wavefunction of two electrons in the laser field [152]. Neglecting the Coulomb correlation between the two electrons one can write:

$$|\,\mathbf{k}_a^{\mathrm{GV}}(t)\,\rangle\otimes|\,\mathbf{k}_b^{\mathrm{GV}}(t)\,\rangle = |\,\mathbf{k}_{\mathrm{CM}}^{\mathrm{GV}}(t)\,\rangle\otimes|\,\mathbf{k}_{\mathrm{rel}}(t)\,\rangle\;, \tag{3.5}$$

where

$$|\,\mathbf{k}_{\mathrm{CM}}^{\mathrm{GV}}(t)\,\rangle \equiv |\,\mathbf{k}_{\mathrm{CM}}\,\rangle \exp\left[-i\int_{-\infty}^{t}\frac{1}{4}\left(\mathbf{k}_{\mathrm{CM}}+\frac{2}{c}\mathbf{A}(t)\right)^2\right] \tag{3.6}$$

is the velocity gauge Gordon-Volkov wavefunction of the *center of mass* of the two electrons. The momentum ket $|\,\mathbf{k}_{\mathrm{CM}}\,\rangle = \exp\left[i\mathbf{k}_{\mathrm{CM}}\cdot\mathbf{r}_{\mathrm{CM}}\right]$ is a plane wave in the center of mass coordinate corresponding to the drift momentum of the center of mass. Physically this separation of the two-electron Gordon-Volkov wavefunction Eq. (3.5) can be interpreted as the signature of two quasi-particles: It can be read as the decoupled product wavefunction of the *center of mass quasi-particle* (of mass 2 a.u.), and the *relative momentum quasi-particle* (of mass 0.5 a.u.). While the former is described by a Gordon-Volkov wavefunction as it couples to the field due to its charge of 2 a.u., the latter behaves as a plane wave $|\,\mathbf{k}_{\mathrm{rel}}\,\rangle$ in the relative coordinate, without electric charge and thus unaffected by the field. The Coulomb interaction of the two electrons only acts on the relative coordinate of the electrons, i.e. it only Coulomb-dresses the plane wave solution for the *relative momentum quasi-particle*. The exact wavefunction of the electron-pair state in the presence of a laser field [152] fully includes this correlation. Thus, the *relative momentum quasi-particle* captures all electron-electron interaction, including the fermionic substructure, while the *center of mass quasi-particle* is unaffected by the inner correlation of the electron-pair state.

To put this observation on a more general level, we may note, that the electron-pair state is a special case of a general charge-pair state of charge Z_{rel} and mass μ. If the charge-to-mass ratios of the two charges is equal, the *relative momentum substate* of the charge-pair state constitutes an uncharged quasi-particle, whose evolution is unaffected by a laser field. An example of a *relative charge-pair state* with nonzero *relative* or *inner charge* is found in the case of the nuclei of a heteronuclear diatomic molecule. Both quasi-particles are bosons, as one of them carries the total spin of the electron pair state, i.e. either a singlet of a triplet while the other one can be considered to be spinless for consistency. While the *relative momentum quasi-particle* captures the inter-Coulombic correlation of the *Coulomb-pair state*, it is reasonable to associate the total spin with the *center of mass Coulomb-pair state*. Thus the *relative Coulomb-pair state* is considered to be a spinless quasi-particle. It is interesting to

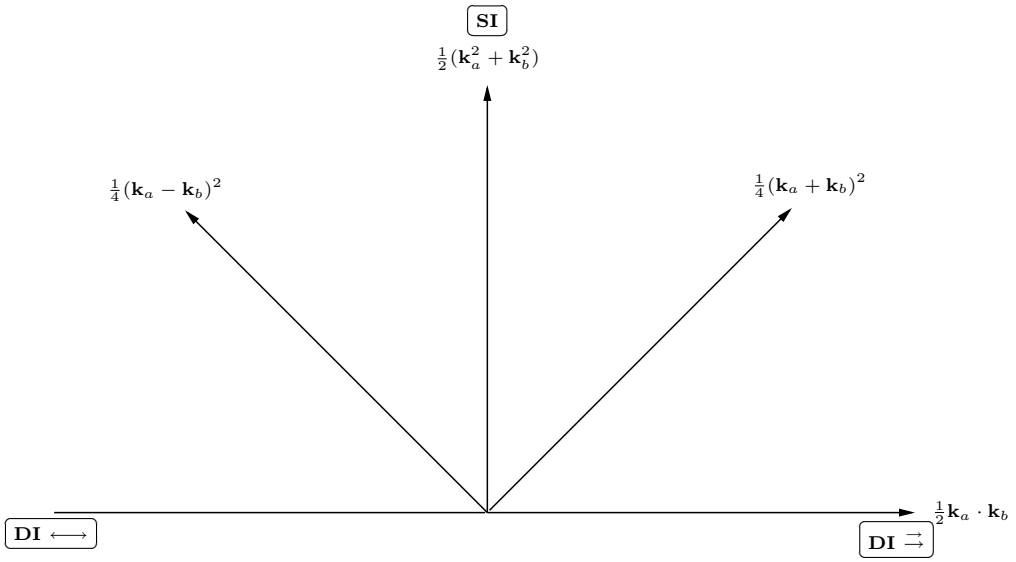

Figure 3.1.: Energy diagram for the two-electron state. Shown are the axis that allow interpretation as double ionization (DI) and single ionization (SI) respectively. The negative part of the DI-axis corresponds to a back-to-back emission, while the positive half-axis corresponds to emission into the same spatial hemisphere. The diagonals correspond to the center of mass and relative energies respectively.

note that the *center of mass Coulomb-pair state* carries the total momentum, while the *relative Coulomb-pair state* carries no momentum as is easily seen by applying the operator of momentum for the particle-pair system:

$$\begin{aligned} \hat{\mathbf{p}}_{12} \left| \mathbf{k}_{\mathrm{rel}} \right\rangle &\equiv \frac{1}{i} \left(\frac{d}{d\mathbf{r}_1} + \frac{d}{d\mathbf{r}_2} \right) \exp\left[i\mathbf{k}_{\mathrm{rel}} \cdot \mathbf{r}_{\mathrm{rel}} \right] \\ &= \frac{1}{i} \left(\frac{d}{d\mathbf{r}_1} + \frac{d}{d\mathbf{r}_2} \right) \exp\left[i\mathbf{k}_{\mathrm{rel}} \cdot (\mathbf{r}_1 - \mathbf{r}_2) \right] = 0 \, . \end{aligned} \tag{3.7}$$

To demonstrate that this interpretation is not devoid of use, we present in Fig. 3.1 an energy diagram for the two-electron state that is derived from it. These observations suggest that an analysis of experimental constellations in terms of *relative energy* and *center of mass energy* could provide an additional tool for the interpretation of physical processes that exhibit a dominant correlation between to charges in the final state. Recently there is experimental indication from kinematically complete *COLTRIMS* [153, 154] experiments that this figure of thought is useful for the interpretation of data from *Nonsequential Double Ionization* (NSDI) or electron impact ionization in a laser field [155]. We point though, that this picture is only asymptotically correct, as it neglects the Coulomb-correlation of the electron-pair with the residual scattering witness, i.e. the parent ion.

The project of the group *Nonlinear Processes in Strong Fields* (NPSF) at the Max

Planck Institute for the Physics of Complex Systems (MPIPKS) has been dubbed "*Virtual NPSF Lab*", as it allows the scientists to make virtual experiments based on a solid theoretical background, that are difficult or impossible to perform in an actual laser laboratory at this degree of parametrical flexibility. E.g. in this virtual laboratory it is easy to obtain predictions of what effect the replacement of one of the electrons by a muon in the system above would have in actual experiments with intense laser fields. Like S-matrix theory it enjoys the advantage of theoretical research, that is easily possible to switch off certain interactions at will to analyze their influence on an experimental observable. Two-dimensional projections of the state of the simulated wavefunction can be obtained at any desired temporal period, stored in native Matlab® [156] format to ease evaluation and visualization of the simulated physical experiment. Currently parallelization of the code is on the way, to make calculations on larger simulation grids feasible at a manageable CPU time. This is necessary to follow the extended quantum paths of the electrons driven by infrared laser fields as well as to more easily manage the number of time steps necessary for attosecond ionization experiments with IR streaking fields, that currently enjoy considerable interest [157].

3.2. Floquet Methods

The other class of techniques usually considers basis functions that are more adapted to the physical nature of the system and evolve the initial condition according to the differential equation restricted to these basis functions. While not as generally applicable as the *TDSE methods*, they offer the possibility to both provide and gain considerably more information about the physical nature of the system under consideration from the interpretation of numerical calculations. Frequently solutions of time independent Schrödinger equations of stationary configurations of the physical system are used as basis functions. If the potentials involved are time dependent, such as in the case of an electric charge in the laser field, the time dependent interaction can sometimes be transformed into the basis states of the description, as in the interaction picture formalism of quantum mechanics.

The computational problem of a continuous set of basis functions quickly enters also this type of approaches, if the discrete set of bound states interacts or couples considerably with the continuous part of the spectrum of eigenfunctions of the physical system. This certainly is the case for increasing strengths of perturbation. Thus it is of utmost importance to choose basis functions that are adapted to the dominant interaction(s). To this end one of the approaches most suitable for laser-atom interactions is the Floquet method [158], which transforms the time-dependent Schrödinger equation, corresponding to a periodic Hamiltonian of a Coulombic system interacting with a laser field, into a set of time-independent coupled equations. Each of these equations corresponds to a certain number of photons that were ab-

sorbed or emitted by the Coulombic system. If the laser field interacting with a molecule is treated classically, the general Hamiltonian can be written as a sum of terms of integer multiple frequency of the laser ([68], eq. (10.2.1.10), p. 247):

$$\begin{aligned} H(t) &= H_0 - \frac{q}{mc}\sum_{i=1}^{N_e}\mathbf{A}(\mathbf{r}_i,t)\cdot\mathbf{p}_i + \frac{q^2}{2mc^2}\sum_{i=1}^{N_e}A^2(\mathbf{r}_i,t) \\ &= H_0 + V^{(1)}(\mathbf{r})e^{-i(\omega t+\delta)} + V^{(-1)}(\mathbf{r})e^{i(\omega t+\delta)} \\ &\quad + V^{(0)} + V^{(2)}(\mathbf{r})e^{-i2(\omega t+\delta)} + V^{(-2)}(\mathbf{r})e^{i2(\omega t+\delta)} \\ &= H(t+T)\ , \end{aligned} \tag{3.8}$$

where $\mathbf{r} = (\mathbf{r}_1,\ldots,\mathbf{r}_{N_e})$ and $T = 2\pi/\omega$. The field is given by the vector potential

$$\mathbf{A}(\mathbf{r}_i,t) = \mathbf{A}_0\frac{1}{2}\sum_{\pm}e^{\pm i(\mathbf{k}\cdot\mathbf{r}_i-\omega t-\delta)} \tag{3.9}$$

of a classical multipole field and

$$\begin{aligned} V^{(\pm1)}(\mathbf{r}) &= -\frac{q}{2mc}\sum_{i=1}^{N_e}\mathbf{A}_0\cdot\mathbf{p}_i e^{\pm i\mathbf{k}\cdot\mathbf{r}_i} \\ V^{(0)} &= \frac{N_e q^2 A_0^2}{4mc^2} \\ V^{(\pm2)}(\mathbf{r}) &= \frac{q^2A_0^2}{8mc^2}\sum_{i=1}^{N_e}e^{\pm i2\mathbf{k}\cdot\mathbf{r}_i}\ . \end{aligned} \tag{3.10}$$

The solutions to the time dependent Schrödinger equation have the general form

$$\psi_\lambda(\mathbf{r},t) = \phi_\lambda(\mathbf{r},t)e^{-i\epsilon_\lambda t}\ , \tag{3.11}$$

where the periodicity of H is reflected in $\phi(\mathbf{r},t) = \phi(\mathbf{r},t+T)$. Thus these functions can be expanded as a Fourier series in overtones of ω

$$\phi_\lambda(\mathbf{r},t) = \sum_{n=-\infty}^{\infty}\phi_{n,\lambda}(\mathbf{r})e^{in(\omega t+\delta)} \tag{3.12}$$

and their spatial part is expanded in the basis of the eigenstates $|j\rangle$ of the field free Hamiltonian H_0 ($H_0|j\rangle = E_j|j\rangle$) to get a full expansion of the (unknown) state of the full Hamiltonian (Eq. (3.8)) in terms of functions with known and physically adapted behavior:

$$\psi_\lambda(\mathbf{r},t) = e^{-i\epsilon_\lambda t}\sum_{n=-\infty}^{\infty}\sum_{j=1}a_{j,n}(\epsilon_\lambda)|jn\rangle\ , \tag{3.13}$$

with the so called *field dressed* or *Floquet states*

$$|jn\rangle = |j\rangle e^{in(\omega t+\delta)} \; . \tag{3.14}$$

Inserting this expansion into the time dependent Schrödinger equation and matching terms of equal frequency, an infinite number of stationary Floquet equations is obtained that determine the expansion coefficients $a_{j,n}(\epsilon_\lambda)$ ([68], eq. (10.2.1.10))

$$(\epsilon_\lambda - \epsilon_{jn}) a_{j,n}(\epsilon_\lambda) = \sum_l \left(\sum_\pm V_{jl}^{(\pm 1)} a_{l,n\pm 1}(\epsilon_\lambda) + V_{jl}^{(\pm 2)} a_{l,n\pm 2}(\epsilon_\lambda) \right) \; , \tag{3.15}$$

where

$$\epsilon_{jn} = E_j + n\omega + V^{(0)} \tag{3.16}$$

denotes the quasi-energy of the *field dressed state* $|jn\rangle$, that is shifted from the field free energy E_j by the absorption or emission of n photons and the time averaged interaction energy of the field. $V_{jl}^{(\pm i)}(\mathbf{r}) = \langle\, j|V^{(\pm i)}(\mathbf{r})|l\,\rangle$ symbolize matrix elements.

The *Floquet states*

$$\psi_n^F(t) = |jn\rangle e^{-i\epsilon_{jn}t} \tag{3.17}$$

satisfy the stationary Floquet-Schrödinger equation

$$i\frac{\partial}{\partial t}\psi_n^F(t) = H_n^F \psi_n^F(t) \; , \tag{3.18}$$

where $H_n^F = H - i\frac{\partial}{\partial t}$.

The biggest disadvantage of the Floquet method is the large dimension of the Hilbert space that needs to be covered. Usually the spectrum of the states $|j\rangle$ is limited to the discrete bound states. Thus conventional Floquet theory is limited to bound-bound transitions and cannot describe transitions to continuum states, that are essential for ionization and dissociation processes. For the description of these processes one needs to extend the method to complex quasi-energies and non-Hermitian Hamiltonians (see [68, 158]).

3.3. Intense-Field Many-Body *S*-Matrix Theory

S-matrix theories analyze the transition amplitudes between known initial and final states of a quantum system under influence of a scattering potential V_i

$$H(t) = H_0 + V_i(t) \; . \tag{3.19}$$

This scattering potential is acting on the system only during a limited time, either because it is switched on and off externally, or because it is an interaction between parts of the total physical system that can be considered as separated for asymptotic

times. H_0 is usually the time independent Hamiltonian of a bound, e.g. molecular, system. In atomic units it is expressed as

$$\begin{aligned} H_0 &= T_e + T_N + V_{\text{mol}} \\ &= \sum_{i=1}^{N_e} \frac{\hat{\mathbf{p}}_i^2}{2} + \sum_{k=1}^{N_N} \frac{\hat{\mathbf{P}}_k^2}{2M_k} \\ &\quad + \sum_{i>j=1}^{N_e} \frac{1}{|\mathbf{r}_i - \mathbf{r}_j|} - \sum_{k=1}^{N_N} \sum_{i=1}^{N_e} \frac{Z_k}{|\mathbf{r}_i - \mathbf{R}_k|} + \sum_{l>k=1}^{N_N} \frac{Z_k Z_l}{|\mathbf{R}_k - \mathbf{R}_l|} \,, \end{aligned} \tag{3.20}$$

where T_e and T_N are the kinetic energies of the electrons and the nuclei respectively. V_{mol} is the potential energy of the molecular system of N_e electrons and N_N nuclei of charge Z_k and mass M_k. $\mathbf{r}_i$ and $\mathbf{R}_k$ denote the electronic and nuclear coordinates respectively.

Note that the state of the laser field can be considered classically. In a full quantum description of the process, the quantization of the field is provided by the introduction of creation and annihilation operators. Due to the high number of photons that are flowing through the laser focus at intensities that are strong enough for intense-field multiphoton ionization, the classical treatment is justified as a case of the correspondence principle [159]. The neglect of the change in the total energy contained in the laser field is justified by the fact that the number of photons exchanged between the field and the bound Coulombic system is very small compared to the number of photons flowing through the focus per unit time. As a consequence, the energetic state of the field is nearly constant on its own scale.

In the conventional perturbative formulation of the S-matrix expansion, initial and final state are eigenstates of the same Hamiltonian that describes the physical system without the interaction [160]

$$\left[i\frac{\partial}{\partial t} - H_0 \right] |\, \phi_{\text{i/f}} \,\rangle = 0 \tag{3.21}$$

in Diracs ket notation, where the spatial coordinates in Eq. (3.21) and the equations below are dropped. The general objective is to find solutions to the Schrödinger equation with the full Hamiltonian:

$$\left[i\frac{\partial}{\partial t} - H(t) \right] |\, \Psi(t) \,\rangle = 0 \,. \tag{3.22}$$

The solutions to this partial differential equation can be written in form of the integral equation

$$|\, \Psi(t) \,\rangle = |\, \phi_{\text{i}}(t) \,\rangle + \int_{-\infty}^{\infty} dt' G(t,t') V_i(t') \, |\, \phi_{\text{i}}(t') \,\rangle \tag{3.23}$$

where G is the Greens operator that satisfies the inhomogeneous Schrödinger equation to the full Hamiltonian

$$\left[i\frac{\partial}{\partial t} - H(t)\right] G(t,t') = \delta(t-t') \; . \tag{3.24}$$

The equivalence is seen by inserting $|\,\Psi(t)\,\rangle$ into the Schrödinger equation Eq. (3.22).

The connection of the solutions to the full Hamiltonian (3.22) to the solutions of the interaction free Hamiltonian (3.21) is found in the expansion of the full Greens operator in terms of the Greens operator G_0 that satisfies

$$\left[i\frac{\partial}{\partial t} - H_0(t)\right] G_0(t,t') = \delta(t-t') \; . \tag{3.25}$$

The formal solution for G_0 can be written as

$$G_0^{\pm}(t,t') = \mp \exp(-iH_0(t-t'))\Theta(\pm(t-t')) \tag{3.26}$$

$$= \pm i\Theta(\pm(t-t')) \sum_j |\,\phi_j(t)\,\rangle\langle\,\phi_j(t')\,| \tag{3.27}$$

where the sign in the superscript selects the direction of time propagation. The *retarded* solution G_0^+ evolves the initial wavefunctions ϕ_i forward in time:

$$|\,\phi(t)\,\rangle = iG_0^+(t,t')\,|\,\phi(t')\,\rangle \quad \text{with } t > t' \tag{3.28}$$

while the *advanced* solution G_0^- propagates the final state wavefunction ϕ_f backwards in time.

In terms of G_0 the full Greens operator can be expressed as:

$$G(t,t') = G_0(t,t') + \int_{-\infty}^{\infty} dt'' G_0(t,t'')V_i(t'')G(t'',t') \; . \tag{3.29}$$

In perturbation theory this recursion is the starting point of the Dyson expansion of the unknown solutions of the full Hamiltonian in terms of the known eigenfunctions of the interaction free Hamiltonian H_0. For this expansion to be meaningful, it is important that the interaction V_i is small enough for the series to converge. A first estimation for the upper bound can be obtained by requiring the term of this recursive expansion that is second order in V_i to be smaller than the term that is of first order in V_i.

In applications to processes in laser fields $V_i(t)$ is the interaction with the radiation field. In dipole approximation and in the form of *minimal coupling* [161, 162] this is given by

$$V_i(t) = V_L^{(\mathrm{VG})}(t) = \sum_{j=1}^{N_e} \left[-\frac{q_j}{c}\hat{\mathbf{p}}_j \cdot \mathbf{A}(t) + \frac{q_j^2}{2c^2}A^2(t)\right] \; , \tag{3.30}$$

where $\mathbf{A}(t) = \mathbf{A}_0 f(t) cos(\omega t)$ is the vector potential of the radiation field in Coulomb gauge ($\nabla \mathbf{A} = 0$), $f(t)$ denoting an envelope function which is slowly varying with respect to the period $2\pi/\omega$ of the carrier. This form of the interaction potential is closely related to the *velocity gauge* form, which implies Coulomb gauge of the field ($\nabla \cdot \mathbf{A} = 0$). The expression for V_i in *length gauge* is obtained by application of the gauge transformation of second kind [163, 164]:

$$\hat{\mathcal{T}}(t) = \exp\left[i \sum_{j=1}^{N_e} \frac{q_j}{c} \chi(\hat{\mathbf{r}}_j; t) \right] \tag{3.31}$$

to the full Hamiltonian $H^{(\mathrm{VG})}(t)$ in velocity gauge. It is generated by the scalar operator $\chi(\hat{\mathbf{r}}; t) = -\hat{\mathbf{r}} \cdot \mathbf{A}(t)$. Transforming the corresponding quantum mechanical state $|\, \Psi(t) \,\rangle$ into length gauge

$$|\, \Psi^{(\mathrm{LG})}(t) \,\rangle = \hat{\mathcal{T}}(t) \, |\, \Psi^{(\mathrm{VG})}(t) \,\rangle \tag{3.32}$$

and inserting it into Eq. (3.22) one finds the relation between $H(t)$ in velocity gauge and the length gauge $H^{(\mathrm{LG})}(t)$:

$$H^{(\mathrm{LG})}(t) = \hat{\mathcal{T}}(t) \left[H^{(\mathrm{VG})}(t) - i \frac{d}{dt} \right] \hat{\mathcal{T}}^\dagger(t) \tag{3.33}$$

$$= \hat{\mathcal{T}}(t) H^{(\mathrm{VG})}(t) \hat{\mathcal{T}}^\dagger(t) + \left(i \frac{d}{dt} \hat{\mathcal{T}}(t) \right) \hat{\mathcal{T}}^\dagger(t) \, . \tag{3.34}$$

While the $\hat{\mathcal{T}}$ operators in the first term just transform the kinematic momenta into canonical momentum operators

$$\hat{\mathcal{T}}(t) \left(\hat{\mathbf{p}}_j - \frac{q_j}{c} \mathbf{A}(t) \right) \hat{\mathcal{T}}^\dagger(t) = \hat{\mathbf{p}}_j \, , \tag{3.35}$$

the second term directly evaluates to the interaction potential in length gauge

$$V_L^{(\mathrm{LG})} = -\mathbf{E}(t) \cdot \sum_{j=1}^{N_e} q_j \hat{\mathbf{r}}_j \, , \tag{3.36}$$

where $\mathbf{E}(t) = -\frac{1}{c} \frac{d}{dt} \mathbf{A}(t)$ is the electric field.

In the interaction with strong laser fields, the criterion of convergence is not met any longer if the intensity $I_0 = \left(\frac{\omega A_0}{c} \right)^2$ of the laser field is of the order of one percent of $4\omega^2$ ([68], Section 2.6), or equivalently if $U_p = \mathcal{O}(0.01)$ in atomic units (e.g. $4.55 \times 10^{12}\,\mathrm{W/cm^2}$ for a Ti:Sapphire laser at its fundamental wavelength of 800 nm). At these intensities the second term of the perturbation series is already comparable in magnitude to one percent of the leading term. Thus it is expected that the lowest order term of the perturbation series is a useful approximation only for intensities

up to about this critical value. This serious limitation in the applicability of the S-matrix expansion for processes in strong laser fields is overcome in the KFR theory [45–47] in connection with the Gordon-Volkov wavefunctions [165, 166] of unbound electrons in a laser field. In this approach, the initial and the final states can be eigenstates of different Hamiltonians. For applications like strong field ionization of molecules, the initial state still is a bound state of the molecular Hamiltonian. The final state in this case is then chosen to be a solution of a Hamiltonian that treats one electron, the ionized one, as interacting fully with the laser field, while the other electrons are not. Neglecting the Coulomb interaction $V_{C,1}$ of the electron in the laser dressed continuum with the residual ion, the Hamiltonian for this system is

$$H_f(t) = \frac{1}{2}\left(\hat{\mathbf{p}}_1 + \frac{1}{c}\mathbf{A}(t)\right)^2 + H_{\mathrm{mol}+} \;, \tag{3.37}$$

where $H_{\mathrm{mol}+}$ is the Hamiltonian of the field free molecular ion. Since the interaction of ion and the electron in the laser field is neglected in this model, the solutions of the corresponding Schrödinger equation are product wavefunctions of the eigenstates of the molecular ion multiplied by the exact eigenstates of the Gordon-Volkov Hamiltonian [166, 53] for the active electron

$$H_{\mathrm{GV}}^{(\mathrm{VG})}(1) = \frac{1}{2}\left(\hat{\mathbf{p}}_1 - \frac{q}{c}\mathbf{A}(t)\right)^2 \;, \tag{3.38}$$

which are given by

$$|\,\Phi_{\mathrm{GV}}^{(\mathrm{VG})}(\mathbf{k},t)\,\rangle = |\,\mathbf{k}\,\rangle \exp\left[-i\int\limits_{-\infty}^{t}\frac{1}{2m_e}\left(\mathbf{k} - \frac{q}{c}\mathbf{A}(t)\right)^2\right] \;. \tag{3.39}$$

In length gauge, the Hamiltonian has the form

$$H_{\mathrm{GV}}^{(\mathrm{LG})}(1) = \frac{1}{2}\hat{\mathbf{p}}_1^2 - q\hat{\mathbf{r}}_1\cdot\mathbf{E}(t) \;, \tag{3.40}$$

and the corresponding eigenstates are found using Eq. (3.32) to be

$$|\,\Phi_{\mathrm{GV}}^{(\mathrm{LG})}(\mathbf{k},t)\,\rangle = |\,\mathbf{k} - \frac{q}{c}\mathbf{A}(t)\,\rangle \exp\left[-i\int\limits_{-\infty}^{t}\frac{1}{2m_e}\left(\mathbf{k} - \frac{q}{c}\mathbf{A}(t)\right)^2\right] \;. \tag{3.41}$$

This ansatz takes into account the interaction of the ionized electron with the field to all orders. It therefore has the potential to describe the essential features of the transfer of a bound electron into the field dressed continuum beyond conventional perturbation theory.

KFR theory thus introduces two partitions of the full Hamiltonian:

$$H(t) = H_i + V_i(t) \tag{3.42}$$
$$= H_f(t) + V_f(t) \ , \tag{3.43}$$

where

$$V_f(t) = \sum_{j=2}^{N_e} V_{L,j}(t) + V_{C,1} \tag{3.44}$$
$$= \sum_{j=2}^{N_e} \left[-\frac{1}{c}\mathbf{p}_j \cdot \mathbf{A}(t) + \frac{1}{2c^2}A^2(t) \right] + \sum_{j=2}^{N_e} \frac{1}{|\mathbf{r}_1 - \mathbf{r}_j|} - \sum_{k=1}^{N_N} \frac{Z_k}{|\mathbf{r}_1 - \mathbf{R}_k|} \ . \tag{3.45}$$

Since the Coulomb field potential is reducing only reciprocal with distance, this model for the final state of the ionized physical system is not exact. Therefore it has originally been developed for the detachment of an electron from a negative ion. The lack of correlation between ionized electron and parent ion can be corrected though by an approximate solution of the Hamiltonian that still considers this interaction ([167] and references therein, [63]). While the Gordon-Volkov wavefunctions are plane waves that fully include the effect of the field in their phases, these Coulomb-Volkov waves are approximations of the field-modified continuum states of the Coulomb potential. If a Coulomb-Volkov wavefunction is used instead of a Gordon-Volkov one to describe the final state, then the Coulomb interaction $V_{C,1}$ of the ionized electron with the residual ion is part of $H_f(t)$ instead of being part of the interaction $V_f(t)$.

There are several approximative approaches of Coulomb corrections to the Gordon-Volkov wavefunctions, that estimate the influence of the Coulomb field on the phases of the Gordon-Volkov functions (see [168, 169] and references there). Among these the semi-classical Wentzel-Kramer-Brillouin (WKB) [170] approximation of Krainov [171, 66, 172], will be used in this work, which has been applied e.g. in single ionization of atoms [173] and molecules [34] as well as in the case of double ionization of He atoms [28] and multiple ionization of Xe [29]. For a comparison with the closely related approximation of Perelemov, Popov and Terent'ev [56], please see [174]. This approximation gives an estimate of the phase factor that is an effect of the Coulomb field of the cation [172]. Details will be given below in section 4.3.1. This approximation corrects the total rates, but it does not influence the angular differential behavior.

Just like for H_i the Greens operator for the final state Hamiltonian satisfying

$$\left[i\frac{\partial}{\partial t} - H_f(t) \right] G_f(t, t') = \delta(t - t') \ . \tag{3.46}$$

is a known object. Analogous to G_i there are retarded and advanced solutions to this equation.

In terms of G_f the full Greens operator can be expanded as

$$G(t,t') = G_f(t,t') + \int_{-\infty}^{\infty} dt'' G_f(t,t'') V_f(t'') G(t'',t') \; . \tag{3.47}$$

Using this expansion in the initial expansion of the wavefunction Eq. (3.23), one obtains

$$\begin{aligned} |\,\Psi(t)\,\rangle = |\,\phi_{\rm i}(t)\,\rangle &+ \int_{-\infty}^{\infty} dt' G_f(t,t') V_i(t') \,|\,\phi_{\rm i}(t')\,\rangle \\ &+ \int_{-\infty}^{\infty} dt' \int_{-\infty}^{\infty} dt'' G_f(t,t'') V_f(t'') G(t'',t') V_i(t') \,|\,\phi_{\rm i}(t')\,\rangle \; . \end{aligned} \tag{3.48}$$

In this form the transition amplitude to the final state Φ_f can be conveniently evaluated as:

$$\begin{aligned} \langle\,\Phi_f(t)\,|\,\Psi(t)\,\rangle = &\langle\,\Phi_f(t)\,|\,\phi_{\rm i}(t)\,\rangle + \int_{-\infty}^{t} dt' \langle\,\Phi_f(t')\,|\,V_i(t')\,|\,\phi_{\rm i}(t')\,\rangle \\ &+ \int_{-\infty}^{\infty} dt' \int_{-\infty}^{t} dt'' \langle\,\Phi_f(t'')\,|\,V_f(t'') G(t'',t') V_i(t')\,|\,\phi_{\rm i}(t')\,\rangle \; , \end{aligned} \tag{3.49}$$

where the diagonal expansion of G_f has been used (see Eq. (3.26)), which brings in the time ordering Heaviside Θ function. $\Theta(t''-t')$ is also present in the full Greens operator $G(t'',t')$, so the integration over t' always has t'' as the upper bound. Incorporating the direct overlap between initial and final state, which does not result in a stationary contribution unless they are the same, the limit $t \to \infty$ is written as

$$\begin{aligned} (S-1)_{fi} = &\int_{-\infty}^{\infty} dt' \langle\,\Phi_f(t')\,|\,V_i(t')\,|\,\phi_{\rm i}(t')\,\rangle \\ &+ \int_{-\infty}^{\infty} dt' \int_{-\infty}^{\infty} dt'' \langle\,\Phi_f(t'')\,|\,V_f(t'') G(t'',t') V_i(t')\,|\,\phi_{\rm i}(t')\,\rangle \; . \end{aligned} \tag{3.50}$$

Recalling that Φ_f is the product wavefunction of the molecular ion with a Gordon-Volkov wave, the first term of this expansion already considers the interaction of the active electron with the field to all orders. I.e. this expansion is qualitatively different from the Dyson perturbation series. It also differs from the usual two-potential scattering formulae [73], since it considers one of the interactions as dominant over the other at different times.

It is interesting to note that, regarding the first term of this expansion, it is possible as well to construct a similar expansion where V_f appears instead of V_i. But from the identity

$$i\frac{\partial}{\partial t}\,|\,\Phi_f(t)\,\rangle = [T_{e,1} + V_{L,1} + H_{\rm mol+}]\,|\,\Phi_f(t)\,\rangle \tag{3.51}$$

$$\Leftrightarrow \quad V_{L,1}\,|\,\Phi_f(t)\,\rangle = i\frac{\partial}{\partial t}\,|\,\Phi_f(t)\,\rangle - [T_{e,1} + H_{\rm mol+}]\,|\,\Phi_f(t)\,\rangle \; , \tag{3.52}$$

where $T_{e,1}$ denotes the kinetic energy operator for the active electron, one finds by partial integration that $V_{L,1}$ is equivalent to $V_{C,1} = H_0 - [T_{e,1} + H_{\mathrm{mol+}}]$ within the matrix element of the first order term. Noting also that

$$V_i - V_f = V_{L,1} - V_{C,1} \tag{3.53}$$

the same holds for the full interaction potentials that include all electrons.

The expression (3.50) for the S-matrix evolution is very elegant, as it projects out G_f on the specific final state. It further allows to choose which approximation of the full Greens operator G to use in the second order matrix element. In this form it provides the basis of the Intense-Field Many-Body S-Matrix Theory (IMST) [25, 26]. In IMST a third partition of the full Hamiltonian can be introduced

$$H(t) = H_m(t) + V_m(t) \tag{3.54}$$

that can include the effect of a physically significant intermediate stage in the transition process. The corresponding intermediate Greens operator G_m provides a time evolution on the subspace of eigenfunctions of H_m. Choosing G_m in the second order term of the IMST expansion, Eq. (3.50), thus takes into account that during the process of ionization the physical system spends a significant time in a configuration that is evolving according to the dynamics of the Hamiltonian H_m. Note that the interactions considered in H_m can be different from those in H_i and H_f, which is found to be particularly useful to analyze NSDI. The second order term is the earliest possible stage in the S-matrix expansion, where this Hamiltonian of a transient configuration can be considered. For the specific case of NSDI, G_m will be given explicitely in section 5.2 to derive the second order term of the IMST expansion.

This derivation is given here for the case of interaction of a bound system with a laser field, but the S-matrix expansion Eq. (3.50) is not limited to this specific case, but can be applied to any physical process where a stationary initial state evolves under the strong influence of an external interaction into an asymptotic final state, progressing through a limited number of physically significant transition stages. The transition states are physically significant in this context, if the time evolution of the system follows the energy surfaces of a corresponding intermediate Hamiltonian H_m for a significant part of the total transition time. It is obvious, that the truncation of the asymptotic S-matrix expansion after as much as one or two terms cannot result in an exact expression for the transition amplitudes. The degree of accurateness cannot even be estimated from the formula alone, contrary to the situation in the perturbation series. The virtue of the IMST expansion lies in the possibility to systematically include possible mechanisms of transition and check their relative amount of contribution to the total transition amplitude. It represents a systematic strategy for the identification of physical transition mechanisms in processes with non-perturbative interactions. The validity of a mechanism is verified by comparison of the various calculated differential transition spectra with experimental data. Once

a mechanism has been identified as significant to a specific kind of process, one can narrow down domains of physical parameters for its relative importance. This way, and by analyzing the analytic properties such as symmetries of the transition matrix elements in Eq. (3.50), a deeper understanding of the evolution of the physical processes can be gained.

4. *S*-Matrix Theory of Inelastic Vibronic Ionization of Molecules in Intense Laser Fields

As explained in section 2.1.1 for the case of an atom, a process of single ionization is called *inelastic* in the scope of this work if more energy is deposited in the ion than necessary to create it from its parent molecule by removal of a specific electron. This is a special case of what Child defines as *open* inelastic scattering channels, who generally defines *inelastic* scattering as a process that changes the internal state of the target [175]. In contrast to the atomic case, energy may also be deposited into the vibrational and rotational states, thus allowing not only electronically excited molecular ions but the more general case of rovibronically excited ones. The process of photoionization of a molecule into excited vibrational states of the molecular cation is referred to as *Inelastic Vibronic Ionization* (IVI).

4.1. Quantum Mechanical Description of Molecules

4.1.1. Born-Oppenheimer Approximation

While in atomic systems only the dynamics of the electrons is described by a central field Hamiltonian, in the case of a molecular system the Hamiltonian H_0 also contains the kinetic energy of the motion of the nuclei in the combined Coulomb field of the electrons and the other nuclei. For a diatomic molecule in its center of mass frame the general Hamiltonian Eq. (3.20) reduces to [161][1]

$$H_{\mathrm{mol}} = T_e + T_N + V_{\mathrm{mol}} \tag{4.1}$$

$$= \sum_{i=1}^{N_e} \frac{1}{2}\hat{\mathbf{p}}_i^2 + \frac{1}{2\mu}\hat{\mathbf{P}}_N^2 - \sum_{k=A,B}\sum_{i=1}^{N_e} \frac{Z_k}{|\mathbf{r}_i - \mathbf{R}_k|} + \sum_{j>i=1}^{N_e} \frac{1}{r_{ij}} + \frac{Z_A Z_B}{R}\,, \tag{4.2}$$

where μ denotes the reduced mass of the two nuclei, $R = |\mathbf{R}_A - \mathbf{R}_B|$ the internuclear and $r_{ij} = |\mathbf{r}_i - \mathbf{r}_j|$ the interelectronic distance. T_N is the kinetic energy of the relative nuclear motion. The extension to molecules with more nuclei is straightforward. Treating the nuclear positions as fixed in the laboratory system of coordinates, one can find electronic wavefunctions that depend parametrically on the internuclear distance R:

$$\left[E_s(\mathbf{R}) - (T_e + V_{\mathrm{mol}})\right] \Phi_s(\mathbf{R}; \mathbf{r}_1, \mathbf{r}_2) = 0\,. \tag{4.3}$$

[1] As usual the mass polarization terms $\frac{1}{8\mu}\left(\sum_{i=1}^{N_e}\hat{\mathbf{p}}_i\right)^2$ [176] are dropped since the mass of the nuclei is much larger than that of the electrons .

Since for each R the set of solutions forms a complete orthogonal basis for the electronic part of the Hilbert space of the problem, the complete solution may be expanded in this basis:

$$\Psi_0(\mathbf{R};\mathbf{r}_1,\mathbf{r}_2) = \sum_q F_q(\mathbf{R})\Phi_q(\mathbf{R};\mathbf{r}_1,\mathbf{r}_2)\ . \tag{4.4}$$

Reinserting this ansatz into the time independent molecular Schrödinger equation and assuming normalization of the electronic wavefunctions one obtains the equations for the functions $F_s(\mathbf{R})$:

$$\langle\, \Phi_s(\mathbf{R};\mathbf{r}_1,\mathbf{r}_2)|\,[E - H_{\mathrm{mol}}]\,|\Psi_0(\mathbf{R};\mathbf{r}_1,\mathbf{r}_2)\,\rangle = 0 \tag{4.5}$$

$$\Leftrightarrow [E - E_s(\mathbf{R})]F_s(\mathbf{R}) - \sum_q \langle\, \overline{\Phi}_s|T_N|\Phi_q\,\rangle F_q(\mathbf{R}) = 0\ , \tag{4.6}$$

where the angle brackets symbolize the integration over the electronic coordinates. The operator of kinetic energy of the nuclei couples the electronic wavefunctions. If its variation with R is small as compared to the R dependence of the functions $F_q(\mathbf{R})$, then this coupling can be neglected and R becomes a parameter for an adiabatic change of the electronic parts Φ_q of the total wavefunction. This ansatz is known as the Born-Oppenheimer approximation [99]. Formally, the Born-Oppenheimer ansatz neglects the coupling terms, resulting in the decoupled equations for the nuclear wavefunctions $F_s(\mathbf{R})$

$$\left[E - E_s(\mathbf{R}) - \frac{1}{2\mu}\hat{\mathbf{P}}_N^2\right] F_s(\mathbf{R}) = 0 \tag{4.7}$$

which describe the movement of the nuclei in the potential energy surface $E_s(\mathbf{R})$ of the electronic state s. For states with zero angular momentum the potential surface is only a function of the internuclear distance while for molecules with more than two atoms this is an energy surface in a configuration space of correspondingly higher dimensionality. This approximation is suitable especially for internuclear distances close to the equilibrium distance R_e, where the electronic potential curve has its minimum.

Separating radial and angular parts of the nuclear wavefunction one finds that the total energy of F_s is composed of three parts, the electronic, the vibrational and the rotational energy. In a first approach, one can treat the molecule as a rigid rotor with fixed internuclear radius, which decouples also the vibrational motion from the centrifugal distortion.

Equation (4.7) leads to a quantization of the energy of vibrational motion of the nuclei. The internuclear distance is no longer a well defined observable or "good" quantum number. In this picture, the quantum of energy needed for a vibronic, that is an electronic and a vibrational, transition depends only on the stationary initial and final states, that are quantized according to their energetic excitation and not on some sort of internuclear distance.

4.1.2. Franck-Condon Approximation

In theoretical works vibrational excitations in processes of electronic transition have been first discussed in the works of Franck and Condon. Using classical [177] as well as arguments of quantum mechanics [178, 179], they showed that electronic transitions can be assumed to be fast with respect to the time scale of nuclear motion, for which the vibrational period of the lightest molecule, H_2, defines the lower bound ($T = 7.58\,\mathrm{fs}$). This suggests that, upon an electronic transition, the state of vibrational motion of the nuclei in the combined Coulombic potential surface of all electronic and nuclear charges is transferred suddenly into the vibrational state of the molecular ion in its respective potential surface. This is known as the Franck-Condon Principle. As such, it still fully allows for any amount of variation of the electronic transition amplitude with the internuclear distance.

The Franck-Condon approximation goes one step further, assuming that the electronic transition amplitude is rather slowly varying over the characteristic internuclear distances. Accordingly, the electronic transition is decoupled from the nuclear motion, which fits well with the Born-Oppenheimer approximation [99] for the wavefunction of bound molecular electrons. Combining the Born-Oppenheimer ansatz with the Franck-Condon separation of transition amplitudes, the projection of the vibrational state of the molecule onto the set of vibrational states of the molecular ion results in the emergence of the Franck-Condon overlap integrals, which are multipliers to the amplitudes of electronic transition to give the total transition amplitude. Fig. 4.1 shows as an example the distribution of the Franck-Condon factors for the first ionizing transitions in H_2 involving vibrational excitation. This model has been successful in explaining experimental results ionization of molecules by synchrotron radiation (e.g. [180, 181]) as well as by impact of fast ions (e.g. [182, 183]) and electrons [184]. It is also used as an important tool in the analysis of pump-probe experiments involving single-photon excitation of molecules (e.g. [185–188]).

On the other hand, there are experimental observations of non-Franck-Condon effects in ionization (by this we mean deviations from the results obtained in the Franck-Condon approximation), e.g. in the electron impact ionization $(e, 2e)$ of H_2 and D_2 [190]. These cases suggest that the basic assumption of a weak variation of the electronic transition matrix element with changing internuclear radius [177, 191] can be too strong for a given bound system.

There are a couple of possible causes for this. It is known theoretically for NO ([192, 193] and references in the latter) as well as for N_2 [194] for more than 25 years, that shape resonances can cause a deviation of the fluorescence spectra from the behavior expected from the Franck-Condon assumption of vertical electronic transitions in single photon ionization processes caused by synchrotron radiation, as they effectively couple nuclear and electronic dynamics. This has been verified experimentally for CO [195, 196] as well as for O_2 [197]. Additionally to shape resonances the variation of the electronic wavefunctions with the internuclear distance can cause Cooper minima,

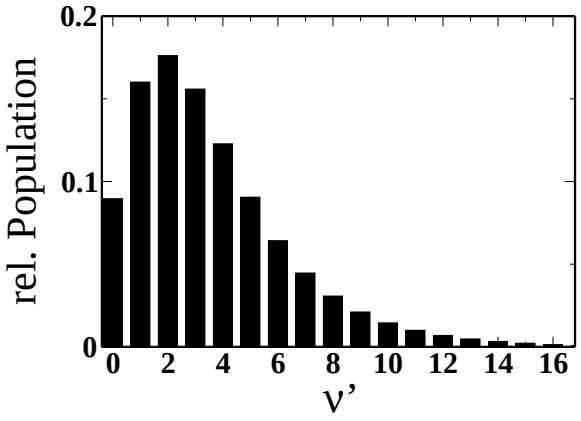

Figure 4.1.: Normalized distribution of Franck-Condon factors for the transition from the vibrational ground state of $H_2(X^1\Sigma_g^+)$ to the vibrational state ν' in $H_2^+(X^2\Sigma_g^+)$ [189].

associated with zeros in the radial electronic transition matrix elements, to vary in the overlap area of the vibrational wavefunctions [198]. Common to these two effects is a localization (or in the case of Cooper minima an anti-localization) of the electronic wavefunction in the course of ionization, that influences the transition amplitude to the continuum and that depends on the molecular geometry [199]. In the case of shape resonances, this localization causes the electron to spend a longer period of time on the boundary of the molecular ion, still influencing the Coulombic internuclear field and thus the process of vibrational transition.

4.2. Observation of Non-Franck-Condon Distributions in Molecular Ions Generated by Intense Laser Fields

The Franck-Condon approximation has also been used to find first estimates for the initial conditions in the theoretical modeling of laser induced processes in molecular ions [142, 200, 117] and seemed to give reasonable results in the analysis of dissociation spectra of molecular ions in intense laser pulses [201]. While the length of the pulses in this specific experiment (150 fs) considerably exceeds the vibrational period of the molecules, the time window for the electronic transitions is much shorter, centered about the points of peak field strength, because the process is a multiphoton one, requiring 10 photons and thus exhibiting a highly nonlinear dependence of the transition rate on the field intensity. Thus, it is reassuring to see that the measured spectrum of vibrational states e.g. of electronically excited N_2^+, produced by inner-shell multiphoton ionization, matches quite well the theoretically predicted one, obtained by multiplication of the Franck-Condon factors into the electronic

transition rate $\Gamma^{(f,i)}(I_0)$ at the given laser intensity [202]:

$$\Gamma^{(f,i)}_{\nu',\nu}(I_0) = \mathcal{O}^{(f,i)}_{\nu,\nu'}\Gamma^{(f,i)}(I_0)\ . \tag{4.8}$$

On the other hand there is theoretical doubt, whether the Franck-Condon approximation is still valid in processes of intense-field multiphoton ionization, where strong mixing of diabatic electronic states is occurring [109]. In the context of the theory of tunnel ionization an approach has been made to define and calculate in-field Franck-Condon overlaps for the ionization of molecules in a static electric field [203]. Considering a homonuclear diatomic molecule the authors simply add an interaction term to the Hamiltonian of internuclear motion that shall consider the effect of the field, which couples a shielded charge of one of the nuclei to the field. First, it is to be noted that the equation should be phrased in the center of mass coordinate system, instead of in the body fixed frame of one of the nuclei, with the reduced mass μ as the inertia of the motion instead of the mass of the remote nucleus. Secondly one recognizes in the center of mass description that the field couples to the internuclear coordinate directly only through its interaction with the *relative charge* of the two nuclei (see section 3.1.1). In case of a homonuclear diatomic, this relative charge is zero. Thus, in this case the effect of the field on the internuclear motion is only mediated by its influence on the electronic wavefunctions. This influence will strongly affect the internuclear potential $V(R)$, given by the adiabatic energy $E_s(R)$ of the electronic wavefunction. The authors of that paper consider this to be the unperturbed Morse potential. Thus, their approach is a decidedly static one, neglecting that the effect of the field on the electrons and on the nuclei occurs on different time scales due to the difference in their respective masses.

First experimental evidence [204, 114, 205, 184] for vibrational distributions deviating from the Franck-Condon distribution has been found in the dissociation spectra of H_2^+ generated via laser induced ionization of the neutral, ground state H_2 molecule. It has been argued that the dissociation spectra are not in agreement with the assumption that the distribution of the vibrational states in the H_2^+ cations is given by the Franck-Condon overlap integrals [189, 206]. For example in one of these experiments the distributions show a narrow peak that suggests a concentration in a single moderately excited vibrational state [205], while in others low vibrational states are found to be favored.

Experimentally it is challenging to get a clear picture of the dynamic state of H_2^+ produced by intense-field multiphoton ionization. Lately it has become feasible by several techniques to infer the vibrational state of the residual ion closely after ionization. Historically the earliest signatures of vibrational states are found in the IR and Raman spectra [207–209] of molecular ions [210]. Other methods have been developed, which dissociate the molecular ion by neutralization into a predissociative state of the molecule and measure the kinetic energy release (KER) of the neutral radical fragments [211]. In a recent experiment this technique has been

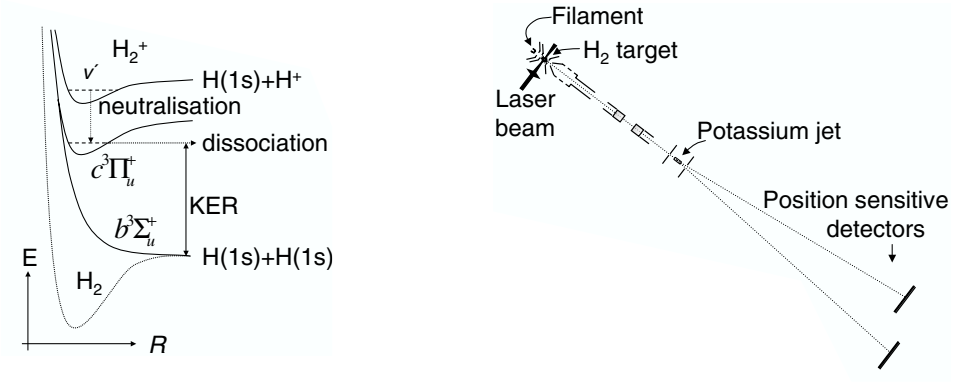

Figure 4.2.: Sketch of the principle of the experiment by Posthumus and coworkers [184], extracted from the original publication.

used to perform a measurement on laser induced ionization of molecular hydrogen [184, 212]. The original schematic overview of the experiment is given in the right panel of Fig. 4.2. The experimental setup consists of an H_2^+ source, an extraction line, a neutralization stage and position sensitive detectors. In the source chamber H_2 molecules are ionized either by electron impact or by application of a laser pulse. The ions are accelerated by an electric field of about 100 V/cm field strength to a final kinetic energy of approximately 4 keV, guiding them towards a jet of potassium vapor. These atoms have an ionization potential of 4.3 eV, which is low compared to the electron affinity of H_2^+, facilitating a neutralization of the molecular ions by charge transfer into an excited state of H_2, that may be characterized as $c^3\Pi_u$ (see left hand side of Fig. 4.2). From this excited state the molecules predissociate due to rotational coupling with the $b^3\Sigma_u^+$ state within a few nanoseconds and their atomic fragments, acquiring a drift velocity of $\mathbf{v}_0 \pm \hat{\mathbf{R}}\sqrt{\mathrm{KER}/M}$, where $\mathbf{v}_0$ is the velocity obtained by the experimental acceleration field, M is the mass of a proton and $\hat{\mathbf{R}}$ is the orientation specific to each molecule. Since apparently the vibrational state is nearly unaffected by the electron capture process, the kinetic energy release of the molecular fragments is related to the vibrational state ν' of the molecular ion according to the energy balance (see Eq. (4.53))

$$\mathrm{KER} = E\left[\mathrm{H}_2 c^3\Pi_u\right] + \omega_e\nu' - \omega_e x_e \nu'(\nu'+1) - \left(E\left[\mathrm{H}_2 X^1\Sigma_g^+\right] + D_0\left[\mathrm{H}_2 X^1\Sigma_g^+\right]\right) \ . \quad (4.9)$$

After traversal of a certain drift length their positions and arrival times are recorded in coincidence by two position sensitive detectors. Electron impact ionization with a projectile energy of 100 eV was used to compare the obtained KER-spectrum with that of an earlier work [190]. This spectrum closely resembles a Franck-Condon distribution of the vibrational states. After this step the experiment was reperformed using laser pulses of different duration and wavelength. The resulting KER spectra that deviate significantly from previous experiment will be analyzed in detail in section 4.4.

Another recent experimental approach is to use pump-probe techniques [213] to perform controlled Coulomb explosion imaging [126–128], where the singly ionized molecular ion is dissociated by means of a subsequent "probe" laser pulse that ionizes a second bound electron. Here the kinetic energy of the charged fragments is measured and the variation of the signal with the time delay between the pumping and the probing laser pulse can be used to recover the superposition of vibrational wavepackets in the molecular ion. In this context one should mention the *COLTRIMS* technique or *reaction microscope* [153, 154] that allows fully differential resolution of the momenta of the charged reaction fragments, representing a very important experimental tool for detection and analysis in the context of ionization and dissociation physics.

Schumacher et al. [204] have attributed the experimentally observed shift to the accumulated effect of dressed state resonances on one hand, the field dependent variation of Franck-Condon integrals in the laser pulse on the other and ultimately to bond softening in the H_2^+ ion. This highlights two possible additional causes of deviation from the Franck-Condon distribution: First, the mechanism of transition can be a process of higher order, involving intermediate, eventually resonant states. There seems to be experimental evidence for this e.g. in the intense-field multiphoton ionization of H_2 at 400 nm [214]. Second, the basis of field free bound states, used to analyze the data, might be one that is inappropriate for the physical process under consideration (either in the state of origin or in the target state). E.g. static field calculations [203] suggest that there is considerable bond softening [112] in the H_2^+ ion, causing that there is no bound states at a peak intensity $I_0 = 1.2 \times 10^{14}\,\mathrm{W/cm^2}$ of the laser pulse. Interestingly these calculations of static field Franck-Condon factors suggest [203] that the vibrational population should shift to higher excitations, contrary to the recent experimental observations [184, 212].

In many of the previous approaches to the problem, the transition probability to continuum for the ionizing electron was assumed to be the same for the transitions to different vibrational states. Thinking of ionization as the breakup of a molecule into two parts, the ion and the electron, this amounts to a neglect of the transition amplitudes for the second, electronic fragment. But a higher excitation of the molecular ion also shifts the possible shell of continuum states for the ionized electron to a lower kinetic energy, and it is argued in this work, that this shift influences the transition rates. This does not rule out other effects that may cause a deviation from the Franck-Condon distribution, but it explains the effect of strong-field ionization on the vibrational state of the molecular ion.

4.3. *S*-Matrix Formulation of the Transition Amplitude

For the case of multiphoton ionization of molecules in strong laser fields vibronic transitions were first considered in the S-matrix description by the introduction of

Franck-Condon overlap integrals into the KFR amplitudes [202]. Lately a second theoretical description on the basis of the Intense-Field Many-Body *S*-Matrix Theory [26] was presented, that treats the transition between the vibrational states during the process of ionization on the same quantum mechanical footing as the electronic transition, without assuming a priori that the vibrational transitions are unaffected by the electronic strong-field transition. In that approach, the internuclear equilibrium distance is assumed to be fixed though during the ionization process, an assumption that is valid in some cases, e.g. for the case of ionization of the outer valence electrons of N_2, but which in general is too limiting for other cases. Another approximation made is that the molecular orbitals are treated as independent of the internuclear motion.

In this work an alternative approach is presented, that explains and predicts the shifted population rates of the unperturbed vibrational states of the H_2^+ ions after the pulse, that hydrogen molecules photoionize into.

4.3.1. Transition Rate

Equipped with the asymptotic boundary conditions of the process, one can describe the effect of the laser field on the bound system in a non-perturbative way by means of the KFR expansion, Eq. (3.50), of the *S*-matrix. The Hamiltonian (4.1) of the diatomic molecule

$$H = \sum_{i=1}^{N_e} \frac{1}{2}\left(\hat{\mathbf{p}}_i + \frac{1}{c}\mathbf{A}(t)\right)^2 + \frac{1}{2\mu}\hat{\mathbf{P}}_N^2 - \sum_{k=A,B}\sum_{i=1}^{N_e}\frac{Z_k}{|\mathbf{r}_i - \mathbf{R}_k|} + \sum_{j>i=1}^{N_e}\frac{1}{r_{ij}} + \frac{Z_A Z_B}{R} \tag{4.10}$$

is reduced to the electronic contribution by following the reasoning of the Born-Oppenheimer approximation, treating the kinetic energy $T_N = \frac{1}{2\mu}\hat{\mathbf{P}}_N^2$ of the internuclear motion as constant on the time scale of electronic motion. This is possible since the relative nuclear coordinate does not couple to the field. Thus, the evolution of electronic part of the many-body system in the laser field is governed by the Hamiltonian

$$H = \sum_{i=1}^{N_e} \frac{1}{2}\left(\hat{\mathbf{p}}_i + \frac{1}{c}\mathbf{A}(t)\right)^2 - \sum_{k=A,B}\sum_{i=1}^{N_e}\frac{Z_k}{|\mathbf{r}_i - \mathbf{R}_k|} + \sum_{j>i=1}^{N_e}\frac{1}{r_{ij}} + \frac{Z_A Z_B}{R} + T_N \tag{4.11}$$

$$= \sum_{i=1}^{N_e} \frac{1}{2}\left(\hat{\mathbf{p}}_i + \frac{1}{c}\mathbf{A}(t)\right)^2 + V_{\text{mol}} \tag{4.12}$$

$$= \underbrace{\sum_{i=1}^{N_e} \frac{1}{c}\hat{\mathbf{p}}_i\mathbf{A}(t) + N_e\frac{A^2(t)}{2c^2}}_{V_L(t)} + H_{\text{mol}} \tag{4.13}$$

while the nuclear part is still approximatively described by the field free nuclear wave equation (4.7). This is justified since already for the molecule of smallest mass, H_2, the reduced mass of the nuclei is about three orders of magnitude larger than that of the electrons, which slows down the nuclear response to the oscillating laser field by just this factor with respect to the electronic one.

In the initial state partition the full electronic Hamiltonian is splitted into $H_i = H_{\mathrm{mol}}$ and $V_i = V_L(t)$. For the final state partition V_f is given in Eq. (3.44) and $H_f(t)$ accordingly in Eq. (3.37) with

$$H_f = H - V_f(t) = H_{\mathrm{GV}}(1) + \sum_{i=2}^{N_e} T_{e,i} + V_{\mathrm{ion}} + T_N \tag{4.14}$$

$$= \frac{1}{2}\left(\hat{\mathbf{p}}_1 + \frac{1}{c}\mathbf{A}(t)\right)^2 + \sum_{i=2}^{N_e}\frac{1}{2}\hat{\mathbf{p}}_i^2 - \sum_{k=A,B}\sum_{i=2}^{N_e}\frac{Z_k}{|\mathbf{r}_i - \mathbf{R}_k|} + \sum_{j>i=2}^{N_e}\frac{1}{r_{ij}} + \frac{Z_A Z_B}{R} + T_N \tag{4.15}$$

In the molecular case the initial state Ψ_i of the system is approximated by the Born-Oppenheimer separated product of a nuclear and an electronic wavefunction

$$\Psi_i(\mathbf{R}; \mathbf{r}_1, \mathbf{r}_j) = \chi_\nu(R - R_e) \otimes \Phi_i(\mathbf{r}_1, \mathbf{r}_j; \underline{\mathbf{R}}_n) \,, \tag{4.16}$$

where χ_ν and Φ_i denote the quantized vibrational and electronic wavefunction respectively. $\mathbf{r}_1$ is the spatial coordinate of the *active* electron, $\mathbf{r}_j$ symbolizes the coordinates of all other electrons and $\underline{\mathbf{R}}_n \equiv \{\mathbf{R}_1, \mathbf{R}_2\}$ is the set of all nuclear coordinates. R_e is the equilibrium value of the scalar internuclear distance $R = |\mathbf{R}_2 - \mathbf{R}_1|$.

Several final states are possible for the system after ionization. Compared to the atomic situation, where different states of electronic excitation of the ion are possible, in molecular ionization also the vibrational state may be excited. The population of these states is likely to be much broader spread as compared to the population of the electronically excited states, as they lie energetically much closer to each other. We therefore consider as final state

$$\Psi_f(\mathbf{R}; \mathbf{k}, \mathbf{r}_j) = \chi'_{\nu'}(R - R'_e) \otimes \Phi_{\mathrm{GV}}(\mathbf{k}) \otimes \Phi_f(\mathbf{r}_j; \underline{\mathbf{R}}_n) \,, \tag{4.17}$$

where Φ_f is an eigenstate of the Hamiltonian of the molecular ion and as such is a function of the coordinates of all electrons remaining bound to the ion. $\mathbf{k}$ is the canonical momentum of the ionized (*active*) electron. The nuclear vibrational wavefunctions $\chi'_{\nu'}$ of the molecular ion will have frequencies that differ from those of the parent molecule, just as the internuclear equilibrium distance R'_e generally deviates from R_e. If the ionized electron is released from a bonding orbital, R'_e will be larger than R_e, as the bonding potential $E_i(R)$, that is created by the electrons occupying the space surrounding the nuclei, is weakened and its minimum thus shifted to a larger value of R. The orientation of the molecule is assumed to stay fixed. The

ionized electron in the laser field is approximately described by a Gordon-Volkov wavefunction $\Phi_{\mathrm{GV}}(\mathbf{k})$ [165, 166] that is an eigenfunction to the corresponding Hamiltonian (Eq. (3.38)). In velocity gauge it has the form (see Eq. (3.39))

$$|\,\Phi_{\mathrm{GV}}(\mathbf{k},t)\,\rangle = |\,\mathbf{k}\,\rangle \exp\left[-i\int_{-\infty}^{t}\frac{1}{2m_e}\left(\mathbf{k}+\frac{1}{c}\mathbf{A}(t)\right)^2\right] . \tag{4.18}$$

As in the atomic case, this ansatz neglects the correlation of the electron in the continuum with its parent ion, treating it as a separated electron of drift momentum $\mathbf{k}$, subject to the oscillations of the electric field component of the laser.

Using the general S-matrix expansion, Eq. (3.50), the first order amplitude [26] for the transition from the initial state in the neutral molecule with vibrational quantum number ν to the vibrational state ν' of the molecular ion, in the general case of an elliptically polarized field, can be written as [215] (see also [173, 26]):

$$\begin{aligned} S_{fi}^{(1)}(t_f,t_i) = &-i\sum_{N=-\infty}^{\infty}\int_{t_i}^{t_f}dt_1\exp\left[i\left(\frac{k^2}{2}+U_p+E_T-N\omega\right)t_1\right](U_p-N\omega)J_N\left(a,b,\eta\right) \\ &\times\langle\,\chi'_{\nu'}(R-R'_e)\,|\,\langle\,\boldsymbol{k}\,|\,\phi_i(\boldsymbol{r}_1;\underline{\mathbf{R}}_n)\,\rangle\langle\,\Phi_f(\mathbf{r}_2;\underline{\mathbf{R}}_n)|\Phi'_i(\mathbf{r}_2;\underline{\mathbf{R}}_n)\,\rangle\,|\,\chi_\nu(R-R_e)\,\rangle \end{aligned} \tag{4.19}$$

where $E_T = E_T(\nu',\nu) = E_{\nu'}^{(f)} - E_{\nu}^{(i)}$ is the IVI transition energy. The first inner brackets of the matrix element denote integration over the spatial coordinates of the active electron. The second inner matrix element represents the overlap between the passive electrons for their transition from the state of the neutral molecule into the ionic state, while the outer brackets represent an integration over the internuclear distance R. For this separation of the matrix elements we have assumed that the multi-electron wavefunction Φ_i is given in Hartree or product form (cf. discussion in section 4.3.2), i.e.

$$\Phi_i(\mathbf{r}_1,\mathbf{r}_j;\underline{\mathbf{R}}_n) = \phi_i(\boldsymbol{r}_1;\underline{\mathbf{R}}_n)\otimes\Phi'_i(\mathbf{r}_j;\underline{\mathbf{R}}_n) . \tag{4.20}$$

$J_N(a,b,\eta)$ are generalized Bessel functions of three arguments (e.g. [173])

$$J_N(a,b,\eta) = \sum_{m=-\infty}^{\infty} J_{N+2m}(a)J_m(b)\exp[i(N+2m)\eta] \tag{4.21}$$

where

$$a = \alpha_0\sqrt{\left(\boldsymbol{\epsilon}_1\cdot\boldsymbol{k}_N\cos\frac{\xi}{2}\right)^2+\left(\boldsymbol{\epsilon}_2\cdot\boldsymbol{k}_N\sin\frac{\xi}{2}\right)^2} \tag{4.22}$$

$$b = \frac{U_p}{2\omega}\cos\xi \tag{4.23}$$

$$\eta = \arctan\left[\tan(\phi_{k,\epsilon})\tan\left(\frac{\xi}{2}\right)\right] , \tag{4.24}$$

where ξ is the ellipticity of the field. Eq. (4.21) reduces to

$$J_N(a,b) = \sum_{m=-\infty}^{\infty} J_{N+2m}(\boldsymbol{\alpha}_0 \cdot \boldsymbol{k}_N) J_m\left(\frac{U_p}{2\omega}\right) \tag{4.25}$$

for linear polarization ($\xi = 0$) and

$$J_N(a) = J_N\left(\frac{\alpha_0}{\sqrt{2}} k_N \sin\theta_{k,\epsilon}\right) \exp[iN\phi_{k,\epsilon}] \tag{4.26}$$

for circular polarization ($\xi = \pi/2$), where $\theta_{k,\epsilon}$ and $\phi_{k,\epsilon}$ are the polar angle and azimuth of $\boldsymbol{k}_N$ in a coordinate system where $\boldsymbol{\epsilon}_1$ and $\boldsymbol{\epsilon}_2$ lie in the x-y plane. For general and asymptotic properties of the generalized Bessel functions and their significance in multiphoton processes see the works by Faisal (e.g. [68]), Reiss and Krainov [47, 216], Leubner [217, 218] as well as Dattoli et al. [219–221] (using the notation ${}^{(2)}J_N(a,-b) = J_N^{(-2)}(-b,a;1) = J_N^{(2)}(b,a;1)$ identical to $J_N(a,b)$ as defined here and $J_N(a,b,\eta) = {}^{(2)}J_N(a,-b;\exp[-i2\eta])\exp[iN\eta]$ [222]). For a recent review see Korsch et al. [223]. Analytically the generalized Bessel functions are obtained by Fourier transformation of the time dependent phase factors in the Gordon-Volkov wavefunctions corresponding to a monochromatic field.

The asymptotic time integral turns the time-dependent phase of Eq. (4.19) into the condition of conservation of energy:

$$\begin{aligned} S_{fi}^{(1)} = -2\pi i \sum_{N=-\infty}^{\infty} \delta\left(\frac{k^2}{2} + U_p + E_T - N\omega\right)(U_p - N\omega) J_N(a,b,\eta) \\ \times \langle\, \chi'_{\nu'}(R - R'_e) |\, \langle\, \boldsymbol{k} \,|\, \phi_i \,\rangle \langle\, \Phi_f | \Phi'_i \,\rangle\, |\, \chi_\nu(R - R_e) \,\rangle\ , \end{aligned} \tag{4.27}$$

where the dependence of the electronic wavefunctions on electronic and nuclear coordinates was dropped. Taking the absolute square of the amplitude by using Eq. (43) of [26], apart from the constant factors C^2 (see discussion below) and N_e, the differential rate of transition from the vibronic state of the neutral molecule with vibrational quantum number ν to the vibrational state labeled by ν' of the molecular ion by the absorption of N photons from a elliptically polarized field of intensity I_0 can be written as:

$$\begin{aligned} \frac{dW_{\nu',\nu}^{(f,i)}}{d\hat{\boldsymbol{k}}_N}(I_0) = 2\pi C^2 N_e k_N (N\omega - U_p)^2 J_N^2(a,b,\eta) \\ \times \left| \langle\, \chi'_{\nu'}(R - R'_e) |\, \langle\, \boldsymbol{k}_N \,|\, \phi_i \,\rangle\, |\, \chi_\nu(R - R_e) \,\rangle \right|^2\ , \end{aligned} \tag{4.28}$$

where

$$k_N = k_N(\nu', \nu) = \sqrt{2\left(N\omega - U_p - \left(E_{\nu'}^{(f)} - E_\nu^{(i)}\right)\right)}\ . \tag{4.29}$$

N_e denotes the number of equivalent electrons (neglecting spin) in the initial molecular orbital and $C^2 = (2k_T E_T/F)^{2Z/k_T}$ is the Coulomb correction factor [66, 172, 34] with $E_T \equiv k_T^2/2$ (see discussion at the end of section 3.3). F is the field strength and Z is the charge of the molecular ion in the final state. The constant factor that has been omitted in the expression for the differential rate is the overlap integral $\langle \Phi_f | \Phi_i' \rangle$ between initial and final electronic bound state wavefunctions, which is on the order of one.

The *total* IVI rate of the vibronic transition from a vibrational level ν of the electronic state i of the molecule into the level ν' of the electronic state f of the molecular ion, is given by integration of Eq. (4.28) over the ejection angles $\hat{\boldsymbol{k}}_N$ of the photoelectron and the summation over the number of photons N absorbed from the field at intensity I_0:

$$\Gamma_{\nu',\nu}^{(f,i)}(I_0) = \sum_{N=N_0}^{\infty} \int d\hat{\boldsymbol{k}}_N \frac{dW_{\nu',\nu}^{(f,i)}}{d\hat{\boldsymbol{k}}_N}(I_0) \;, \tag{4.30}$$

where N_0 is the minimum number of photons needed to be absorbed to allow the transition of interest, i.e. $N_0 = \lfloor (E_T + U_p)/\omega \rfloor_{\text{int.}} + 1$, which depends on the field intensity. When N_0 increases with rising intensity, one calls this the "closing of the N_0 photon channel" for the specific transition. The above formula for the total rate, Eq. (4.30), is valid both in the corresponding *multiphoton* ($\gamma = \sqrt{E_T/2U_p} \gg 1$, and in the *tunneling* ($\gamma \ll 1$) regimes of ionization. In the tunneling limit it is also possible to evaluate Eq. (4.30) approximately by, first, using the integral representation of the generalized Bessel function and evaluating it by the stationary phase method [224, 225], and next by replacing the sum over N by an integral over $1/\omega \; d(N\omega)$ (see e.g. [54] or [26]). From this it follows that the present S-matrix formalism predicts that even in the tunneling limit, it is the eigen-energy difference between the asymptotic initial and final vibronic states, which is the *transition* energy E_T defined above, rather than the difference with respect to the potential energy curves, which controls the IVI process.

In this S-matrix analysis, the R-dependence of the ionization rate enters through the variation of the molecular orbitals due to the changing location on the potential surface, while the transition energy E_T refers to the transition between two adiabatic vibronic states, which as such does not depend on R. The transition energy accounts not only for the difference in potential energy but also for the kinetic energy of the states. (This definition is also applied in [117] in combination with tunneling theory.) The R-dependence of the molecular orbitals makes the electronic ionization rate R-dependent too. This R-dependence of the electronic matrix element has early been identified to be a possible source of experimentally observed deviations from the pure Franck-Condon distribution in the case of electron-impact ionization [190].

The approaches based on ADK tunneling theory analyze the ionization process in terms of in-field molecular behavior, taking into account the effect of the field by con-

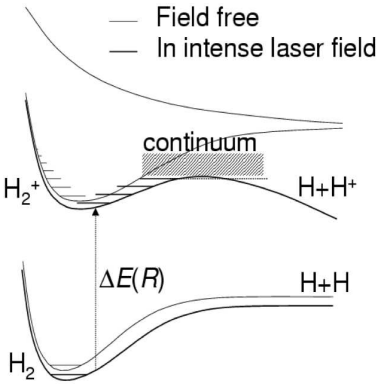

Figure 4.3.: Sketch of field distorted potential curves of the H_2/H_2^+ system in the ADK picture, taken from [184]

sidering the distortion of the molecular potential surfaces (for a sketch see Fig. 4.3) and by introducing an imaginary part to them. The imaginary part determines the decay of the states due to (tunneling) ionization.

In the terms of tunneling theory, the ionization rate depends on the internuclear separation R due to the R-dependence of the ionization potential (difference of electronic initial and final state potential curves) [108]. While the Franck-Condon approximation has been used also successfully for the calculation of total vibronic ionization rates in connection with tunneling theory [117], its formal foundation in the context of the tunneling picture is a matter of debate [108]. At first sight, the notion of a *sudden electronic transition* seems to be at odds with the finite time for the tunneling process that is assumed e.g. in the derivation of the Keldysh adiabaticity parameter (Eq. (2.7)). On the other hand, comparing the time scales for the processes, for 800 nm light the period of oscillation is 2.67 fs and thus, the electron is assumed to tunnel the potential barrier into a continuum state in less than 1.33 fs [45]. In the hydrogen molecule, showing the highest vibration frequency of all molecules, the period of vibration is 7.58 fs. First, this shows that, while the tunneling transition is surely not *sudden* on the typical time scale of the electron (1 a.u. = 24.2 as), it is still happening at least three times faster than the characteristic oscillation time of the neutral hydrogen molecule. This indicates that for the hydrogen molecule the transition is close to the border of being Franck-Condon like. Second, it shows that the in-field potential curves, that govern the tunneling theory analysis, are too rapidly changing to accommodate vibrational states of stationary nature. In fact, in tunneling theory only the contributions at times around maximum field amplitude are considered, as ionization rates peak nonlinearly with field intensity. Thus it is very interesting that the analysis in terms of in-field vibrational states on the field-bent potential curves produces good results [184], even though the states are very transient and diabatic transitions between in-field vibrational states

of like symmetry might be expected. The relative accuracy of the description on the basis of in-field vibrational states indicates, that the details of the anharmonic vibrational wavefunctions and their energetic shifts are not influencing the process dominantly.

4.3.2. Electronic Wavefunctions

In the molecular orbital (MO) description of wavefunctions for molecules, the electronic state of the bound system is given on the basis of a product wavefunction of orbital wavefunctions for individual electrons. This product wavefunction is antisymmetrized by forming a Slater determinant from the occupied orbital wavefunctions. Each orbital wavefunction for an individual electron is a product of a spin and a spatial part. The orbital wavefunctions are orthogonal to another, either due to orthogonality of the spatial or of the spin component. This constraint imposes the Pauli exclusion principle.

The determination of these orbital wavefunctions is the objective of quantum chemical calculations based on the Hartree-Fock method (see e.g. [226]). In these analytical functions of a suitable type are taken as an ansatz for the radial behavior of the orbitals, and a variational principle is used to adapt their parameters in such a way, that the total energy of the bound multi-electron system is minimized. From the analytical solutions for the radial wavefunctions of the Hydrogen atom, Slater-type orbitals (or exponential type orbitals) of the form $\phi(r) = c\exp(-ar)$ provide the best fit functions to model the radial behavior of any Coulombic bound system. The use these types of functions in the context of the Hartree-Fock method results in integrals over a product of four functions of this type (known as two-center, three- or four-electron integrals, [226]), that are hard to perform in a computationally efficient way. While lately there is considerable progress in the mathematical evaluation strategies for these integrals [227–232] and by now already two programs for quantum chemistry based on Slater-type orbitals have been published [233–235], the lions share of quantum chemical calculations is done on the basis of a modified ansatz for the radial functions, where a single Slater-type orbital is approximated by a superposition of a suitable number of so called "primitive" Gaussian functions with different exponents [236, 226]. The advantage of this procedure is, that the four center integral over Gaussian functions are equivalent to an integral over two Gaussians centered at separate places.

The molecular orbitals can be expressed as linear combinations of atomic orbitals:

$$\Phi(\boldsymbol{r};\underline{\mathbf{R}}_n) = \sum_{n=1}^{N_N}\sum_{j} b_{n,j}(R)\phi_{n,j}(\boldsymbol{r};\mathbf{R}_n)\ , \tag{4.31}$$

where $\boldsymbol{r}$ is the coordinate of the electron and $\underline{\boldsymbol{R}}_n$ are the coordinates of the N_N nuclei. The orbital coefficients $b_{n,j}$ can been obtained by a variational self consistent field

method employed e.g. in quantum chemical program codes such as GAMESS [237]. In the calculation of the mixed Gaussian and plane wave matrix elements in the S-matrix expression below, the recursions of Obara and Saika have been employed [238].

If the atomic orbitals are expressed as linear combinations of Cartesian Gaussians, the index j turns into set of indices $(i, \mathbf{m})$:

$$\Phi(\boldsymbol{r}; \underline{\mathbf{R}}_n) = \sum_{n=1}^{N_N} \sum_{i=1}^{N_g} \sum_{|\mathbf{m}|=0}^{l_{\max}} b_{n,i,\mathbf{m}}(R) \mathcal{G}(\mathbf{r} - \mathbf{R_n}; \mathbf{m}, \zeta_i) \ , \tag{4.32}$$

where N_g is the number of so-called "primitive" (i.e. uncontracted), unnormalized Cartesian Gaussian basis functions $\mathcal{G}$ and $\mathbf{m}$ is a three component multi-index running up to a length of total angular momentum $l_{\max}$ [226]. The parametrization of the corresponding Cartesian Gaussians is given by

$$\mathcal{G}(\mathbf{r} - \mathbf{R}; \mathbf{m}, \zeta_i) = (r_x - R_x)^{m_x} (r_y - R_y)^{m_y} (r_z - R_z)^{m_z} \exp\left[-\zeta_i (\mathbf{r} - \mathbf{R})^2\right] \ . \tag{4.33}$$

The Cartesian Gaussian functions are a simplification of the spherical Gaussian functions, that contain Cartesian prefactors instead of spherical harmonics [239]. They are the default basis functions of most quantum chemical programs. For brevity of notation, we adapt the general notation of Obara and Saika [238], representing the generic type of terms appearing in the evaluation of the Fourier integral over a single Cartesian Gaussian by the following bracket expression:

$$[\mathbf{q}|\mathbf{m}] = (-ik_x)^{q_x} (-ik_y)^{q_y} (-ik_z)^{q_z} \int d\mathbf{r} \, \exp\left[-i\mathbf{k}\mathbf{r}\right] \mathcal{G}(\mathbf{r} - \mathbf{R}; \mathbf{m}, \zeta) \ , \tag{4.34}$$

where $\mathbf{q}$ is a multi-index just like the multi-index $\mathbf{m}$. The index i of the Gaussian exponent ζ_i has been dropped to avoid confusion with the imaginary number. The objective of the recursion is to successively lower the exponents of the Cartesian factors $(\mathbf{r} - \mathbf{R})_\mu = \mathbf{r}_\mu - \mathbf{R}_\mu$ in the integral. In each step the maximal value of component $\mathbf{m}_\mu$ is reduced by one until all components are zero. This is achieved by repeated evaluation of the following formula that basically represents the result of an integration by parts with respect to the nuclear coordinate $\mathbf{R}$:

$$[\mathbf{q}|\mathbf{m}] = \frac{1}{2\zeta} \left([\mathbf{q} + \mathbb{1}_\mu | \mathbf{m} - \mathbb{1}_\mu] + (\mathbf{m}_\mu - 1)[\mathbf{q}|\mathbf{m} - 2\mathbb{1}_\mu] \right) \ . \tag{4.35}$$

Here, $\mathbb{1}_\mu$ denotes the μth column of the 3x3 identity matrix. When the reduction is complete, a trivial Fourier transformation over a Gaussian function is left at the center:

$$[\mathbf{q}|\mathbf{0}] = \left(\frac{\pi}{\zeta}\right)^{3/2} (-ik_x)^{q_x} (-ik_y)^{q_y} (-ik_z)^{q_z} \exp\left[-i\mathbf{k}\left(\mathbf{R} - \frac{i\mathbf{k}}{4\zeta}\right)\right] \ . \tag{4.36}$$

While this recursion is fairly trivial, it allows the evaluation of transition matrix elements containing single-electron wavefunctions of arbitrary quantum chemical quality, without restriction in the maximal angular momentum $l_{\max}$. Similar recursions have also been formulated for spherical Gaussian basis functions [240, 241].

When one electron is ionized, without further processes, its state in the orbital it originates from stays unoccupied. This orbital is called *the active orbital*. The orbital wavefunctions of the other electrons are modified slightly, since the electron-electron correlation with the formerly occupied orbital is not acting on them any longer. This change is considered to be small, when the active orbital is the outermost one, when comparing the radial dependence and the energetic ordering of the orbitals. This orbital is called the *highest occupied molecular orbital* (HOMO).

In recent experiments, it was possible to measure the probability density of the active orbital from the harmonic spectrum that is emitted when the ionized electron re-occupies the active orbital [242]. From this probability density it is encouraging to see that even in an intense laser field a strong similarity to the highest occupied molecular orbital of the undisturbed molecule is apparent. In the context of S-matrix theory the use of the field free molecular orbitals is justified on a completely other and rigorous basis, since they are used to describe the asymptotic initial and final bound electronic state.

4.3.3. Vibrational Wavefunctions

4.3.3.1. Diatomic Molecules

There are different approximations to the electronic potential that forms the one dimensional well for the nuclear vibrational motion. For small variations of the internuclear separation from the equilibrium distance, the potential can be approximated by a harmonic potential, corresponding to the leading quadratic term in the Taylor expansion of the potential about its minimum at $R = R_e$. The harmonic wavefunctions [243]

$$\psi_\nu(x) = \left(\frac{\gamma}{\pi}\right)^{\frac{1}{4}} (2^\nu \nu!)^{-\frac{1}{2}} e^{-\gamma x^2/2} H_\nu(\gamma^{\frac{1}{2}} x) \;, \quad \nu \in \mathbb{N}_0 \;, \tag{4.37}$$

with $\gamma = \mu\omega/\hbar$, are solutions to the Schrödinger equation corresponding to the one dimensional harmonic potential

$$V = \frac{1}{2} k x^2 = \frac{\hbar^2}{2\mu} \gamma^2 x^2 \tag{4.38}$$

where μ is the reduced mass of the two-particle system that is performing the stretching motion. $\omega/2\pi$ is the characteristic base-frequency of the vibration, corresponding to the force constant k. $x = R - R_e$ denotes the displacement of the nuclei from the

equilibrium separation R_e. The Hermite H_ν polynomials are defined as

$$H_\nu(z) = (-1)^\nu e^{z^2} \frac{d^\nu}{dz^\nu} e^{-z^2} \ , \quad \nu \in \mathbb{N}_0 \tag{4.39}$$

and thus the ground vibrational state $\nu = 0$ is a Gaussian distribution over the displacement x. The parity of the states under reflection $x \mapsto -x$ corresponds to the parity of the quantum number ν.

A higher order approximation to the internuclear binding potential is obtained by a heuristic anharmonic potential introduced by P. M. Morse [244], that takes into account the finite dissociation energy:

$$E_i(R) \approx E_i(R \to \infty) + D_e \left(e^{-2\alpha(R-R_e)} - 2e^{-\alpha(R-R_e)} \right) \tag{4.40}$$

$$= E_i(R_e) + D_e \xi^2 \ , \tag{4.41}$$

where ξ is frequently called the *Morse coordinate* and D_e is the *dissociation* or *bonding energy*:

$$\xi = 1 - e^{-\alpha(R-R_e)} = 1 - \frac{y}{2a} \tag{4.42}$$

$$D_e = E_i(R \to \infty) - E_i(R_e) \ . \tag{4.43}$$

The Morse wavefunctions, defined by this potential, are given by (e.g. [245])

$$\chi_\nu(x) = \sqrt{\frac{2\alpha q_\nu \nu!}{\Gamma(2a-\nu)}} \exp\left[-\frac{y(x)}{2} \right] y(x)^{q_\nu} L_\nu^{2q_\nu}(y(x)) \ , \tag{4.44}$$

where $L_\nu^{2q_\nu}$ are generalized Laguerre polynomials of degree ν and order $2q_\nu$. The parameters are

$$y(x) = 2a\, e^{-\alpha x} \text{ and } x = R - R_e \tag{4.45}$$

$$q_\nu = a - (\nu + \frac{1}{2}) \tag{4.46}$$

$$\alpha = \omega_e \sqrt{\frac{\mu}{2D_e}} \tag{4.47}$$

$$a = \frac{2D_e}{\omega_e} = \frac{\omega_e}{2\omega_e x_e} \tag{4.48}$$

and their energy eigenvalues follow the anharmonic law

$$E_{\text{vib},\nu} = -\omega_e x_e (j-\nu)^2 \tag{4.49}$$

$$= -D_e + \omega_e(\nu + \frac{1}{2}) - \omega_e x_e (\nu + \frac{1}{2})^2 \tag{4.50}$$

where $\omega_e x_e$ is the so called anharmonicity constant (see e.g. [246]), and $\nu \in \{0, \ldots, \lfloor j \rfloor\}$, with $j = a - \frac{1}{2}$. Thus, the discrete vibronic energy levels of a diatomic, vibrationally anharmonic molecular system can be written as

$$E_{i,\nu} = E_i(R \to \infty) + E_{\mathrm{vib},\nu} \tag{4.51}$$

$$= E_0 + \frac{D_e}{a^2}(2j\nu - \nu^2) \tag{4.52}$$

$$= E_0 + \omega_e \nu - \omega_e x_e \nu(\nu + 1) \ , \tag{4.53}$$

where E_0 is the sum of the energy of the electronic state and the vibrational zero-point energy. The values for the constants are determined by numerical fits to data obtained by molecular spectroscopy (e.g. [247] for H_2/H_2^+). For homonuclear diatomic molecules, the nuclei vibrate symmetrically with respect to the center of mass but for heteronuclear diatomic molecules the ratio of masses breaks this symmetry.

4.3.3.2. Polyatomic Molecules

Vibrations of molecules with more than two atomic centers have long provided a challenge for efficient theoretical description. The first and most obvious point is the choice of coordinates. There are several sets of so called *internal coordinates* proposed, that are defined in terms of internuclear separations and angles (for an overview and latest developments see e.g. [248–250]). These are specifically adapted to the molecule at hand, as well from the geometric aspect as from the aspect of resulting in a decoupled expression for the potential energy. But they come at the price of coupling in the kinetic energy operator.

The oscillations of the molecule, that are coupled in the internal coordinates, can be decoupled by transformation to *normal coordinates* [210]. I.e. the operator of kinetic energy has a diagonal representation in them [251]. In the harmonic approximation (see below) the potential energy operator decouples as well. These decoupled vibrations are called *normal modes* and are widely used as a nomenclature for the vibrational state of a molecule. The normal mode vibrations have two characteristic features: first, the local bond vibrations are phase-locked with respect to each other, i.e. either they are either in phase (symmetric modes) or out of phase by π (anti-symmetric modes) with respect to each other. Second, for each separate mode all local bond vibrations have the same frequency. These two constraints ensure that the center of mass stays fixed. Apart from their general use as an analytic tool, they are well adapted e.g. for the description of symmetric linear triatomic molecules, where the oscillations of both bonds are in resonance [252, 253]. For higher excited states of bonds between strongly asymmetric mass distributions on the other hand, local mode vibrations in anharmonic potentials are found to be more suitable [254–257].

The choice of coordinates also has an effect on the general quality of the basis functions that are introduced to describe the vibrational states. The most straight

forward basis functions are of direct product or Hartree type

$$\Phi_{i_1,i_2,\ldots,i_f} = \phi_{i_1}(q_1)\phi_{i_2}(q_2)\ldots\phi_{i_f}(q_f) \tag{4.54}$$

where q_k are the displacement coordinates corresponding to the f vibrational degrees of freedom. It can be shown [210] that the vibrational wavefunction decouples like this in the normal coordinate representation. In the general case the vibrational wavefunction is constructed as a superposition of these basis functions.

In first approximation the potential energy surface that determines the molecular motion is assumed to be of harmonic form about the point of equilibrium for each coordinate. Higher terms in the expansion of the potential introduce coupling between the normal mode vibrations, which may be treated in a perturbative way [210]. These terms become important for higher excited vibrational states, which cover internuclear distances that are not infinitesimal in the sense of the harmonic approximation. For the determination of eigenstates of the nuclear vibrational Hamiltonian several schemes have been developed, e.g. perturbative methods and strategies similar to those used in electronic quantum chemistry, such as the Vibrational Self Consistent Field (VSCF) [258] or Vibrational Multi-Configuration Self-Consistent-Field (V-MCSCF) [259] methods. Some of these systematic approaches are already available as software packages [260] to take into account the coupling terms. Additionally to the general ab-initio calculations, approaches have been made to decouple vibrational modes that act on different time scales by adiabatic treatment [261].

In the case of triatomic molecules the coupling between the normal modes can be avoided by the choice of curvilinear internal coordinates (Jacobi, Radau and hyperspherical coordinates), that are as well orthogonal in the sense that the kinetic energy operator decouples [262]. E.g. for H_2O Radau coordinates are a good choice [263] as the momentum of inertia of the central atom is much larger than that of the two hydrogen atoms. Lately, there is renewed interest in *variable curvature* [264] or *generalized internal* vibrational coordinates [248] that are parametrically adaptable and comprise the Jacobi, Radau and hyperspherical coordinates as special cases, but are not necessarily orthogonal in the kinetic energy.

In the approximation of the potential energy surfaces beyond the harmonic model Morse potentials have been successfully employed [265] for the stretching coordinates [266] of linear (HCN [267, 268], CO_2 [269]) as well as bent triatomic molecules (e.g. H_2O [270, 263, 271, 248] and N_2O [272, 269, 273]). These result in higher (usually up to fourth) order expansions of the potential in terms of *Morse coordinates* [269]. These potentials represent generalizations of the usual Morse potential (Eq. (4.40)), as they are higher order expansions of the potential in terms of the Morse coordinates (Eq. (4.42)) that have the property to asymptotically reach the value of 1 as the linear displacement of respective valence coordinate goes to infinity in the limit of dissociation. For the bending motion the Pöschl-Teller potential (one possible generalization of the Morse potential [274, 275]) is frequently chosen. For comparative studies of different empirical internuclear potentials see [276, 277].

Since Franck-Condon factors are very significant for the analysis of molecular spectra, techniques for their evaluation for polyatomic molecules have been developed first for harmonic potentials [278, 279] and later, after significant research on the algebraic treatment of anharmonicity in polyatomic molecules [280, 254, 281], as well for anharmonic potentials (e.g. the *vibron model* [282–284]). While these techniques are strive for efficient evaluation in the polyatomic case, the basic matrix elements for Morse wavefunctions already have been obtained much earlier [285].

4.3.4. Rate Equations and Transition Yields

Using the LCAO description of the electronic wavefunction above, the expression (4.28) for the ionization rate into a specific vibrational state of the molecular cation can be written as:

$$\frac{dW^{(f,i)}_{\nu',\nu}}{d\hat{\boldsymbol{k}}_N}(I_0) = 2\pi C^2 N_e k_N (N\omega - U_p)^2 J_N^2\,(a,b,\eta) \tag{4.55}$$
$$\times \left| \sum_{n=1}^{2} \sum_{j} \langle\, \chi'_{\nu'}(R - R'_e)\,|\, b_{n,j}(R) \exp\left[-i\boldsymbol{k}_N \cdot \hat{\mathbf{R}}_n \frac{\mu R}{m_n} \right] |\, \chi_\nu(R - R_e)\,\rangle \tilde{\phi}_{n,j}(\boldsymbol{k}_N) \right|^2$$

in the center of mass frame of the molecule, where the vector $\frac{\mu R_e}{m_n}\hat{\mathbf{R}}_n$ points to the equilibrium position of the nth nucleus in the initial electronic state and μ denotes the reduced mass of the molecular system. $\tilde{\phi}_{n,j}(\boldsymbol{k}_N)$ is the Fourier transform of the atomic orbital $\phi_{n,j}$ (see section 4.3.2). The magnitude $|\mathbf{k}_N|$ of the electron momentum after the absorption on N photons is given by Eq. (4.29).

The orientation of the molecule in space is determined in Eq. (4.55) by the unit vectors $\hat{\mathbf{R}}_n = \pm\hat{\mathbf{R}}$. For diatomic molecules, the orientations of the body-fixed frames (with the molecular axis chosen along the polar axis) of an ensemble of molecules can be taken into account by averaging over their distribution in the space-fixed laboratory frame. In the theoretical results presented below, a random distribution of the molecular axes is generally assumed and the orientation averaging is carried out, unless stated explicitly otherwise. Finally to obtain total ionization rates for a given vibronic transition, the differential rate (4.55) was integrated over all emission directions and summed over all contributing photon orders according to Eq. (4.30). The order of integration was chosen this way to obtain physically meaningful results in each step as well as to minimize evaluation of the **k** dependent orbitals:

$$\Gamma^{(f,i)}_{\nu',\nu}(I_0) \equiv \sum_{N=N_0}^{\infty} \int d\Omega_{\mathbf{k}_N} \frac{1}{4\pi} \int d\Omega_{\mathbf{R}} \frac{dW^{(f,i)}_{\nu',\nu}}{d\hat{\boldsymbol{k}}_N}(I_0, \hat{\mathbf{R}}) \tag{4.56}$$
$$= \sum_{N=N_0}^{\infty} \int_0^1 d\cos\vartheta_k \int_0^{2\pi} c(\varphi_k) d\varphi_k \frac{1}{4\pi} \int_0^1 d\cos\vartheta_R \int_{\varphi_k}^{\varphi_k+\pi} d\varphi_R \frac{dW^{(f,i)}_{\nu',\nu}}{d\hat{\boldsymbol{k}}_N}(I_0, \hat{\mathbf{R}})\ ,$$

where $c(\phi_k)$ is a characteristic function that chooses the interval of integration according to the symmetry of the ionized orbital e.g. $c(\varphi_k) = 2\pi\delta(\varphi_k)$ for a σ orbital and $c(\varphi_k) = 2\Theta(\pi - \varphi_k)$ for an orbital of π symmetry.

In order to compare the predictions of the theory with experimental data one needs to consider the fact that the experimental data for IVI are obtained as production rates or *yields* of ions generated in the focus of a pulsed laser beam. The gas jet transversing the focus provides an initial ensemble of neutral target molecules that interact with the laser field during a time interval of the order of the pulse duration, and within a spatial volume of the order of the focal volume. The IVI yield distributions, therefore, are constructed by substituting the basic theoretical rates of the IVI transitions (*single molecule response*) into the rate equations that govern the relative populations of interest. The normalized yield distributions are then obtained, at a given point in the laser focus, by integrating the rate equations over the time-profile of the laser pulse and adding the contributions from all the points within the focus (see e.g. [37]).

The rate equations for the normalized populations in the final vibrational channels are given by [202]:

$$\frac{dN_{\nu'}^{(f)}(t)}{dt} = \Gamma_{\nu',0}^{(f,X)}(I_0(\boldsymbol{r},t)) \left(1 - \sum_{\nu'} N_{\nu'}^{(f)}(t)\right), \tag{4.57}$$

where it is assumed that the target molecule is initially prepared in the lowest vibrational level ($\nu = 0$) of its electronic ground state ($i = X$). Furthermore the analysis is restricted to one specific final electronic state; contributions from ionization to any higher charge states and/or possible fragments are not considered. In actual computations, the rate equations were solved assuming a typical Gaussian temporal laser pulse profile with an (experimentally given) pulse length τ centered around $t = 0$ [82]. The results are integrated over the spatial intensity distribution of a Gaussian TEM_{00} mode [286], characterized by the (experimentally given) peak pulse intensity, I_0, the beam waist, and the Rayleigh length of the beam.

4.4. S-Matrix analysis of Non-Franck-Condon Distributions in Small Diatomics

4.4.1. Comparison with Experimental Data

The results of the calculations are discussed on a relative scale, as usual for processes induced by strong laser fields. This is done for the sake of comparison with experimental data, which is given on relative scales due to a *minimal* uncertainty of about 10% in the determination of peak laser intensities at the precision achievable with current experimental techniques [287]. Additionally the initial total number of

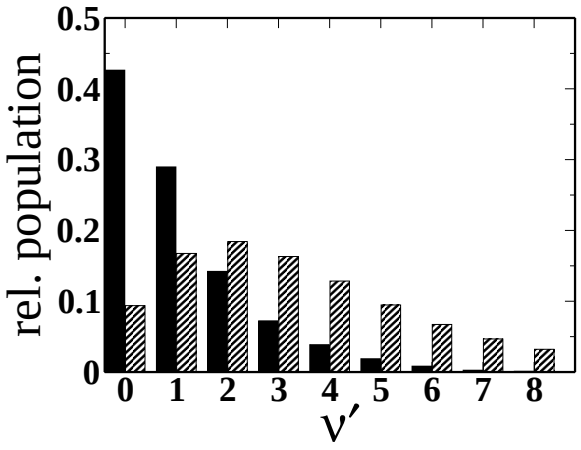

Figure 4.4.: Comparison of the calculations of the IVI yield distribution (normalized to the total ion yield of all vibrational channels) of the different vibrational levels of H_2^+ (solid bars) and the corresponding Franck-Condon distribution (hatched bars) [215]. Laser parameters: $\lambda = 800\,\text{nm}$, $I_0 = 3\times10^{13}\,\text{W/cm}^2$ and $\tau = 45\,\text{fs}$.

molecules in the focus of the laser pulse can usually only be estimated on a statistical basis from the experimental conditions.

In Fig. 4.4 the result of a calculation (solid bars) for the IVI distribution of population in different vibrational levels of the H_2^+ ion [215] is presented. The orientation of the internuclear axis for the ensemble of molecules has been assumed to be random and an averaging over the orientations was carried out. For reference the Franck-Condon overlap distribution for the present transition [189] are included in the figure (hatched bars). The figure reveals a strong difference between the calculated IVI distribution and the Franck-Condon overlap integrals. While the present result shows a maximum at $\nu' = 0$ followed by a continuous decrease toward the higher levels, the Franck-Condon distribution is peaked at $\nu' = 2$ and decreases only slowly. As a consequence, the Franck-Condon distribution strongly underestimates the laser induced populations in the two lowest vibrational levels, and systematically overestimates those from the third level onwards. This is similar to a strong shift toward the lower excitation levels as predicted theoretically earlier [108, 202, 288, 184] and observed in the experiment [184] subsequently.

Fig. 4.5 compares the results of the present theory (solid bars) to the experimental data of Urbain et al. (hatched bars, [184]) at two different wavelengths (a-c: 800 nm, d: 1064 nm) and four different peak laser intensities: (a) $I_0 = 3\times10^{13}\,\text{W/cm}^2$, (b) $I_0 = 4.8\times10^{13}\,\text{W/cm}^2$, (c) $I_0 = 1.5\times10^{14}\,\text{W/cm}^2$, and (d) $I_0 = 10^{14}\,\text{W/cm}^2$. A shift toward the lowest vibrational states is clearly present in all the cases shown in the figure. Although the calculated individual heights are not quite the same, the major characteristics of the theoretical results, including the monotonic decrease of the heights with increasing vibrational excitation in case (a), and the occurrence of a

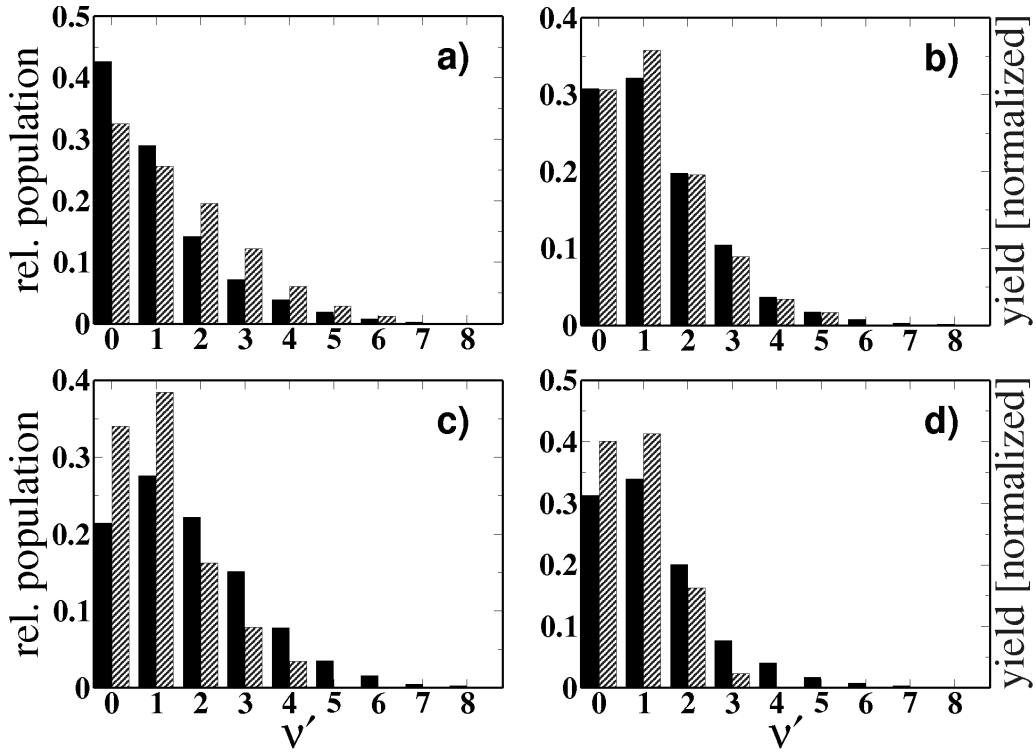

Figure 4.5.: Comparison of the normalized populations (branching ratios) of the vibrational levels in H_2^+ (solid bars) [215] with the normalized experimental yields taken from [184] (hatched bars). Laser parameters are: a) – c) $\lambda = 800\,\text{nm}$, $\tau = 45$ fs at $I_0 = 3{\times}10^{13}\,\text{W/cm}^2$ (panel a), $I_0 = 4.8{\times}10^{13}\,\text{W/cm}^2$ (panel b) and $I_0 = 1.5{\times}10^{14}$ W/cm^2 (panel c); d) $\lambda = 1064\,\text{nm}$, $\tau = 6\,\text{ns}$ at $I_0 = 10^{14}\,\text{W/cm}^2$.

peak-reversal in the cases (b), (c) and (d) are fully consistent with the experimental data. More specifically, the theory correctly reproduces the position of the maximum in every distribution (a) to (d), namely in 800 nm radiation at the lowest intensity (Fig. 4.5 a), it occurs at $\nu' = 0$, while in all the other cases the maximum is located at $\nu' = 1$, both in the experimental data as well as in the theoretical results.

The dominant population of the vibronic ground state in the calculation occurs in the interval of intensity between $2.5{\times}10^{13}\,\text{W/cm}^2$ and $4.1{\times}10^{13}\,\text{W/cm}^2$ for 800 nm (see right panel of Fig. 4.6). This peak reversal is due to *channel closing* effects in the transition rates [289] that can be seen in the left panel of Fig. 4.6. As the intensity of the laser is increased, the increasing ponderomotive energy of the continuum states is rising the necessary energy for a transition. At some point the minimal number of photons $N_0(I_0, I_p, \nu, \nu')$ that used to be sufficient does not cover the increased transition energy any longer and the N_0-photon channel for the ionization process closes. This first affects the higher excited states, as also visible in the calculated rates. In a laser pulse, there is a spatio-temporal distribution of intensities is the focal

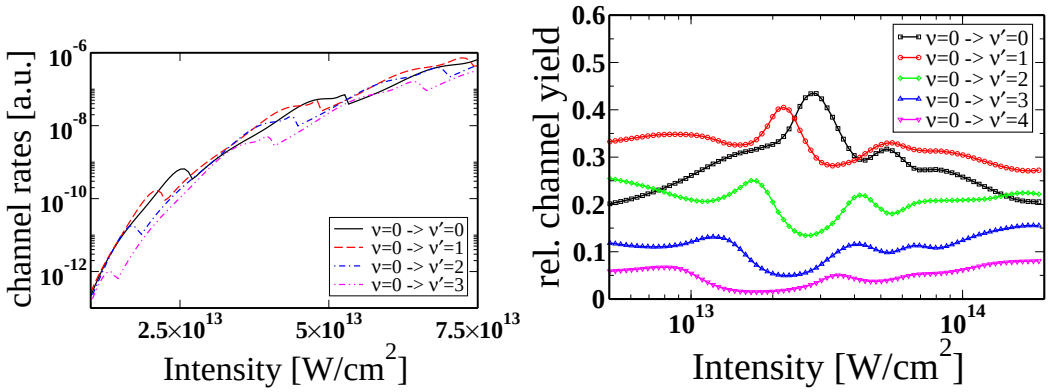

Figure 4.6.: Predicted intensity dependence of the IVI process for the transitions to the ground and first few excited vibrational states of H_2^+ due to ionization of H_2 in vibronic ground state by a linearly polarized laser with a carrier frequency of 800 nm.
Left: Calculated transition rates to different final states. Right: Normalized calculated transition yields obtained in a Gaussian laser pulse of 45 fs duration (logarithmic intensity scale) .

volume, which is integrated over to obtain ionization yields that are comparable with experimental results. Nevertheless, as can be seen from Fig. 4.6 as well as from the experimental results [212, 184], there is an accumulated signature of this detectable in the yields, leading to the *peak reversal* in an intensity interval slightly above the intensity of the first channel closing for the $\nu' = 0$ state in the presented intensity window. The next channel closing only brings the population of the $\nu' = 1$ state close to the one of the $\nu' = 0$ state, without surpassing it.

Fig. 4.7 shows the variation of the transition rates to the first few vibrational states as a function of the laser wavelength at a given intensity, clearly showing the importance of channel closing effects for the final vibrational state. It is interesting to note that for increasing wavelength the second excited state, which is dominant in the Franck-Condon distribution, is predicted to be predominantly less populated than the zeroth and first excited state. The decrease of the photon energy has the tendency to separate the contributions of the different vibronic ionization channels. Even though for longer wavelengths the Keldysh parameter is reaching the tunneling regime already at this moderate intensity, this wavelength dependent picture is beyond the predictive scope of tunneling theory (section 2.1.2) and can currently only be obtained by the S-matrix theory discussed in sections 3.3 and 4.3.

The remaining difference between the experimental and the calculated yields apparent in Fig. 4.5 might be due to two reasons: First, there is an estimated uncertainty of about 20% in the measurement of the peak intensity in the *current* experimental data [184]. In the calculations we have noted that the actual heights

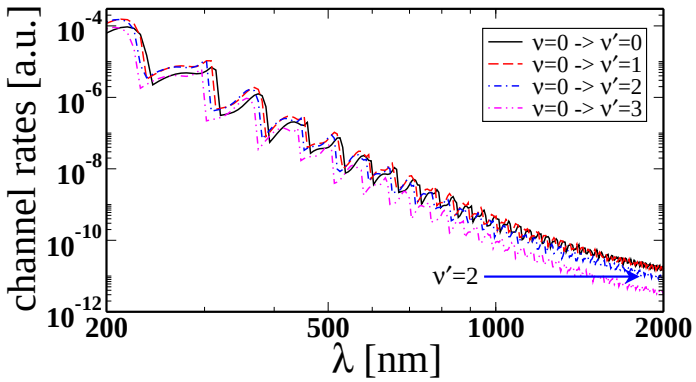

Figure 4.7.: Calculated wavelength dependence of the IVI transition rate to the ground and first few excited vibrational states of H_2^+ due to ionization of H_2 in vibronic ground state by a linearly polarized laser at an intensity of $I_0 = 3 \times 10^{13}\,\mathrm{W/cm^2}$.

are sensitive to the peak intensity of the laser (cf. Fig. 4.6, right hand panel). Second, a possible effect of fragmentation or dissociation of the hydrogen molecular ion is not taken into account in the computations. In fact, Urbain et al. [184] have pointed out that depending on the orientation of the molecular ion and the laser intensity, a possible dissociation of the ion into a proton and a hydrogen atom may occur from the higher vibrational states of the ion. This could lead to a depletion of the higher vibrational levels in the experiment and might also be responsible for the overestimations by the present calculations (cf. Fig. 4.5c and d) which neglect a possible fragmentation or dissociation induced effect.

The calculated distributions depend on the choice of the vibrational wavefunctions. The influence can be seen from Fig. 4.8, where a comparison is shown between the IVI distributions obtained with the Morse wavefunctions (solid bars) and with the simple harmonic oscillator wavefunctions (hatched bars). The results from the calculations with the harmonic oscillator wavefunctions show a considerably weaker shift toward lower vibrational states than those obtained from the Morse wavefunctions. This is not only a quantitative difference but also can lead to a qualitative change. For example, the shift of the position of the distribution maximum from $\nu' = 1$ to $\nu' = 0$ at the lowest field intensity (cf. Fig. 4.8a) is not reproduced by the simple harmonic oscillator wavefunctions. This is due to the delicate dependence of the channel closings on the total transition energies, which are different for the equally spaced harmonic states and the energy shifted anharmonic ones.

4.4.2. Alignment and Polarization Effects

It has been shown recently (e.g. [290, 37]) that for diatomic molecules both the total ionization rates and the photoelectron angular distributions depend on the ori-

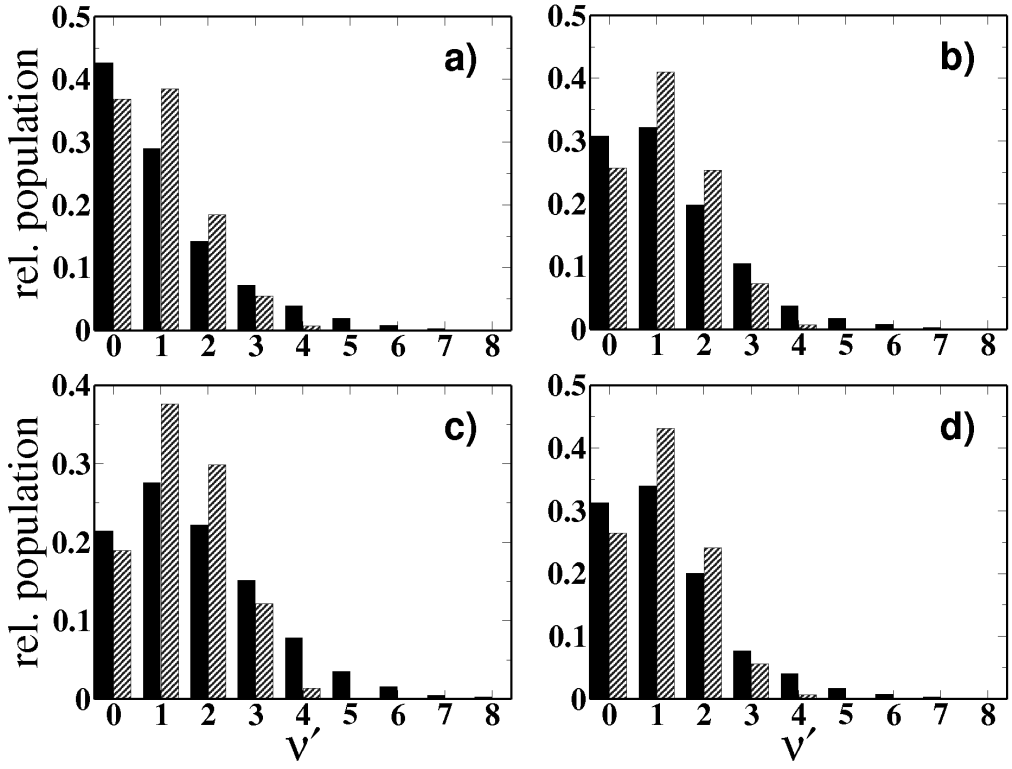

Figure 4.8.: Effect of the choice of vibrational wavefunctions on the predicted populations in the molecular H_2^+ ion. Shown is a comparison between the results obtained with Morse (solid bars) wavefunctions and harmonic oscillator wavefunctions (hatched bars) [215]. Laser parameters are the same as in Fig. 4.5.

entation of the internuclear axis. In contrast, in the present calculations (and in agreement with results from the static field theory [184]) it is found that the effect of the alignment of the molecule is rather small or negligible for the IVI populations in the vibrational levels of the hydrogen molecular ion (at least as long as the fragmentation channels can be considered to be rather improbable). This is exemplified in Fig. 4.9, where the results for the alignment of the internuclear axis, parallel and perpendicular to the direction of (linear) polarization of the laser, are compared. It can be seen that the distributions hardly differ in the two cases.

Please note again that relative populations are compared, which does not reflect that the absolute ionization yields vary with the degree of alignment of the internuclear axis with respect to the polarization of the field [37]. While the coupling to the field strongly determines the direction of emission of the ionized electron, the probability of which depends on the symmetry of the molecular orbital, the field does not directly couple to the internuclear relative coordinate in the leading order of the S-matrix expansion for this process. This term corresponds to a physical process where only the active electron interacts with the field and shares the above threshold

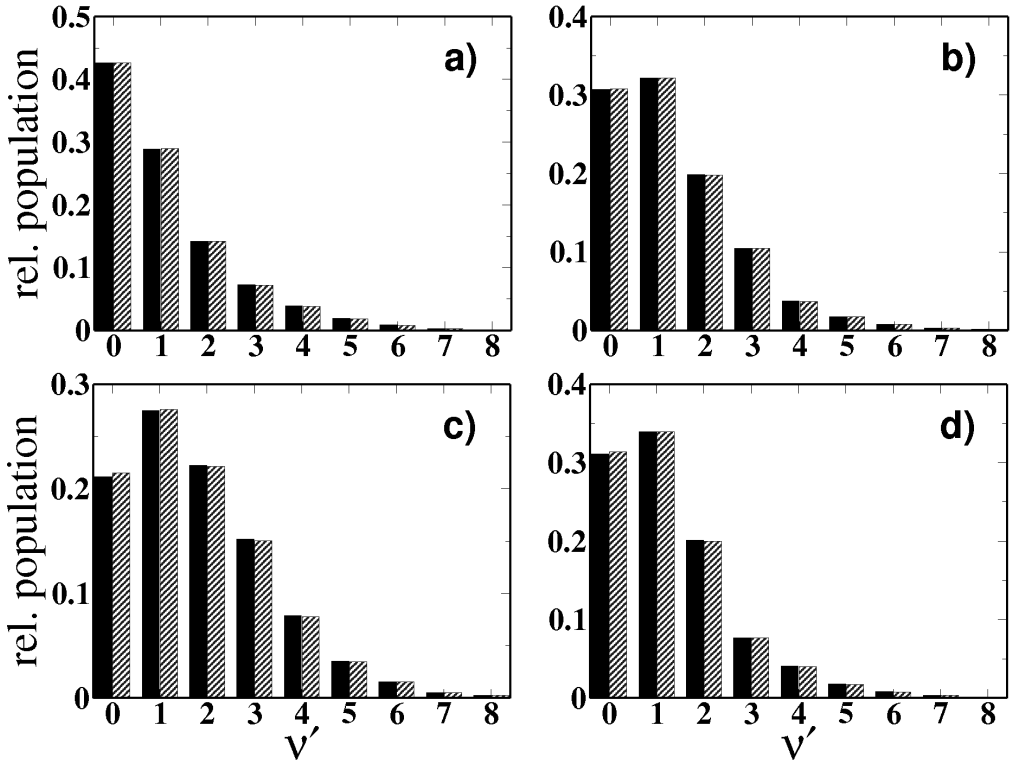

Figure 4.9.: Comparison of the IVI populations for the alignment of the internuclear axis parallel (solid bars) and perpendicular (hatched bars) to the laser polarization direction [215]. Laser parameters are the same as in Fig. 4.5.

part of the absorbed energy with the parent molecular ion. This energy transfer is isotropic, while the directed momentum transfer between electron and the molecular ion is of minor importance (see discussion in section 4.4.4) in intense-field multiphoton ionization. Thus, the mutual alignment of field and molecular axis has no direct effect on the vibrational dynamics.

To check the possible effect of the laser polarization on the IVI distributions calculations with circular polarization of the laser field have been performed. In Fig. 4.10 the calculated IVI yields are shown at the same intensities and frequencies of the laser as in the case of linear polarization (Fig. 4.5). Interestingly, for circular polarization the dominant population is found to be in the vibronic ground state $\nu' = 0$, not only for a limited interval of intensities, but increasingly also for all intensities below a certain threshold intensity, $I_0 = 8.2{\times}10^{13}\,\mathrm{W/cm^2}$ for 800 nm (see Fig. 4.11), or $I_0 = 1.04{\times}10^{14}\,\mathrm{W/cm^2}$ for 1064 nm. As a result, while a channel closing effect apparently accounts for the peak reversals in the case of linear polarization (see Fig. 4.6 [289]), in the circular polarization case the vibronic ground state of the molecular ion is favored for all intensities below the above mentioned thresholds.

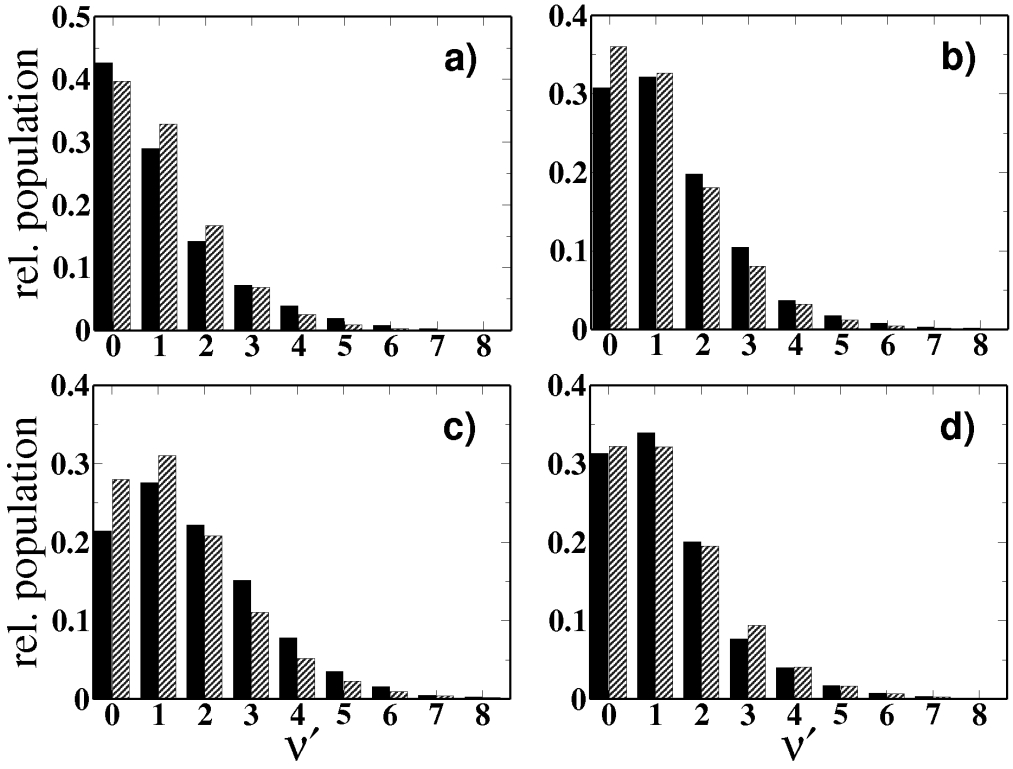

Figure 4.10.: Comparison of the IVI populations for linear (solid bars) vs. circular polarization (hatched bars) of the laser light [215]. Laser parameters are the same as in Fig. 4.5.

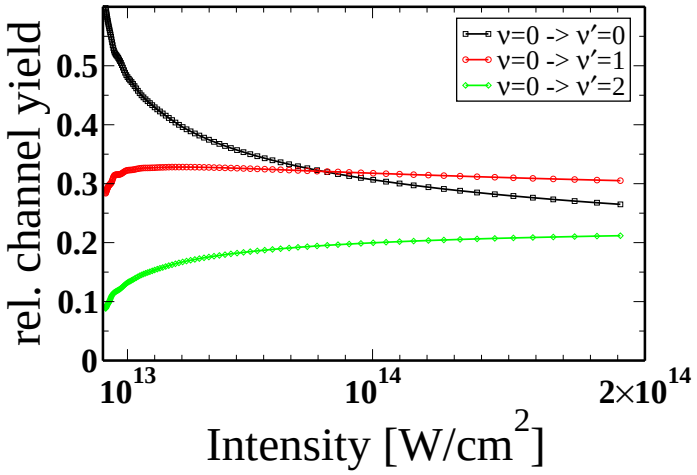

Figure 4.11.: Intensity dependence of the normalized yields for the IVI transitions to the ground and first two excited vibrational states of H_2^+ due to ionization of H_2 in a circularly polarized Gaussian laser pulse of 45 fs duration and 800 nm carrier frequency.

4.4.3. Origin of the Shift to Lower Vibrational States

In order to analyze the origin of the stronger population of lower vibrational levels than in the Franck-Condon distribution, first it has been investigated whether the overlap approximation is violated in this process. In the expression for the differential IVI rate (Eq. (4.55)), the electronic and the vibrational matrix elements are coupled by two factors that depend on the internuclear distance R, namely the molecular orbital coefficients, $b_{n,j}(R)$, and the dynamical phase of the atomic orbitals appearing in the exponential function. In order to analyze the influence of both these factors, the MO coefficients were treated as constants in a first step, evaluated at the molecular equilibrium separation, while the dynamical phase was allowed to vary with R. In this approximation the IVI rate is given by the formula

$$\frac{dW^{(f,i)}_{\nu',\nu}}{d\hat{\boldsymbol{k}}_N}(I_0) \approx 2\pi C^2 N_e k_N (N\omega - U_p)^2 J_N^2\,(a,b,\eta) \tag{4.58}$$
$$\times \left| \sum_{n=1}^{2} \sum_{j} b_{n,j}(R_e)\tilde{\phi}_{n,j}(\boldsymbol{k}_N) \langle\, \chi'_{\nu'}(R-R'_e)\,|\exp\left[-i\boldsymbol{k}_N\cdot\hat{\mathbf{R}}_n\tfrac{\mu R}{m_n}\right]|\,\chi_\nu(R-R_e)\,\rangle \right|^2$$

This approximation for a transition from the vibrational ground state is the special case of the general Franck-Condon approximation to locate transitions at the points of maximal wavefunction amplitude. A theoretically more accurate option for excited vibrational initial states is to take the r-centroids [291, 292] as the radii of transition, which are the expectation values for the internuclear distance for a specific vibrational transition (instead of for a single vibrational state). These have been shown for harmonic as well as for Morse potentials to be the distances, where it is consistent to assume vertical (Franck-Condon) transitions to occur [293, 294].

Fig. 4.12 compares results obtained within this assumption from the above equation to those from the full calculations, Eq. (4.55). As can be seen, in all cases considered, the shift toward the lowest vibrational levels is somewhat smaller in the calculations with the 'frozen' MO coefficients, however, the distinct differences to the Franck-Condon distribution, the shift toward lower vibrational states and the reversal of the peak position, are still present.

To analyze the effect of the variation of the dynamic phase factor of the atomic orbitals, with the internuclear distance R, for the specific case of ionization of a homonuclear diatomic molecule from its ground state Eq. (4.58) can be rewritten as [295, 37, 100]:

$$\frac{dW^{(f,i)}_{\nu',\nu}(I_0)}{d\hat{\boldsymbol{k}}_N} = 2\pi C^2 N_e k_N (N\omega - U_p)^2 J_N^2\,(a,b,\eta) \left|\tilde{\phi}(\boldsymbol{k}_N)\right|^2 \tag{4.59}$$
$$\times \underbrace{4\langle\, \chi'_{\nu'}(R-R'_e)\,|\cos[\arg(\tilde{\phi}(\boldsymbol{k}_N)) + \boldsymbol{k}_N\cdot\mathbf{R}/2]\,|\,\chi_\nu(R-R_e)\,\rangle^2}_{\left|t_{\nu',\nu}(\boldsymbol{k}_N)\right|^2}$$

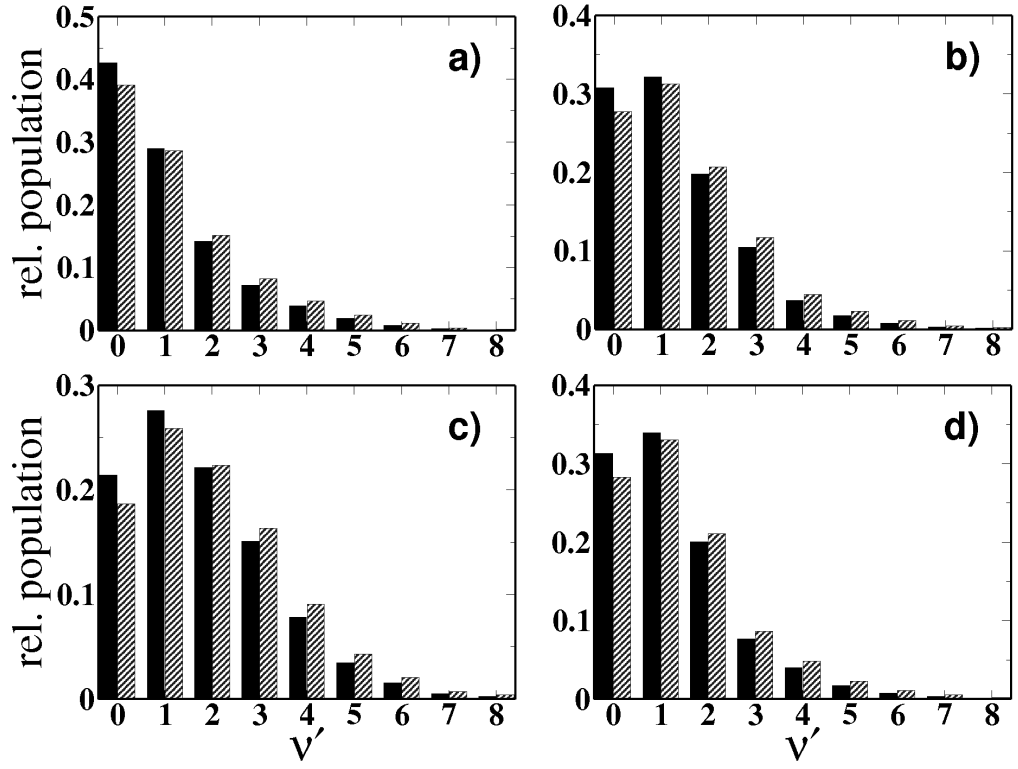

Figure 4.12.: Comparison of the vibrational populations in the molecular H_2^+ ion as obtained from S-matrix calculations with fully R-dependent molecular orbitals (solid bars) and with fixed molecular orbital coefficients (hatched bars) [215]. Laser parameters are the same as in Fig. 4.5.

where

$$\tilde{\phi}(\boldsymbol{k}_N) = \sum_j b_j(R_e) \langle\, \boldsymbol{k}_N | \phi_j(\boldsymbol{r}; -\mathbf{R}_e/2) \,\rangle \tag{4.60}$$

is the Fourier transform of the part of the molecular wavefunction localized at the nucleus at $\mathbf{R}_1 = -\mathbf{R}_e/2$ and $\hat{\mathbf{R}}_e$ points along the molecular axis away from that nucleus.

In the overlap approximation it is assumed that the electronic $\boldsymbol{k}$ dependence decouples in the matrix element between the vibrational wavefunctions, and reduces the latter to:

$$|t^{(FC)}_{\nu',\nu}(\boldsymbol{k})|^2 = 4\cos^2[\arg(\tilde{\phi}(\boldsymbol{k}_N)) + \boldsymbol{k}_N \cdot \mathbf{R}_e/2] \langle\, \chi'_{\nu'}(R - R'_e) \,|\, \chi_\nu(R - R_e) \,\rangle^2 \tag{4.61}$$

In Fig. 4.13 we present the ratio of the partial matrix element $|t_{\nu',0}(\boldsymbol{k})|^2$ to $|t^{(FC)}_{\nu',0}(\boldsymbol{k})|^2$, averaged over all angles of electron ejection, $\hat{\boldsymbol{k}}$, as a function of k and for different vibrational numbers ν'. As can be seen from the figure, the ratio is close to 1 for small values of k. This may be simply understood from the leading constant term of

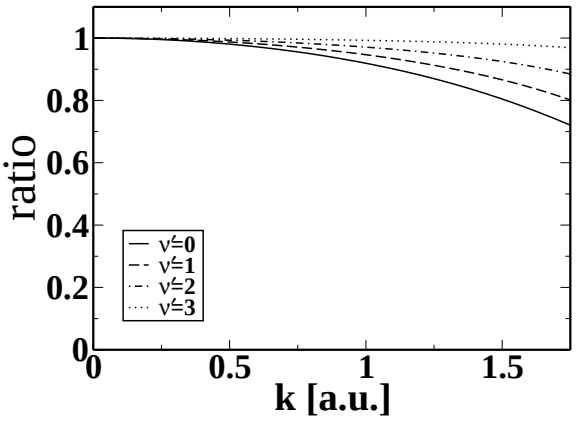

Figure 4.13.: Variation of the ratio $|t_{\nu',0}(\boldsymbol{k})|^2$ to $|t^{(FC)}_{\nu',0}(\boldsymbol{k})|^2$ as a function of $\boldsymbol{k}$ for different ν' (see legend) [215].

the Taylor expansion of the phase factor. Thus, since the rate of laser induced ionization is dominated by the emission of slow electrons, the conditions for the overlap approximation should be well fulfilled in the present case (cf. Fig. 4.13). To check the expectation, test calculations were performed where the term $|t_{0,\nu'}(\boldsymbol{k})|^2$ was replaced by $|t^{(FC)}_{0,\nu'}(\boldsymbol{k})|^2$ in Eq. (4.58). Fig. 4.14 shows the results of these calculations. As can be seen from the figure the results (hatched bars) are nearly identical. Deviations can occur however in case higher kinetic energies are observed. This is e.g. the case for X-ray Raman scattering from core excited CO, where typical photoelectron energies are above 300 eV and thus $\boldsymbol{k}R \geq 1$. A generalized Franck-Condon (GFC [296]) approximation has been proposed for this case, which includes the dynamic variation of the photoelectron phase terms.

Combined with Fig. 4.12 this shows, that the overlap approximation, which has been assumed before in S-matrix calculations in an *ad hoc* way [202, 289], is a qualitatively good approximation at the present field parameters. Therefore, the main cause for the shift in the distribution of the IVI transition probabilities to lower vibrational quantum numbers, deviating from the Franck-Condon distribution, lies in the nonlinear dependence of the ionization rate on the transition energy $E_T = E^{(f)}_{\nu'} - E^{(i)}_{\nu}$. As has been noted before [202, 289] and as can be seen from Fig. 4.15, the increase of the transition energy results in a strong decrease of the electronic transition rate itself. A Franck-Condon like distribution of IVI would have resulted only if ionization rates for different inelastic vibrational channels would have been approximately a constant. This is clearly not the case. Rather, due to the strong decrease of the ionization rates with increasing inelasticity, the population of the higher vibrational states in IVI is *suppressed* below the Franck-Condon distribution. Thus, in the process of IVI less energy is deposited in the molecule than expected from the unsuppressed Franck-Condon distribution.

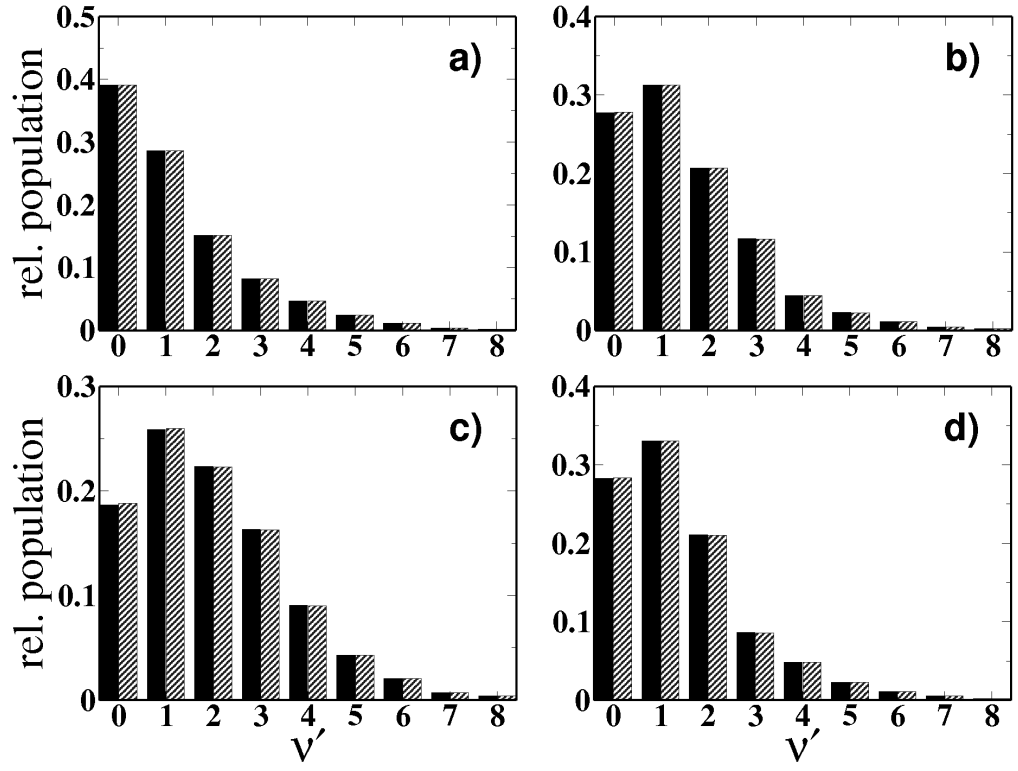

Figure 4.14.: Comparison of the results (solid bars) of calculations in which the molecular orbital coefficients are fixed at $R = R_e$ (keeping the R dependence of the phase) to those in which the overlap approximation has been assumed (hatched bars) [215]. Laser parameters are the same as in Fig. 4.5.

Some insight into the scaling of the effect can be obtained by looking at the effect of the vibrational excitation in the energy balance:

$$\begin{aligned} N\omega &= E_T(\nu',\nu) + U_p + E_{\mathrm{kin},N}(\nu',\nu) \\ &= E_T(0,0) + U_p + E_{\mathrm{kin},N}(\nu',\nu) + \Delta E_{\mathrm{vib}}(\nu',\nu) \\ &= E_T(0,0) + U_p + E_{\mathrm{kin},N}(0,0) \end{aligned} \tag{4.62}$$

Here $E_{\mathrm{kin},N}(0,0)$ is the kinetic energy, that an electron would gain from the ionizing absorption of N electrons, starting from the molecule and leaving the ion in their respective vibrational ground states:

$$E_{\mathrm{kin},N}(0,0) = N\omega - U_p - (E^{(f)}_{\nu'=0} - E^{(i)}_{\nu=0}) \tag{4.63}$$

$$\Delta E_{\mathrm{vib}}(\nu',\nu) = E^{(f)}_{\mathrm{vib}}(\nu') - E^{(i)}_{\mathrm{vib}}(\nu) \tag{4.64}$$

$$E^{(f)}_{\mathrm{vib}}(\nu') = E^{(f)}_{\nu'} - E^{(f)}_{\nu'=0} = \omega^{(f)}_e \nu' - (\omega_e x_e)^{(f)}(\nu'+1)\nu' \ , \tag{4.65}$$

where the last identity is specific for a Morse potential (see Eq. (4.53)), and holds

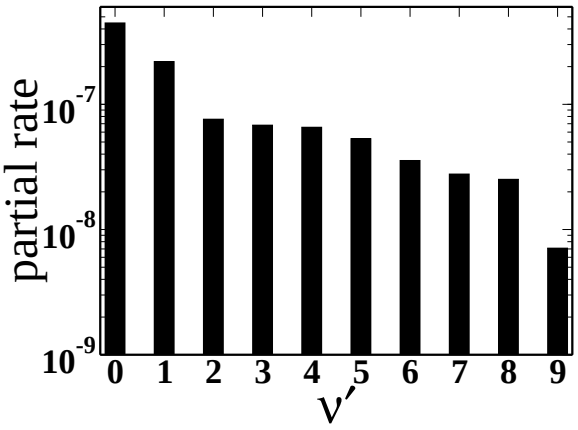

Figure 4.15.: Variation of the electronic part of the transition rate to $H_2^+(\nu')$ at a peak intensity of $I_0 = 4.8\times10^{13}\,\mathrm{W/cm^2}$ for the linear polarized 800 nm case [215]. Note that there are two channel closings at $\nu' = 2$ and $\nu' = 9$ at this particular intensity.

mutatis mutandis for the initial state. Thus

$$\begin{aligned} |\boldsymbol{k}_N(\nu',\nu)| &= \sqrt{2\left(E_{\mathrm{kin},N}(0,0) - \Delta E_{\mathrm{vib}}(\nu',\nu)\right)} \\ &= \sqrt{2E_{\mathrm{kin},N}(0,0)}\sqrt{1 - x_N(\nu',\nu)} \\ &= |\boldsymbol{k}_N(0,0)|\sqrt{1 - x_N(\nu',\nu)}\,, \end{aligned} \tag{4.66}$$

where $x_N(\nu',\nu) = \Delta E_{\mathrm{vib}}(\nu',\nu)/E_{\mathrm{kin},N}(0,0)$.

At a given constant photon number ΔE_{vib} must be smaller than $E_{\mathrm{kin},N}(0,0)$, thus $x_N < 1$. Then the first cylindrical Bessel function in the product pairs that add up to the generalized Bessel function (Eq. (4.25)) can be written as

$$J_{N+2m}(\boldsymbol{\alpha}_0 \cdot \boldsymbol{k}_N(\nu',\nu)) = J_{N+2m}(\sqrt{1 - x_N(\nu',\nu)}\boldsymbol{\alpha}_0 \cdot \boldsymbol{k}_N(0,0))\,. \tag{4.67}$$

Since $\boldsymbol{\alpha}_0 = q\sqrt{I_0}/(m_e\omega^2)$, an increase of x_N corresponds to a linear down-scaling of the laser intensity with respect to the quiver radius, while the ponderomotive energy U_p in the second cylindrical Bessel function stays unaffected:

$$J_N(\boldsymbol{\alpha}_0 \cdot \boldsymbol{k}_N(\nu',\nu), \frac{U_p}{2\omega}) = \sum_{m=-\infty}^{\infty} J_{N+2m}(\sqrt{1 - x_N(\nu',\nu)}\boldsymbol{\alpha}_0 \cdot \boldsymbol{k}_N(0,0)) J_m\left(\frac{U_p}{2\omega}\right)\,. \tag{4.68}$$

It is interesting to see how the strong non-linearity in the intense-field multiphoton IVI spectra changes when the ionization occurs in a single photon process instead, e.g. under synchrotron conditions. In the low intensity limit, the generalized Bessel

function can be approximated by the contributions of the lowest order cylindrical Bessel functions. To find these, it is useful to expand Eq. (4.25) for odd N as

$$J_N(a,b) = -\sum_{m=1}^{\infty} J_{2m-1}(a)\left[J_{(N+1)/2-m}(b) - J_{(N-1)/2+m}(b)\right] . \tag{4.69}$$

Thus, for a single-photon process $J_1(a,b) \approx -J_1(a)J_0(b)$. Applying the Taylor-expansion of the Bessel functions

$$J_m(a) = \sum_{l=0}^{\infty} \frac{(-1)^l}{l!(m+l)!}\left(\frac{a}{2}\right)^{2l+m} \tag{4.70}$$

and considering again only the lowest order term

$$J_1\left(\boldsymbol{\alpha}_0\cdot\boldsymbol{k}_1, \frac{U_p}{2\omega}\right) \approx -\frac{1}{2}\boldsymbol{\alpha}_0\cdot\boldsymbol{k}_1 = -\frac{1}{2}\sqrt{1-x_1}\boldsymbol{\alpha}_0\cdot\boldsymbol{k}_1(0,0) . \tag{4.71}$$

A single photon process is only possible if the photon energy is large enough to cover the transition energy to continuum and the change in vibrational energy. If the photon energy is so high that the kinetic energy of the ionized electron is large on the scale of the dissociation energy of the molecular ion, the dimensionless ratio x_1 will be small and $\sqrt{1-x_1} \approx 1 - x_1/2 - x_1^2/8$. I.e. in the case of a high energy photoeffect process, the nonlinear variation of the electronic transition amplitude, which is characteristic for the intense-field multiphoton IVI process, will become smaller. This smaller variation is known e.g. from Helium-resonance-line photoelectron spectroscopy on molecular targets [297].

4.4.4. Momentum Conservation

From a more general perspective, it is interesting to note the physical meaning of the dynamic photoelectron phase terms. As part of the matrix elements over the nuclear coordinate, they are the interaction potential that couples electronic momentum to the nuclear coordinates. In the diatomic case the central matrix elements are expressed in Dirac notation as:

$$\langle\, \chi'_{\nu'}[R'_e]|e^{-i\boldsymbol{k}_e\mathbf{R}_n}|\chi_\nu[R_e]\,\rangle \tag{4.72}$$

$$= \langle\, \chi'_{\nu'}| \int d\mathbf{K}'\, |\,\mathbf{K}'\,\rangle\langle\,\mathbf{K}'|\, e^{-i\boldsymbol{k}_e\mathbf{R}_n} \int d\mathbf{K}\; |\,\mathbf{K}\,\rangle\langle\,\mathbf{K}\,|\,\chi_\nu\,\rangle \tag{4.73}$$

$$= \int d\mathbf{K}' \int d\mathbf{K}\, \langle\, \chi'_{\nu'}\,|\,\mathbf{K}'\,\rangle \underbrace{\langle\,\mathbf{K}'|\, e^{-i\boldsymbol{k}_e\cdot\mathbf{R}_n}\,|\,\mathbf{K}\,\rangle}\langle\,\mathbf{K}\,|\,\chi_\nu\,\rangle\ , \tag{4.74}$$

where the nuclear state kets $|\,\chi_\nu[R_e]\,\rangle$ are written independent of coordinates ($\mathbf{R} = R\hat{\mathbf{R}}$ is the internuclear coordinate while the equilibrium distance R_e just a parameter,

which is dropped for brevity of notation). The coordinates of the nuclei in the center of mass frame are connected to the internuclear distance as $\mathbf{R}_n = \pm\mathbf{R}\mu/m_n$. The symbol $|\mathbf{K}\rangle$ denotes an eigenstate of the relative nuclear momentum conjugate to the internuclear coordinate $\mathbf{R}$. The closure relation $\int d\mathbf{K}\,|\,\mathbf{K}\,\rangle\langle\,\mathbf{K}\,|= \mathbb{1}$ has been inserted twice, to express the vibrational state kets as a linear combination of eigenstates of the internuclear momentum operator. The projections $\tilde{\chi_\nu}(\mathbf{K}) \equiv \langle\,\mathbf{K}\,|\,\chi_\nu\,\rangle$ are the expansion coefficients that are identical to the Fourier-transformed wavefunction of the internuclear coordinate $\langle\,\mathbf{R}\,|\,\chi_\nu[R_e]\,\rangle \equiv \chi_\nu(R - R_e)$. The integrals in this context extend over the full Hilbert space of the respective state. The underbraced term can be seen to be equivalent to a delta distribution:

$$\begin{aligned}\langle\,\mathbf{K}'\,|\,e^{-i\boldsymbol{k}_e\mathbf{R}_n}|\,|\,\mathbf{K}\,\rangle &= \int d\mathbf{R}\,\langle\,\mathbf{K}'\,|\,\mathbf{R}\,\rangle e^{\mp i\boldsymbol{k}_e\frac{\mu}{m_n}\mathbf{R}}\langle\,\mathbf{R}\,|\,\mathbf{K}\,\rangle \\ &= \int d\mathbf{R}\,\exp\left[i\left(\mathbf{K}\mp\frac{\mu}{m_n}\boldsymbol{k}_e - \mathbf{K}'\right)\mathbf{R}\right] \\ &= \underbrace{\delta\left(K\mp\frac{\mu}{m_n}\boldsymbol{k}_e\cdot\hat{\mathbf{R}} - K'\right)}\ . \end{aligned} \tag{4.75}$$

This matrix element establishes the condition of momentum conservation in the center of mass frame of the molecule, where a share of the electronic drift momentum is transferred to the momenta of the molecular nuclei, distributed according to the ratio of their masses. The sign is selected according to which nucleus the partial wave of the ionizing electron originates from. E.g. in the homonuclear case, if we denote the projection of the electron momentum on the internuclear axis by $\boldsymbol{k}'_e \equiv (\boldsymbol{k}_e\cdot\hat{\mathbf{R}})\hat{\mathbf{R}}$, the relative nuclear momentum K will be increased by $k'_e/2$ in the contribution originating from the nucleus at $-\mathbf{R}/2$, while it will be decreased by the same amount due to the contribution from the nucleus at $+\mathbf{R}/2$. Equation (4.75) establishes the selection rule for the change in relative internuclear momentum in process of IVI in the basis of eigenstates of relative internuclear momentum. Inserted back into expression (4.72), the central matrix element over the nuclear coordinates becomes:

$$\begin{aligned}&\iint d\mathbf{K}'\,d\mathbf{K}\,\langle\,\chi'_{\nu'}\,|\,\mathbf{K}'\,\rangle\delta\left(\mathbf{K}\mp\frac{\mu}{m_n}\boldsymbol{k}'_e - \mathbf{K}'\right)\langle\,\mathbf{K}\,|\,\chi_\nu\,\rangle \\ &= \int d\mathbf{K}\,\langle\,\chi'_{\nu'}\,|\,\mathbf{K}\mp\frac{\mu}{m_n}\boldsymbol{k}'_e\,\rangle\langle\,\mathbf{K}\,|\,\chi_\nu\,\rangle\ ,\end{aligned} \tag{4.76}$$

which describes the effect of the conservation of total momentum on the transition amplitude between vibrational states occurring in strong field ionization of molecules. We may transform back into the position representation, to extract the expression for the molecular vibrational wavefunction after ionization, i.e. before it gets projected

onto the set of specific possible wavefunctions of the molecular ion:

$$\int d\mathbf{R}\,\langle\,\chi'_{\nu'}\,|\,\mathbf{R}\,\rangle \underbrace{\int d\mathbf{K}\,\langle\,\mathbf{R}\,|\,\mathbf{K}\mp\frac{\mu}{m_n}\boldsymbol{k}'_e\,\rangle\langle\,\mathbf{K}\,|\,\chi_\nu\,\rangle} \tag{4.77}$$
$$= \int dR\,\chi_{\nu'}(R-R'_e)\underbrace{\int dK\,\mathcal{F}\left[\chi_\nu(R-R_e)\right](K)\exp\left[i\left(K\mp\frac{\mu}{m_n}k'_e\right)R\right]}\ .$$

The underbraced term represents the essential term of the nuclear vibrational wavefunction of the molecule after the emission of the active electron. It has the form of a wavepacket, made up by a superposition of plane waves of internuclear motion that are shifted by the mass-ratio scaled electron momentum into the opposite direction of electron emission (all projected onto the internuclear axis) with respect to the initial distribution of internuclear momentum, that is given by the Fourier transformed initial vibrational wavefunction $\tilde{\chi}_\nu(K) \equiv \mathcal{F}\left[\chi_\nu(R-R_e)\right](K)$. Note that in the homonuclear case the opposite signs of the momentum shift do not result in a cancellation of the effect (this would only be true, in case the positions R_e and R'_e of the troughs in the vibrational potentials coincide and the potentials are symmetric). The component of the electron momentum that is perpendicular to the molecular axis has two effects: It results in a shift of the momentum of the center of mass of the molecule and for heteronuclear molecules it also induces a change of the rotational state, which is not explicitly considered here.

This analysis of momentum conservation highlights an additional aspect in the interpretation of the matrix elements given in the IMST and KFR theories, where the conservation of energy appears naturally. While the conservation of energy is a result of temporal phase matching in S-matrix theory the conservation of momentum results from spatial phase matching. Since atomic systems are commonly described in a body fixed frame, the conservation of total momentum usually does not appear explicitly in the formula describing their single ionization. In molecular systems this condition has an effect on the internal, relative dynamics of the system and thus emerges explicitly from the matrix elements. This derivation also clarifies why the dynamic photoelectron phase terms have only minimal effect on the internuclear dynamics, as a change of internuclear momentum translates to a much smaller change in the velocity of internuclear motion, due to the high mass of the nuclei (in terms of electron mass, i.e. atomic units). The discussion of further issues concerning the consideration of momentum conservation in S-matrix theory and specifically the role of the ionic momentum is continued in section 5.1.3 in the context of the second part of the thesis, which analyzes electron impact ionization of diatomic molecules in the presence of an intense laser field.

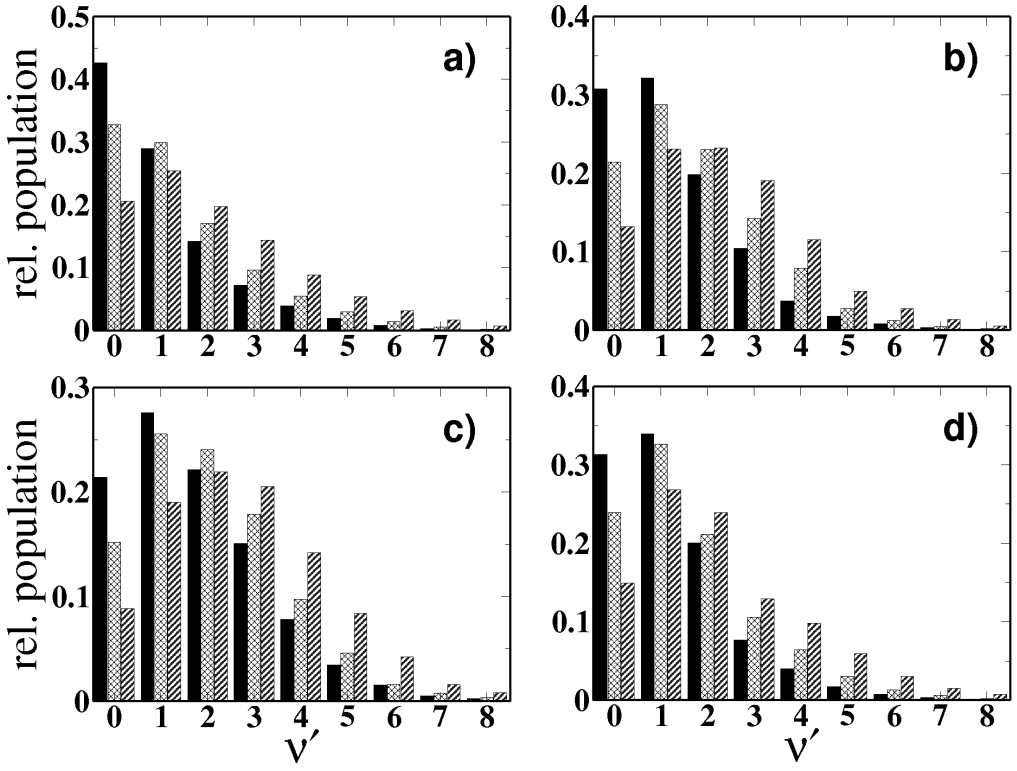

Figure 4.16.: Normalized populations of the vibrational states in H_2^+ (solid bars), HD^+ (cross hatched bars) and D_2^+ (hatched bars) for IVI of H_2, HD and D_2, from their respective ground states [215]. Laser parameters are the same as in Fig. 4.5.

4.4.5. Application to HD and D_2

Next, the present theory is applied to investigate possible isotopic effects in the IVI processes. To this end, the IVI distributions from two isotopes of the hydrogen molecule, HD and D_2, were calculated. While for the neutral species the molecular constants needed for the Morse wavefunctions are available in literature [298], for the molecular ions the anharmonicity parameter $\omega_e x_e = \omega_e^2/(4D_e)$, which determines the eigen-energies of the vibrational states, was calculated from the experimental values [299] of the energy $D_0 = D_e - \omega_e/2$. The vibrational constants are given in table 4.1.

Fig. 4.16 presents the results for the calculated IVI distributions from the ground vibronic states of the isotopes. The computations have been carried out at the same laser parameters as for the hydrogen molecule (cf. Fig. 4.5). A small but clear *isotopic shift* of the IVI distributions of the *heavier* isotopes of H_2 toward the higher vibrational levels is predicted. As the decrease of the electronic part of the transition rate as a function of the inelastic vibrational excitations is rather similar for the three molecules, the differences in the distributions are mainly due to the different behavior of the vibrational part. This is also seen from the Franck-Condon factors for

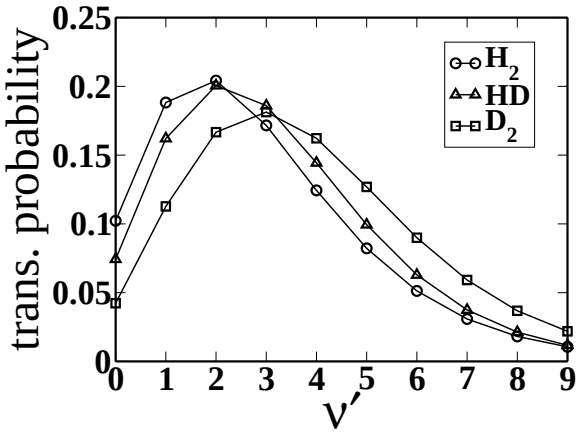

Figure 4.17.: Calculated Franck-Condon distributions for H_2^+, HD^+ and D_2^+ after direct transition out of the ground state of the respective molecule [215].

	R_e [Å]	D_0 [eV]	ω_e[cm^{-1}]	$\omega_e x_e$[cm^{-1}]	μ_A [a.m.u.][a]	I_p [eV]
$H_2\,(X^1\Sigma_g^+)$	0.741	4.478	4401.21	121.33	0.5076	15.42593
$H_2^+\,(X^2\Sigma_g^+)$	1.052	2.65	2322.0	66.2[b]	0.5076	-
$HD\,(X^1\Sigma_g^+)$	0.74142	4.513789	3813.1	91.65	0.672	15.44465
$HD^+\,(X^2\Sigma_g^+)$	1.057	2.667682	1913.1	40.72[b]	0.672	-
$D_2\,(X^1\Sigma_g^+)$	0.74152	4.556256	3115.5	61.82	1.007	15.46658
$D_2^+\,(X^2\Sigma_g^+)$	1.0559	2.691919	1577.3	27.64[b]	1.007	-

[a] $m_e = 5.4858\times10^{-4}$ a.m.u. [300]
[b] calculated values

Table 4.1.: Molecular constants [299, 298, 300].

the molecules, as presented in Fig. 4.17, that are obtained from the overlap integrals of the Morse wavefunctions, as used for the calculations shown in Fig. 4.16.

4.5. Inelastic Vibronic Ionization of Other Molecules

4.5.1. Other Diatomics: O_2 and CO

The present theory can also be applied to more complex molecules if their behavior in strong fields is well representable in a single active electron ansatz. The discussed *ad hoc* approach to IVI, multiplying the Franck-Condon overlaps into the KFR ionization rates to vibrationally resolved final states, has been applied to the ionization of N_2 before [202]. In the course of this work full IVI calculations were performed on the ionization of O_2 into the electronic ground ($X^2\Pi_g$) and first excited ($A^2\Pi_u$) states of O_2^+ as well as on the ionization of CO into the first ($A^2\Pi$) and second ($B^2\Sigma^+$) electronically excited states of CO^+. In figure 4.18 the Franck-Condon overlaps

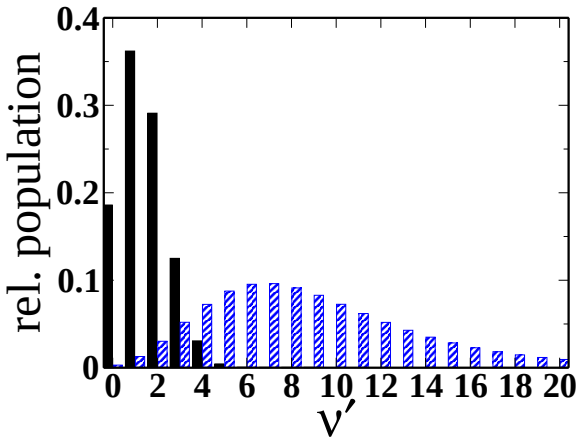

Figure 4.18.: Franck-Condon factors for the transition $O_2 X^3\Sigma_g^- \rightarrow O_2^+ X^2\Pi_g$ (solid bars) and $O_2 X^3\Sigma_g^- \rightarrow O_2^+ A^2\Pi_u$ (hatched bars) [301].

for the transitions in O_2 are given. The $O_2^+ X^2\Pi_g$ is created by the ionization of an electron from the antibonding highest occupied molecular orbital $1\pi_g$ (HOMO), thus the internuclear distance relaxes to a smaller value in the ion ($R_e' = 1.1164\,\text{Å}$) as compared to the neutral molecule ($R_e = 1.20752\,\text{Å}$). For the formation of the $O_2^+ A^2\Pi_u$ state an electron is removed from a bonding molecular orbital ($1\pi_u$), which weakens the bond to a stretched internuclear distance of ($R_e' = 1.409\,\text{Å}$) . This change in internuclear distance is caused by a shift of the minimum of the potential curve of the ionic state with respect to the minimum of the potential curve of the neutral molecule. The vertical electronic transition from the neutral to the ionic potential curve takes place in the vicinity of R_e. In the case of the $O_2^+ A^2\Pi_u$, the increase of the internuclear distance causes the steeper slope of the anharmonic potential curve to be shifted into the target region, while the shift of the $O_2^+ X^2\Pi_g$ potential curve causes transitions to happen into its shallower side. Thus, transitions from the ground vibrational state of the neutral O_2 cover a much broader spectrum of vibrational states in the $O_2^+ A^2\Pi_u$ state than transitions to the $O_2^+ X^2\Pi_g$ state, and the vibrational state of the electronically excited O_2 is more probable to be a much higher excited one than in the electronic ground state.

Figure 4.19 shows the relative IVI population yields of $O_2^+ X^2\Pi_g$ created by a Gaussian 45 fs pulse of an 800 nm Ti:Sapphire laser for two different intensities. The experimental vibrational constants are taken from [298]. While the vibrational spectrum generated by the more intense field is qualitatively the same at other intensities too, the spectrum at $I_0 = 3 \times 10^{12}\,\text{W/cm}^2$ is shown as a special case in which the ground vibrational level is predominantly populated. This peak reversal only happens in a small interval of intensities around the one picked here. In any case, the distributions show the characteristic trend for IVI-generated molecular ions to lower vibrational excitation.

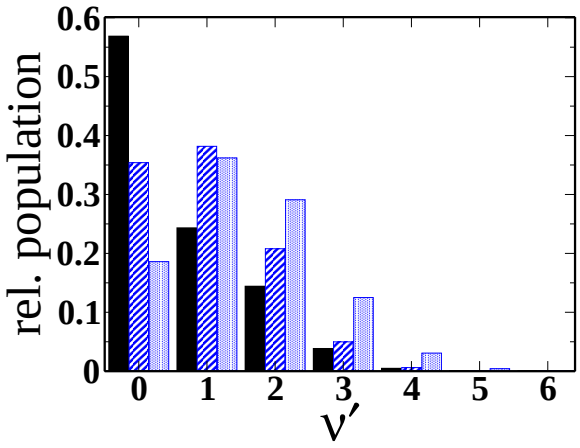

Figure 4.19.: Relative IVI populations in $O_2^+ X^2\Pi_g$ created by a Gaussian 45 fs pulse at 800 nm and intensities of $I_0 = 3\times10^{12}\,\mathrm{W/cm^2}$ (solid bars) and $I_0 = 6\times10^{12}\,\mathrm{W/cm^2}$ (hatched bars) respectively. The grey bars show the Franck-Condon overlaps for the sake of comparison.

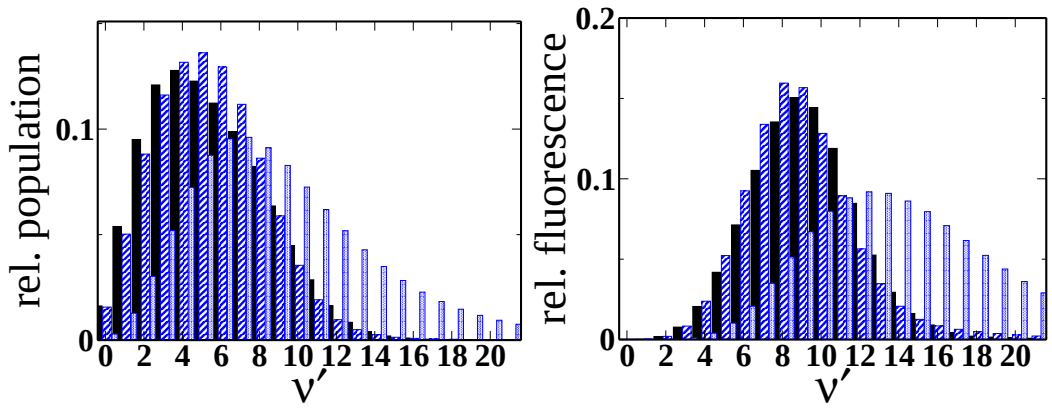

Figure 4.20.: Left: Same as in Fig. 4.19 but for the $O_2^+ A^2\Pi_u$ state.
Right: Calculated relative fluorescence signals from the vibrationally excited states of $O_2^+ A^2\Pi_u$, created by IVI in a Gaussian 45 fs pulse at 800 nm and $I_0 = 3\times10^{12}\,\mathrm{W/cm^2}$ (solid bars) and $I_0 = 6\times10^{12}\,\mathrm{W/cm^2}$ (hatched bars) respectively. Transitions are chosen to occur into the ground state of $O_2^+ X^2\Pi_g$. The grey bars show for comparison the relative fluorescence strengths as expected from a Franck-Condon distribution of the vibrational states of $O_2^+ A^2\Pi_u$.

The relative populations for the excited $O_2^+ A^2\Pi_u$ state are given in the left panel of figure 4.20. The comparison to the Franck-Condon distribution confirms the IVI shift of the vibrational population. In this case the maximum of the Franck-Condon distribution is at $\nu = 8$, while the representative IVI distribution, obtained after

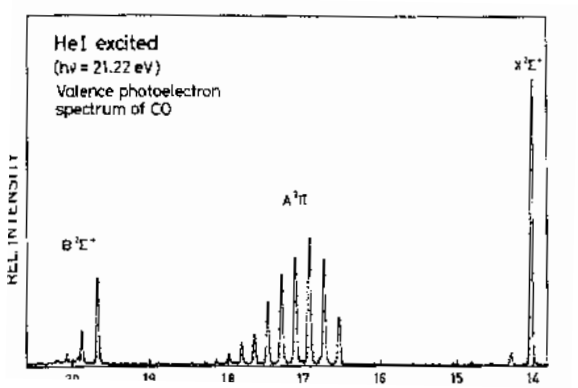

Figure 4.21.: Experimental He I spectrum of CO by Wannberg et al. from [305]

ionization in a laser pulse at a maximum intensity of $I_0 = 6 \times 10^{12}\,\mathrm{W/cm^2}$, peaks at $\nu' = 5$. A slight peak reversal between the $\nu' = 4$ and the $\nu' = 5$ state is also visible in the comparison of the two spectra taken at $I_0 = 3 \times 10^{12}\,\mathrm{W/cm^2}$ and $I_0 = 6 \times 10^{12}\,\mathrm{W/cm^2}$ respectively.

The creation of an electronically excited molecular state opens a possible way to detect the IVI shift of the vibrational spectrum by means of fluorescence. To this end, the vibrational distribution was multiplied with the corresponding Einstein coefficients [302] for the transition $O_2^+ A^2\Pi_u\,(\nu') \rightarrow O_2^+ X^2\Pi_g\,(\nu'' = 0)$ [303]. As shown in the right hand panel of Fig. 4.20 the small effect of the peak reversal in the vibrational population of $O_2^+ A^2\Pi_u$ is canceled by the strong suppression of the electronic transitions at low vibrational quantum numbers, apparent from the Einstein coefficients. The IVI shift of the fluorescence spectrum from $\nu' = 12$ to $\nu' = 8$ is still visible in the direct comparison of the calculated relative fluorescence strengths and might be detectable in experiment by direct comparison of the fluorescence spectrum from IVI generated $O_2^+ A^2\Pi_u$ to that of ions prepared in this state by other means, e.g. electron impact or single photon ionization by radiation from synchrotron sources.

As a representative case for a heteronuclear diatomic molecule the ionization of carbon monoxide is treated in the IVI formalism. It is isoelectronic to N_2 with a molecular orbital description of $(1\sigma_g)^2(1\sigma_u)^2(2\sigma_g)^2(2\sigma_u)^2(1\pi_u)^4(3\sigma_g)^2$ and a $^1\Sigma^+$ symmetry term. The transformation to the center of mass coordinate system, needed for the treatment of heteronuclear diatomic molecules is already included in the general derivation of the IVI transition rates (Eq. (4.55)). Ionizing transitions into the vibrational states of first ($A^2\Pi$) and second ($B^2\Sigma^+$) electronically excited states of CO^+ have been calculated. The transition to the ionic electronic ground state was not considered, as the experimental Franck-Condon factors for this transition [304] already predict a 96% population of the ground vibrational state, followed by 3.8% in the first excited vibration (see Fig. 4.21). Only a small quantitative shift would be obtained by the additional IVI suppression of the excited states.

The $CO^+ A^2\Pi$ state is reached from the ground state of CO by removal of a 1π

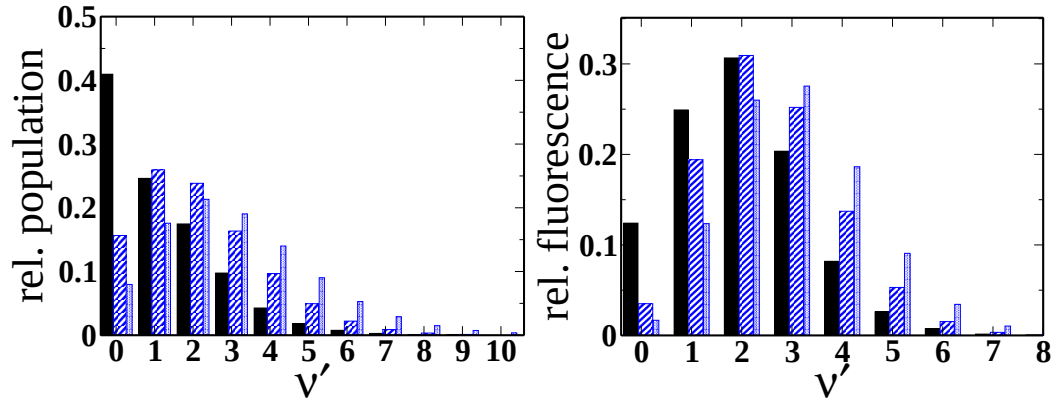

Figure 4.22.: Left: Relative IVI populations of $CO^+ A^2\Pi$ created by a Gaussian 45 fs pulse at 800 nm and peak intensities of $I_0 = 6 \times 10^{12}\,\mathrm{W/cm^2}$ (solid bars) and $I_0 = 1.5 \times 10^{14}\,\mathrm{W/cm^2}$ (hatched bars). For comparison the thinner grey bars show the Franck-Condon overlaps.
Right: Calculated relative fluorescence signals from the vibrationally excited states of $CO^+ A^2\Pi$ to its ground state. Laser parameters as in the left panel. For comparison the thinner grey bars show the relative fluorescence strengths as expected from a Franck-Condon distribution of the vibrational states of $CO^+ A^2\Pi$.

electron. The ionization potential for this transition ($E_B = 16.544\,\mathrm{eV}$) has been obtained from the experimental He *I* spectrum [305]. Alternatively it can be estimated as the sum of the ionization potential ($I_p = 14.014\,\mathrm{eV}$) into the ground state $X^2\Sigma$ of the ion and the excitation energy of the $A^2\Pi$ state ($T_e = 2.57\,\mathrm{eV}$). For the molecular orbital calculations a simple Gaussian set of basis functions was used, denoted as 4-31G+ in Pople notation [226]. The experimental parameters for the vibrational wavefunctions were taken from [306].

The left hand panel of figure 4.22 shows the relative IVI population yields of $CO^+ A^2\Pi$ as obtained from the ionization by a Gaussian 45 fs pulse at 800 nm for two peak intensities. The vibrational spectrum obtained at $I_0 = 1.5 \times 10^{14}\,\mathrm{W/cm^2}$ is typical for a wide range of intensities and compared to the Franck-Condon overlaps its maximum is shifted down by one to $\nu' = 1$. As in the case of the electronic ground state of O_2^+, there is a small window of intensities, around $I_0 = 6 \times 10^{12}\,\mathrm{W/cm^2}$ in this case, where the ground state is dominantly populated.

The shift of the vibrational IVI spectrum will cause the maximum of the fluorescence spectrum to shift as well with respect to the one expected from a Franck-Condon distribution in the excited $CO^+ A^2\Pi$ state as can be seen from the right hand panel of Fig. 4.22. These spectra were obtained by multiplying the corresponding Einstein A coefficients for the so-called comet-tail system $A^2\Pi\,(\nu') \rightarrow X^2\Sigma^+\,(\nu'' = 0)$ [307] into the vibrational IVI spectrum. The peak-reversal effect in the vibrational population caused by the ionization at a peak intensity of $I_0 = 6 \times 10^{12}\,\mathrm{W/cm^2}$ is

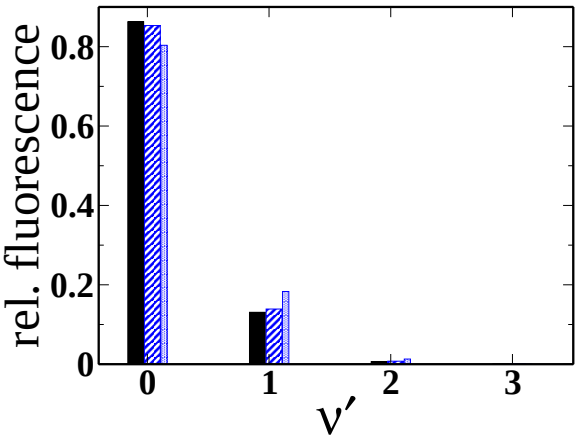

Figure 4.23.: Calculated relative fluorescence signals from the vibrationally excited states of $CO^+ B^2\Sigma^+$ created by IVI in a Gaussian 45 fs pulse at 800 nm and peak intensities of $I_0 = 3 \times 10^{13}\,\mathrm{W/cm^2}$ (solid bars) and $I_0 = 1.5 \times 10^{14}\,\mathrm{W/cm^2}$ (hatched bars) to the ground state of CO^+ (Einstein A coefficients from [306]). For comparison the thinner grey bars show the relative fluorescence strengths as expected from a plain Franck-Condon distribution in the vibrational states of $CO^+ B^2\Sigma^+$.

not strong enough to manifest in the fluorescence spectrum.

Finally, the $CO^+ B^2\Sigma^+$ state is obtained by ionization of an inner-shell $2\sigma_u$ electron from ground state CO at a transition energy of $E_B = 19.672\,\mathrm{eV}$ [305]. Like in the ionic ground state the internuclear distance ($R_e' = 1.1687\,\text{Å}$) in this excited electronic state is quite close to that in the ground state ($R_e = 1.1283\,\text{Å}$) of neutral CO, and thus the vibrational spectrum peaks strongly at $\nu' = 0$. Thus the shift of the IVI spectrum is only of quantitative nature, as depicted in the theoretical predictions of the fluorescence spectrum in Fig. 4.23.

4.5.2. Extension to Polyatomic Molecules

On a systematic way to an analysis of polyatomic molecules, linear triatomic systems, as e.g. HCN, constitute the first class of objects to be studied [199]. For these, it is convenient to start the kinematic description in Jacobi coordinates [308]. These transform to one dimensional Cartesian coordinates of the atoms as

$$\begin{aligned} R_3' &= \frac{\mu_{23}}{m_3} r \\ R_2' &= -\frac{\mu_{23}}{m_2} r \\ R_1' &= -R\,, \end{aligned} \tag{4.78}$$

where $\mu_{23} = \frac{m_2 m_3}{m_2 + m_3}$ is the reduced mass of the bi-atomic system of atom 2 and 3, that are separated by r. R denotes the scattering coordinate of atom 1 with respect to the

center of masses of the bi-atomic system of atom 2 and 3. From these coordinates one transforms to the center of mass coordinates as follows:

$$\begin{aligned} SP' &= -\frac{m_1}{M}R \\ R_3 &= R_3' - SP' = \frac{m_1}{M}R + \frac{\mu_{23}}{m_3}r \\ R_2 &= R_2' - SP' = \frac{m_1}{M}R - \frac{\mu_{23}}{m_2}r \\ R_1 &= -\frac{m_2+m_3}{M}R\,, \end{aligned} \tag{4.79}$$

where SP' is the center of mass in the system of Jacobi coordinates and M is the total mass of the molecule. If the vibrational potentials to be used are not given in Jacobi coordinates, they can be expressed in terms of the bond coordinates $r_1 = R - r/2$ and $r_2 = r$:

$$\begin{aligned} R_3 &= \frac{m_1}{M}r_1 + \left(\frac{m_1}{2M} + \frac{\mu_{23}}{m_3}\right)r_2 \\ R_2 &= \frac{m_1}{M}r_1 + \left(\frac{m_1}{2M} - \frac{\mu_{23}}{m_2}\right)r_2 \\ R_1 &= -\frac{m_2+m_3}{M}r_1 - \frac{m_2+m_3}{2M}r_2\,. \end{aligned} \tag{4.80}$$

Using these equations the vibrational dynamics of the internuclear distances is coupled to the coordinates of the electronic wavefunctions.

Next the question of the representation of the vibrations has to be addressed. Note that HCN is restricted here to be in a single configuration of its isotopomeres [309]. For linear triatomic systems with strongly asymmetric mass distribution like HCN the harmonic oscillator description is found to be an inefficient basis for the calculation of energy levels [310]. Much better results were obtained modeling the strongly mass-asymmetric bond by a Morse potential, thus describing the total vibration in a product basis combined of one harmonic and one Morse wavefunction [310–312]. If this ansatz is extended to molecules with several equivalent bonds, e.g. to benzene [254], Fermi-resonances between the equivalent oscillators have to be considered [313]. For linear triatomic molecules with more symmetric mass distributions like S_2O calculations with a product of harmonic wavefunctions proved to be sufficiently accurate for the calculation of excitations up to 3rd to 4th excited local mode state [310], i.e. a description in terms of normal modes is appropriate in this case (see discussion in section 4.3.3.2).

On this basis the IVI model can be used to calculate transition rates to the fundamental ($\nu_i = 1$) and the overtones ($\nu_i > 1$) of the local vibration modes as well as to the combination modes. To be applicable to the ionization of molecules in experimentally determined geometries, for the majority of cases it is important to allow for bend configurations the excitation of angular vibrational modes. These

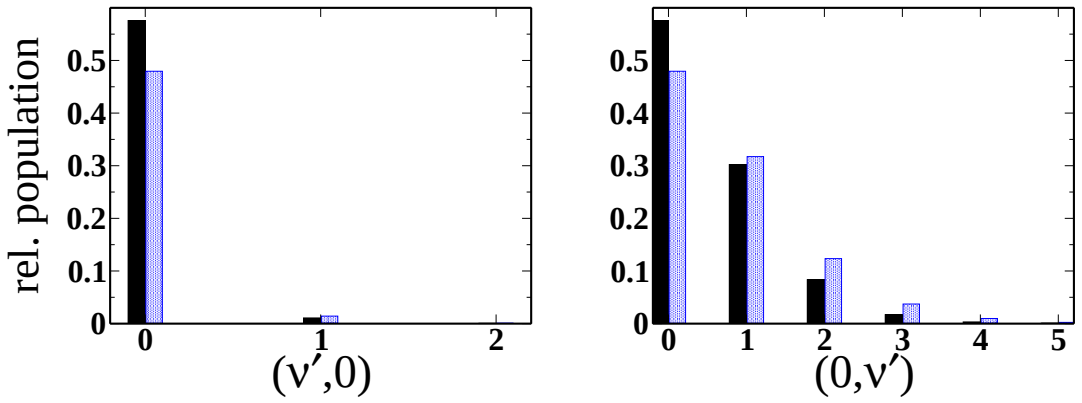

Figure 4.24.: Relative IVI populations in $HCN^+ X^2\Pi$ created from ground state HCN by a linearly polarized Gaussian 15 fs laser pulse at 800 nm with a peak intensity of $I_0 = 1 \times 10^{14}\,\mathrm{W/cm^2}$ (solid bars). The grey bars show the Franck-Condon overlaps for comparison.
Left: Selective excitation of the HC bond. Right: Same for the CN bond.

can be included in the local mode framework by the extension of the geometric description of the molecular structure to two dimensions, using the bond angle as an additional internal coordinate, and extending the product basis by a set of bending wavefunctions [310, 314, 275]. The present theory does not consider the subsequent intramolecular vibrational redistribution (IVR), that will start after the initial preparation of the vibrational wavepacket in the molecular ion, mediated by the hitherto neglected coupling between the oscillators, that may be modeled as a harmonic coupling [315, 256, 316] of the internal vibrational displacement coordinates. More accurate descriptions of the inter-mode coupling are obtained by coupling the Morse coordinates of anharmonic local mode vibrations [317, 318].

It is interesting to note, that in HCN the highest occupied molecular orbital has π symmetry and stretches only between carbon and nitrogen. Nevertheless on removal of one of the bonding valence electrons both bond lengths increase. The change is small (0.025 Å for the HC and 0.06 Å for the CN bond[2]), which allows that this triatomic system maintains its linear geometry upon ionization. As a consequence, the overlap of the ground state vibrational wavefunction of the neutral molecule with the vibrational wavefunctions of the molecular ion favors the ground state of the molecular ion. Thus one only expects a quantitative change in the occupation probability of the ionic vibrational ground state comparing the Franck-Condon distribution with the vibrational spectrum of strong field IVI. The calculations were performed using

[2]Molecular data for HCN are taken from experimental results reviewed in [319] and data for $HCN^+ X^2\Pi$ are from "corrected CI-SD" results in [320]

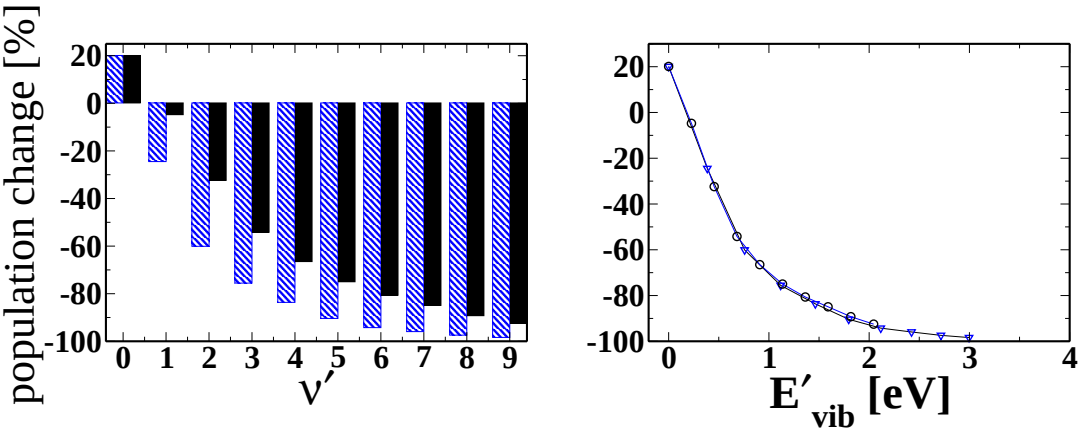

Figure 4.25.: Relative change of IVI populations in $HCN^+X^2\Pi$ with respect to the Franck-Condon overlaps for the HC (left: hatched bars, right: triangles) and CN bond (left: solid bars, right: circles) as a function of vibrational quantum numbers (left panel) and as a function of excitation energy (right panel; lines are drawn to guide the eye). Laser parameters as in Fig. 4.24.

the approximation of 'frozen' MO-coefficients corresponding to Eq. (4.58), as the effect of the variation of the molecular orbital coefficients was found to be small in the case of H_2, which strongly speeds up the calculations. As shown in figure 4.24, the vibration of the HC bond is strongly localized in the ground state, while the vibration of the CN bond has a broader spectrum. (As a consequence in the overlap for transitions from an excited CN vibration one finds local minima of interference due to the difference in the vibrational frequencies.) To better point out the differences, figure 4.25 shows the percentage of change in the occupation of the vibrational overtones of the two bonds relative to the respective Franck-Condon overlaps. The stronger suppression of the HC vibration apparent in the left panel is due to its larger characteristic energy quanta as compared to the CN vibration. In the right hand panel, where the population is plotted against the excitation energy of the states, the effect of IVI on the vibrational excitation is seen to be very similar for both bonds.

5. Nonsequential Double Ionization of Diatomic Molecules

The recollision mechanism of *Nonsequential Double Ionization* (NSDI, section 2.2) can be thought of as a three-step process [23, 26], first, a single electron is ionized, which is then propagated in the laser-dressed continuum. In the third step it recollides with the parent ion and by electron-electron interaction provides the energy and momentum for the ionization of a second electron. The combined process is well described in an IMST formulation of second order, which treats the propagation of the electron in the second step as a coherent quantum process (see section 2.2). To set the context of this chapter let us briefly recall the significant interactions in NSDI. In figure 5.1 the Feynman diagram for the dominant term of the IMST expansion is given, which has been discussed in section 2.2. Here we include a schematic visualization of the exchange of photons (represented by the dotted lines) between the photon field (dashed upward line) and the fermions (solid upward lines). Additionally to the direct interaction of the primary electron with the field at t_1, the photon exchange of the two-electron system with the field is considered at time t_2 when the second interaction takes place. This is due to the inherent coupling of the phases of the Gordon-Volkov states with the vector potential of the field.

Experimental observations show that dication yields from NSDI of diatomic molecules vary with the alignment angle between the internuclear axis and the polarization of the laser field. For N_2 preferential emission is found for parallel alignment [321, 322] while for O_2 the ionization yield is found to show a maximum at about 45° and 135° [322]. The two experiments differ in the way that molecular alignment was resolved. In [322] it was detected after double ionization from the fragments of dissociated molecules. Thus, this experiment considers only transitions to excited, antibonding states of the molecular dication. In cases where ionization initiates dissociation, the angular dependence of dissociation is connected to the symmetry of the ionizing molecular orbital. If the ionization rate is enhanced for a specific alignment of the molecular axis with respect to the fixed polarization axis of the laser field, the dissociation rate will be found to exhibit a maximum at that angle. The experiment reported in [321] on the other hand actively controls molecular alignment by application of weak 'pump' laser pulse that creates a rotational wave packet [323, 324], which results in preferential alignment parallel or perpendicular to the polarization of the 'pump' pulse at certain rephasing or 'revival' times after the pulse. Thus this experiment also detects molecular dications that are not transfered to an excited electronic state during NSDI.

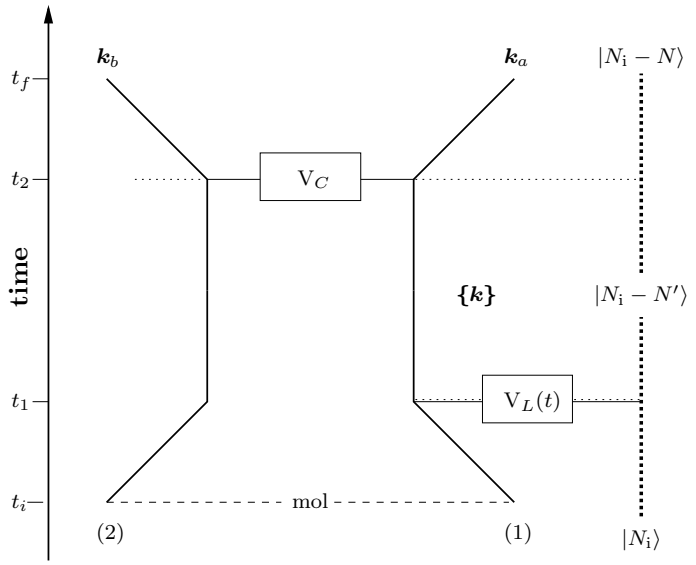

Figure 5.1.: Feynman diagram of the second order process that gives the dominant contribution to *Nonsequential Double Ionization* (NSDI) in infrared laser fields. The laser field is represented by the dashed line and the dotted lines symbolize the exchange of photons. The photon balance can be seen from the Fock-states.

This chapter gives a theoretical account of the alignment dependence of the *Nonsequential Double Ionization* of diatomic molecules. This is done from two perspectives. The first part of this chapter analyzes the effect of alignment on the ionization behavior in laser assisted electron impact on diatomic molecules, i.e. on the final step of NSDI. To this end, the recollision process is analyzed in section 5.1 within a first order KFR ansatz (see section 3.3) considering the effect of spin correlation between projectile and target electron on the rate for exchange scattering. On the other hand, to assess the alignment dependence of the full NSDI process a model formula for the *Nonsequential Double Ionization* of atoms is adapted to the molecular case in section 5.2. This formula combines the two separate first order S-matrix expressions for the initial step (intense-field multiphoton ionization) and the final step (laser assisted electron impact ionization) to obtain an approximation for the rates of NSDI of diatomic molecules. It is extended to allow the consideration of vibronic excitation of the molecule and its mono- and dications in the process. Additionally to the alignment dependence of the NSDI rates the distribution of the vibrational states of the molecular dication after NSDI is predicted within the limits of the approximations applied. Since there is no bound state of doubly ionized H_2 the analysis as well as the model formula is applied to the molecules N_2 and O_2, which experimentally are the most readily accessible diatomic molecular species.

5.1. Electron impact ionization in a laser field

The first two steps of the total NSDI process, above threshold ionization of a single electron (see section 2.1) and its quasi-classical propagation in the field, are quite well understood. Specifically the dependence of the rate for intense-field multiphoton ionization on the alignment of the internuclear axis of a diatomic molecule with respect to the polarization of the laser field has been shown theoretically [325, 37]. Thus, it is interesting to analyze the third step separately, which resembles an $(e, 2e)$ electron impact ionization in the laser field. Recently this ansatz has been used to give a heuristic interpretation of angular resolved differential kinetic energy release (KER) spectra, obtained from dissociative double ionization of N_2 and O_2, in terms of the electronic orbital occupied by the two active electrons in their initial state [322].

5.1.1. Characteristic spin correlated states

In the application to multi-electron systems it is essential to note that the contributions from interactions with inner-shell electrons, which are part of the interaction potential $V_i(t)$, can usually be neglected. For the intense-field multiphoton ionization of the primary electron in the NSDI process this approximation is justified because of the higher energy barrier the inner-shell electrons have to overcome to reach continuum. In the KFR formula the factors responsible for the reduction of the transition amplitude are the generalized Bessel functions that depend nonlinearly on the number of photons absorbed or emitted. An analysis of their asymptotic behavior [47] shows that the transition amplitude for linear polarization scales like $\exp\left[-\frac{2}{3}\sqrt{(2E_b)^3/I_0}\right]$ with the binding energy E_b. This coincides with the dependence obtained from tunneling theory (Eq. (2.8)). The secondary electron in NSDI is ionized by a coherent combination of inelastic electron impact and intense-field multiphoton absorption. For the laser intensities considered (around $2 \times 10^{14}\,\mathrm{W/cm^2}$) the impact energy of the rescattering primary electron can be high enough for direct impact ionization of a HOMO electron. The ionization of inner-shell electrons either needs the assistance of a higher order multiphoton absorption or higher field intensities acceleration the primary electron. In the first case the ionization of the outer-shell electron(s) gives higher ionization rates. The case of N_2 is particularly interesting. While the primary electron in the double ionization of N_2 preferentially originates from the $3\sigma_g$ HOMO, the singlet-spin companion electron in the singly occupied $3\sigma_g$ HOMO of N_2^+ is only slightly weaker bound (on the scale of energies involved in the process) than the electrons in the $1\pi_u$ orbital, opening two channels for secondary ionization that are energetically close enough to contribute.

The spins of the two emitted electrons are correlated in the same way as in the initial state of the neutral molecule. Therefore the situation is different to the conventional $(e, 2e)$ ionization of singly charged molecular ions in an electron beam,

where the incoming electrons are in general uncorrelated to the spins of the molecular electrons. In the case of O_2, if one only considers the outer valence electrons, this means that the system stays in a specific spin triplet state throughout the process. In this model the higher order transition channels that involve interaction with the inner-shell electrons are neglected. In the case of N_2 the two outer valence electrons form a singlet spin system in the molecular ground state. Considering only these two electrons, N_2 can be treated like Para-H_2. There has been a debate about the assignment of the electronic ground state of N_2^{2+}. Since too few experimental data is available, it is established solely by quantum chemical MR-CI calculations that the ground state is the singlet state $X^1\Sigma_g^+$, which lies 43.0 eV above the ground state of N_2, while the lowest triplet state $a^3\Pi_u$ has additional 0.57 eV of energy [139, 326]. This has been attributed partially to a correlated relaxation effect in the dication, since the minimum of the ab-initio potential curve of the singlet state $A^1\Pi_u$ shown in [327] lies about 1.4 eV above the minimum of the triplet curve. Also the $A^2\Pi_u$ state in the singly ionized N_2^+ lies 1.14 eV above the ground state $X^2\Sigma_g^+$ [298]. Since the $3\sigma_g$ and $1\pi_u$ orbitals in N_2^+ are very close in energy and to our knowledge the final total spin of N_2^{2+} has not been selected in measurements up to now, it is interesting to calculate the triplet channel as well, where the primary $3\sigma_g$ electron impact-ionizes an electron from the $1\pi_u$ orbital of N_2^+.

5.1.1.1. O_2

The anti-symmetrized wavefunctions of the two electron system, occupying the highest occupied molecular orbital (HOMO) of the O_2 molecule can be described as

$$|\Phi_i^{(T=+1)}\rangle = |\pi_{(g,x)}\uparrow, \pi_{(g,y)}\uparrow\rangle\rangle \tag{5.1}$$

$$= \frac{1}{\sqrt{2}}\big(|\pi_{(g,x)}, \pi_{(g,y)}\rangle - |\pi_{(g,y)}, \pi_{(g,x)}\rangle\big) \otimes \underbrace{|\uparrow\uparrow\rangle}_{|T^+\rangle} \tag{5.2}$$

$$|\Phi_i^{(T=-1)}\rangle = |\pi_{(g,x)}\downarrow, \pi_{(g,y)}\downarrow\rangle\rangle \tag{5.3}$$

$$= \frac{1}{\sqrt{2}}\big(|\pi_{(g,x)}, \pi_{(g,y)}\rangle - |\pi_{(g,y)}, \pi_{(g,x)}\rangle\big) \otimes \underbrace{|\downarrow\downarrow\rangle}_{|T^-\rangle} \tag{5.4}$$

$$|\Phi_i^{(T=0)}\rangle = \frac{1}{\sqrt{2}}\big(|\pi_{(g,x)}\uparrow, \pi_{(g,y)}\downarrow\rangle\rangle - |\pi_{(g,y)}\uparrow, \pi_{(g,x)}\downarrow\rangle\rangle\big) \tag{5.5}$$

$$= \frac{1}{\sqrt{2}}\big(|\pi_{(g,x)}, \pi_{(g,y)}\rangle - |\pi_{(g,y)}, \pi_{(g,x)}\rangle\big) \otimes \underbrace{\frac{1}{\sqrt{2}}\big(|\uparrow\downarrow\rangle + |\downarrow\uparrow\rangle\big)}_{|T^0\rangle}\,. \tag{5.6}$$

Here T denotes the total spin of the two electrons in the triplet state and $|\,\phi_a\phi_b\,\rangle\rangle$ is an abbreviating notation for the Slater determinant of the spin orbitals

$$|\,\phi_a\phi_b\cdots\phi_n\,\rangle\rangle \equiv \frac{1}{\sqrt{n!}}\begin{vmatrix} \phi_a(1) & \phi_b(1) & \cdots & \phi_n(1) \\ \phi_a(2) & \phi_b(2) & \cdots & \phi_n(2) \\ \vdots & & & \\ \phi_a(n) & \phi_b(n) & \cdots & \phi_n(n) \end{vmatrix}, \tag{5.7}$$

in contrast to the unsymmetrized Hartree product wavefunction

$$|\,\phi_a\phi_b\cdots\phi_n\,\rangle \equiv \phi_a(1)\phi_b(2)\cdots\phi_n(n)\;. \tag{5.8}$$

From these possible initial states one of the two electrons is eventually driven to a continuum state, while the other one stays bound. This situation corresponds to the second stage of the three-step process and the states of the system are called intermediate to distinguish them from the final state, where both electrons are found in the continuum. The intermediate states are eigenstates to the intermediate Hamiltonian H_m (see Eq. (3.54)). The possible spin correlated intermediate states after single ionization of the electron from the $\pi_{(g,y)}$ orbital are:

$$|\,\Phi^{(T=0,\pm)}_{+,x}\,\rangle = \frac{1}{\sqrt{2}}(|\,\boldsymbol{k}_0^{\mathrm{GV}},\pi_{(g,x)}\,\rangle - |\,\pi_{(g,x)},\boldsymbol{k}_0^{\mathrm{GV}}\,\rangle)\otimes\begin{cases}|\,T^+\,\rangle\\|\,T^0\,\rangle\\|\,T^-\,\rangle\end{cases} \tag{5.9}$$

and the intermediate state for ionization from the $\pi_{(g,x)}$ orbital is formed analogously

$$|\,\Phi^{(T=0,\pm)}_{+,y}\,\rangle = \frac{1}{\sqrt{2}}(|\,\boldsymbol{k}_0^{\mathrm{GV}},\pi_{(g,y)}\,\rangle - |\,\pi_{(g,y)},\boldsymbol{k}_0^{\mathrm{GV}}\,\rangle)\otimes\begin{cases}|\,T^+\,\rangle\\|\,T^0\,\rangle\\|\,T^-\,\rangle\end{cases}\;. \tag{5.10}$$

Upon recollision of the continuum electron, there is a certain probability for the second electron to be also transferred into the continuum of the doubly ionized O_2 molecule. The possible spin correlated final double continuum states can be assumed to be constructed like the initially bound electron wavefunctions:

$$|\,\Phi^{(T=0,\pm)}_{f}\,\rangle = \frac{1}{\sqrt{2}}(|\,\boldsymbol{k}_a^{\mathrm{GV}},\boldsymbol{k}_b^{\mathrm{GV}}\,\rangle - |\,\boldsymbol{k}_b^{\mathrm{GV}},\boldsymbol{k}_a^{\mathrm{GV}}\,\rangle)\otimes\begin{cases}|\,T^+\,\rangle\\|\,T^0\,\rangle\\|\,T^-\,\rangle\end{cases}\;. \tag{5.11}$$

The continuum states $|\,\boldsymbol{k}_0^{\mathrm{GV}}\,\rangle$, $|\,\boldsymbol{k}_a^{\mathrm{GV}}\,\rangle$ and $|\,\boldsymbol{k}_b^{\mathrm{GV}}\,\rangle$ are Gordon-Volkov states (Eq. (4.18)), i.e. they are solutions of the Hamiltonian that governs the evolution of the unbound electron in the laser field.

Before proceeding, we may discuss whether the two triplet sets in the intermediate state could be replaced by one using the coherent superposition $(\pi_x+\pi_y)/\sqrt{2}$. In this

respect, one has to note that the real valued atomic orbital functions p_x and p_y that construct the molecular π_x and π_y orbitals are not eigenfunctions of L_z, they are a merely convenient linear combination of the complex valued $Y_{1,1}$ and $Y_{1,-1}$ spherical harmonics (multiplied with the radial part that corresponds to the nuclear charge and the main quantum number). The angular parts are

$$p_x(\theta,\varphi) = \frac{1}{\sqrt{2}}\big(Y_{1,-1}(\theta,\varphi) - Y_{1,1}(\theta,\varphi)\big) \tag{5.12}$$

$$p_y(\theta,\varphi) = \frac{i}{\sqrt{2}}\big(Y_{1,-1}(\theta,\varphi) + Y_{1,1}(\theta,\varphi)\big)\ . \tag{5.13}$$

This corresponds to a change of basis for the description of the angular part of the electronic wave function. Likewise, one could use $(\pi_x+\pi_y)/\sqrt{2}$ as one basis function, but then, to span the same functional space, one would also have to consider the linear combination $(\pi_x-\pi_y)/\sqrt{2}$. Together these two states would provide just a rotated version of the π_x, π_y basis and the description would be equivalent.

5.1.1.2. N_2

As explained above, for N_2^+ there are two channels of electron impact ionization, that are energetically quite close. The first one is the ionization of the unpaired electron in the $3\sigma_g$ orbital which forms a singlet spin state with the projectile electron. In this case, the two active electrons both originate from the $3\sigma_g$ HOMO of N_2 and there is only one anti-symmetrized singlet wavefunction:

$$|\,\Phi_i^{(S)}\,\rangle = |\,\sigma_g\uparrow, \sigma_g\downarrow\,\rangle\rangle \tag{5.14}$$

$$= |\,\sigma_g, \sigma_g\,\rangle \otimes \underbrace{\frac{1}{\sqrt{2}}\big(\,|\uparrow\downarrow\rangle - |\downarrow\uparrow\rangle\big)}_{|S\rangle}\ . \tag{5.15}$$

If one of the two active electrons is ionized into the continuum of the molecular ion, the system is transferred into the corresponding singlet spin correlated intermediate state

$$|\,\Phi_+^{(S)}\,\rangle = \frac{1}{\sqrt{2}}\big(\,|\,\boldsymbol{k}_0^{\mathrm{GV}}\uparrow, \sigma_g'\downarrow\,\rangle\rangle + |\,\sigma_g'\uparrow, \boldsymbol{k}_0^{\mathrm{GV}}\downarrow\,\rangle\rangle\big) \tag{5.16}$$

$$= \frac{1}{\sqrt{2}}\big(\,|\,\boldsymbol{k}_0^{\mathrm{GV}}, \sigma_g'\,\rangle + |\,\sigma_g', \boldsymbol{k}_0^{\mathrm{GV}}\,\rangle\big) \otimes |\,S\,\rangle \tag{5.17}$$

where the $3\sigma_g'$ of N_2^+ slightly differs from the $3\sigma_g$ in N_2. Finally, after ionization of the second active electron by recollision, the system is left in the double continuum

state

$$|\Phi_f^{(S)}\rangle = \frac{1}{\sqrt{2}}\big(|\boldsymbol{k}_a^{\mathrm{GV}}\uparrow, \boldsymbol{k}_b^{\mathrm{GV}}\downarrow\rangle\rangle + |\boldsymbol{k}_b^{\mathrm{GV}}\uparrow, \boldsymbol{k}_a^{\mathrm{GV}}\downarrow\rangle\rangle\big) \tag{5.18}$$

$$= \frac{1}{\sqrt{2}}\big(|\boldsymbol{k}_a^{\mathrm{GV}}, \boldsymbol{k}_b^{\mathrm{GV}}\rangle + |\boldsymbol{k}_b^{\mathrm{GV}}, \boldsymbol{k}_a^{\mathrm{GV}}\rangle\big) \otimes |S\rangle\,. \tag{5.19}$$

If on the other hand the primary electron impact ionizes one of the two $1\pi_{(u,x/y)}$ electrons of opposite spin, their combined spin forms a triplet, and the N_2^{2+} dication is left as well in a triplet state. In this case the anti-symmetrized wavefunction of the active electrons of this process in N_2 can be described as

$$|\Phi_{i,x/y}^{(T)}\rangle = \frac{1}{\sqrt{2}}\big(|\sigma_g, \pi_{(u,x/y)}\rangle - |\pi_{(u,x/y)}, \sigma_g\rangle\big) \otimes \begin{cases} |T^+\rangle \\ |T^0\rangle \\ |T^-\rangle \end{cases}. \tag{5.20}$$

The intermediate state is given as

$$|\Phi_{+,x/y}^{(T=0,\pm)}\rangle = \frac{1}{\sqrt{2}}(|\boldsymbol{k}_0^{\mathrm{GV}}, \pi_{(u,x/y)}\rangle - |\pi_{(u,x/y)}, \boldsymbol{k}_0^{\mathrm{GV}}\rangle) \otimes \begin{cases} |T^+\rangle \\ |T^0\rangle \\ |T^-\rangle \end{cases}, \tag{5.21}$$

and the final state is given by Eq. (5.11).

5.1.2. Collision dynamics in the laser field

Now, with the spin correlated essential states of the three-step process identified, we focus on the third stage, the $(e, 2e)$-collision in the presence of the laser field. In the proposed recollision mechanism of *Nonsequential Double Ionization* (NSDI) the primary ionized electron is driven by the laser field and still interacts with its parent ion via the Coulomb interaction. This intermediate state of NSDI is now the initial state of the $(e, 2e)$-collisional process. Thus, the Hamiltonian of the system can be split up into two parts, the reference Hamiltonian describes the dynamics of the bound system and the primary continuum electron in the laser field, and the second considering the interaction between these two. In velocity gauge this is

$$H = \underbrace{\frac{1}{2}\left(\mathbf{p}_1 + \frac{1}{c}\mathbf{A}(t)\right)^2 + H_{\mathrm{mol}^+}}_{H_{\mathrm{i}}} + \underbrace{V_C^{(1,\mathrm{mol}^{(2+)})} + V_C^{(1,2)} + V_L^{(2)}(t)}_{V_{\mathrm{i}}} \tag{5.22}$$

where $V_C^{(1,2)} = 1/|\mathbf{r}_1 - \mathbf{r}_2|$ is the Coulomb interaction between the bound and the continuum electron and $V_C^{(1,\mathrm{mol}^{(2+)})}$ denotes the interaction between the continuum electron and the remaining charged constituents of the nascent dication:

$$V_C^{(1,\mathrm{mol}^{(2+)})} = \sum_{i=3}^{N_e} \frac{1}{|\mathbf{r}_1 - \mathbf{r}_i|} - \sum_{j=1}^{N_n} \frac{1}{|\mathbf{r}_1 - \mathbf{R}_j|}\,. \tag{5.23}$$

The summations extend over all N_n nuclei at their respective positions R_j and up to the number of electrons N_e. The third interaction term $V_L^{(2)}(t)$ in Eq. (5.22) considers the interaction of the secondary electron with the laser field:

$$V_L^{(2)}(t) = \frac{1}{c}\mathbf{p}_2 \cdot \mathbf{A}(t) + \frac{1}{2c^2}A^2(t) \; . \tag{5.24}$$

The first order contribution of this last term corresponds to an intense-field multiphoton ionization of the secondary electron, uncorrelated to the primary one. In the following this term will not be considered, as in the double ionization process it would constitute the second step of sequential ionization, which is known to be of minor importance at the intensities where rescattering is effective.

Applying the general framework of S-matrix theory (section 3.3) we may start with Eq. (3.49) where in this case V_f denotes the interaction of the correlated electrons in the double continuum state among each other and with the residual molecular dication:

$$V_f = \frac{1}{|\mathbf{r}_1 - \mathbf{r}_2|} + \sum_{m=1}^{2}\left(\sum_{i=3}^{N_e}\frac{1}{|\mathbf{r}_m - \mathbf{r}_i|} - \sum_{j=1}^{N_n}\frac{Z_j}{|\mathbf{r}_m - \mathbf{R}_j|}\right) \; . \tag{5.25}$$

This final state interaction corresponds to a splitting of the full Hamiltonian into $H = H_f - V_f$ where H_f is the Hamiltonian of the three separate, non-interacting parts of this system:

$$H_f = \frac{1}{2}\left(\mathbf{p}_1 + \frac{1}{c}\mathbf{A}(t)\right)^2 + \frac{1}{2}\left(\mathbf{p}_2 + \frac{1}{c}\mathbf{A}(t)\right)^2 + H_{\mathrm{mol}^{(2+)}} \; , \tag{5.26}$$

where $H_{\mathrm{mol}^{(2+)}}$ represents the molecular Hamiltonian of the dication.

The initial states are assumed to be of the form of the spin correlated singly ionized states $\Phi_+^{(S/T)}$ discussed above (Eqns. (5.9), (5.10), (5.16), (5.21)). The final states are taken to be the spin correlated double continuum states $\Phi_f^{(S/T)}$ described above (Eqns. (5.11), (5.18)). The asymptotic first order transition amplitude between two states of either total spin then is

$$A_{fi}^{(1)} = \langle\, \Phi_f^{(S/T)} \,|\, \Phi_+^{(S/T)} \,\rangle - i\int_{t_i}^{\infty} dt_1 \langle\, \Phi_f^{(S/T)}(t_1) \,|\, V_{\mathrm{i}} \,|\, \Phi_+^{(S/T)}(t_1) \,\rangle \; . \tag{5.27}$$

Figure 5.2 shows the Feynman diagrams corresponding to the two interactions considered, direct electron-electron scattering and scattering of the primary electron with the residual molecular dication. Since in the latter process there is no directed momentum transfer between the primary and the secondary electron, it can be interpreted as a variation of the *Shake-Off* process in NSDI in second order. The spin correlation of the two electrons is symbolized by the chained lines connecting them at t_i and t_f, baring in mind that it is present during the whole process.

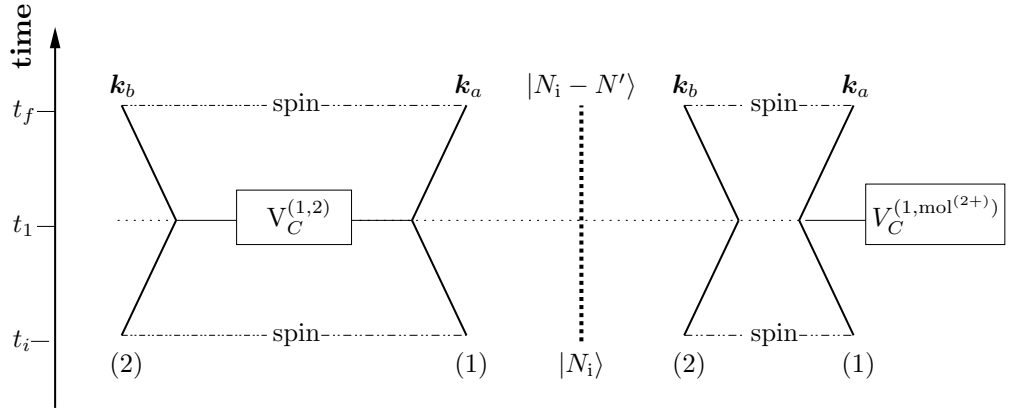

Figure 5.2.: Feynman diagrams of the $(e + N\omega, 2e)$ process. Left: Direct collision of the active electrons, Right: Collision with the residual molecular dication. The laser field is represented by the dashed line and the exchange of photons with it is symbolized by the dotted lines. The photon balance can be seen from the Fock state kets. The diagrams are added coherently.

For singlet states the first order amplitude evaluates to

$$S_{fi}^{(1,S)} = A_{fi}^{(1)} - \langle\, \Phi_f^{(S)} \,|\, \Phi_+^{(S)} \,\rangle \tag{5.28}$$

$$= -i \int_{t_i}^{\infty} dt_1 \langle\, \boldsymbol{k}_a^{\mathrm{GV}}, \boldsymbol{k}_b^{\mathrm{GV}}(t_1) |\, V_\mathrm{i}\, [1 + \mathcal{P}_{12}] \,|\, \boldsymbol{k}_0^{\mathrm{GV}}, \sigma_g(t_1) \,\rangle \tag{5.29}$$

where the zeroth order vanishing overlap $\langle\, \Phi_f^{(S)} \,|\, \Phi_+^{(S)} \,\rangle$ has been subtracted. The spin wavefunctions project out in the expression and the permutation operator $\mathcal{P}_{12}$ takes account of the exchange of the electrons. Thus, the amplitude is the coherent sum of the so-called *direct* and *exchange* terms. Note that both outgoing electrons enter the continuum at the same instant of time with their phases correlated by the scattering interaction.

For triplet states one has three amplitudes corresponding to the different total spins of the two electrons during the process and for molecular orbitals of π symmetry one has two contributions depending on which of the two (x/y) orbitals is considered in the initial state. So e.g. for O_2 one has:

$$S_{fi,x}^{(1,T=0,\pm)} = -i \int_{t_i}^{\infty} dt_1 \langle\, \boldsymbol{k}_a^{\mathrm{GV}}, \boldsymbol{k}_b^{\mathrm{GV}}(t_1) |\, V_\mathrm{i}\, [1 - \mathcal{P}_{12}] \,|\, \boldsymbol{k}_0^{\mathrm{GV}}, \pi_{(g,x)}(t_1) \,\rangle \tag{5.30}$$

$$S_{fi,y}^{(1,T=0,\pm)} = -i \int_{t_i}^{\infty} dt_1 \langle\, \boldsymbol{k}_a^{\mathrm{GV}}, \boldsymbol{k}_b^{\mathrm{GV}}(t_1) |\, V_\mathrm{i}\, [1 - \mathcal{P}_{12}] \,|\, \boldsymbol{k}_0^{\mathrm{GV}}, \pi_{(g,y)}(t_1) \,\rangle \tag{5.31}$$

The antisymmetric spatial wavefunction of the triplet states causes the sign flip on permutation of the electrons. These two contributions are added coherently, as they are part of the possible quantum paths of the ionization process:

$$S_{fi}^{(1,T=0,\pm)} = -i \int_{t_i}^{\infty} dt_1 \langle\, \boldsymbol{k}_a^{\mathrm{GV}}, \boldsymbol{k}_b^{\mathrm{GV}}(t_1) |\, V_{\mathrm{i}}\, [1 - \mathcal{P}_{12}]\, |\, \boldsymbol{k}_0^{\mathrm{GV}}, (\pi_{(g,x)} + \pi_{(g,y)})(t_1) \,\rangle \quad (5.32)$$

To evaluate the amplitude, the time integral has been performed first [26]. Letting $t_i \to -\infty$, the time integral imposes the condition of energy conservation on the terms:

$$\begin{aligned} S_{fi}^{(1,S/T)} = &-2\pi i \sum_{N=N_0}^{\infty} \delta\left(\frac{k_a^2}{2} + \frac{k_b^2}{2} + U_p + E_T - N\omega - \frac{k_0^2}{2}\right) \\ &\times J_N\left(\boldsymbol{\alpha}_0 \cdot (\boldsymbol{k}_a + \boldsymbol{k}_b - \boldsymbol{k}_0), \frac{U_p}{2\omega}\right) \\ &\times \langle\, \boldsymbol{k}_a, \boldsymbol{k}_b(t_1) |\, V_{\mathrm{i}}\, [1 \pm \mathcal{P}_{12}]\, |\, \boldsymbol{k}_0, \Phi_i(t_1) \,\rangle \end{aligned} \quad (5.33)$$

where $N_0 = \lceil (U_p + E_T - \frac{k_0^2}{2})/\omega \rceil$ is large enough to allow energy conservation. Here, a linear polarization of the laser is assumed, consistent with the relevant situation in the rescattering process.

From the direct scattering term $V_C(1,2)$ in the remaining matrix element one obtains two coupled Fourier transformations

$$\langle\, \boldsymbol{k}_a, \boldsymbol{k}_b |\, V_C(1,2)\, |\, \boldsymbol{k}_0, \Phi_i \,\rangle = \frac{4\pi}{|\boldsymbol{k}_0 - \boldsymbol{k}_a|^2} \langle\, \boldsymbol{k}_a + \boldsymbol{k}_b - \boldsymbol{k}_0 | \Phi_i \,\rangle\, . \quad (5.34)$$

For a homonuclear diatomic, where the nuclear charge $Z_j = N_e/2$, the indirect scattering term $V_C(1, \mathrm{mol}^{(2+)})$ is approximated as

$$V_C(1, \mathrm{mol}^{(2+)}) = \sum_{i=3}^{N_e} \frac{1}{|\mathbf{r}_m - \mathbf{r}_i|} - \sum_{j=1}^{2} \frac{Z_j}{|\mathbf{r}_m - \mathbf{R}_j|} \quad (5.35)$$

$$\approx -\tilde{Z} \sum_{j=1}^{2} \frac{1}{|\mathbf{r}_m - \mathbf{R}_j|}\ , \quad (5.36)$$

with a screened charge $\tilde{Z} \approx 1$, and thus

$$\langle\, \boldsymbol{k}_a, \boldsymbol{k}_b |\, V_C(1, \mathrm{mol}^{(2+)})\, |\, \boldsymbol{k}_0, \Phi_i \,\rangle = -\frac{8\pi}{|\boldsymbol{k}_0 - \boldsymbol{k}_a|^2} \langle\, \boldsymbol{k}_b | \Phi_i \,\rangle \tilde{Z} \cos[(\boldsymbol{k}_0 - \boldsymbol{k}_a)\mathbf{R}_e/2]\ , \quad (5.37)$$

if $\mathbf{R}_j = \pm \mathbf{R}_e/2$.

The ionization rate is obtained as the absolute square of the first order amplitude $S_{fi}^{(1)}$, using the identity $\delta^2(x) = \lim_{\tau\to\infty} \frac{\tau}{2\pi}\delta(x)$ for the square of Dirac's delta-distribution [26]. The differential cross section is found by dividing by the incident flux.

$$\begin{aligned}\frac{d^9\sigma^{(1,S/T)}}{d\boldsymbol{k}_0 dE_a d\Omega_a dE_b d\Omega_b} =& \frac{4|\boldsymbol{k}_a||\boldsymbol{k}_b|}{(2\pi)^3|\boldsymbol{k}_0|}C^2 \sum_{N=-\infty}^{\infty} J_N^2\left(\boldsymbol{\alpha}_0\cdot(\boldsymbol{k}_a+\boldsymbol{k}_b-\boldsymbol{k}_0), \frac{U_p}{2\omega}\right)\\ &\times\Bigg[\left(\frac{1}{|\boldsymbol{k}_0-\boldsymbol{k}_a|^2}\pm\frac{1}{|\boldsymbol{k}_0-\boldsymbol{k}_b|^2}\right)\tilde{\Phi}_i(\boldsymbol{k}_a+\boldsymbol{k}_b-\boldsymbol{k}_0)\\ &-\frac{2}{|\boldsymbol{k}_0-\boldsymbol{k}_a|^2}\cos[(\boldsymbol{k}_0-\boldsymbol{k}_a)\mathbf{R}_e/2]\tilde{\Phi}_i(\boldsymbol{k}_b)\\ &\mp\frac{2}{|\boldsymbol{k}_0-\boldsymbol{k}_b|^2}\cos[(\boldsymbol{k}_0-\boldsymbol{k}_b)\mathbf{R}_e/2]\tilde{\Phi}_i(\boldsymbol{k}_a)\Bigg]^2\\ &\times\delta\left(\frac{k_a^2}{2}+\frac{k_b^2}{2}+U_p+E_T-N\omega-\frac{k_0^2}{2}\right)\\ =&|f\pm g|^2\end{aligned} \tag{5.38}$$

where C is the Coulomb correction factor for the dication discussed in section 3.3. As noted in the last line of this equation, the cross section for *exchange scattering* can be written as a sum of a *direct* term f and an *exchange* term g.

The limits of this first order Born approximation (FBA) [161] to the process and the description of the continuum electrons in terms of Gordon-Volkov waves deserve some attention. This model is an extension of the Plane Wave Born Approximation (PWBA) to laser dressed continuum states [42]. It is known, that the Plane Wave Born Approximation only gives reasonable results for high energetic processes, as it neglects the Coulomb correlation (or "distortion" from the perspective of plane waves) of the ionized electrons with the parent ion and between each other (see e.g. [328]). There are several aspects to this. First it has been noted that at lower energies the effect of electron exchange becomes more important [161, 329], which is the reason why spin correlation is considered in the present ansatz. On the other hand there are several specialized Distorted Wave Born Approximations (DWBA [73], molecular DWBA [330]) such as the Coulomb/Continuum Distorted Wave (CDW, see references and discussion in [331]), BBK [332, 333] and Molecular BBK (Brauner-Briggs-Klar [334]), that incorporate Coulomb correlation between some or all particles in the final state description (see [335] for a discussion). For the high energy $(e, 2e)$ processes the Impulse Approximation [336] in its plane wave form (PWIA [337]) has been widely used as a tool of analysis to map the momentum space wavefunction of the scattering target (see [338] for a discussion of the limits). The approximation of Coulomb continuum wavefunctions forms a whole area of research of its own and the calculation of integrals containing these wavefunctions still is an

analytically and numerically challenging task. Thus, if the experimental situation is such, that it selectively measures electrons with a strongly asymmetric distribution of kinetic energy, only the slow electron is modeled as a Coulomb wave, while the fast electron (usually identical to the projectile) may be treated as a plane wave. In most theoretical treatments, the incoming electron is described by a plane wave or in the eikonal approximation (CDW-EIS [339]). It is to be noted, that the descriptions differ mostly in the relative angular differential dependencies, while they give rather good predictions for the total ionization rate. Since in the current state of the analysis of the $(e + N\omega, 2e)$ rescattering process in the laser field the focus lies on cross sections that are differential in the initial but total in the final state, the Gordon-Volkov description is chosen, which has the benefit to include the interaction with the intense laser field to all orders.

Quite early the success of Orthogonalized Plane Waves (OPW) in solid state physics [340] has found adaption in the approximative description of electron scattering of atomic systems, usually in the form of Orthogonalized Coulomb Waves (OCW [341–343] and references in the latter). Already the OPW approximation considerably improves the threshold behavior of the predicted ionization cross sections [344], while retaining the simplicity of the plane wave description (see e.g. [345]). Thus, a Gordon-Volkov wave orthogonalized to the bound electron wavefunction represents a candidate for the next order of approximation for the correlation between the electrons and the parent ion. For a discussion of the importance of the choice of gauge and the limitations in this approach see [346]. The correlation between the two electrons in the field can be considered exactly [152], again at the expense of simple integrability.

Using a simple ansatz of orthogonalization for ionization of the secondary electron, one can estimate that the contribution of the indirect scattering term due to $V_C(1, \mathrm{mol}^{(2+)})$ will not contribute. As this indirect scattering term does not couple the two active electrons, it separates into a product:

$$\langle\, \boldsymbol{k}_a, \boldsymbol{k}_b \,|\, V_C(1, \mathrm{mol}^{(2+)}) \,|\, \boldsymbol{k}_0, \Phi_i \,\rangle = \langle\, \boldsymbol{k}_a \,|\, V_C(1, \mathrm{mol}^{(2+)}) \,|\, \boldsymbol{k}_0 \,\rangle \langle\, \boldsymbol{k}_b \,|\, \Phi_i \,\rangle \;. \tag{5.39}$$

If the $|\, \boldsymbol{k}_b \,\rangle$ is now replaced by a $|\, \boldsymbol{k}'_b \,\rangle$ that is orthogonal to the initial orbital $|\, \Phi_i \,\rangle$, e.g.

$$|\, \boldsymbol{k}'_b \,\rangle \equiv (|\, \boldsymbol{k}_b \,\rangle - |\, \Phi_i \,\rangle \langle\, \Phi_i \,|\, \boldsymbol{k}_b \,\rangle) \, \frac{1}{1 - |\langle\, \mathbf{k}_b \,|\, \Phi_i \,\rangle|^2} \;, \tag{5.40}$$

the matrix element of indirect scattering vanishes. Thus Eq. (5.38) simplifies to

$$\begin{aligned}\frac{d^9\sigma^{(1,S/T)}}{d\boldsymbol{k}_0 dE_a d\Omega_a dE_b d\Omega_b} =& \frac{4|\boldsymbol{k}_a||\boldsymbol{k}_b|}{(2\pi)^3|\boldsymbol{k}_0|}C^2 \sum_{N=-\infty}^{\infty} J_N^2\left(\boldsymbol{\alpha}_0\cdot\boldsymbol{\Delta k}, \frac{U_p}{2\omega}\right) \\ &\times\left(\frac{1}{|\boldsymbol{k}_0-\boldsymbol{k}_a|^2}\pm\frac{1}{|\boldsymbol{k}_0-\boldsymbol{k}_b|^2}\right)^2 \tilde{\Phi}_i^2(\boldsymbol{\Delta k}) \\ =& |f\pm g|^2 \,,\end{aligned} \tag{5.41}$$

where again f and g denote the terms of *direct* and *exchange* scattering respectively and $\boldsymbol{\Delta k}\equiv\boldsymbol{k}_a+\boldsymbol{k}_b-\boldsymbol{k}_0$. Eq. (5.41) is evaluated on the energy shell defined by

$$\frac{k_a^2}{2}+\frac{k_b^2}{2}+U_p+E_T = N\omega+\frac{k_0^2}{2}\,. \tag{5.42}$$

5.1.3. Ionic Recoil Momentum in Laser Assisted Electron Impact Ionization

As $\boldsymbol{\Delta k}$ corresponds to a change of the momentum of molecular ion, it is necessary to discuss its missing consideration in the first order S-matrix model. In a first order process, i.e. a process where each constituent of the physical system is involved at most in a single interaction, the secondary electron can only be ionized by direct interaction with the primary electron. As a consequence, to first order the impinging electron does not directly affect the momentum of the molecule. Also, the coupling of the laser field on the molecular ion can be considered to be negligible due to the large inertia of the molecular mass and the high frequency of the laser field. This is evident from the quiver radius of 5.1×10^{-4} a.u. for the hydrogen molecular cation in an 800 nm laser of $1\times10^{14}\,\mathrm{W/cm^2}$ intensity.

One may compare the situation considered here to the collision of two unbound electrons in the presence of a laser field. The first order S-matrix element for this process corresponding to equations (5.28) and (5.32) is given by

$$\begin{aligned}S_{fi}^{(1)} &= -i\int_{t_i}^{\infty} dt_1 \langle\, \boldsymbol{k}_a^{\mathrm{GV}}, \boldsymbol{k}_b^{\mathrm{GV}}(t_1)\,|\, V_{\mathrm{i}}\,[1\pm\mathcal{P}_{12}]\,|\,\boldsymbol{k}_0^{\mathrm{GV}}, \boldsymbol{k}_1^{\mathrm{GV}}(t_1)\,\rangle \\ &= -2\pi i\sum_{N=N_0}^{\infty}\delta\left(\frac{k_a^2}{2}+\frac{k_b^2}{2}-\frac{k_0^2}{2}-\frac{k_1^2}{2}-N\omega\right) \\ &\quad\times J_N\left(\boldsymbol{\alpha}_0\cdot(\boldsymbol{k}_a+\boldsymbol{k}_b-\boldsymbol{k}_0-\boldsymbol{k}_1)\right)\langle\,\boldsymbol{k}_a,\boldsymbol{k}_b\,|\,V_{\mathrm{i}}\,[1\pm\mathcal{P}_{12}]\,|\,\boldsymbol{k}_0,\boldsymbol{k}_1\,\rangle\,,\end{aligned} \tag{5.43}$$

where $\boldsymbol{k}_1$ is the momentum of the secondary electron, which for the length of this paragraph is assumed to be a freely drifting particle in a Gordon-Volkov eigenstate.

By the orthonormality of momentum eigenstates one obtains

$$\begin{aligned} S_{fi}^{(1)} = -2\pi i \sum_{N=N_0}^{\infty} \delta\left(\frac{k_a^2}{2} + \frac{k_b^2}{2} - \frac{k_0^2}{2} - \frac{k_1^2}{2} - N\omega\right) \\ \times \left(\frac{4\pi}{|\boldsymbol{k}_0 - \boldsymbol{k}_a|^2} \pm \frac{4\pi}{|\boldsymbol{k}_0 - \boldsymbol{k}_b|^2}\right) \delta\left(\boldsymbol{k}_a + \boldsymbol{k}_b - \boldsymbol{k}_0 - \boldsymbol{k}_1\right) \ , \end{aligned} \tag{5.44}$$

where $\delta(\boldsymbol{r}) \equiv \delta(x)\delta(y)\delta(z)$. Thus, if $\boldsymbol{k}_1$=0 initially, one also has $\boldsymbol{\Delta k}$=0, as demanded by momentum conservation.

Due to the Coulomb correlation of the secondary electron with the molecular system, which it is bound to in the initial state, the residual ion may compensate a nonzero electronic momentum balance. This effect can be discovered in the leading order of the S-matrix expansion Eq. (5.33), if additionally to the electronic state one considers the state of motion of molecular ion. Describing the physical system in a frame of reference where the molecular ion is at rest initially, its final momentum can be included as a plane wave in the final state[1]. This way the first order electronic S-matrix transition amplitude turns into an effective scattering potential acting on the molecular coordinates due to their appearance in the molecular wavefunction Φ_i. Without going into details which are beyond the scope of current interest, the derivation may be understood from the following qualitative argument. In a frame of reference where the ion was at rest before the collision, the ion momentum will change due to matrix elements of the form

$$\langle\, \mathbf{K}_{\text{ion}} |\, \exp\left[-i\boldsymbol{\Delta k} \cdot \mathbf{R}_{\text{CM}}\right] |\, \mathbf{0}\,\rangle \ , \tag{5.45}$$

where $\mathbf{R}_{\text{CM}}$ is the center of mass coordinate and $|\,\mathbf{0}\,\rangle$ and $|\,\mathbf{K}_{\text{ion}}\,\rangle$ denote the initial and final state momentum states respectively of the center of mass of the molecular ion. These matrix elements appear due to the effective potential

$$\begin{aligned} V_{\text{eff}} \equiv \sum_{N=-\infty}^{\infty} \delta\left(\frac{k_a^2}{2} + \frac{k_b^2}{2} + U_p + E_T - N\omega - \frac{k_0^2}{2}\right) \\ \times J_N\left(\boldsymbol{\alpha}_0 \cdot \boldsymbol{\Delta k}, \frac{U_p}{2\omega}\right) \\ \times \left(\frac{1}{|\boldsymbol{k}_0 - \boldsymbol{k}_a|^2} \pm \frac{1}{|\boldsymbol{k}_0 - \boldsymbol{k}_b|^2}\right) \tilde{\Phi}_i(\boldsymbol{\Delta k}) \ , \end{aligned} \tag{5.46}$$

[1] Actually, this is only an approximation for a Gordon-Volkov wavefunction, but this approximation is justified due to the large mass of the nuclei relative to the electronic mass. With a Gordon-Volkov wavefunction for the molecular ion, the arguments of the generalized Bessel function e.g. in Eq. (5.46) change to $J_N\left(\boldsymbol{\alpha}_0 \cdot \boldsymbol{\Delta k} + \boldsymbol{\alpha}_M^{(2)} \cdot \mathbf{K}_{\text{ion}}, \left(U_p + U_{p,M}^{(2)} - U_{p,M}\right)/(2\omega)\right)$, where $\boldsymbol{\alpha}_M^{(2)}$ and $U_{p,M}^{(2)}$ denote the quiver radius and ponderomotive energy respectively of the molecular dication (charge $q = +2$ and mass $M \equiv M_{\text{ion}}$), while $U_{p,M}$ denotes the ponderomotive energy of the molecular ion (nearly same mass but a charge of $q = +1$). Likewise, the energy balance would be changed by the term $U_{p,M}^{(2)} - U_{p,M}$. Since both, $\boldsymbol{\alpha}_M^{(q)}$ and $U_{p,M}^{(q)}$, scale with the mass as $1/M$ (see definitions (2.2) and (1.3)), they are negligible compared to their electronic counterparts.

and are weighted according to the electronic transition matrix elements contained. Here, the kinetic energy of the ion is neglected in the energy conservation, as it can be considered to be small in comparison to the electronic energies. As discussed in section 4.4.4 the matrix element (5.45) corresponds to a shift in the space of internuclear momentum by $\mathbf{K}_{\text{ion}} = -\boldsymbol{\Delta k}$.

In terms of the separated kinetic energy of the center of mass and of the relative motion of the outgoing electrons respectively (see section 3.1.1) $\boldsymbol{\Delta k}$ amounts to the difference between center of mass momentum $\boldsymbol{k}_{\text{CM}}$ of the outgoing electrons and the momentum $\boldsymbol{k}_0$ of the incoming electron:

$$\boldsymbol{\Delta k} = \boldsymbol{k}_{\text{CM}} - \boldsymbol{k}_0 \Rightarrow \boldsymbol{k}_0 = \boldsymbol{k}_{\text{CM}} + \mathbf{K}_{\text{ion}} \,, \tag{5.47}$$

where the last equation establishes the momentum conservation under the approximation that the total momentum transfer from the field due to multiphoton absorption is negligible. Note that the total momentum transfer affects the drift momentum of the electron in the laser field, not the ponderomotive motion. The momentum transfer from the field can be considered to be small as one photon carries a momentum of ω/c, which amounts to 4×10^{-4} a.u. for 800 nm photons. I.e. the field is a source (or drain) of energy, but its momentum exchange with the scattering system is negligible. The contrary holds for the molecular ion: It exchanges momentum with the scattering electrons, but due to its large inertial mass its energy exchange with the electrons can be neglected.

Since under these kinematic conditions, to the first order in the S-matrix expansion, the center of mass momentum $\boldsymbol{k}_{\text{CM}}$ is determined by Eq. (5.47), once the impact momentum and the recoil momentum of the molecular ion are given, all additional energy transfer by the intense-field multiphoton process affects only the relative kinetic energy of the electron pair. In other words, using the interpretation of section 3.1.1, it then changes the energy of the *relative electron-pair state*. It is interesting to note the similarity to the situation in the IVI process considered in chapter 4, where the active electron couples to the field and shares the absorbed energy with the vibrational substate of the molecule, which does not directly couple to the field. Here as well, the *relative electron-pair state* does not couple to the field, but its energy consumption is provided by the active *center of mass electron-pair state* that couples to the laser field due to its charge of 2 a.u..

The momentum transfer will lie predominantly along the direction of the acting forces, i.e. the coinciding polarization axis of the field and the impact direction of the primary electron. If photons are absorbed from the field, i.e. $N_0 > 0$ in expression (5.41), the generalized Bessel functions promote a momentum transfer to the center of mass of the electron pair along the field polarization. As in first order S-matrix approximation $\boldsymbol{k}_{\text{CM}}$ is not affected by any Coulomb interaction with the nuclei, the only coulomb interaction considered is the binary collision of the two electrons. The terms $1/q_i^2 = 1/|\boldsymbol{k}_0 - \boldsymbol{k}_i|^2$ that arise from this interaction correspond

to the Rutherford amplitude [73] and favor an emission of one of the electrons at a momentum $\boldsymbol{k}_i$ close to $\boldsymbol{k}_0$. Together with energy conservation these terms create an anisotropy in the preferred directions of emission, since, without absorption of photons from the field,

$$\frac{k_0^2}{2} - \frac{k_a^2}{2} - U_p - E_T = \frac{k_b^2}{2} > 0 \,, \tag{5.48}$$

i.e. without a high transfer of energy from the field k_a will be smaller than k_0. The anisotropy is stronger for the electron with the larger final momentum and it favors a change of momentum $\boldsymbol{q}_i$ in the direction of $-\boldsymbol{k}_0$. In the following discussion we assume that k_a is larger than k_b if not stated otherwise. In this case a relevant quantity is the momentum difference $\boldsymbol{q} \equiv \boldsymbol{k}_0 - \boldsymbol{k}_a$.

Thus, under the conditions considered here, the momentum transfer $\boldsymbol{\Delta k} = \boldsymbol{k}_b - \boldsymbol{q}$ to the center of mass will also be parallel to the incoming momentum $\boldsymbol{k}_0$ and to the laser polarization. To calculate a spectrum of the center of mass momentum, one would integrate Eq. (5.41) over all configurations of relative motion of the two electrons, that constitute the possible *internal* or *relative electron-pair states*, taking into account the relation of energy conservation in terms of kinetic energy of center of mass and relative motion (see section 3.1.1):

$$\frac{1}{4}k_{\mathrm{CM}}^2 = N\omega - U_p - E_T - \frac{1}{2}k_0^2 - k_{\mathrm{rel}}^2 \,. \tag{5.49}$$

Finally it is interesting to understand, why $\boldsymbol{\Delta k}$ appears as the argument of the Fourier-transformed molecular orbital instead of the momentum of the ionized electron, which appears in the corresponding term of the first order S-Matrix amplitude for single ionization. Since $\boldsymbol{k}_b = \boldsymbol{\Delta k} + \boldsymbol{k}_0 - \boldsymbol{k}_a$, the quantity $\boldsymbol{\Delta k}$ is the initial momentum that the secondary electron contributes to the collision. The possible initial momenta for the secondary electron are determined by its Fourier transformed wavefunction, just as in the case of single ionization. The appearance of the Fourier transformed molecular orbital can be interpreted as a probing of the molecular orbital that constitutes part of the initial conditions for the many-body $(e + N\omega, 2e)$ process.

5.1.4. Alignment Dependence for Different Orbital Symmetries

The molecular orbitals were approximated by the *natural orbitals* [347, 348, 48] obtained by a Multi-Configuration SCF calculation with Fully Optimized Reaction Space (FORS) on the basis of a 6-311(2d,1f) set of Gaussian type orbitals. The ionization potentials of N_2^+ were taken from [349] (with the lower ionization potential for the $^1\Sigma_g^+$ state, consistent with [350, 102]) and the one for O_2^+ was estimated as the difference between the double and single ionization potentials of O_2 [351–356] to be 24 eV, which agrees with experimental estimates [102, 357]. The initial energy of

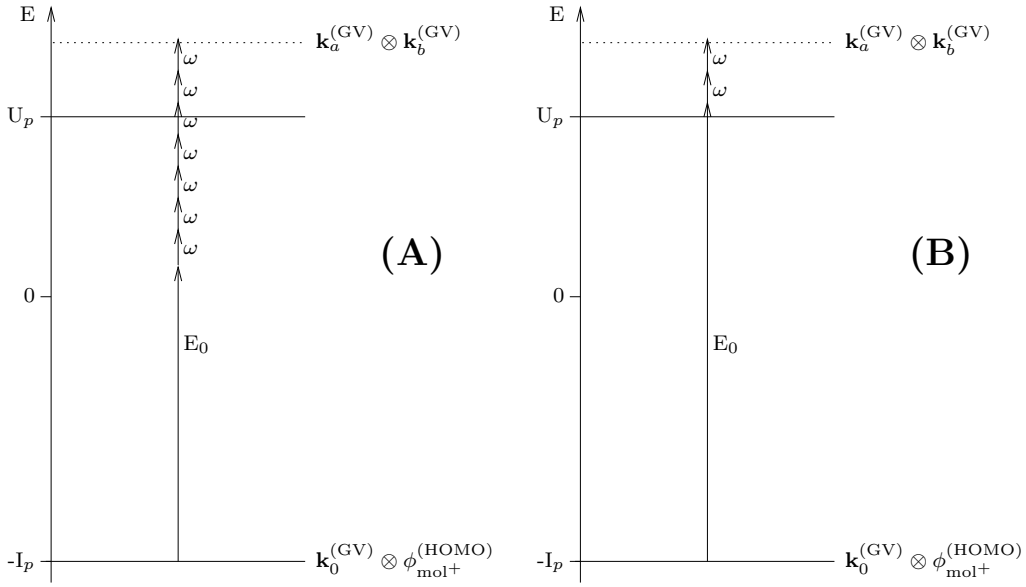

Figure 5.3.: Energy diagrams of the $(e + N\omega, 2e)$ process in an infrared laser field.
Left (A): E_0 five photons below dressed continuum threshold.
Right (B): E_0 at threshold.

the primary electron was fixed to a set of possible values, below, at and above the $(e+N\omega, 2e)$ ionization threshold for the specific molecular ion. For the sub-threshold energies the absorption of photons from the laser field allows energy conservation (see Fig. 5.3).

The laser wavelength was fixed to 800 nm and the intensity was adapted such that the chosen impact energy of the primary electron matches the maximal kinetic energy of about $3.17\,U_p$ at the moment of rescattering. This value is expected from a classical estimate for the field propagation, where it is assumed that its initial energy after ionization is negligible [74]. The ionization threshold of the secondary electron can be reached by the kinetic energy of the recolliding primary electron without additional photon absorption if $I_p^{(+)} + U_p \leq E_0 = 3.17\,U_p$, i.e. if the intensity is higher than $I_{\mathrm{thresh}} = 4\omega^2 I_p^{(+)}/2.17$, where $I_p^{(+)}$ is the ionization potential of the molecular cation.

The alignment angle of the molecule with respect to the linearly polarized laser was varied from parallel to perpendicular alignment and for each angle the total cross section for the $(e + N\omega, 2e)$ process was calculated. To this end, the contributions for the emission of the two electrons were integrated over their two full solid angles (4π) and the possible ways to share the energy – given at a certain order of photon absorption – between the two electrons. This 5-dimensional integral was evaluated numerically by Monte-Carlo integration ([358] using Sobol quasi-random numbers [359]). Finally the result of this integration was summed over the possible number of absorbed photons. If the kinetic energy of the incoming electron is already high

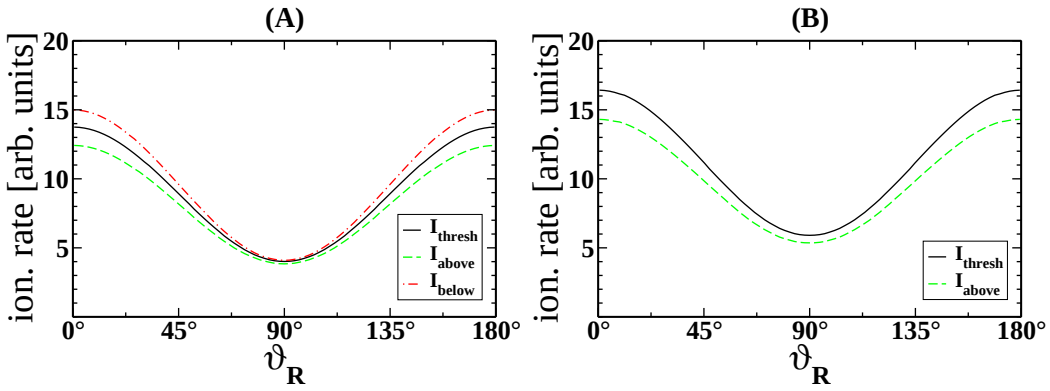

Figure 5.4.: Total singlet ionization rates for the $3\sigma_g$ orbital of $N_2^+ X^2\Sigma_g$ by the direct $(e + N\omega, 2e)$ process in a laser field of 800 nm wavelength ($\omega = 1.55$ eV).
(I_{below}= 1.5×10^{14} W/cm^2, I_{thresh}= 2.096×10^{14} W/cm^2 and I_{above}= 2.7×10^{14} W/cm^2).
Left: Impact energies 5 photons below threshold.
(E_0= 28.41 eV, E_0= 32.0 eV, and E_0= 35.64 eV)
Right: Impact energies matching threshold (E_0= 39.7 eV and E_0= 43.39 eV).

enough to achieve ionization of the target electron, the photon number is also allowed to be negative, corresponding to the emission of photons during the scattering process.

Fig. 5.4 shows the results for the electron impact ionization of the $3\sigma_g$ orbital of $N_2^+ X^2\Sigma_g$ in a laser field at 800 nm wavelength. In this calculation only the direct $(e + N\omega, 2e)$ scattering term of V_i was considered. Three intensities are chosen to result in maximal rescattering energies of the primary electron that lie 5 photons below (chained line), at (solid line) or 5 photons above ionization threshold (dashed line). Note that the threshold is intensity dependent due to the ponderomotive potential. The figure shows the dependence of the total ionization rate on the alignment angle of the molecule with respect to the polarization axis, which in a process of *Nonsequential Double Ionization* by a linearly polarized laser field coincides with the momentum of the returning electron. Since the molecule is homonuclear the rates are symmetric with respect to the orientation of the molecular axis.

In the context of rescattering the two active electrons are treated as a singlet system. This target shows a significantly enhanced ionization rate for the aligned molecule as compared to the anti-aligned configuration. The behavior can be interpreted in terms of the S-matrix expression (5.41) for the differential ionization rate. The alignment dependence enters through the Fourier transformed molecular orbital. Just focusing on the angular dependence of the Fourier transformed molecular orbitals $\tilde{\Phi}_i(\boldsymbol{\Delta k})$ in Eq. (5.41), by expanding the plane wave $\exp[-i\boldsymbol{r}\boldsymbol{\Delta k}]$ in the Fourier integral in terms of spherical harmonics (e.g. [161], eq. (A4.27)), one obtains

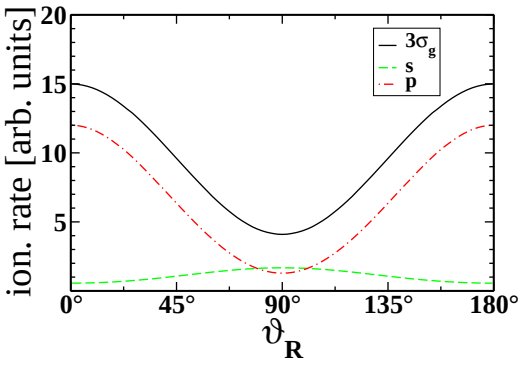

Figure 5.5.: Separate contributions of s and p atomic orbitals in the molecular $3\sigma_g$ orbital to the total singlet ionization rates of $N_2^+ X^2\Sigma_g$ ($E_0 = 28.41\,\mathrm{eV}$ in a laser field of intensity I_{below} and frequency $\omega = 1.55\,\mathrm{eV}$).

[34, 37, 100]:

$$\begin{aligned}\tilde{\Phi}_{3\sigma_g}(\boldsymbol{\Delta k}) =& 2c_s\tilde{\phi}_{s\text{-AO}}(\boldsymbol{\Delta k})\cos\left(\boldsymbol{\Delta k}\cdot\boldsymbol{R}_e/2\right)\\ &+i2c_p\tilde{\phi}_{p_z\text{-AO}}(\boldsymbol{\Delta k})\sin\left(\boldsymbol{\Delta k}\cdot\boldsymbol{R}_e/2\right)\ ,\end{aligned} \tag{5.50}$$

where $\tilde{\phi}_{\text{s-AO}}(\boldsymbol{\Delta k})$ is the Fourier transformed atomic s-orbital located at one of the nuclei (see Eq. (4.60)) and $\tilde{\phi}_{\text{p-AO}}$ is the corresponding Fourier transformed atomic p-orbital. Note that the momentum balance $\boldsymbol{\Delta k} = \boldsymbol{k}_a + \boldsymbol{k}_b - \boldsymbol{k}_0$ can be nonzero due to the recoil momentum of the ion (see discussion in section 5.1.3).

Fig. 5.5 shows the separate contributions of the s and p atomic orbitals in the molecular $3\sigma_g$ orbital. The p component clearly dominates the behavior. From Eq. (5.51) and Eq. (5.52) one sees that the atomic p-orbitals of the $3\sigma_g$ orbital induce a $\cos(\vartheta_{\boldsymbol{\Delta k}}) = \widehat{\boldsymbol{\Delta k}}\cdot\widehat{\boldsymbol{R}}_e$ characteristic, while the $1\pi_u$ exposes a $\sin(\vartheta_{\boldsymbol{\Delta k}}) = |\widehat{\boldsymbol{\Delta k}}\times\widehat{\boldsymbol{R}}_e|$ dependence. I.e. while the former favors a momentum transfer of $\boldsymbol{\Delta k}$ to the center of mass of the dication along the molecular axis, the latter promotes a momentum transfer perpendicular to this axis.

More generally we find the following alignment dependencies for molecular orbitals of different symmetries:

$$\begin{aligned}\tilde{\Phi}_{3\sigma_g}(\boldsymbol{\Delta k}) =& \quad 2c_s\tilde{R}_{s\text{-AO}}(|\Delta k|)\cos\left(\boldsymbol{\Delta k}\cdot\boldsymbol{R}_e/2\right)\\ &+ i2c_p\tilde{R}_{p_z\text{-AO}}(|\Delta k|)\widehat{\boldsymbol{\Delta k}}\cdot\widehat{\boldsymbol{R}}_e\sin\left(\boldsymbol{\Delta k}\cdot\boldsymbol{R}_e/2\right)\end{aligned} \tag{5.51}$$

$$\tilde{\Phi}_{1\pi_u}(\boldsymbol{\Delta k}) = \quad 2c_p\tilde{R}_{p_{x/y}\text{-AO}}(|\Delta k|)\left|\widehat{\boldsymbol{\Delta k}}\times\widehat{\boldsymbol{R}}_e\right|\cos\left(\boldsymbol{\Delta k}\cdot\boldsymbol{R}_e/2\right) \tag{5.52}$$

$$\tilde{\Phi}_{1\pi_g}(\boldsymbol{\Delta k}) = \quad 2c_p\tilde{R}_{p_{x/y}\text{-AO}}(|\Delta k|)\left|\widehat{\boldsymbol{\Delta k}}\times\widehat{\boldsymbol{R}}_e\right|\sin\left(\boldsymbol{\Delta k}\cdot\boldsymbol{R}_e/2\right) \tag{5.53}$$

$$\begin{aligned}\tilde{\Phi}_{3\sigma_u}(\boldsymbol{\Delta k}) =& \quad 2c_s\tilde{R}_{s\text{-AO}}(|\Delta k|)\sin\left(\boldsymbol{\Delta k}\cdot\boldsymbol{R}_e/2\right)\\ &+ i2c_p\tilde{R}_{p_z\text{-AO}}(|\Delta k|)\widehat{\boldsymbol{\Delta k}}\cdot\widehat{\boldsymbol{R}}_e\cos\left(\boldsymbol{\Delta k}\cdot\boldsymbol{R}_e/2\right)\ ,\end{aligned} \tag{5.54}$$

where $\tilde{R}_{s\text{-AO}}$, $\tilde{R}_{p_z\text{-AO}}$ and $\tilde{R}_{p_{x/y}\text{-AO}}$ are the radial parts of the Fourier transformed s and p atomic orbitals respectively.

Assuming that the momentum transfer is small compared to the inverse internuclear distance, the interference terms in Eqns. (5.51-5.54) can be expanded up to second order in $|\boldsymbol{\Delta k}\cdot\boldsymbol{R}_e|$ as:

$$\begin{aligned}
\tilde{\Phi}_{3\sigma_g}(\boldsymbol{\Delta k}) \approx\ & 2c_s\tilde{R}_{s\text{-AO}}(|\Delta k|)\left(1-\frac{1}{2}(\boldsymbol{\Delta k}\cdot\boldsymbol{R}_e/2)^2\right)\\
&+ ic_p\tilde{R}_{p_z\text{-AO}}(|\Delta k|)\cos(\vartheta_{\boldsymbol{\Delta k}})\boldsymbol{\Delta k}\cdot\boldsymbol{R}_e\\
=\ & c_s\tilde{R}_{s\text{-AO}}(|\Delta k|)\frac{1}{4}\left(8-|\boldsymbol{\Delta k}|^2|\boldsymbol{R}_e|^2+|\boldsymbol{\Delta k}|^2|\boldsymbol{R}_e|^2\sin^2(\vartheta_{\boldsymbol{\Delta k}})\right)\\
&+ ic_p\tilde{R}_{p_z\text{-AO}}(|\Delta k|)|\boldsymbol{\Delta k}||\boldsymbol{R}_e|\cos^2(\vartheta_{\boldsymbol{\Delta k}})
\end{aligned} \tag{5.55}$$

$$\begin{aligned}
\tilde{\Phi}_{1\pi_u}(\boldsymbol{\Delta k}) \approx\ & c_p\tilde{R}_{p_{x/y}\text{-AO}}(|\Delta k|)\sin(\vartheta_{\boldsymbol{\Delta k}})\left(1-\frac{1}{2}(\boldsymbol{\Delta k}\cdot\boldsymbol{R}_e/2)^2\right)\\
=\ & c_p\tilde{R}_{p_{x/y}\text{-AO}}(|\Delta k|)\sin(\vartheta_{\boldsymbol{\Delta k}})\frac{1}{4}\left(8-|\boldsymbol{\Delta k}|^2|\boldsymbol{R}_e|^2+|\boldsymbol{\Delta k}|^2|\boldsymbol{R}_e|^2\sin^2(\vartheta_{\boldsymbol{\Delta k}})\right)
\end{aligned} \tag{5.56}$$

$$\begin{aligned}
\tilde{\Phi}_{1\pi_g}(\boldsymbol{\Delta k}) \approx\ & 2c_p\tilde{R}_{p_{x/y}\text{-AO}}(|\Delta k|)\sin(\vartheta_{\boldsymbol{\Delta k}})\boldsymbol{\Delta k}\cdot\boldsymbol{R}_e/2\\
=\ & c_p\tilde{R}_{p_{x/y}\text{-AO}}(|\Delta k|)|\boldsymbol{\Delta k}||\boldsymbol{R}_e|\frac{1}{2}\sin(2\vartheta_{\boldsymbol{\Delta k}})
\end{aligned} \tag{5.57}$$

$$\begin{aligned}
\tilde{\Phi}_{3\sigma_u}(\boldsymbol{\Delta k}) \approx\ & c_s\tilde{R}_{s\text{-AO}}(|\Delta k|)\boldsymbol{\Delta k}\cdot\boldsymbol{R}_e\\
&+ i2c_p\tilde{R}_{p_z\text{-AO}}(|\Delta k|)\cos(\vartheta_{\boldsymbol{\Delta k}})\left(1-\frac{1}{2}(\boldsymbol{\Delta k}\cdot\boldsymbol{R}_e/2)^2\right)\\
=\ & c_s\tilde{R}_{s\text{-AO}}(|\Delta k|)|\boldsymbol{\Delta k}||\boldsymbol{R}_e|\cos(\vartheta_{\boldsymbol{\Delta k}})\\
&+ ic_p\tilde{R}_{p_z\text{-AO}}(|\Delta k|)\cos(\vartheta_{\boldsymbol{\Delta k}})\frac{1}{4}\left(8-|\boldsymbol{\Delta k}|^2|\boldsymbol{R}_e|^2+|\boldsymbol{\Delta k}|^2|\boldsymbol{R}_e|^2\sin^2(\vartheta_{\boldsymbol{\Delta k}})\right)\ .
\end{aligned} \tag{5.58}$$

Thus the alignment dependence of the $3\sigma_g$ orbital of $N_2^+X^2\Sigma_g$ (Fig. 5.4) is different to the behavior found in the ionization of an electron from the $1\pi_u$ orbital of $N_2^+X^2\Sigma_g$. In this case there are two possible spin orientations of the secondary electron. Here we consider the case where the primary and secondary electrons form a triplet, finally leaving the dication in the triplet state $a^3\Pi_u$. The corresponding data are presented in Fig. 5.6. The main difference between the $3\sigma_g$ and the $1\pi_u$ orbitals in N_2 is the orientation of the contributing atomic orbitals with respect to the internuclear axis (the effect of spin will be discussed in the next section). While the atomic p_z orbitals in a molecular $3\sigma_g$ orbital are directed along the internuclear axis, the atomic $p_{x/y}$ (or rather $m=\pm1$) orbitals that form the molecular $1\pi_u$ orbital are aligned perpendicular to it. This is the origin of the $\sin(\vartheta_{\boldsymbol{\Delta k}})$ term in the alignment dependence of the transition matrix element (see Eq. (5.52)).

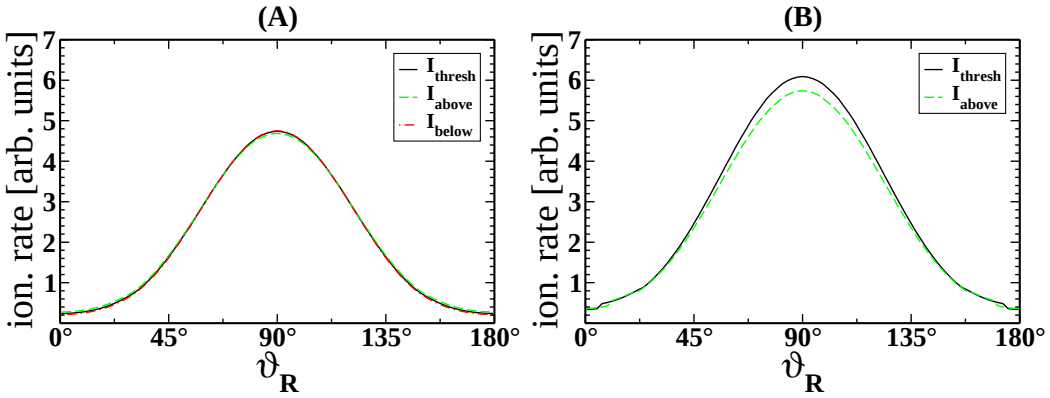

Figure 5.6.: Total triplet ionization rates for the $1\pi_u$ orbital of $N_2^+ X^2\Sigma_g$ by the direct $(e + N\omega, 2e)$ process in a laser field of 800 nm wavelength ($\omega = 1.55$ eV).
(I_{below}=1.6×10^{14} W/cm^2, I_{thresh}=2.14×10^{14} W/cm^2 and I_{above}=2.75×10^{14} W/cm^2).
Left: Impact energies 5 photons below threshold.
(E_0= 30.3 eV, E_0= 32.8 eV, and E_0= 36.6 eV)
Right: Impact energies matching threshold (E_0= 40.5 eV and E_0= 44.4 eV).

It is interesting to compare this to the alignment dependence of $(e + N\omega, 2e)$ ionization from the HOMO of $O_2^+ X^2\Pi_g$ presented in Fig. 5.7. It shows maxima at 45°, which corresponds to the characteristic found in multiphoton single ionization by an intense laser field [37]. Equations (5.57) and (5.57) contain a sine term for p_x and p_y, which has been interpreted as destructive interference of the outgoing partial waves of the ionizing electron from the two nuclear centers [34]. The local maxima result from the product of two competing terms, the angular characteristic of the $1\pi_g$ orbital favoring momentum transfer at right angles to the molecular axis, counteracted by the destructive interference in that direction due to the opposite phases of the partial waves emitted from both sides of the molecular Coulombic double-well. As the interference term changes its phase depending on the electronic momentum balance (and internuclear distance), it suppresses momentum transfer completely at right angles to the molecular axis. The expansion (5.57) shows that the product of both effects results in the maximum at 45°.

The difference to the behavior of the $1\pi_u$ orbital of $N_2^+ X^2\Sigma_g$ can again be interpreted in terms of the symmetry of the molecular orbital that is probed by the ionization. The highest occupied orbital in $O_2^+ X^2\Pi_g$ is antibonding, exhibiting a node along the plane perpendicular to the intramolecular axis, cutting it at the molecular center of mass. Note that the contributing atomic orbitals have p_x or p_y character. The $1\pi_u$ orbital in the nitrogen case in contrast does not show this nodal plane, thus allowing more electron density to form in the space between the nuclei, around the internuclear axis. (Note that the spherical harmonics $Y_{1,1}$ and $Y_{1,-1}$, from which the Cartesian orbitals p_x or p_y are constructed, show no preferential directedness along

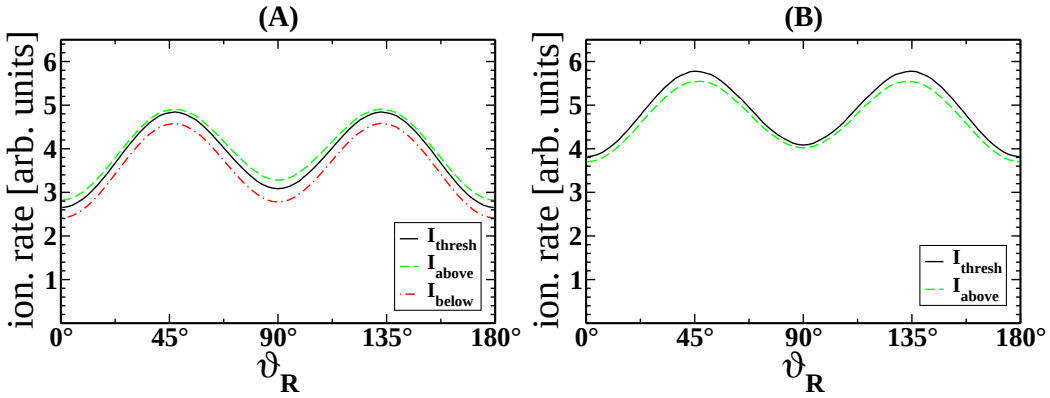

Figure 5.7.: Total ionization rates for $O_2^+ X^2\Pi_g$ by the direct $(e + N\omega, 2e)$ process in a laser field of 800 nm wavelength ($\omega = 1.55\,\text{eV}$). Variation with alignment angle of the molecular axis with respect to the polarization/impact direction. Intensities of the laser are chosen such that the maximal impact energy of the electron lies either above, at or below ionization threshold ($I_p + U_p(I_0)$).
(I_{below}= 1.30×10^{14} W/cm^2, I_{thresh}= 1.85×10^{14} W/cm^2 and I_{above}= 2.5×10^{14} W/cm^2).
Left: Impact energies 5 photons (7.75 eV) below threshold
(E_0= 24.6 eV, E_0= 27.4 eV, and E_0= 31.9 eV).
Right: Impact energies matching threshold (E_0= 35.1 eV and E_0= 39.6 eV).

the x- or y-axis). More importantly, both atomic p orbitals of the molecular $1\pi_u$ orbital of $N_2^+ X^2\Sigma_g$ are in phase, causing a constructive interference of the outgoing partial waves of the ionizing electron from the two nuclear centers. I.e. the suppression that is characteristic for the HOMO of molecular oxygen is not present in this case.

5.1.5. Spin Effects

Fig. 5.8 shows the effect of the *exchange scattering* due to the Pauli principle for identical fermions (see Eq. (5.41)). The figure compares the cross sections obtained by consideration of the antisymmetry of the total electronic wavefunction with different approximations. The complete neglect of the fermionic character of the electrons results in the incoherent sum $|f|^2 + |g|^2$ of the *direct* and *exchange* scattering amplitudes. It is interesting to note that this 'classical' result is closer to $2|f|^2$ than to the value of $|f|^2$ that is usually expected in nearly elastic scattering ($|\boldsymbol{k}_a|^2 \approx |\boldsymbol{k}_0|^2$), where the *straight-line approximation* $|\boldsymbol{q}|^2 \approx 4|\boldsymbol{k}_0|^2 \sin(\vartheta_{\boldsymbol{k}_a \boldsymbol{k}_0}/2) \approx 0$ can be made, turning f into a singular integral kernel which causes the contribution of g to be negligible. Here, in the strongly inelastic scattering process, this singularity can only occur if the secondary electron can overcome the ionization threshold to the field dressed continuum just by absorption of photons from the laser-field. It is more likely that the

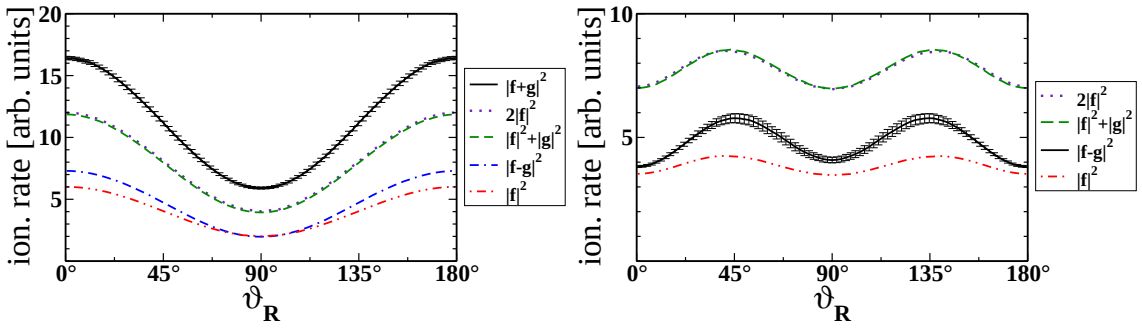

Figure 5.8.: Effect of antisymmetry of the total electronic wavefunction on the total singlet ionization rates.
Left: Singlet scattering $|f+g|^2$ on $3\sigma_g$ orbital of $N_2^+ X^2\Sigma_g$ ($E_0 = 28.41\,\mathrm{eV}$ at I_{thresh})
Right: Triplet scattering $|f-g|^2$ on $1\pi_g$ orbital of $O_2^+ X^2\Pi_g$ ($E_0 = 35.1\,\mathrm{eV}$ at I_{thresh}).

primary electron shares its energy, which makes the size of the *exchange scattering* term comparable to that of the *direct scattering* term and thus $|f|^2 + |g|^2 \approx 2|f|^2$ (consequently the dotted line is nearly indistinguishable from the dashed line). As expected from the formula the result for singlet exchange scattering lies above the 'classical' value, while the result for triplet exchange scattering lies below this value and actually quite close to the $|f|^2$ approximation. It is disputable to interpret the latter as a signature of the Pauli hole in the triplet momentum wavefunction, which disallows both outgoing electrons to acquire the same momentum state, as this rule only suppresses cases where both electron momenta go in the same direction with exactly equal momenta. Generally, the effect of the wavefunction antisymmetry is found to affect the total cross sections but to have only little influence on their alignment dependence. It should be noted that the fermionic character of the electrons also shows signatures in differential cross sections that resolve electron-electron correlation in *Nonsequential Double Ionization* [360–362].

5.1.6. Relation to Experiment

Field-free transient alignment of molecules can be generated using techniques of strong-field induction of rotational wave packets (see [323, 324] and references therein). This allows the controlled preparation of the initial conditions for subsequent physical processes that are sensitive to alignment. For N_2 specifically an experiment of NSDI was performed using this technique [321], that confirms the preferential emission for parallel alignment that was shown here to be characteristic for the $3\sigma_g$ HOMO of molecular nitrogen in the $(e + N\omega, 2e)$ process. It did not resolve ionization at intermediate alignment angles though, which does not rule out an admixture of ionization

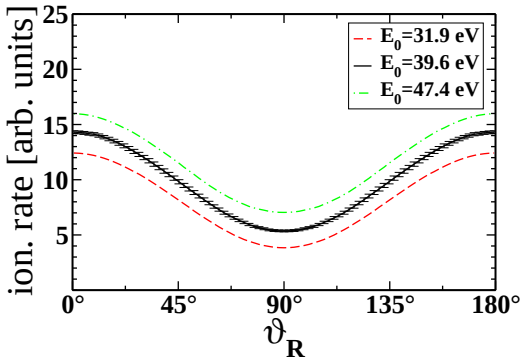

Figure 5.9.: Total singlet ionization rates for the $3\sigma_g$ orbital of $N_2^+ X^2\Sigma_g$ at a constant laser intensity of $I_{\text{above}} = 2.7 \times 10^{14}\,\text{W/cm}^2$ and varying energy of the primary (projectile) electron.
($E_0 = 35.6\,\text{eV}$, $E_0 = 43.4\,\text{eV}$ and $E_0 = 51.1\,\text{eV}$).

from the molecular $1\pi_u$ orbital, causing a superposition of the respective alignment dependencies which can result in a small local maximum for the *Nonsequential Double Ionization* at perpendicular alignment of the N_2 molecule with respect to the laser polarization.

In the experiment reported in [322] on the other hand a different technique is applied: The orientation of the molecules is detected after the double ionization process by observing the direction of emission of the fragments of the dissociating molecules in kinetic energy release spectra. This technique is selective to ionization channels that leave the dication in an excited state. The authors interpret the observed results in a three step model. In the first step an electron from the HOMO is ionized in an intense-field multiphoton process. After propagation in the laser field (which, contrary to the usual counting, is not considered as a separate step in [322]), it rescatters in the second step with a secondary bound electron. In contrast to the process considered in this chapter the authors assume that the secondary electron is transfered to an excited bound state in this rescattering event. In the final step this secondary, excited electron would then ionize in a subsequent maximum of the oscillating laser field. To leave the dication itself in an excited, dissociating state without interactions of higher order, the secondary electron must originate from a molecular orbital that lies energetically below the HOMO.

For the dissociation of N_2^{2+} from the $A^1\Pi_u$ state the spectra in [322] show a strong predominance for parallel alignment. This is at odds with the expectations from the analysis of the $(e + N\omega, 2e)$ process, as the major electronic configuration of the $A^1\Pi_u$ state is considered to be the $\pi_u^{-1}3\sigma_g^{-1}$ configuration (with respect to the neutral molecule); i.e. the primary electron from the $3\sigma_g$ HOMO of N_2 must have excited an electron from a π_u orbital in the rescattering event. It would be expected that the different characteristic of the rescattering ionization would have a stronger influence

on the dissociation pattern, resulting in additional maxima perpendicular to the direction of laser polarization. This can be an indication that rescattering ionization is not the dominant process in this particular case. Without further analysis the authors propose rescattering excitation as the dominant mechanism. On the other hand it is known that multi-electron correlation is important for inner-valence electrons [363], which suggests that the description of the single electron wavefunction for the secondary electron used in the theoretical calculation and analysis should be improved, e.g. by the use of Dyson orbitals [48–50, 364]. Other observed states of N_2^{2+} correspond to higher order processes and will not be considered here.

In the case of O_2^{2+} it is interesting to see that the measured dissociation spectra show relatively stable maxima at about 40° for different excited states of the dication ($W^3\Delta_u$, $B^3\Sigma_u^-$ and $1^1\Delta_u$). In these states the electronic configuration $\pi_u^{-1}\pi_g^{-1}$ (relative to the neutral molecule) is dominant. This is in contrast to the spectrum measured for the $B^3\Pi_g$ state of the dication with an electronic configuration of $3\sigma_g^{-1}\pi_g^{-1}$. It shows that the scattering of the primary π_g (HOMO) electron with a lower lying $3\sigma_g$ 'fills up' the minimum at zero degrees that is present for the $\pi_u^{-1}\pi_g^{-1}$ configuration. This can be interpreted as the interplay of the alignment characteristic of the intense-field multiphoton ionization of the primary electron, which has a maximum at 45° [37] and a minimum at both zero and 90°, with the corresponding dependence of the secondary $(e + N\omega, 2e)$ ionization step of a $3\sigma_g$ electron, which has its maximum at zero degrees. This observation suggests that the characteristics of the two individual steps of the process will generally interplay in the full NSDI process. In the following section a model formula for the combined process will be derived that involves two active electrons. It will be applied to the HOMO electrons of N_2 and O_2.

5.2. Model Formula for Nonsequential Double Ionization of Molecules

The electron impact ionization of different states of a molecular ion, considered in the previous sections of this chapter, is the second step in the coherent process of *Nonsequential Double Ionization* of molecules. To establish the connection of the second step with the full NSDI process, its initial conditions must be matched with the boundary conditions of the first step, the above threshold ionization of the primary electron. According to chapter 4, the molecular ion can be transferred to different vibronically excited states due to the first ionization step. These intermediate states are coupled to corresponding continuum states of the primary electron that rescatters in the second step. The coherent evolution of the primary ionized electron and the molecular ion in its possible transition states is defined by the intermediate separation of the full Hamiltonian as described by Eq. (3.54). Thus, the quantum mechanical representation of the time evolution connecting the initial and final step

of the three-step process is given by the Greens operator of the separated two-particle (Volkov electron-ion) system, which can be expressed as

$$G_m(t,t') = \frac{1}{i\hbar}\Theta(t-t')\exp\left[-\frac{i}{\hbar}\int_{t'}^{t} d\tau H_m(\tau)\right] . \tag{5.59}$$

It is a formal solution to the Schrödinger equation to the intermediate Hamilton operator H_m

$$\left[i\hbar\frac{\partial}{\partial t} - H_m(t)\right] G_m(t,t') = \delta(t-t') , \tag{5.60}$$

where the intermediate H_m is identical to the 'final' Hamiltonian Eq. (4.14) of the IVI process discussed in chapter 4 and the 'initial' Hamiltonian Eq. (5.22) of the recollision process:

$$H_m = H_{\mathrm{GV}}(1) + H_{\mathrm{mol+}}(2) . \tag{5.61}$$

In the product-basis of the eigenstates $|\,\Psi_m^{(j)}\,\rangle \equiv |\,\mathbf{k}^{\mathrm{GV}}\,\rangle\otimes\,|\,\Phi_m^{(j)}\,\rangle$ of H_m the Greens operator G_m is represented by the following expansion (see e.g. [68]):

$$\begin{aligned} G_m(t,t') =& \frac{1}{i\hbar}\Theta(t-t')\int d\mathbf{k}\,|\,\mathbf{k}\,\rangle\langle\,\mathbf{k}\,|\otimes\sum_j |\,\Phi_m^{(j)}\,\rangle\langle\,\Phi_m^{(j)}\,| \\ &\times\sum_{N=-\infty}^{\infty}\exp\left[-i(E_k+U_p+E_j-N\omega)t\right] J_N\left(\mathbf{k}\cdot\boldsymbol{\alpha}_0,\frac{U_p}{2\omega}\right) \\ &\times\sum_{N'=-\infty}^{\infty}\exp\left[i(E_k+U_p+E_j-N'\omega)t'\right] J_{N'}\left(\mathbf{k}\cdot\boldsymbol{\alpha}_0,\frac{U_p}{2\omega}\right) , \end{aligned} \tag{5.62}$$

where $E_k = k^2/2$ is the intermediate kinetic drift energy of the primary electron and E_j is the energy of the transition state $|\,\Phi_m^{(j)}\,\rangle$ of the molecular ion after the primary ionization.

The Greens operator G_m of the intermediate partition of the Hamiltonian is essential in the general framework of the IMST (section 3.3) to obtain a physically well defined expression for the second order term of the IMST expansion Eq. (3.50). To this end the Greens operator to the full Hamiltonian is now expanded in terms of G_m as:

$$G(t,t') = G_m(t,t') + \int_{-\infty}^{\infty} dt'' G(t,t'')V_m G_m(t'',t') . \tag{5.63}$$

Inserting this recursive expansion into the general S-matrix equation Eq. (3.50), the second order term is found to be

$$(S-1)_{fi}^{(2)} = \int_{-\infty}^{\infty} dt \int_{-\infty}^{\infty} dt' \langle\,\Psi_f(t)\,|\,V_f(t)G_m(t,t')V_i(t')\,|\,\Psi_{\mathrm{i}}(t')\,\rangle , \tag{5.64}$$

where

$$|\,\Psi_f(t)\,\rangle \equiv |\,\mathbf{k}_a^{\mathrm{GV}}(t)\,\rangle \otimes |\,\mathbf{k}_b^{\mathrm{GV}}(t)\,\rangle \otimes |\,\Phi_f^{(2+)}(t)\,\rangle \tag{5.65}$$

is approximated as a product state of two Gordon-Volkov states with the state of the molecular dication. As already discussed earlier, the correlation between the two outgoing electrons can be considered by using a exact fully correlated two-electron Gordon-Volkov wavefunction [152] or approximations of it, while the correlation between the outgoing electrons and the dication can only be treated approximately, e.g. by the inclusion of a Coulomb correction factor. $V_i(t')$ denotes the interaction of the primary electron with the laser field (see chapter 4). Neglecting ionization of the secondary electron by interaction with the field alone, corresponding to the sequential channel of double ionization, the interaction V_f is identical to the 'initial' interaction V_i of Eq. (5.22), corresponding to a Coulombic collision process. Thus, in this specific case V_f is an entirely internal interaction of parts of the molecular system which does not depend on the external time parameter [365]. As already explained before, the simultaneous interaction with the environment, in this case represented by the state of the laser field, is taken into account to all orders by the Gordon-Volkov waves.

Performing the integrations over t' and t in Eq. (5.64) and exploiting the addition theorem for generalized Bessel functions (see e.g. [223]), the second order S-matrix term takes the well known form [32]:

$$\begin{aligned}(S-1)_{fi}^{(2)} = &\sum_{N=-\infty}^{\infty} 2\pi\delta\left(E_a + E_b + 2U_p + E_f - E_i - N\omega\right) \\ &\times \int d\mathbf{k} \sum_j \langle\, \Phi_f \,|\, V_f\, [1 \pm \mathcal{P}_{12}] \,|\, \Phi_m^{(j)} \,\rangle J_N\left((\mathbf{k}_a + \mathbf{k}_b - \mathbf{k})\cdot\boldsymbol{\alpha}_0, \frac{U_p}{2\omega}\right) \\ &\times \sum_{N'=-\infty}^{\infty} \frac{(U_p - N'\omega)}{E_k + U_p + E_T[j,i] - N'\omega + i0} J_{N'}\left(\mathbf{k}\cdot\boldsymbol{\alpha}_0, \frac{U_p}{2\omega}\right) \langle\, \Phi_m^{(j)} \,|\, \Phi_i \,\rangle\ ,\end{aligned} \tag{5.66}$$

where $E_T[j,i] = E_m^{(j)} - E_i$ is the transition energy between the initial state of the neutral molecule and the state $|\,\Phi_m^{(j)}\,\rangle$ of the molecular ion. E_a and E_b are the kinetic energies of the outgoing electrons. According to the discussion of the orthogonality of bound and continuum states in the collision process the final interaction V_f in this specific mechanism of double-ionization reduces to the Coulomb interaction between the bound and the continuum electron $V_C^{(1,2)} = 1/|\mathbf{r}_1 - \mathbf{r}_2|$ (see end of section 5.1.2). Additional scattering with the nuclei (before or after the electron-electron interaction) constitutes a higher order process which cannot be considered consistently in the second order description of *Nonsequential Double Ionization*.

In the context of IVI (see chapter 4) the intermediate states j are vibrational substates ν' of specific electronic states s' of the singly ionized molecule, i.e. $i \equiv (s,\nu)$, $j \equiv (s',\nu')$ and $f \equiv (s'',\nu'')$. The molecular initial, transition and final states $|\,\Phi_i\,\rangle$,

$|\,\Phi_m^{(j)}\,\rangle$ and $|\,\Phi_f\,\rangle$ are approximated by the Born-Oppenheimer separated product of a nuclear and an electronic part (see section 4.3.1). Focusing on the two active electrons while the passive electrons are considered in their combined effect as the creators of the internuclear binding potential that determines the molecular vibrational states, the molecular state in the three stages is represented by

$$\Phi_i(\mathbf{R};\mathbf{r}_1,\mathbf{r}_2) = \chi_\nu(R-R_e)\otimes\phi_{s,1}(\mathbf{r}_1;\underline{\mathbf{R}}_n)\phi_{s,2}(\mathbf{r}_2;\underline{\mathbf{R}}_n) \tag{5.67}$$

$$\Phi_m^{(j)}(\mathbf{R};\mathbf{r}_2) = \chi'_{\nu'}(R-R'_e)\otimes\phi'_{s',2}(\mathbf{r}_2;\underline{\mathbf{R}}'_n) \tag{5.68}$$

$$\Phi_f(\mathbf{R};) = \chi''_{\nu''}(R-R''_e)\;, \tag{5.69}$$

where the orientation of the molecule is assumed to stay fixed during the process. This holds for diatomic molecules and can be extended to polyatomic molecules based on the criterion of invariance of symmetry elements.

The approximative treatment of the vibrational degree of freedom by the Franck-Condon approximation (Eq. (4.8)) reduces the computational resources such that the treatment of a higher order process as the *Nonsequential Double Ionization* of molecules can be considered. Applying this approximation and restricting the considered transition channels of the molecular ion to the vibrational substates ν' of a specific electronic state s' as well as neglecting the overlaps between the inactive electrons one can transform Eq. (5.66) to:

$$\begin{aligned}(S-1)^{(2)}_{fi}(\nu'',\nu)|_{s'} = 2\pi \sum_{N=-\infty}^{\infty} &\delta\left(E_a+E_b+2U_p+E_f-E_i+N\omega\right)\\ &\times\int d\mathbf{k}\langle\,\mathbf{k}_a,\mathbf{k}_b\,|\,V_f\,[1\pm\mathcal{P}_{12}]\,|\,\mathbf{k},\phi'_{s',2}\,\rangle\langle\,\mathbf{k}\,|\,\phi_{s,1}\,\rangle\\ &\times J_N\left((\mathbf{k}_a+\mathbf{k}_b-\mathbf{k})\cdot\boldsymbol{\alpha}_0,\frac{U_p}{2\omega}\right)\sum_{N'=-\infty}^{\infty}J_{N'}\left(\mathbf{k}\cdot\boldsymbol{\alpha}_0,\frac{U_p}{2\omega}\right)\\ &\times\sum_{\nu'}\frac{\langle\,\chi''_{\nu''}\,|\,\chi'_{\nu'}\,\rangle(U_p-N'\omega)\langle\,\chi'_{\nu'}\,|\,\chi_\nu\,\rangle}{E_k+U_p+E_T[(s',\nu'),(s,\nu)]-N'\omega+i0}\;,\end{aligned} \tag{5.70}$$

where

$$E_T[(s',\nu'),(s,\nu)] \equiv E_{(s',\nu')} - E_{(s,\nu)} \tag{5.71}$$

and $E_f - E_i = E_{(s'',\nu'')} - E_{(s,\nu)}$ is the total energy difference of initial and final state. Note that just as in the case of IVI (chapter 4), the molecular dication can be left in an excited vibrational (or generally vibronic) state. The Franck-Condon approximation applied here throughout the process is justified by the analysis of chapter 4 strictly only for the first ionization step. This analysis of vibrational excitation in the first step can however be considered to be representative for nonlinear processes in intense laser fields. We may point out that the application of the Franck-Condon approximation in both steps is independent on the one hand and just a matter of

reduction of computational cost on the other hand. In general, the expressions derived by the Franck-Condon overlap approximation can be replaced by the 'frozen' MO or fully coherent calculations (in Born-Oppenheimer approximation). For the first ionization step this is accomplished by the formulae derived in chapter 4, while for the $(e + N\omega, 2e)$ step the corresponding expression can be derived starting from Eq. (5.28) by the additional consideration of the vibrational transition along the same lines as for the IVI process, finally arriving at an expression similar to Eq. (5.33), with a modified energy balance and a matrix element that includes integration of the vibrational transition amplitude over the internuclear relative coordinate. Since the energies involved in the laser induced recollision in NSDI are relatively high compared to the photon energy and even more so compared to the energies of vibrational excitation, the deviation from the Franck-Condon distribution for the vibrational transition rates in this process is generally expected to be smaller than in the IVI process.

Computationally it is still a very time consuming task to perform the full integrations in Eq. (5.66). This encourages to seek for an approximative solution based on reasonable physical assumptions. The integration over intermediate momenta of the primary electron can be evaluated using the approximations of [27, 28], where the electron is assumed to be predominantly emitted along the direction of laser polarization and the radial integral over its intermediate kinetic drift energy is performed by using the definition of the Dirac-Heitler ζ function (see e.g. [68], Eq. (3.9.1.1), [366, 367]), also known as Sokhotsky-Plemelj identity [368]

$$\lim_{\epsilon \to 0} \frac{1}{E - H \pm i\epsilon} = P.V. \left(\frac{1}{E - H} \right) \mp i\pi\delta(E - H) \,, \tag{5.72}$$

and neglecting off-shell contributions from the Cauchy Principal Value ($P.V.$) term (pole approximation). The modulus squared result is a generalization of the model formula given in [28] to processes of *Nonsequential Double Ionization* in molecules where not only a single but several vibronic states are allowed as transition states for the singly ionized molecular ion:

$$\frac{dW^{(2)}(\mathbf{k}_a, \mathbf{k}_b)}{d\mathbf{k}_a d\mathbf{k}_b} \approx \sum_{N'=N_0'}^{\infty} \sum_j \Gamma_{(e+N\omega,2e)} \left(\mathbf{k}_a, \mathbf{k}_b; \mathcal{E}_{j,i}^{(N')} \right) \frac{\pi k_{j,i}^{(N')}}{2} \Gamma_{\mathrm{ATI}}^{(N')} \left(k_{j,i}^{(N')} \parallel \hat{\mathbf{A}}, \Phi_m^{(j)} \right) \,. \tag{5.73}$$

$\Gamma_{\mathrm{ATI}}^{(N')} \left(k_{j,i}^{(N')} \parallel \hat{\mathbf{A}}, \Phi_m^{(j)} \right)$ is the ATI rate for the ionization of the neutral molecule into a specific vibronic state $|\, \Phi_m^{(j)} \,\rangle$ of the molecular ion due to absorption of N' photons from the laser field (with a minimal N_0' due to energy conservation). Only electron momenta parallel to the polarization axis of the laser, along $\hat{\mathbf{A}}$, are considered. In chapter 4, where ATI transitions to vibrational substates of specific electronic states were considered, the expression for this rate is obtained in Eq. (4.28). In this case the magnitude of the drift momenta $k_{j,i}^{(N')}$ after ATI is given analogously to Eq. (4.29)

by

$$k_{j,i}^{(N')} = \sqrt{2E_k^{(N')}} \equiv \sqrt{2\left(N'\omega - U_p - (E_m^{(j)} - E_i)\right)} \,. \tag{5.74}$$

The rate for the second step of the process is given by the absolute square of the amplitude given in Eq. (5.33):

$$\begin{aligned}\Gamma_{(e+N\omega,2e)}\left(\mathbf{k}_a, \mathbf{k}_b; \mathcal{E}_{j,i}^{(N')}\right) \approx & C^2 \sum_{N=-\infty}^{\infty} \frac{dW_{(e+N\omega,2e)}^{(1)}(\mathbf{k}_a, \mathbf{k}_b)}{d\mathbf{k}_a d\mathbf{k}_b}\left(\mathcal{E}_{j,i}^{(N')}\right) \\ = & \sum_{N=N_0}^{\infty} 2\pi\delta\left(E_a + E_b + U_p + E_f - E_m^{(j)} - N\omega - \mathcal{E}_{j,i}^{(N')}\right) \\ & \times \left|\langle\, \mathbf{k}_a, \mathbf{k}_b \,|\, V_f\, [1 \pm \mathcal{P}_{12}] \,|\, \mathbf{k}_{\text{rescat}}, \Phi_m^{(j)} \,\rangle\right|^2 \\ & \times J_N^2\left((\mathbf{k}_a + \mathbf{k}_b - \mathbf{k}_{\text{rescat}}) \cdot \boldsymbol{\alpha}_0, \frac{U_p}{2\omega}\right) \,,\end{aligned} \tag{5.75}$$

where also the Coulomb correction $C^2 = \left(k_T^{3/2}/F\right)^{2Z/k_T}$ for the ionized secondary electron is applied with $k_T = \sqrt{2\left(E_f - E_m^{(j)}\right)}$ (see section 4.3.1). Consistently with the previous discussion the primary electron is considered to rescatter with the maximal classically allowed energy of $\mathcal{E}_{j,i}^{(N')} \approx 3.17\, U_p$ (see also footnote 18 of [28]), i.e. its initial kinetic energy after ionization is set to zero, independent of the number N' of photons absorbed.

If the transition occurs between the two electronic ground states of the molecule and the dication and one considers only vibrationally excited transition states $(0, \nu')$ of the singly ionized molecular ion in its electronic ground state, the transition energy for the primary ionization in Eq. (5.70) is given by $E_T[(0,\nu'),(0,\nu)] = I_p + \Delta E_{\text{vib}}(\nu', \nu)$. In this case, the momentum of the electron after *Inelastic Vibronic Ionization* (Eq. (4.29)) is given by:

$$k_{j,i}^{(N')} \equiv k_{(0,\nu'),(0,\nu)}^{(N')} = \sqrt{2\left(N'\omega - U_p - I_p - \Delta E_{\text{vib}}(\nu', \nu)\right)} \,, \tag{5.76}$$

and accordingly the transition energy in Eq. (5.75) for the secondary ionization can be written as:

$$E_f - E_m^{(j)} = I_p^{(+)} + \Delta E_{\text{vib}}(\nu'', \nu) - \Delta E_{\text{vib}}(\nu', \nu) \,, \tag{5.77}$$

where $I_p^{(+)}$ represents the ionization potential of the singly ionized molecule and $\Delta E_{\text{vib}}(\nu'', \nu)$ is the difference of the vibrational energy in the initial and the final state.

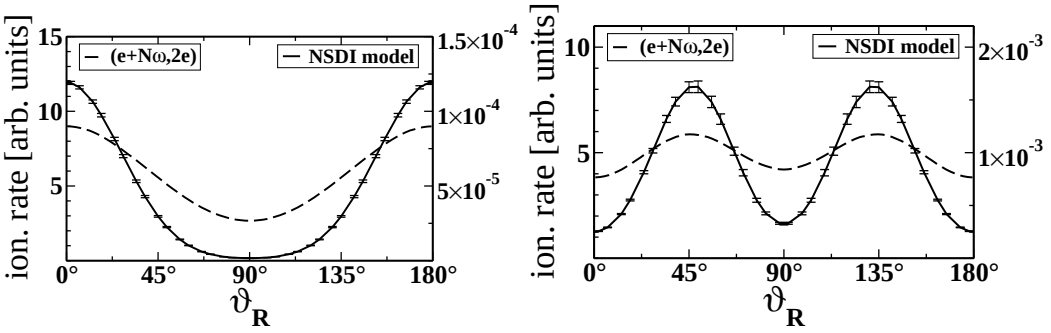

Figure 5.10.: Alignment dependence of IV-NSDI rates for the $(\nu'' = 0, \nu = 0)$ transition compared to the corresponding rates of the $(e + N\omega, 2e)$ process alone. Intensities are chosen such that classical impact energies are matching ionization threshold $(I_p^{(+)} + U_p)$ for the $(e + N\omega, 2e)$ process.
Left: $N_2^{2+}X^1\Sigma_g^+ \leftarrow N_2X^1\Sigma_g^+$ (I_{thresh}= $2.096\times10^{14}\,\text{W/cm}^2$)
Right: $O_2^{2+}X^1\Sigma_g^+ \leftarrow O_2X^3\Pi_g^-$ (I_{thresh}= $1.85\times10^{14}\,\text{W/cm}^2$).

5.2.1. Results for N_2 and O_2

In Fig. 5.10 the alignment dependence of total NSDI rates is presented as obtained from calculations of the model formula derived above. For comparison the rates for the $(e + N\omega, 2e)$ process are shown, which constitutes the second step of the total process. As it becomes evident from the figure, the alignment dependence is stronger for the combined NSDI process than for the $(e + N\omega, 2e)$ process alone. For O_2 the ratio lies between the minima and maxima between 1.6 and 1.8 for the separate $(e + N\omega, 2e)$ step, while it lies between 4.4 to 5.2 for the full NSDI process at the threshold intensity of $O_2^+X^2\Pi_g$. For N_2 the ratio increases from 2.8 for the separate $(e + N\omega, 2e)$ process to about 4.5 for the full NSDI process, both calculated at the threshold intensity of $N_2^+X^2\Sigma_g^+$. This amplification of the alignment dependence is anticipated as a result of the constructive interplay of the separate primary and secondary steps of ionization. Both processes independently show qualitatively a similar alignment dependence in their analytical first order S-matrix expressions [37, 100]. As a consequence the signature of the symmetry of the ionized molecular orbital is amplified in NSDI compared to the individual processes.

Fig. 5.11 shows the relative populations of the vibrational states of the dications after *Nonsequential Double Ionization* in parallel alignment. These are obtained from the normalized, i.e. relative IV-NSDI rates for the $(\nu'', \nu = 0)$ transitions as calculated by the IV-NSDI model formula in Franck-Condon approximation (IV-NSDI(FC)) derived in section 5.2. Experimental values have been used for the vibrational constants of the electronic ground states of N_2^{2+} [369, 370] and O_2^{2+} [371, 372].

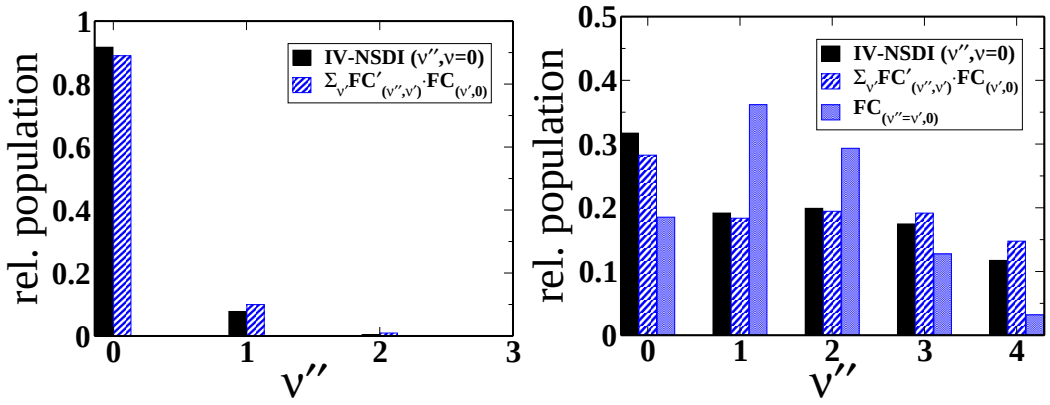

Figure 5.11.: Relative populations of the vibrational states in the dication of a diatomic molecule after *Nonsequential Double Ionization* in parallel alignment as calculated from the model formula described in section 5.2. For comparison the figure shows the products of the Franck-Condon factors for the IVI and the subsequent $(e+N\omega, 2e)$ process, summed over the possible vibrational transition states. For O_2 the Franck-Condon factors for the first (IVI) transition are shown as well, for N_2 these coincide with the IV-NSDI(FC) population. Intensities are chosen as in Fig. 5.10.
Left: $N_2^{2+}X^1\Sigma_g^+(\nu'') \leftarrow N_2X^1\Sigma_g^+(\nu=0)$
Right: $O_2^{2+}X^1\Sigma_g^+(\nu'') \leftarrow O_2X^3\Pi_g^-(\nu=0)$.

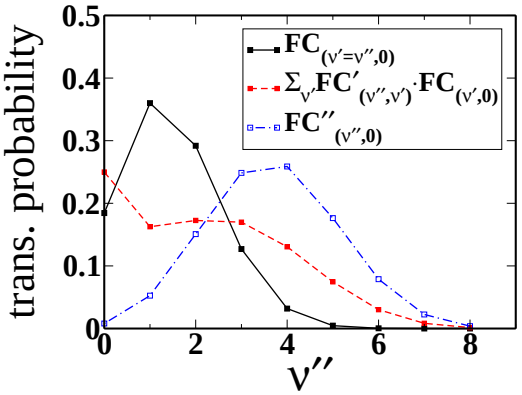

Figure 5.12.: Franck-Condon overlaps for transitions between the vibrational states of the electronic ground states of O_2 and its mono- and dications. $FC_{(\nu'=\nu'',0)}$ denotes the transition of the neutral $O_2X^3\Pi_g^-(\nu=0)$ to the vibrationally excited states $O_2^+X^2\Pi_g(\nu')$ of the cation in its electronic ground state while $FC''_{(\nu'',0)}$ refers to the direct transition of the neutral $O_2X^3\Pi_g^-(\nu=0)$ to the vibrationally excited states $O_2^{2+}X^1\Sigma_g^+(\nu'')$ of the dication in its electronic ground state. The $\Sigma_{\nu'}FC'_{(\nu'',\nu')} \cdot FC_{(\nu',0)}$ denotes the products of the Franck-Condon factors for the IVI and the subsequent $(e+N\omega, 2e)$ process, summed over the possible vibrational transition states.

As in the context of IVI, the relative populations are shifted towards lower vibrational states, an effect that was shown in chapter 4 to be a relative one, resulting from a suppression of the ionizing transitions into higher excited vibronic states. Note that the IV-NSDI(FC) distributions are compared to the products of the Franck-Condon factors for the IVI and the subsequent $(e+N\omega, 2e)$ process, summed over the possible vibrational transition states.

For N_2 one finds that the final distribution is nearly indistinguishable from the Franck-Condon distribution for the first (IVI) step alone. This in an incidental coincidence, as can be seen from the right hand panel of Fig. 5.11 which shows a strong deviation of the IV-NSDI(FC) population from the Franck-Condon distribution of the first transition in the case of O_2. For further reference Fig. 5.12 shows the normalized Franck-Condon distributions for different transitions: the one for the first (IVI) transition and the before-mentioned product-sum over possible two-step transitions are compared to the direct Franck-Condon overlaps between the electronic ground state of the neutral molecule and the dication respectively. The latter two were calculated from the overlap integrals of the respective Morse wavefunctions and good agreement with experimental data is found for the neutral to dication transition [373]. This comparison is necessary to confirm the numerical validity of the product-sum distribution. Comparing the relative IV-NSDI(FC) population with the Franck-Condon distribution for the direct neutral to dication transition, it is evident that the IV-NSDI process is not a direct transition between the neutral molecule and the dication, but that the IVI transitions to the vibrational states of the singly charged $O_2^+ X^2\Pi_g$ ion in the first step of the process are significant.

6. Conclusions and Outlook

This thesis presents an analysis of the interplay of molecular degrees of freedom with ionization processes in intense laser fields. The two most salient features of molecules in comparison to atoms are the anisotropy of their electronic state and their internal state of vibration. Thus, the analysis focusses on two aspects of the ionization of molecules in intense laser fields, the influence of intense-field multiphoton ionization on the concomitant transitions between vibrational states on the one hand and the dependence of certain ionization processes on the alignment of diatomic molecules with respect to the acting forces on the other hand.

In chapter 4 the vibrational state of a molecule after ionization in an intense laser field has been analyzed in the framework of S-Matrix theory. As a formal result a first order expression for the transition amplitude in the general process of *Inelastic Vibronic Ionization* (IVI) has been derived. It has been shown that the overlap approximation, which has been assumed before in S-Matrix calculations in an *ad hoc* way [202, 289], is a qualitatively good approximation in the domain of field parameters considered here (see section 4.4.3).

The shift in the distribution of the IVI transition probabilities to lower vibrational quantum numbers, deviating from the Franck-Condon distribution, has been shown to have its origin in the nonlinear dependence of the ionization rate on the transition energy $E_T = E_{\nu'}^{(f)} - E_{\nu}^{(i)}$. It is pointed out that the *Franck-Condon Principle* is a general principle of quantum mechanics, while the validity of results obtained by the *Franck-Condon approximation* has to be checked for each particular transition (see section 4.1.2). Two different levels of approximation have been identified, the 'frozen' MO approximation on the one hand – a special case of the generalized Franck-Condon (GFC [296]) approximation which includes the dynamic variation of the photoelectron phase terms – and the overlap approximation on the other hand, which corresponds to the original approximation of Franck and Condon. While the first one neglects the variation of the electronic wavefunctions within the range of the internuclear distances covered by the overlap of the vibrational wavefunctions, the latter also neglects the effect of the recoil momentum of the ionized electron on the internuclear motion. In the specific case of multiphoton ionization of H_2 in an intense laser field, the latter is found to be negligible compared to the former one. Both levels of approximation agree qualitatively well with the fully coherent calculations in this case, which confirms the usefulness of the Franck-Condon approximation for ionization processes in intense laser fields. This validation of the Franck-Condon approximation for the experimentally accessible case of intense-field multiphoton ionization of H_2 provides a better understanding on how this approximation has to

be applied to give valid results in strongly nonlinear processes.

It has been derived how momentum conservation emerges from the S-Matrix formalism (see section 4.4.4) as a result of spatial phase matching, which complements the emergence of energy conservation from temporal phase matching inherent to the theory. For the specific case of the IVI process the photoelectron phase terms appearing in the transition amplitudes have been shown to induce small momentum shifts in the eigenspace of the operator of internuclear momentum. The theory has been applied to isotopic variations of the H_2 molecule (HD and D_2) to analyze isotope effects. These effects are found to be very well described in terms of the Franck-Condon overlaps of the different vibrational wavefunctions.

As examples of more complex molecules the theory was applied to the homonuclear molecule O_2 and to the heteronuclear molecule CO. To obtain experimentally accessible observables, transition rates to vibronically (i.e. vibrationally as well as electronically) excited states have been calculated which define the initial conditions for the subsequent process of spontaneous emission. The resulting fluorescence spectra were presented. Using the example of the HCN molecule in one of its linear isotopomeric configurations it was shown how to apply the theory to polyatomic molecules.

In chapter 5 electron impact ionization of a molecule in the presence of an intense laser field was studied (abbreviated as $(e + N\omega, 2e)$). This process is the final step of *Nonsequential Double Ionization* of a molecule. To this end a first order S-matrix expression was derived from the principles of the Intense-Field Many-Body S-Matrix Theory (IMST). Beyond the standard approach the possibility of exchange scattering was taken into account to assess the influence of the two different spin correlations in the highest occupied molecular orbitals (HOMOs) of N_2 and O_2 (see section 5.1.5).

The influence of the different orbital symmetries on the alignment dependence of total ionization rates has been analyzed for electron impact ionization in the presence of an intense laser field (section 5.1.4), extending a previous analysis for intense-field multiphoton ionization by other authors [34, 36, 35]. To complete the interpretation of the resulting formulae, the role of momentum conservation in the established framework of IMST was considered based on the following two key results obtained in the previous chapters: On the one hand it builds on the analysis of an electron-pair state in the presence of a laser field (section 3.1.1), to understand the different roles of *center of mass momentum* and relative motion of the two outgoing electrons in an intense laser field. On the other hand the analysis of momentum conservation in the context of *Inelastic Vibronic Ionization* (IVI) (section 4.4.4) was extended to consider the *center of mass momentum* of the molecular ion.

To relate the results back to the specific context of *Nonsequential Double Ionization* an approximative model formula was used to calculate estimates for the influence of orbital symmetry on the alignment dependence of transition rates for *Nonsequential Double Ionization*. An amplification of the alignment dependence is found, as anticipated, as a result of the constructive interplay of the separate primary and

secondary steps of ionization. Both processes separately show a qualitatively similar alignment dependence in their analytical expressions derived from the first order IMST [37, 100]. As a consequence the signature of the symmetry of the ionized molecular orbital is amplified in NSDI compared to the individual processes. The theoretical results agree with the experimental data of a preferential emission for parallel alignment in the *Nonsequential Double Ionization* of N_2 [321]. This behavior was shown in the analysis of section 5.1.4 as well as in the numerical results obtained from the model formula in section 5.2 to be characteristic for the $3\sigma_g$ HOMO of molecular nitrogen.

Based on the analysis of *Inelastic Vibronic Ionization* (IVI) in chapter 4, the vibrational excitation of the molecular dication after *Nonsequential Double Ionization* was assessed using an approximative Franck-Condon treatment. Similar to the results obtained for IVI, the population of the vibrational states in the dication was found to be slightly *suppressed* below the product of the Franck-Condon factors of the individual ionization steps (summed over the vibrational transition states).

From this perspective different lines of future research arise. Using the techniques described in this thesis, the vibrational state of a molecule can be tracked coherently throughout processes comprising several steps of ionization, rescattering and recombination (e.g. [374]). As the basic approach developed in chapter 4 (within the Born-Oppenheimer approximation) operates without the Franck-Condon approximation, it allows an analysis on non-Franck-Condon effects (see sections (4.1.2) and (4.2)). In future applications of the formalism it will be interesting to apply it as well to overtone spectra of local mode vibrations [256] as well as to combine its general principle with other descriptions of vibrational states. The application to more complex molecules involves the quantum mechanical description of coupled anharmonic molecular vibrations in more than one dimension. Additionally the change of the rotational state of the molecule, which is neglected in the present analysis, can be considered along lines similar to the ones presented here for the vibrational state.

Combined with the electronic molecular orbitals, the coherent integration over all molecular degrees of freedom will however quickly exceed the current practical limits of numerical simulation. This underlines the importance to assess the validity of the different levels of approximation. If certain degrees of freedom can effectively be decoupled, the complexity of the problem reduces considerably, which frees up computational resources and allows their investment into the treatment of more complex physical processes instead.

The application to the dissociative double ionization of N_2 and O_2 [322] is considered to demand the inclusion of multi-electronic correlation beyond the two active electron model, as electrons from inner-valence orbitals are ionized and adiabatic relaxation of the multi-electron state becomes important [363]. An elegant way would be the use of Dyson orbitals [48–50] (see section 2.1.1) instead of their approximation by Hartree-Fock or natural orbitals. These consider the full electronic correlation in the initial and final bound state as well as the relaxation occurring in the transi-

tion. These orbitals are considered to be the physical quantities probed in electron momentum or (e,2e) spectroscopy (see [51] and references therein) as well as in the recently demonstrated molecular orbital tomography using *High Harmonic Generation* [242, 364]. The challenge lies in the calculation of these orbitals. Currently there are two approaches of approximation for them: The first family of methods originates from electron propagator theory [375, 376]. The second approach is to calculate the overlap between high quality wavefunctions for initial and (excited) final bound states, e.g. from Multi-Reference Configuration Interaction calculations with single and double excitations (MRCI(SD) or MRSD-CI) [51].

Since the fully coherent simulation of the three step process of *Nonsequential Double Ionization* still is a computationally demanding task, the propagation of the electronic wavepacket though the laser driven continuum is taken into account only very roughly in this work, based on a classical calculation of an upper bound for the energy transfer from the field. To push the quantum mechanical analysis a step further it might be worth to pursue an approach that is based on the stationary phase approximation of quantum trajectories [377] for the propagation of the field driven electronic wave packet, which on the one hand would reduce the integration space over the intermediate electronic continuum states, but on the other hand would consider the fact that the electron enters the continuum with nonzero velocity and that there is a weighted distribution of recollision energies to sum over.

It will also be interesting to treat the related phenomenon of *High Harmonic Generation* upon recombination for the case of diatomic molecules using a second order IMST approach. For this process experimental results for N_2 and O_2 show an alignment dependence of the intensity of the harmonic radiation that is related to the one found for NSDI [378].

Generally, the main strength of the IMST approach lies in its potential to analyze mechanisms of processes in intense laser fields. Once a mechanism has been identified the analytical form of the corresponding matrix elements allows the analysis of functional dependencies between physical degrees of freedom and parameters as well as the deliberate neglect of selected terms to assess their role in the process under consideration. The usefulness of each separate approximation provides a piece of information about the relevant physical interactions. These possibilities by far compensate for the limitations due to the restriction to individual terms of the S-matrix expansion as well as those imposed by the approximations used to describe the initial, transition and final states, since they can be addressed in a systematic way. This approach is therefore of high value to guide the physical intuition and to assist the interpretation of data obtained from experiments as well as from numerical ab-initio calculations.

Appendix

A. Atomic Units

In atomic units, four fundamental physical constants are set to unity:

$$\hbar = e = a_0 = m_e = 1 \; . \tag{A.1}$$

Since the Bohr radius is defined as

$$a_0 = \frac{4\pi\epsilon_0\hbar^2}{m_e e^2} \tag{A.2}$$

this system of units is of the Gaussian type, where $\epsilon_0 = \frac{1}{4\pi}$. The atomic unit of energy is the Hartree, with

$$1\,\text{Hartree} = \frac{e^2}{4\pi\epsilon_0 a_0} = 27.2116\,\text{eV} \tag{A.3}$$

The atomic unit of time is derived from the atomic unit of energy as

$$\hbar = \text{a.u.}_{\text{energy}} \times \text{a.u.}_{\text{time}} \Rightarrow \text{a.u.}_{\text{time}} = \frac{\hbar a_0}{e^2} = 24.2 \times 10^{-18}\,\text{s} \tag{A.4}$$

The atomic field strength in ground state of the hydrogen atom is obtained from the Coulomb law

$$|E_0| = \frac{e}{4\pi\epsilon_0 a_0^2} = 5.14 \times 10^9\,\frac{\text{V}}{\text{cm}} \tag{A.5}$$

and from this one derives the atomic unit of intensity as

$$1\,\text{a.u. of Intensity} = \frac{1}{2} c\epsilon_0 E_0^2 = 3.51 \times 10^{16}\,\text{W/cm}^2 \; . \tag{A.6}$$

Acknowledgments

I want to thank my supervisors for having given me the chance to discover more of quantum physics and for guiding me in discussions with their experience and intuition. I feel honored by the creative and encouraging discussions with Farhad H. M. Faisal Ph.D. and to be given the chance to build my research upon the fascinating power and clarity of the Intense-Field Many-Body S-Matrix Theory.

I want to thank Dr. Andreas Becker, who granted me continued support and the chance to benefit from the scientific atmosphere of his research group *Nonlinear Processes in Strong Laser Fields* at the Max Planck Institute for the Physics of Complex Systems in the city of Dresden.

I am also grateful for the code for the generalized Bessel function that was developed by former members of the group *Theoretische Atom-, Molekül- und Laserphysik* as well as for the various packages opensource software which constitute an essential part of the means of production necessary for the research for and preparation of this thesis ([237, 379–397]). I also acknowledge the fine documentation and course materials made available by numerous scientists on the web (e.g. [398–402]).

I would like to thank my friends who were patient with my absent-minded states as well as with my esoteric sounding reports and who supported me emotionally.

Finally I'm thanking my family for their support and foremost my parents, who in addition convinced me to learn maths and encouraged me to follow my scientific interests.

Bibliography

[1] A. Einstein, Ann. d. Phys. **17**, 132 (1905).

[2] M. Goeppert, Naturw. **17**, 932 (1929).

[3] M. Goeppert-Mayer, Ann. Phys. **9**, 273 (1931).

[4] V. W. Hughes and L. Grabner, Phys. Rev. **79**, 314 (1950).

[5] W. Kaiser and C. G. B. Garrett, Phys. Rev. Lett. **7**, 229 (1961).

[6] J. P. Gordon, H. J. Zeiger, and C. H. Townes, Phys. Rev. **95**, 282 (1954).

[7] T. H. Maiman, Nature **187**, 493 (1960).

[8] A. L. Schawlow and C. H. Townes, Phys. Rev. **112**, 1940 (1958).

[9] G. S. Voronov and N. B. Delone, Sov. Phys. JETP Lett. **1**, 66 (1965), [Zh. Éksp. Teor. Fiz. Pis'ma Red. **1**, 42 (1966)].

[10] P. Agostini, G. Barjot, J. F. Bonnal, G. Mainfray, and C. Manus, IEEE J. Quant. Electron. **4**, 667 (1968).

[11] A. D. Strickland and G. Mourou, Opt. Commun. **56**, 219 (1985).

[12] P. Maine and G. Mourou, Opt. Lett. **13**, 467 (1988).

[13] P. Maine, D. Strickland, P. Bado, M. Pessot, and G. Mourou, IEEE J. Quantum Electron. **24**, 398 (1988).

[14] J. D. Bonlie, F. Patterson, D. Price, B. White, and P. Springer, Appl. Phys. B **70**, S155 (2000).

[15] S.-W. Bahk, P. Rousseau, T. A. Planchon, V. Chvykov, G. Kalintchenko, A. Maksimchuk, G. A. Mourou, and V. Yanovsky, Opt. Lett. **29**, 2837 (2004).

[16] T. Brabec and F. Krausz, Rev. Mod. Phys. **72**, 545 (2000).

[17] A. Scrinzi, M. Y. Ivanov, R. Kienberger, and D. M. Villeneuve, J. Phys. B. **39**, R1 (2006).

[18] M. Hentschel, R. Kienberger, Ch. Spielmann, G. A. Reider, N. Milosevic, T. Brabec, P. Corkum, U. Heinzmann, M. Drescher, and F. Krausz, Nature **414**, 509 (2001).

[19] P. Antoine, A. L'Huillier, and M. Lewenstein, Phys. Rev. Lett. **77**, 1234 (1996).

[20] M. J. Rosker, M. Dantus, and A. H. Zewail, J. Chem. Phys. **89**, 6113 (1988).

[21] E. D. Potter, J. L. Herek, S. Pedersen, Q. Lui, and H. Zewail, Nature **355**, 66 (1992).

[22] A. H. Zewail, Science **242**, 1645 (1988).

[23] F. H. M. Faisal and A. Becker, *Selected Topics on Electron Physics* (Plenum, New York, 1996), p. 397.

[24] F. H. M. Faisal and A. Becker, *Multiphoton Processes*, vol. 154 of *Intl. Conf. Ser.* (Institute of Physics Publ. (Bristol), 1997).

[25] F. H. M. Faisal, A. Becker, and J. Muth-Böhm, Laser Physics **9**, 115 (1999).

[26] A. Becker and F. H. M. Faisal, J. Phys. B **38**, R1 (2005).

[27] F. H. M. Faisal and A. Becker, Laser Phys. **7**, 684 (1997).

[28] A. Becker and F. H. M. Faisal, Phys. Rev. A **59**, R1742 (1999).

[29] A. Becker and F. H. M. Faisal, Phys. Rev. A **59**, R3182 (1999).

[30] A. Becker and F. H. M. Faisal, Phys. Rev. Lett. **84**, 3546 (2000).

[31] A. Becker and F. H. M. Faisal, Opt. Expr. **8**, 383 (2001).

[32] A. Becker and F. H. M. Faisal, Phys. Rev. Lett. **89**, 193003 (2002).

[33] U. Saalmann, C. Siedschlag, and J.-M. Rost, J. Phys. B **39**, R39 (2006).

[34] J. Muth-Böhm, A. Becker, and F. H. M. Faisal, Phys. Rev. Lett. **85**, 2280 (2000).

[35] F. Grasbon, G. G. Paulus, S. L. Chin, H. Walther, J. Muth-Böhm, A. Becker, and F. H. M. Faisal, Phys. Rev. A **63**, 041402(R) (2001).

[36] J. Muth-Böhm, A. Becker, S. L. Chin, and F. H. M. Faisal, Chem. Phys. Lett. **337**, 313 (2001).

[37] A. Jaroń-Becker, A. Becker, and F. H. M. Faisal, Phys. Rev. A **69**, 023410 (2004).

[38] P. Agostini, F. Fabre, G. Mainfray, G. Petite, and N. K. Rahman, Phys. Rev. Lett. **42**, 1127 (1979).

[39] P. Kruit, J. Kimman, H. G. Muller, and M. J. van der Wiel, Phys. Rev. A **28**, 248 (1983).

[40] R. R. Freeman, P. H. Bucksbaum, H. Milchberg, S. Darack, D. Schumacher, and M. E. Geusic, Phys. Rev. Lett. **59**, 1092 (1987).

[41] R. R. Freeman and P. H. Bucksbaum, J. Phys. B **24**, 325 (1991).

[42] N. M. Kroll and K. M. Watson, Phys. Rev. A **8**, 804 (1973).

[43] F. H. M. Faisal, J. Phys. B **6**, L312 (1973).

[44] N. K. Rahman, Phys. Rev. A **10**, 440 (1974).

[45] L. V. Keldysh, Sov. Phys. JETP **20**, 1307 (1965), [Zh. Éksp. Teor. Fiz. **47**, 1945 (1964)].

[46] F. H. M. Faisal, J. Phys. B **6**, L89 (1973).

[47] H. R. Reiss, Phys. Rev. A **22**, 1786 (1980).

[48] B. T. Pickup, Chem. Phys. **19**, 193 (1977).

[49] O. W. Day Jr., Int. J. Quant. Chem. **56**, 547 (1995).

[50] I. G. Kaplan, B. Barbiellini, and A. Bansil, Phys. Rev. B **68**, 235104 (2003).

[51] C. E. Brion, G. Cooper, Y. Zheng, I. V. Litvinyuk, and I. E. McCarthy, Chem. Phys. **270**, 13 (2001).

[52] M. J. DeWitt and R. J. Levis, J. Chem. Phys. **108**, 7739 (1998).

[53] L. D. Landau and E. M. Lifshitz, *Quantum Mechanics* (Addison Wesley, 1958).

[54] A. M. Perelomov, V. S. Popov, and M. V. Terent'ev, Sov. Phys. JETP **23**, 924 (1966), [Zh. Éksp. Teor. Fiz. **50**, 1393 (1966)].

[55] A. M. Perelomov, V. S. Popov, and M. V. Terent'ev, Sov. Phys. JETP **24**, 207 (1967), [Zh. Éksp. Teor. Fiz. **51**, 309 (1966)].

[56] A. M. Perelomov, V. S. Popov, and M. V. Terent'ev, Sov. Phys. JETP **25**, 336 (1967), [Zh. Éksp. Teor. Fiz. **52**, 514 (1967)].

[57] M. V. Ammosov, N. B. Delone, and V. P. Krainov, Sov. Phys. JETP **64**, 1191 (1986), [Zh. Éksp. Teor. Fiz. **91**, 2008 (1986)].

[58] F. A. Ilkov, J. E. Decker, and S. L. Chin, J. Phys. B **25**, 4005 (1992).

[59] H. B. v. Linden v.d. Heuvell and H. G. Muller, *Multiphoton processes* (Cambridge University Press, 1988), vol. 8 of *Studies in Modern Optics*, chap. Limiting cases of excess-photon ionization, p. 25.

[60] T. F. Gallagher, Phys. Rev. Lett. **61**, 2304 (1988).

[61] R. Moshammer, J. Ullrich, B. Feuerstein, D. Fischer, A. Dorn, C. D. Schröter, J. R. Crespo Lopez-Urrutia, C. Hoehr, H. Rottke, C. Trump, et al., Phys. Rev. Lett. **91**, 113002 (2003).

[62] A. Rudenko, K. Zrost, C. D. Schröter, V. L. B. de Jesus, B. Feuerstein, R. Moshammer, and J. Ullrich, J. Phys. B **37**, L407 (2004).

[63] F. H. M. Faisal and G. Schlegel, J. Phys. B **38**, L223 (2005).

[64] F. H. M. Faisal and G. Schlegel, J. Mod. Opt. **53**, 207 (2006).

[65] S. Augst, D. Strickland, D. D. Meyerhofer, S. L. Chin, and J. H. Eberly, Phys. Rev. Lett. **63**, 2212 (1989).

[66] V. P. Krainov, J. Opt. Soc. Am. B **14**, 425 (1997).

[67] V. S. Popov, Phys.-Usp. **47**, 855 (2004), [Usp. Fiz. Nauk **174**, 921 (2004)].

[68] F. H. M. Faisal, *Theory of Multiphoton Processes* (Plenum Press (NY), 1987).

[69] Y. Gontier and M. Trahin, J. Phys. B **13**, 4383 (1980).

[70] F. Fabre, G. Petite, P. Agostini, and M. Clement, J. Phys. B **15**, 1353 (1982).

[71] H. G. Muller, A. Tip, and M. J. van der Wiel, J. Phys. B **16**, L679 (1983).

[72] T. W. B. Kibble, Phys. Rev. **150**, 1060 (1966).

[73] C. J. Joachain, *Quantum Collision Theory* (North-Holland Publishing Co., 1979).

[74] P. B. Corkum, Phys. Rev. Lett. **71**, 1994 (1993).

[75] G. G. Paulus, W. Nicklich, H. Xu, P. Lambropoulos, and H. Walther, Phys. Rev. Lett. **72**, 2851 (1994).

[76] G. G. Paulus, W. Becker, W. Nicklich, and H. Walther, J. Phys. B **27**, L703 (1994).

[77] L. F. DiMauro and P. Agostini, Adv. At. Mol. Opt. Phys. **35**, 79 (1995).

[78] D. N. Fittinghoff, P. R. Bolton, B. Chang, and K. C. Kulander, Phys. Rev. Lett. **69**, 2642 (1992).

[79] B. Walker, B. Sheehy, L. F. DiMauro, P. Agostini, K. J. Schafer, and K. C. Kulander, Phys. Rev. Lett. **73**, 1227 (1994).

[80] S. F. J. Larochelle, A. Talebpour, and S. L. Chin, J. Phys. B **31**, 1201 (1998).

[81] S. Speiser and J. Jortner, Chem. Phys. Lett. **44**, 399 (1976).

[82] M. R. Cervenan and N. R. Isenor, Opt. Comm. **13**, 175 (1975).

[83] R. Dörner, Th. Weber, M. Weckenbrock, A. Staudte, M. Hattass, and H. Schmidt-Böcking, Adv. At. Mol. Opt. Phys. **48**, 1 (2002).

[84] A. Becker, R. Dörner, and R. Moshammer, J. Phys. B **38**, S753 (2005).

[85] A. Kheifets, J. Phys. B **34**, L247 (2001).

[86] J. H. McGuire, N. Berrah, R. J. Bartlett, J. A. R. Samson, J. A. Tanis, C. L. Cocke, and A. S. Schlachter, J. Phys. B **28**, 913 (1995).

[87] B. A. Zon, Sov. Phys. JETP **89**, 219 (1999), [Zh. Éksp. Teor. Fiz. **116**, 410 (1999)].

[88] U. Eichmann, M. Dörr, H. Maeda, W. Becker, and W. Sandner, Phys. Rev. Lett. **84**, 3550 (2000).

[89] I. V. Litvinyuk, F. Légaré, P. W. Dooley, D. M. Villeneuve, P. B. Corkum, J. Zanghellini, A. Pegarkov, C. Fabian, and T. Brabec, Phys. Rev. Lett. **94**, 033003 (2005).

[90] K. C. Kulander, J. Cooper, and K. J. Schafer, Phys. Rev. A **51**, 561 (1995).

[91] M. Y. Kuchiev, Sov. Phys. JETP Lett. **45**, 404 (1987), [Zh. Éksp. Teor. Fiz. Pis'ma Red. **45**, 319 (1987)].

[92] M. Y. Kuchiev, J. Phys. B **28**, 5093 (1995).

[93] P. Dietrich, N. H. Burnett, M. Ivanov, and P. B. Corkum, Phys. Rev. A **50**, 3585 (1994).

[94] D. N. Fittinghoff, P. R. Bolton, B. Chang, and K. C. Kulander, Phys. Rev. A **49**, 2174 (1994).

[95] B. Feuerstein, R. Moshammer, D. Fischer, A. Dorn, C. D. Schröter, J. Deipenwisch, J. R. Crespo Lopez-Urrutia, C. Höhr, P. Neumayer, J. Ullrich, et al., Phys. Rev. Lett. **87**, 043003 (2001).

[96] M. Weckenbrock, M. Hattass, A. Czasch, O. Jagutzki, L. Schmidt, T. Weber, H. Roskos, T. Löffler, M. Thomson, and R. Dörner, J. Phys. B **34**, L449 (2001).

[97] E. Eremina, X. Liu, H. Rottke, W. Sandner, A. Dreischuh, F. Lindner, F. Grasbon, G. G. Paulus, H. Walther, R. Moshammer, et al., J. Phys. B **36**, 3269 (2003).

[98] V. L. B. de Jesus, B. Feuerstein, K. Zrost, D. Fischer, A. Rudenko, F. Afaneh, C. D. Schröter, R. Moshammer, and J. Ullrich, J. Phys. B **37**, L161 (2004).

[99] M. Born and J. R. Oppenheimer, Ann. d. Physik **84**, 457 (1927).

[100] A. Jaron-Becker, A. Becker, and F. H. M. Faisal, Phys. Rev. A **72**, 069907(E) (2004).

[101] A. Talebpour, C.-Y. Chien, and S. L. Chin, J. Phys. B **29**, L677 (1996).

[102] C. Guo, M. Li, J. P. Nibarger, and G. N. Gibson, Phys. Rev. A **58**, R4271 (1998).

[103] S. M. Hankin, D. M. Villeneuve, P. B. Corkum, and D. M. Rayner, Phys. Rev. A **64**, 013405 (2001).

[104] B. Friedrich and D. Herschbach, J. Phys. Chem. **99**, 15686 (1995).

[105] B. Friedrich and D. Herschbach, Phys. Rev. Lett **74**, 4623 (1995).

[106] H. Sakai, C. P. Safvan, J. J. Larsen, K. M. Hilligsøe, K. Hald, and H. Stapelfeldt, J. Chem. Phys. **110**, 10235 (1999).

[107] J. J. Larsen, H. Sakai, C. P. Safvan, I. Wendt-Larsen, and H. Stapelfeldt, J. Chem. Phys. **111**, 7774 (1999).

[108] A. Saenz, J. Phys. B **33**, 4365 (2000).

[109] A. D. Bandrauk and M. L. Sink, J. Chem. Phys. **74**, 1110 (1981).

[110] P. H. Bucksbaum, A. Zavriyev, H. G. Muller, and D. W. Schumacher, Phys. Rev. Lett. **64**, 1883 (1990).

[111] P. Dietrich and P. B. Corkum, J. Chem. Phys. **97**, 3187 (1992).

[112] A. Saenz, Phys. Rev. A **66**, 063407 (2002).

[113] G. H. Yao and S. I. Chu, Phys. Rev. A **48**, 485 (1993).

[114] L. J. Frasinski, J. H. Posthumus, J. Plumridge, K. Codling, P. F. Taday, and A. J. Langley, Phys. Rev. Lett. **83**, 3625 (1999).

[115] S. Chelkowski, T. Zuo, O. Atabek, and A. D. Bandrauk, Phys. Rev. A **52**, 2977 (1995).

[116] T. Zuo and A. D. Bandrauk, Phys. Rev. A **52**, R2511 (1995).

[117] A. Talebpour, S. Larochelle, and S. L. Chin, J. Phys. B **31**, L49 (1998).

[118] G. R. Hanson, J. Chem. Phys. **62**, 1161 (1975).

[119] K. Codling and L. J. Frasinski, J. Phys. B **26**, 783 (1993).

[120] A. S. Alnaser, B. Ulrich, X. M. Tong, I. V. Litvinyuk, C. M. Maharjan, P. Ranitovic, T. Osipov, R. Ali, S. Ghimire, Z. Chang, et al., Phys. Rev. A **72**, 030702 (2005).

[121] H. Yu, T. Zuo, and A. D. Bandrauk, Phys. Rev. A **54**, 3290 (1996).

[122] A. Saenz, Phys. Rev. A **61**, 051402 (2000).

[123] M. J. DeWitt, E. Wells, and R. R. Jones, Phys. Rev. Lett. **87**, 153001 (2001).

[124] D. Dundas and J. M. Rost, Phys. Rev. A **71**, 013421 (2005).

[125] H. Moriyama, Y. Wasada-Tsutsui, M. Sekiya, and H. Tatewaki, J. Chem. Phys. **118**, 5413 (2003).

[126] H. Stapelfeldt, E. Constant, and P. B. Corkum, Phys. Rev. Lett. **74**, 3780 (1995).

[127] S. Chelkowski, P. B. Corkum, and A. D. Bandrauk, Phys. Rev. Lett. **82**, 3416 (1999).

[128] S. Chelkowski and A. D. Bandrauk, Phys. Rev. A **65**, 023403 (2002).

[129] T. A. Carlson and R. M. White, J. Chem. Phys. **44**, 4510 (1966).

[130] A. S. Coolidge, H. M. James, and R. D. Present, J. Chem. Phys. **4**, 193 (1936).

[131] G. Herzberg, Annu. Rev. Phys. Chem. **9**, 315 (1958).

[132] J. Tellinghuisen, Adv. Chem. Phys. **LX**, 299 (1985).

[133] F. B. Yousif, B. G. Lindsay, and C. J. Latimer, J. Phys. B **21**, 4157 (1988).

[134] R. Schinke, *Photodissociation Dynamics* (Cambridge University Press, 1995).

[135] H. Niikura, F. Légaré, R. Hasbani, A. D. Bandrauk, M. Yu. Ivanov, D. M. Villeneuve, and P. B. Corkum, Nature **417**, 917 (2002).

[136] J. H. Eberly, J. Javanainen, and K. Rzazewski, Phys. Rep. **204**, 331 (1991).

[137] K. C. Kulander, Phys. Rev. A **35**, 445 (1987).

[138] K. J. Schafer and K. C. Kulander, Phys. Rev. A **42**, 5794 (1990).

[139] P. R. Taylor and H. Partridge, J. Phys. Chem. **91**, 6148 (1987).

[140] R. Kosloff and D. Kosloff, J. Comput. Phys. **63**, 363 (1986).

[141] U. V. Riss and H.-D. Meyer, J. Phys. B **31**, 2279 (1998).

[142] S. Chelkowski, C. Foisy, and A. D. Bandrauk, Phys. Rev. A **57**, 1176 (1998).

[143] C. Ruiz, L. Plaja, R. Taïeb, V. Véniard, and A. Maquet, Phys. Rev. A **73**, 063411 (2006).

[144] E. S. Smyth, J. S. Parker, and K. T. Taylor, Comp. Phys. Comm. **114**, 1 (1998).

[145] J. S. Parker, L. R. Moore, D. Dundas, and K. T. Taylor, J. Phys. B **33**, L691 (2000).

[146] C. Ruiz, L. Plaja, L. Roso, and A. Becker, Phys. Rev. Lett. **96**, 053001 (2006).

[147] S. Baier, C. Ruiz, L. Plaja, and A. Becker, Phys. Rev. A **74**, 033405 (2006).

[148] H. Bachau, E. Cormier, P. Decleva, J. E. Hansen, and F. Martín, Rep. Prog. Phys. **64**, 1815 (2001).

[149] A. Becker, C. Ruiz, S. Baier, F. He, A. Requate, M. F. Ciappina, and P. Panek, (unpublished), Nonlinear Processes in Strong Fields/Max Planck Institute of the Physics of Complex Systems (MPIPKS) (2006), URL `http://planet.pks.mpg.de/trac/npsflib/wiki/NpsfLibReadme`.

[150] W. H. Press, S. A. Teukolsky, W. T. Vettering, and B. P. Flannery, *Numerical recipes in C++* (Cambridge University Press, 2002).

[151] M. Cline, G. Lomow, and M. Girou, *C++ FAQs* (Addison Wesley Professional, 1998), 2nd ed.

[152] F. H. M. Faisal, Phys. Lett. A **187**, 180 (1994).

[153] R. Dörner, V. Mergel, O. Jagutzki, L. Spielberger, J. Ullrich, R. Moshammer, and H. Schmidt-Böcking, Phys. Rep. **330**, 95 (2000).

[154] J. Ullrich, R. Moshammer, A. Dorn, R. Dörner, L. Ph. H. Schmidt, and H. Schmidt-Böcking, Rep. Prog. Phys. **66**, 1463 (2003).

[155] R. Dörner, in *Atomic Physics Workshop* (MPIPKS, 2006), URL `http://www.mpipks-dresden.mpg.de/~atom2006/program1.html`.

[156] Tech. Rep., MATLAB®is a registered trademark of The MathWorks, Inc. (2007).

[157] J. Itatani, F. Quéré, G. L. Yudin, M. Yu. Ivanov, F. Krausz, and P. B. Corkum, Phys. Rev. Lett. **88**, 173903 (2002).

[158] S. I. Chu and D. A. Telnov, Phys. Rep. **390**, 1 (2004).

[159] G. Q. Hassoun and D. H. Kobe, Am. J. Phys. **57**, 658 (1989).

[160] L. I. Schiff, *Quantum Mechanics* (McGraw-Hill, 1968).

[161] B. H. Bransden and C. J. Joachain, *Physics of atoms and molecules* (Addison Wesley Longman, 1983).

[162] J. D. Jackson, *Classical electrodynamics* (J. Wiley & Sons, 1999), 3rd ed.

[163] C. Cohen-Tannoudji, B. Diu, and F. Laloe, *Quantum Mechanics*, vol. 1 (J. Wiley & Sons, 1978).

[164] L. B. Madsen, Phys. Rev. A **65**, 053417 (2002).

[165] W. Gordon, Z. Phys. **40**, 117 (1926).

[166] D. M. Volkov, Z. Phys. **94**, 250 (1935).

[167] J. Z. Kamiński, A. Jaroń, and F. Ehlotzky, Phys. Rev. A **53**, 1756 (1996).

[168] C. C. Chirilã and R. M. Potvliege, Phys. Rev. A **71**, 021402(R) (2005).

[169] O. Smirnova, M. Spanner, and M. Ivanov, J. Phys. B **39**, S307 (2006).

[170] D. Bohm, *Quantum theory* (Prentice-Hall, 1951).

[171] V. P. Krainov and B. Shokri, Sov. Phys. JETP **80**, 657 (1995), [Zh. Éksp. Teor. Fiz. **107**, 1180 (1995)].

[172] N. B. Delone and V. P. Krainov, Phys.-Usp. **41**, 469 (1998), [Usp. Fiz. Nauk **168**, 531 (1998)].

[173] A. Becker, L. Plaja, P. Moreno, M. Nurhuda, and F. H. M. Faisal, Phys. Rev. A **64**, 023408 (2001).

[174] S. F. J. Larochelle, A. Talebpour, and S. L. Chin, J. Phys. B **31**, 1215 (1998).

[175] M.S. Child, *Molecular Collision Theory* (Dover, 1996).

[176] W. Kołos and L. Wolniewicz, Rev. Mod. Phys. **35**, 473 (1963).

[177] J. Franck, Trans. Faraday Soc. **21**, 536 (1925).

[178] E. U. Condon, Proc. Nat. Acad. Sci. **13**, 462 (1927).

[179] E. U. Condon, Phys. Rev. **32**, 858 (1928).

[180] T. D. Thomas, L. J. Saethre, S. L. Sorensen, and S. Svensson, J. Chem. Phys. **109**, 1041 (1998).

[181] M. Coreno, M. de Simone, K. C. Prince, R. Richter, M. Vondráček, L. Avaldi, and R. Camilloni, Chem. Phys. Lett. **306**, 209 (1999).

[182] N. G. Johnson, R. N. Mello, M. E. Lundy, J. Kapplinger, E. Parke, K. D. Carnes, I. Ben-Itzhak, and E. Wells, Phys. Rev. A. **72**, 052711 (2005).

[183] G. Laurent, J. Fernández, S. Legendre, M. Tarisien, L. Adoui, A. Cassimi, X. Fléchard, F. Frémont, B. Gervais, E. Giglio, et al., Phys. Rev. Lett. **96**, 173201 (2006).

[184] X. Urbain, B. Fabre, E. M. Staicu-Casagrande, N. de Ruette, V. M. Andrianarijaona, J. Jureta, J. H. Posthumus, A. Saenz, E. Baldit, and C. Cornaggia, Phys. Rev. Lett. **92**, 163004 (2004).

[185] M. Gruebele and A. H. Zewail, J. Chem. Phys. **98**, 883 (1993).

[186] I. Fischer, D. M. Villeneuve, M. J. J. Vrakking, and A. Stolow, J. Chem. Phys. **102**, 5566 (1995).

[187] M. J. J. Vrakking, D. M. Villeneuve, and A. Stolow, Phys. Rev. A **54**, R37 (1996).

[188] C. J. Hammond, K. L. Reid, and K. L. Ronayne, J. Chem. Phys. **124**, 201102 (2006).

[189] G. H. Dunn, J. Chem. Phys. **44**, 2592 (1966).

[190] F. Busch and G. H. Dunn, Phys. Rev. A **5**, 1726 (1972).

[191] E. U. Condon, Phys. Rev. **28**, 1182 (1926).

[192] G. Caprace, J. Delwiche, P. Natalis, and J. Collin, Chem. Phys. **13**, 43 (1976).

[193] E. Hertz, G. Nersisyan, N. A. Papadogiannis, and D. Charalambidis, J. Chem. Phys. **118**, 595 (2003).

[194] J. L. Dehmer, D. Dill, and S. Wallace, Phys. Rev. Lett. **43**, 1005 (1979).

[195] R. Stockbauer, B. E. Cole, D. L. Ederer, J. B. West, A. C. Parr, and J. L. Dehmer, Phys. Rev. Lett. **43**, 757 (1979).

[196] B. E. Cole, D. L. Ederer, R. Stockbauer, K. Codling, A. C. Parr, J. B. West, E. D. Poliakoff, and J. L. Dehmer, J. Chem. Phys. **72**, 6308 (1980).

[197] P. Erman, A. Karawajczyk, E. Rachlew-Källne, J. Rius i Riu, M. Stankiewicz, K. Yoshiki Franzén, A. Weider Moen, and L. Veseth, Physica Scripta **62**, 294 (2000).

[198] R. M. Rao and E. D. Poliakoff, Phys. Rev. Lett. **76**, 2666 (1996).

[199] G. J. Rathbone, Ph.D. thesis, Louisiana State University/Department of Chemistry (2002), URL `http://etd.lsu.edu/docs/available/etd-1114102-161158/unrestricted/Rathbone_dis.pdf`.

[200] T. D. G. Walsh, F. A. Ilkov, S. L. Chin, F. Châteauneuf, T. T. Nguyen-Dang, S. Chelkowski, A. D. Bandrauk, and O. Atabek, Phys. Rev. A **58**, 3922 (1998).

[201] T. D. G. Walsh, F. A. Ilkov, and S. L. Chin, J. Phys. B **30**, 2167 (1997).

[202] A. Becker, A. D. Bandrauk, and S. L. Chin, Chem. Phys. Lett. **343**, 345 (2001).

[203] M. E. Sukharev and V. P. Krainov, Sov. Phys. JETP **83**, 457 (1996), [Zh. Éksp. Teor. Fiz. **110**, 832 (1996)].

[204] A. Zavriyev, P. H. Bucksbaum, H. G. Muller, and D. W. Schumacher, Phys. Rev. A **42**, 5500 (1990).

[205] C. Trump, H. Rottke, M. Wittmann, G. Korn, W. Sandner, M. Lein, and V. Engel, Phys. Rev. A **62**, 063402 (2000).

[206] D. Villarejo, J. Chem. Phys. **49**, 2523 (1968).

[207] C. V. Raman and K. S. Krishnan, Nature **121**, 501 (1928).

[208] G. S. Landsberg and L. I. Mandelstam, Naturw. **16**, 557 (1928).

[209] I. L. Fabelinskii, Phys.-Usp. **46**, 1105 (2003), [Usp. Fiz. Nauk **173**, 1137 (2003)].

[210] E. B. Wilson, J. C. Decius, and P. C. Cross, *Molecular Vibrations* (Dover, 1955).

[211] D. P. de Bruijn and J. Los, Rev. Sci. Instr. **53**, 1020 (1982).

[212] B. Fabre, J. H. Posthumus, L. Malfaire, E. M. Staicu-Casagrande, J. Jureta, C. Cornaggia, E. Baldit, and X. Urbain, Laser Phys. **14**, 468 (2004).

[213] T. Ergler, A. Rudenko, and B. Feuerstein, Phys. Rev. Lett. **95**, 093001 (2005).

[214] D. Normand, C. Cornaggia, and J. Morellec, J. Phys. B **19**, 2881 (1986).

[215] A. Requate, A. Becker, and F. H. M. Faisal, Phys. Rev. A **73**, 033406 (2006).

[216] H. R. Reiss and V. P. Krainov, J. Phys. A **38**, 527 (2005).

[217] C. Leubner, Phys. Rev. A **23**, 2877 (1981).

[218] C. Leubner and E. M. Strohmaier, J. Phys. A **14**, 509 (1981).

[219] G. Dattoli, L. Giannessi, L. Mezi, and A. Torre, N. Cim. B **105**, 327 (1990).

[220] G. Dattoli, A. Torre, S. Lorenzutta, G. Maino, and C. Chiccoli, N. Cim. B **106**, 21 (1991).

[221] G. Dattoli, C. Chiccoli, S. Lorenzutta, G. Maino, M. Richetta, and A. Torre, J. Sci. Comp. **8**, 69 (1993).

[222] A. Torre, in *Advanced special functions and applications. Proceedings of the workshop (Melfi, PZ, Italy, 9-12 May 1999)* (Aracne, 2000), pp. 75–92.

[223] H. J. Korsch, A. Klumpp, and D. Witthaut, J. Phys. A **39**, 14947 (2006).

[224] N. Bleistein and R. A. Handelsman, *Asymptotic Expansions of Integrals* (Dover, 1986), 2nd ed.

[225] C. M. Bender and S. A. Orszag, *Advanced Mathematical Methods for Scientists and Engineers* (McGraw-Hill/Springer('99), 1978).

[226] A. Szabo and N. S. Ostlund, *Modern quantum chemistry* (Dover, 1982).

[227] J. Fernández Rico, J. J. Fernández, I. Ema, R. López, and G. Ramírez, Int. J. Quant. Chem. **78**, 83 (2000).

[228] I. I. Guseinov and B. A. Mamedov, Int. J. Quant. Chem. **78**, 146 (2000).

[229] I. I. Guseinov and B. A. Mamedov, Int. J. Quant. Chem. **81**, 117 (2001).

[230] I. I. Guseinov and B. A. Mamedov, Int. J. Quant. Chem. **86**, 450 (2001).

[231] C. Guidotti, O. Salvetti, N. Durante, U. T. Lamanna, and G. P. Arrighini, Int. J. Quant. Chem. **93**, 59 (2003).

[232] J. J. Fernández, R. López, I. Ema, G. Ramírez, and J. Fernández Rico, Int. J. Quant. Chem. **106**, 1986 (2006).

[233] A. Bouferguene, M. Fares, and P. E. Hoggan, Int. J. Quant. Chem. **57**, 801 (1996).

[234] J. Fernández Rico, R. López, A. Aguado, I. Ema, and G. Ramírez, Int. J. Quant. Chem. **19**, 1284 (1998).

[235] J. Fernández Rico, R. López, A. Aguado, I. Ema, and G. Ramírez, Int. J. Quant. Chem. **81**, 148 (2001).

[236] S. F. Boys, Proc Roy. Soc. **200**, 542 (1950).

[237] M. W. Schmidt, K. K. Baldridge, J. A. Boatz, S. T. Elbert, M. S. Gordon, J. H. Jensen, S. Koseki, N. Matsunaga, K. A. Nguyen, S. J. Su, et al., J. Comput. Chem. **14**, 1347 (1993), URL `http://www.msg.ameslab.gov/GAMESS/GAMESS.html`.

[238] S. Obara and A. Saika, J. Chem. Phys. **89**, 1540 (1988).

[239] H. B. Schlegel and M. J. Frisch, Int. J. Quant. Chem. **54**, 83 (1995).

[240] J. Kuang and C. D. Lin, J. Phys. B **30**, 2529 (1996).

[241] J. Kuang and C. D. Lin, J. Phys. B **30**, 2549 (1997).

[242] J. Itatani, J. Levesque, D. Zeidler, H. Niikura, H. Pépin, J. C. Kieffer, P. B. Corkum, and D. M. Villeneuve, Nature **432**, 867 (2004).

[243] I. N. Levine, *Molecular Spectroscopy* (J. Wiley & Sons, 1975).

[244] P. M. Morse, Phys. Rev. **34**, 57 (1929).

[245] J. P. Dahl and M. Springborg, J. Chem. Phys. **88**, 4535 (1988).

[246] J. C. Lopez-Viera, A. L. Rivera, Y. F. Smirnov, and A. Frank, Int. J. Quant. Chem. **88**, 280 (2002).

[247] T. E. Sharp, Atom. Data **2**, 119 (1971).

[248] J. Zúñiga, M. Alacid, A. Bastida, F. J. Carvajal, and A. Requena, J. Chem. Phys. **110**, 6339 (1999).

[249] T. Carrington, *Encyclopedia of Computational Chemistry* (J. Wiley & Sons, 1998), vol. 5, chap. Vibrational Energy Level Calculations, pp. 3157–3166.

[250] J. Zúñiga, J. A. G. Picón, A. Bastida, and A. Requena, J. Chem. Phys. **122**, 224319

(2005).

[251] J. K. G. Watson, Mol. Phys. **15**, 479 (1968).

[252] E. V. Doktorov, I. A. Malkin, and V. I. Man'ko, J. Phys. B **9**, 507 (1976).

[253] G. Longhi, S. Abbate, C. Zagano, G. Botto, and L. Ricard-Lespade, Theor. Chem. Acc. (Theor. Chim. Act.) **82**, 321 (1992).

[254] B. R. Henry and W. Siebrand, J. Chem. Phys. **49**, 5369 (1968).

[255] R. Wallace, Chem. Phys. **11**, 189 (1975).

[256] M. S. Child and L. Halonen, Adv. Chem. Phys. **57**, 1 (1984).

[257] I. M. Mills and A. G. Robiette, Mol. Phys. **56**, 743 (1985).

[258] R. B. Gerber and J. O. Jung, *Computational Molecular Spectroscopy* (J. Wiley & Sons, 2000), chap. 11, pp. 365–390.

[259] F. Culot and J. Livin, Theor. Chem. Acc. (Theor. Chim. Act.) **89**, 227 (1994).

[260] J. M. Bowman, S. Carter, and X. Huang, Int. Rev. Phys. Chem. **22**, 533 (2003).

[261] P. C. Ojha and R. S. Berry, Mol. Phys. **63**, 909 (1988).

[262] J. Zúñiga, A. Bastida, M. Alacid, and A. Requena, J. Phys. Chem. **99**, 11051 (1995).

[263] D. W. Schwenke, Chem. Phys. Lett. **189**, 91 (1992).

[264] D. T. Colbert and E. L. Sibert, J. Chem. Phys. **91**, 350 (1989).

[265] P. Jensen, J. Mol. Spectrosc. **128**, 478 (1988).

[266] L. Halonen, J. Phys. Chem. **93**, 3386 (1989).

[267] S. Carter, N. C. Handy, and I. M. Mills, Phil. Trans. Phys. Sci. Eng. **332**, 309 (1990).

[268] J. Botina and N. Rahman, Phys. Rev. A **51**, 3088 (1995).

[269] J. Zúñiga, M. Alacid, A. Bastida, F. J. Carvajal, and A. Requena, J. Mol. Spectrosc. **195**, 137 (1999).

[270] P. Jensen, J. Mol. Spectrosc. **133**, 438 (1989).

[271] H. Wei and T. Carrington, J. Chem. Phys. **97**, 3029 (1992).

[272] D. Xie and G. Yan, Mol. Phys. **88**, 1349 (1996).

[273] J. Zúñiga, M. Alacid, A. Bastida, and A. Requena, J. Chem. Phys. **105**, 6099 (1996).

[274] G. Pöschl and E. Teller, Z. Physik **83**, 143 (1933).

[275] A. Requena, M. Alacid, A. Bastida, and J. Zúñiga, Int. J. Quant. Chem. **52**, 165 (1994).

[276] Y. P. Varshni, Rev. Mod. Phys. **29**, 664 (1957).

[277] D. Steele, E. R. Lippincott, and J. T. Vanderslice, Rev. Mod. Phys. **34**, 239 (1962).

[278] T. E. Sharp and H. M. Rosenstock, J. Chem. Phys. **41**, 3453 (1964).

[279] A. Toniolo and M. Persico, J. Comp. Chem. **22**, 968 (2001).

[280] W. Siebrand and D. F. Williams, J. Chem. Phys. **49**, 1860 (1968).

[281] W. M. Gelbart, P. R. Stannard, and M. L. Elert, Int. J. Quant. Chem. **XIV**, 703 (1978).

[282] F. Iachello and S. Oss, J. Mol. Spectrosc. **153**, 225 (1992).

[283] T. Müller, P. Dupré, P. H. Vaccaro, F. Pérez-Bernal, M. Ibrahim, and F. Iachello,

Chem. Phys. Lett. **292**, 243 (1998).

[284] T. Müller, P. H. Vaccaro, F. Pérez-Bernal, and F. Iachello, J. Chem. Phys. **111**, 5038 (1999).

[285] M. L. Sage, Chem. Phys. **35**, 375 (1978).

[286] P. Milonni and J. H. Eberly, *Lasers* (J. Wiley & Sons, 1988), chap. 14.5.

[287] A. S. Alnaser, X. M. Tong, T. Osipov, S. Voss, C. M. Maharjan, B. Shan, Z. Chang, and C. L. Cocke, Phys. Rev. A **70**, 023413 (2004).

[288] A. Saenz, Phys. Rev. A **66**, 063408 (2002).

[289] T. K. Kjeldsen and L. B. Madsen, Phys. Rev. Lett. **95**, 073004 (2005).

[290] A. Jaroń-Becker, A. Becker, and F. H. M. Faisal, J. Phys. B **36**, L375 (2003).

[291] P. A. Fraser, Can. J. Phys. **32**, 515 (1954).

[292] R. W. Nicholls and W. R. Jarmain, Proc. Phys. Soc. **69**, 253 (1956).

[293] R. W. Nicholls and W. R. Jarmain, Proc. Phys. Soc. **74**, 133 (1959).

[294] R. W. Nicholls, Proc. Phys. Soc. **89**, 181 (1966).

[295] A. Rozendaal and E. J. Baerends, Chem. Phys. **95**, 57 (1985).

[296] P. Salek, F. Gel'mukhanov, H. Agren, O. Björneholm, and S. Svensson, Phys. Rev. A **60**, 2786 (1999).

[297] D. W. Turner and D. P. May, J. Chem. Phys. **45**, 471 (1966).

[298] *NIST Chemistry WebBook (Standard Reference Database Number 69)* (2005), URL `http://webbook.nist.gov/chemistry/`.

[299] Y. P. Zhang, C. H. Cheng, J. T. Kim, J. Stanojevic, and E. E. Eyler, Phys. Rev. Lett. **92**, 203003 (2004).

[300] A. A. Radzig and B. M. Smirnov, *Reference Data on Atoms, Molecules and Ions* (Springer, 1985).

[301] F. R. Gilmore, R. R. Laher, and P. J. Espy, J. Phys. Chem. Ref. Dat. **21(5)**, 1005 (1992), URL `http://www.nist.gov/srd/reprints.htm`.

[302] R. C. Hilborn, Am. J. Phys. **50**, 982 (1082).

[303] R. Laher, IPAC Webpage (1999), URL `http://spider.ipac.caltech.edu/staff/laher/fluordir/fluorindex.html`.

[304] D. C. Jain and R. C. Sahni, Trans. Faraday Soc. **64**, 3169 (1968).

[305] B. Wannberg, D. Nordfors, and K. L. Tan, J. Electr. Spectr. Rel. Phen. **47**, 147 (1988).

[306] K. Okada and S. Iwata, J. Chem. Phys. **112**, 1804 (2000).

[307] D. C. Jain, J. Phys. B **5**, 199 (1971).

[308] G. J. Harris, O. L. Polyansky, and J. Tennyson, Spectr. Act. A **58**, 673 (2002).

[309] G. W. Drake, ed., *Springer Handbook of Atomic, Molecular, and Optical Physics* (Springer, 2006), sect. 31.1.2.

[310] S. Carter and N. C. Handy, Mol. Phys. **47**, 1445 (1982).

[311] S. Carter and N. C. Handy, Mol. Phys. **57**, 175 (1986).

[312] U. Manthe, H. Köppel, and L. S. Cederbaum, J. Chem. Phys. **95**, 1708 (1991).

[313] M. S. Child, Acc. Chem. Res. **18**, 45 (1985).

[314] H. Wei and Q. Zhu, J. Phys. B **24**, 137 (1991).

[315] M. S. Child and R. T. Lawton, Faraday Discuss. **71**, 273 (1981).

[316] S. Li, J. R. Schmidt, S. A. Corcelli, C. P. Lawrence, and J. L. Skinner, J. Chem. Phys. **124**, 204110 (2006).

[317] J. E. Baggott, G. L. Caldow, and I. M. Mills, J. Chem. Soc. **84**, 1407 (1988).

[318] M. M. Law and J. L. Duncan, Mol. Phys. **93**, 809 (1998).

[319] P. Botschwina, M. Horn, M. Matuschewski, E. Schick, and P. Sebald, J. Mol. Struct. (THEOCHEM) **400**, 119 (1997).

[320] K. A. Peterson, R. C. Mayrhofer, and R. C. Woods, J. Chem. Phys. **93**, 4946 (1990).

[321] D. Zeidler, A. Staudte, A. B. Bardon, D. M. Villeneuve, R. Dörner, and P. B. Corkum, Phys. Rev. Lett. **95**, 203003 (2005).

[322] A. S. Alnaser, S. Voss, X. -M. Tong, C. M. Maharjan, P. Ranitovic, B. Ulrich, T. Osipov, B. Shan, Z. Chang, and C. L. Cocke, Phys. Rev. Lett. **93**, 113003 (2004).

[323] H. Stapelfeldt and T. Seideman, Rev. Mod. Phys. **75**, 543 (2003).

[324] P. W. Dooley, I. V. Litvinyuk, K. F. Lee, D. M. Rayner, M. Spanner, D. M. Villeneuve, and P. B. Corkum, Phys. Rev. A **68**, 023406 (2003).

[325] Z. X. Zhao, X. M. Tong, and C. D. Lin, Phys. Rev. A **67**, 043404 (2003).

[326] J. Senekowitsch, S. ONeil, and W. Meyer, Theor. Chem. Acc. **84**, 85 (1992).

[327] M. Lundqvist, D. Edvardsson, P. Baltzer, and B. Wannberg, J. Phys. B **29**, 1489 (1996).

[328] M. R. Rudge, Rev. Mod. Phys. **40**, 564 (1968).

[329] J. R. Oppenheimer, Phys. Rev. **32**, 361 (1928).

[330] C. Champion, J. Hanssen, and P. A. Hervieux, Phys. Rev. A **65**, 022710 (2002).

[331] D. S. F. Crothers and L. J. Dubé, Adv. At., Mol., Opt. Phys. **30**, 287 (1991).

[332] M. Brauner, J. S. Briggs, and H. Klar, J. Phys. B **22**, 2265 (1989).

[333] M. Brauner and J. S. Briggs, J. Phys. B **24**, 2227 (1991).

[334] C. R. Stia, O. A. Fojón, P. F. Weck, J. Hanssen, B. Joulakian, and R. D. Rivarola, Phys. Rev. A **66**, 052709 (2002).

[335] J. McGuire, *Electron Correlation Dynamics in Atomic Collisions* (Cambridge University Press, 1997), (revised edition: URL `http://www.physics.tulane.edu/Jim_McGuire/bk.html`).

[336] J. S. Briggs, J. Phys. B **10**, 3075 (1977).

[337] I. E. McCarthy and E. Weigold, Rep. Prog. Phys. **51**, 299 (1988).

[338] I. E. McCarthy, Z. Phys. D **23**, 287 (1992).

[339] D. S. F. Crothers and J. F. McCann, J. Phys. B **21**, 287 (1988).

[340] C. Herring, Phys. Rev. **57**, 1169 (1940).

[341] L. L. Lohr Jr., in *Electron Spectroscopy: Proceedings of an International Conference*

held at Asilomar, 1971, edited by D. A. Shirley (Elsevier, 1972), pp. 245–258.

[342] M. Mishra and Y. Öhrn, Int. J. Quant. Chem. Symp. **S14**, 335 (1980).

[343] M. Deleuze, B. T. Pickup, and J. Delhalle, Mol. Phys. **83**, 655 (1994).

[344] G. De Miranda Seabra, Ph.D. thesis, Kansas State University (2005).

[345] F. O. Ellison, J. Chem. Phys. **61**, 507 (1974).

[346] M. Mohraz and L. L. Lohr Jr., Int. J. Quant. Chem. **10**, 811 (1976).

[347] C. W. Bauschlicher Jr. and P. R. Taylor, Theor. Chem. Acc. (Theor. Chim. Act.) **74**, 63 (1988).

[348] O. Goscinski and P. Lindner, J. Math. Phys. **11**, 1313 (1970).

[349] *NIST Physical Reference Data*, URL `http://physics.nist.gov/PhysRefData/`.

[350] C. Cornaggia and P. Hering, J. Phys. B **31**, L503 (1998).

[351] P. H. Krupenie, J. Phys. Chem. Ref. Dat. **1**, 423 (1972).

[352] T. D. Märk, J. Chem. Phys. **63**, 3731 (1975).

[353] J. H. Agee, J. B. Wilcox, L. E. Abbey, and T. F. Moran, Chem. Phys. **61**, 171 (1981).

[354] T. Masuoka, Z. Phys. D **4**, 43 (1986).

[355] M. Larsson, P. Baltzer, S. Svensson, B. Wannberg, N. Martensson, A. Naves de Brito, N. Correia, M. P. Keane, M. Carlsson-Gothe, and L. Karlsson, J. Phys. B **23**, 1175 (1990).

[356] J. Fournier, P. G. Fournier, M. L. Langford, M. Mousselmal, J. M. Robbe, and G. Gandara, J. Chem. Phys. **96**, 3594 (1992).

[357] H. Cherkani-Hassani, D. S. Belic, J. J. Jureta, and P. Defrance, J. Phys. B **39**, 5105 (2006).

[358] M. Galassi, J. Davies, J. Theiler, B. Gough, G. Jungman, M. Booth, and F. Rossi, *GNU Scientific Library Reference Manual* (2006), 2nd ed.

[359] P. Bratley and B. L. Fox, ACM TOMS **14**, 88 (1988).

[360] C. Ruiz, L. Plaja, J. R. Vázquez de Aldana, and L. Roso, Phys. Rev. A **68**, 023409 (2003).

[361] C. Ruiz, L. Plaja, J.R. Vázquez de Aldana, and L. Roso, Appl. Phys. B **78**, 829 (2004).

[362] C. Ruiz, L. Plaja, and L. Roso, Laser Phys. **16**, 600 (2006).

[363] L. S. Cederbaum, J. Schirmer, W. Domcke, and W. v. Niessen, J. Phys. B **10**, L549 (1977).

[364] S. Patchkovskii, Z. Zhao, T. Brabec, and D. M. Villeneuve, J. Chem. Phys. **126**, 114306 (2007).

[365] J. S. Briggs and J. M. Rost, Found. Phys. **31**, 693 (2001).

[366] P. A. M. Dirac, *The Principles of Quantum Mechanics* (Oxford University Press, 1930), 4th ed., §15, p. 61.

[367] W. Heitler, *The Quantum Theory of Radiation* (Dover (originally published by Clarendon Press), 1954), 3rd ed., §8.1, p. 69.

[368] F. Constantinescu, *Distributionen und ihre Anwendungen in der Physik* (Teubner,

1974).

[369] B. J. Olsson, G. Kindvall, and M. Larsson, J. Chem. Phys. **88**, 7501 (1988).

[370] M. Ahmad, P. Lablanquie, F. Penent, J. G. Lambourne, R. I. Hall, and J. H. D. Eland, J. Phys. B **39**, 3599 (2006).

[371] L. G. M. Pettersson and M. Larsson, J. Chem. Phys. **94**, 818 (1991).

[372] M. Lundqvist, D. Edvardsson, P. Baltzer, M. Larsson, and B. Wannberg, J. Phys. B **29**, 499 (1996).

[373] R. Feifel, J. H. D. Eland, and D. Edvardsson, J. Chem. Phys. **122**, 144308 (2005).

[374] S. Baker, J. S. Robinson, C. A. Haworth, H. Teng, R. A. Smith, C. C. Chirila, M. Lein, J. W. G. Tisch, and J. P. Marangos, Science **312**, 424 (2006).

[375] W. v. Niessen, J. Schirmer, and L. S. Cederbaum, Comp. Phys. Rep. **1**, 57 (1984).

[376] V. G. Zakrzewski, O. Dolgounitcheva, and J. V. Ortiz, Int. J. Quant. Chem. **75**, 607 (1999).

[377] P. Salières, B. Carré, L. Le Déroff, F. Grasbon, G. G. Paulus, H. Walther, R. Kopold, W. Becker, D. B. Milosevic, A. Sanpera, et al., Science **292**, 902 (2001).

[378] J. Itatani, D. Zeidler, J. Levesque, M. Spanner, D. M. Villeneuve, and P. B. Corkum, Phys. Rev. Lett. **94**, 123902 (2005).

[379] *GCC, the GNU Compiler Collection*, URL `http://gcc.gnu.org/`.

[380] *GSL - GNU Scientific Library*, URL `http://www.gnu.org/software/gsl/`.

[381] *CLHEP - A Class Library for High Energy Physics*, URL `http://cern.ch/clhep/`.

[382] N. M. O'Boyle, *GaussSum*, URL `http://gausssum.sourceforge.net/`.

[383] R. Muller, *PyQuante - Python Quantum Chemistry*, URL `http://pyquante.sourceforge.net/`.

[384] T. D. Crawford, C. D. Sherrill, E. F. Valeev, and R. A. King, *PSI3 - an ab initio quantum chemistry program*, URL `http://www.psicode.org/`.

[385] G. v. Rossum, *The Python Programming Language*, URL `http://www.python.org/`.

[386] T. Hahn, Comp. Phys. Comm. **168**, 78 (2005), eDoc URL `http://edoc.mpg.de/228268`, homepage URL `http://www.feynarts.de/cuba/`.

[387] P. Koval and S. Fritzsche, Comp. Phys. Comm. **152**, 191 (2003).

[388] *Xmgrace*, URL `http://plasma-gate.weizmann.ac.il/Grace/`.

[389] *Pybliographer*, URL `http://pybliographer.org/`.

[390] *Kile - an integrated LaTeX environment*, URL `http://kile.sourceforge.net/`.

[391] H. T. Thanh, P. Sojka, J. Zlatuska, M. Schröder, et al., *pdfeTeX*, URL `http://sarovar.org/projects/pdftex/`.

[392] L. Lamport, *LaTeX*, URL `http://www.latex-project.org/`.

[393] M. Kohm, *KOMA-Script*, URL `http://www.komascript.de/`.

[394] American Mathematical Society, *AMS-LaTeX*, URL `http://www.ams.org/tex/`.

[395] D. P. Carlisle and S. P. Q. Rahtz, *graphicx package*.

[396] S. P. Q. Rahtz, *Hyperref*, URL `http://www.tug.org/applications/hyperref/`.

[397] P. W. Daly, *natbib.sty package*.

[398] A. Becker, S. L. Chin, N. Moiseyev, and K. Yamanouchi, eds., *International Seminar and Workshop on Intense Laser-Matter Interaction and Pulse Propagation* (2005), URL `http://www.mpipks-dresden.mpg.de/~lmipp05/PROGRAM/seminar.html`.

[399] A. Becker, R. Dörner, and M. Walter, eds., *International Wilhelm and Else Heraeus Summerschool: Few-body dynamics in atomic and molecular systems* (2006), URL `http://nano.jyu.fi/summerschool06/`.

[400] H. Schmidt-Böcking and R. Dörner, *Experimental Atomic Physics at Frankfurt University*, URL `http://hsbpc1.ikf.physik.uni-frankfurt.de/web/`.

[401] A. Jaeck, ed., *Virtual Chemistry Library* (2007), URL `http://www.chemlin.net/chemistry/quantum_chemistry.htm`.

[402] M. S. Gordon, *Tutorials by Mark Gordon's Quantum Theory Group*, URL `http://www.msg.ameslab.gov/Group/Tutorials/GroupTutor.html`.